VOL. 606 NO. 1 JULY 31, 1992

JOURNAL OF CHROMATOGRAPHY

INCLUDING ELECTROPHORESIS AND OTHER SEPARATION METHODS

ELSEVIER

JOURNAL OF CHROMATOGRAPHY

INCLUDING ELECTROPHORESIS AND OTHER SEPARATION METHODS

Scope. The *Journal of Chromatography* publishes papers on all aspects of chromatography, electrophoresis and related methods. Contributions consist mainly of research papers dealing with chromatographic theory, instrumental development and their applications. The section *Biomedical Applications*, which is under separate editorship, deals with the following aspects: developments in and applications of chromatographic and electrophoretic techniques related to clinical diagnosis or alterations during medical treatment; screening and profiling of body fluids or tissues with special reference to metabolic disorders; results from basic medical research with direct consequences in clinical practice; drug level monitoring and pharmacokinetic studies; clinical toxicology; analytical studies in occupational medicine.

Submission of Papers. Manuscripts (in English; *four* copies are required) should be submitted to: Editorial Office of *Journal of Chromatography*, P.O. Box 681, 1000 AR Amsterdam, Netherlands, Telefax (+31-20) 5862 304, or to: The Editor of *Journal of Chromatography, Biomedical Applications*, P.O. Box 681, 1000 AR Amsterdam, Netherlands. Review articles are invited or proposed by letter to the Editors. An outline of the proposed review should first be forwarded to the Editors for preliminary discussion prior to preparation. Submission of an article is understood to imply that the article is original and unpublished and is not being considered for publication elsewhere. For copyright regulations, see below.

Publication. The *Journal of Chromatography* (incl. *Biomedical Applications*) has 39 volumes in 1992. The subscription prices for 1992 are:

J. Chromatogr. (incl. *Cum. Indexes, Vols. 551–600*) + *Biomed. Appl.* (Vols. 573–611):
Dfl. 7722.00 plus Dfl. 1209.00 (p.p.h.) (total *ca.* US$ 4880.25)

J. Chromatogr. (incl. *Cum. Indexes, Vols. 551–600*) only (Vols. 585–611):
Dfl. 6210.00 plus Dfl. 837.00 (p.p.h.) (total *ca.* US$ 3850.75)

Biomed. Appl. only (Vols. 573–584):
Dfl. 2760.00 plus Dfl. 372.00 (p.p.h.) (total *ca.* US$ 1711.50).

Subscription Orders. The Dutch guilder price is definitive. The US$ price is subject to exchange-rate fluctuations and is given as a guide. Subscriptions are accepted on a prepaid basis only, unless different terms have been previously agreed upon. Subscriptions orders can be entered only by calender year (Jan.–Dec.) and should be sent to Elsevier Science Publishers, Journal Department, P.O. Box 211, 1000 AE Amsterdam, Netherlands, Tel. (+31-20) 5803 642, Telefax (+31-20) 5803 598, or to your usual subscription agent. Postage and handling charges include surface delivery except to the following countries where air delivery via SAL (Surface Air Lift) mail is ensured: Argentina, Australia, Brazil, Canada, China, Hong Kong, India, Israel, Japan*, Malaysia, Mexico, New Zealand, Pakistan, Singapore, South Africa, South Korea, Taiwan, Thailand, USA. *For Japan air delivery (SAL) requires 25% additional charge of the normal postage and handling charge. For all other countries airmail rates are available upon request. Claims for missing issues must be made within three months of our publication (mailing) date, otherwise such claims cannot be honoured free of charge. Back volumes of the *Journal of Chromatography* (Vols. 1–572) are available at Dfl. 217.00 (plus postage). Customers in the USA and Canada wishing information on this and other Elsevier journals, please contact Journal Information Center, Elsevier Science Publishing Co. Inc., 655 Avenue of the Americas, New York, NY 10010, USA, Tel. (+1-212) 633 3750, Telefax (+1-212) 633 3990.

Abstracts/Contents Lists published in Analytical Abstracts, Biochemical Abstracts, Biological Abstracts, Chemical Abstracts, Chemical Titles, Chromatography Abstracts, Clinical Chemistry Lookout, Current Contents/Life Sciences, Current Contents/Physical, Chemical & Earth Sciences, Deep-Sea Research/Part B: Oceanographic Literature Review, Excerpta Medica, Index Medicus, Mass Spectrometry Bulletin, PASCAL-CNRS, Pharmaceutical Abstracts, Referativnyi Zhurnal, Research Alert, Science Citation Index and Trends in Biotechnology.

US Mailing Notice. *Journal of Chromatography* (main section ISSN 0021-9673, *Biomedical Applications* section ISSN 0378-4347) is published (78 issues/year) by Elsevier Science Publishers (Sara Burgerhartstraat 25, P.O. Box 211, 1000 AE Amsterdam, Netherlands). Annual subscription price in the USA US$ 4880.25 (subject to change), including air speed delivery. Application to mail at second class postage rate is pending at Jamaica, NY 11431. **USA POSTMASTERS:** Send address changes to *Journal of Chromatography*, Publications Expediting, Inc., 200 Meacham Avenue, Elmont, NY 11003. Airfreight and mailing in the USA by Publication Expediting.

See inside back cover for Publication Schedule, Information for Authors and information on Advertisements.

0021-9673/92/$05.00

Printed in the Netherlands

CONTENTS

(Abstracts/Contents Lists published in Analytical Abstracts, Biochemical Abstracts, Biological Abstracts, Chemical Abstracts, Chemical Titles; Chromatography Abstracts, Current Awareness in Biological Sciences (CABS) Current Contents/Life Sciences, Current Contents/Physical, Chemical & Earth Sciences, Deep-Sea Research/Part B: Oceanographic Literature Review, Excerpta Medica, Index Medicus, Mass Spectrometry Bulletin, PASCAL-CNRS, Referativnyi Zhurnal, Research Alert and Science Citation Index)

REGULAR PAPERS

Column Liquid Chromatography

Gas Chromatography

Electrophoresis

(Continued overleaf)

JOURNAL OF CHROMATOGRAPHY

VOL. 606 (1992)

JOURNAL of CHROMATOGRAPHY

INCLUDING ELECTROPHORESIS AND OTHER SEPARATION METHODS

ELSEVIER

AMSTERDAM — LONDON — NEW YORK — TOKYO

0021-9673/92/$05.00

Printed in the Netherlands

Journal of Chromatography, 606 (1992) 1–8
Elsevier Science Publishers B.V., Amsterdam

CHROM. 24 243

Effects of molecular structure on the *S* index in the retention equation in reversed-phase high-performance liquid chromatography

Nong Chen, Yukui Zhang and Peichang Lu

National Chromatographic R. & A. Centre, Dalian Institute of Chemical Physics, Chinese Academy of Sciences, 116011 Dalian (China)

(First received August 27th, 1991; revised manuscript received March 17th, 1992)

ABSTRACT

The *S* index in the retention equation $\log k' = \log k'_w - S\varphi$ in reversed-phase high-performance liquid chromatography was systematically investigated as the function of molecular structure parameters. The *S* index, which has been observed to be nearly constant for a specific solute even when column systems with different C_{18} packing materials are used, was quantitatively correlated with the solvatochromic parameters of the solutes. The coefficients in the correlation of the *S* index with the solvatochromic parameters of the solutes were investigated and were found to be consistent with the results of using a solvatochromic comparison method. For non-polar compounds, a simplified linear relationship between *S* and the Van der Waals volume of the solute was observed. For homologues, a linear relationship between *S* and carbon number was found. Therefore, when other factors remain the same, increasing the size of the solute results in an increase in *S* whereas increasing the dipolarity or hydrogen bonding ability of the solute will result in a decrease in *S*.

INTRODUCTION

The selectivity of the chromatographic system in reversed-phase high-performance liquid chromatography (RP-HPLC) is generally manipulated by changing the composition of the mobile phase. The linear relationship between the logarithm of capacity factors and the composition of the mobile phase in RP-HPLC has found considerable application and has been shown to be fairly reliable in practice, as expressed by the equation [1–3]

$$\log k' = \log k'_w - S\varphi \quad (1)$$

where k' is the capacity factor, φ is the volume fraction of strong solvent in a binary mobile phase, $\log k'_w$ is the extrapolated value for the capacity factor in pure water and *S* is defined as the negative of the slope of the plot of $\log k'$ *versus* volume fraction (φ).

The *S* value in eqn. 1 plays an important role in understanding the interactions in binary mobile phases and in computer simulations of RP-HPLC [3,4]. It has been suggested that *S* should be a constant, characterizing the solvent strength [1,2]; however, it has been found that *S* is variable tending to increase with increasing solute retention, and there is a general trend of increasing *S* in RP-HPLC as the molecular size of the solute increases. It has been observed that *S* values can be approximately related to the molecular weight (*M*) of the solute [3], and therefore it may be questioned whether *S* is a characteristic constant of the solvent. In several other studies, a linear relationship between *S* and $\log k'_w$ has been found [5–11].

It has also been found that *S* depends on the structure of the eluites [4,12–14]. One study showed

Correspondence to: Dr. N. Chen, National Chromatographic, R. & A. Centre, Dalian Institute of Chemical Physics, Chinese Academy of Sciences, 116011 Dalian, China.

0021-9673/92/$05.00

S increasing for the following benzene derivatives [11,12]: aniline < alkylbenzene < chlorobenzene < ether < aldehydes, ketones < nitriles < unsubstituted polyaromatics < nitro compounds < phthalates < phenylalkanols.

It has been found when other factors remain the same, there is a tendency for more polar compounds to exhibit smaller values of S. All the above results show that S is a solute-related constant.

In a previous paper [4], the S index (the "hydrophilic index") was observed to be nearly constant for a specific solute even when column systems with different C_{18} packing materials are used. The S index quantitatively describes the difference betwee n the free-energy change of the solute in a weak solvent and a strong solvent, and it is therefore a function of the molecular structural parameters of the solute. This paper describes the effect of molecul ar structure on S in RP-HPLC. The S index was quantitatively correlated with the solvatochromic parameters of the solutes. The coefficients in the correlation of S with the solvatochromic parameters of the solutes are discussed based on the solvatochro mic comparison method.

EXPERIMENTAL

Detailed chromatographic conditions have been described in a previous paper [4]. All data were processed with a BASIC program on an IBM-AST 286 microcomputer. Other experimental results utilized in this work were taken from papers by Hammers *et al.* [6], Hafkenscheid and Tomlinson [15], Harnisch *et al.* [16] and Hanai and Hubert [17], which gave exact descriptions of the chromatographic conditions employed.

RESULTS AND DISCUSSION

The S index quantitatively describes the difference in free-energy change between solute–weak solvent and solute–strong solvent systems, as is shown by the following equation [4]:

$$S = (\Delta G^0_{A,C} - \Delta G^0_{A,B})/RT \quad (2)$$

where $\Delta G^0_{A,C}$ and $\Delta G^0_{A,B}$ are the free-energy change between solute–weak solvent and solute–strong solvent, respectively, R is the gas constant and T is the column absolute temperature.

The non-electrostatic free-energy change can be separated into Van der Waals interactions [ΔG^0 (van)] and hydrogen bonding interactions [ΔG^0(H)]:

$$\Delta G^0 = \Delta G^0(\text{van}) + \Delta G^0(\text{H}) \quad (3)$$

Dispersion, dipole–dipole (dipolarity) and dipole–induced dipole (polarization) interactions are included in the Van der Waals interactions. These interactions can be characterized by using solvatochromic parameters which have been shown to be useful in evaluating and identifying the physicochemical properties governing aqueous solubilities [18–23]. As in linear solvation energy relationships (LSERs), solvent-dependent properties depend on three types of terms according to the following equation:

$$SP = SP_0 + \text{cavity term} + \text{dipolar term} + \text{hydrogen bonding terms} \quad (4)$$

The general LSER for solutes has taken the form

$$SP = SP_0 + mv_w/100 + d\pi^* + b\beta + a\alpha \quad (5)$$

where v_w measures the cavity term and is the Van der Waals molecular volume, and can be calculated by using Bondi's method [24], π^* is a measure of solute dipolarity/polarizability, α is the hydrogen bond donor ability (HBD) or HBD acidity and β is the hydrogen bond acceptor ability (HBA) or HBA basicity.

The parameters v_w, π^*, β and α characterize the solutes and the coefficients m, d, b and a characterize the solvents. The solvent property complementary to solute HBA basicity is solvent HBD acidity. According to the solvatochromic comparison method [20], solvent-dependent properties are given by the following equation:

$$SP = SP_0 + mv_w/100 + d\pi^* + b\beta + a\alpha \quad (6)$$

where

$$m = f(\delta^2_C - \delta^2_B) \quad (7)$$

$$d = g(\pi^*_B - \pi^*_C) \quad (8)$$

$$b = h(\alpha_B - \alpha_C) \quad (9)$$

$$a = l(\beta_B - \beta_C) \quad (10)$$

where δ_C and δ_B the solubility parameters for weak solvent and strong solvent, respectively, π^*_B, α_B and β_B are solvatochromic parameters for the strong

TABLE I

SOLUBILITY AND SOLVATOCHROMIC PARAMETERS FOR METHANOL AND WATER

Solubility and solvatochromic parameters taken from refs. 18 and 10, respectively.

Parameter	Methanol	Water
π^*	0.60	1.09
β	0.62	0.18
α	0.93	1.17
$\delta(\text{cal/ml})^{1/2}$	14.5	23.4

solvent, π^*_C, α_C and β_B are solvatochromic parameters for the weak solvent and f, g, h and l are constants.

In RP-HPLC, the difference in free-energy change between solute–weak solvent and solute–strong solvent can be directly correlated with the solvatochromic parameters, hence SP in eqn. 6 refers to the S index. Therefore, S can be quantitatively correlated with the solvatochromic parameters.

In eqn. 6, the magnitude of m denotes the difference in the solubility parameters for the weak solvent and the strong solvent, d is determined mainly by the difference between the strong solvent and the weak solvent in the dipolarity/polarizability parameters, b shows the difference in hydrogen donor ability of the strong solvent and the weak solvent and a shows the difference in hydrogen acceptor ability of the strong solvent and the weak solvent. The solvatochromic and solubility parameters for methanol and water are given in Table I.

Table II gives the experimental S values and the S values calculated from the solvatochromic parameters; the resulting equation obtained by least-squares regression is

$$S = (1.09 \pm 0.14) + (4.55 \pm 0.15)v_w/100 - (0.252 \pm 0.13)\pi^* - (2.50 \pm 0.17)\beta + (0.0948 \pm 0.15)\alpha \quad (11)$$

$$n = 49;\ R = 0.987;\ \text{S.D.} = 0.156$$

In this and all the regression equations that follow, n is the number of data points in the regression, R is the coefficient of the regression and S.D. is the standard deviation.

The sign of the coefficients is determined by whether the term represents an exoergic or endoergic factor in the retention process. The coefficients of the m, d, b and a terms have the expected signs. The value of solubility parameter for water is greater than that for methanol (see Table I), whereas the dipolarity of water ($\pi^*_C = 1.09$) is higher than that of methanol ($\pi^*_B = 0.60$), which leads to m having a positive sign and d a negative sign.

As methanol ($\beta_B = 0.62$) is more basic than water ($\beta_C = 0.18$), this leads to a value of a that is positive, whereas water is a stronger HB acid ($\alpha_C = 1.17$) than methanol ($\alpha_B = 0.93$), so b is negative.

The contribution of the α term to S is not very significant compared with β. There is no deterioration in the statistical goodness of fit when the α term is omitted, which is consistent with earlier conclusions for the acetonitrile–water system [23] and the methanol–water system [22], but we use a different approach. We believe that if the relationship between the logarithmic capacity factors and the mobile phase composition is linear (plots of $\log k'$ *vs.* φ are less linear when acetonitrile is used instead of methanol as the organic modifier), the parameters $\log k'_w$ and the S would be sufficiently unbiased to be useful as input data for solvatochromic comparison studies. Log k'_w or S is correlated well with the solvatochromic parameters (see Tables II–IV). Log k'_w and S do offer some advantages over log k' at a particular eluent composition when correlated with the solvatochromic parameters. Log k'_w and S contain the retentions over a wide range of concentrations of the mobile phase for a particular solute. The slope of $\log k'$ *vs.* φ is determined by the mobile phase effect, whereas the intercept of the plots is determined mainly by the properties of the stationary phases. Therefore, the mobile phase effects have been separated from the stationary phase effects by using this approach.

Eqn. 11 shows that increasing hydrogen bonding interaction results in a dramatic decrease in S when other conditions remain the same. This is consistent with the practical observations that when other factors remain the same, more polar compounds will have decreased S values, whereas increasing the size of the solute leads to an increase in S. Therefore, there is a general trend that as the solute becomes increasingly hydrophobic, S will become increasingly positive; in contrast, as the solute becomes more hydrophilic and more polar, S will decrease when other conditions remain the same.

Table III shows the results of another example,

TABLE II

VALUES OF SOLVATOCHROMIC PARAMETERS AND COMPARISON OF EXPERIMENTAL *S*-VALUES WITH CALCULATED VALUES FOR VARIOUS AROMATICS

Column, Lichrosorb RP-C_{18}; eluent, methanol–water (methanol from 30 to 90%, v/v). *S* values from ref. 6; solvatochromic parameters from ref. 18.

Compound	$v_w/100$	π^*	β	α	*S*(exp.)	*S*(calc.)[a]	Δ
Benzene	0.491	0.59	0.10	0	2.71	2.92	0.21
Toluene	0.592	0.55	0.11	0	3.28	3.37	0.09
1,2-Dimethylbenzene	0.668	0.51	0.12	0	3.64	3.70	0.06
1,3-Dimethylbenzene	0.668	0.51	0.12	0	3.74	3.70	−0.04
1,4-Dimethylbenzene	0.668	0.51	0.12	0	3.69	3.70	0.01
1,3,5-Trimethylbenzene	0.769	0.47	0.13	0	4.23	4.16	−0.07
1,2,3,4-Tetramethylbenzene	0.867	0.43	0.15	0	4.45	4.55	0.10
1,2,3,5-Tetramethylbenzene	0.867	0.43	0.15	0	4.48	4.55	0.07
Pentamethylbenzene	0.965	0.39	0.17	0	4.90	4.96	0.06
Hexamethylbenzene	1.063	0.35	0.19	0	5.40	5.36	−0.04
Ethylbenzene	0.668	0.53	0.12	0	3.77	3.70	−0.07
n-Propylbenzene	0.769	0.51	0.12	0	4.43	4.16	−0.27
n-Butylbenzene	0.867	0.49	0.12	0	4.95	4.61	−0.34
Naphthalene	0.753	0.70	0.15	0	4.03	3.97	−0.06
Fluorene	0.960	1.18	0.22	0	4.53	4.61	0.08
Phenanthrene	1.015	0.80	0.20	0	4.80	5.01	0.21
Anthracene	1.015	0.80	0.20	0	4.95	5.01	0.06
Pyrene	1.156	0.90	0.25	0	5.18	5.50	0.32
Biphenyl	0.92	1.18	0.20	0	4.68	4.48	−0.20
Bibenzyl	1.116	1.10	0.22	0	5.33	5.34	0.01
Fluorobenzene	0.520	0.62	0.07	0	2.99	3.12	0.13
Chlorobenzene	0.581	0.71	0.07	0	3.36	3.38	0.02
Bromobenzene	0.624	0.79	0.06	0	3.42	3.58	0.16
1,2-Dichlorobenzene	0.671	0.80	0.03	0	3.88	3.87	−0.01
1,3-Dichlorobenzene	0.671	0.75	0.03	0	3.93	3.88	−0.05
1,4-Dichlorobenzene	0.671	0.70	0.03	0	3.90	3.89	−0.01
1,2,3-Trichlorobenzene	0.761	0.85	0	0	4.33	4.34	0.01
1,2,4-Trichlorobenzene	0.761	0.75	0	0	4.35	4.36	0.01
1,3,5-Trichlorobenzene	0.761	0.70	0	0	4.45	4.38	−0.07
1,2,3,4-Tetrachlorobenzene	0.851	0.80	0	0	4.75	4.76	0.01
1,2,3,5-Tetrachlorobenzene	0.851	0.80	0	0	4.80	4.76	−0.04
1,2,4,5-Tetrachlorobenzene	0.851	0.70	0	0	4.80	4.79	−0.01
Pentachlorobenzene	0.941	0.75	0	0	5.25	5.18	−0.07
Hexachlorobenzene	1.031	0.70	0	0	5.70	5.61	−0.09
2-Chloroaniline	0.652	0.83	0.40	0.25	2.84	2.87	0.03
3-Chloroaniline	0.652	0.78	0.40	0.31	2.91	2.89	−0.02
4-Chloroaniline	0.653	0.73	0.40	0.31	2.96	2.91	−0.05
3-Chlorophenol	0.626	0.77	0.23	0.69	3.34	3.23	−0.11
4-Chlorophenol	0.626	0.72	0.23	0.67	3.35	3.25	−0.10
Aniline	0.562	0.73	0.50	0.26	1.98	2.24	0.26
Phenol	0.536	0.72	0.33	0.61	2.35	2.58	0.23
Benzyl alcohol	0.634	0.99	0.52	0.39	2.55	2.46	−0.09

TABLE II (*continued*)

Compound	$v_w/100$	π^*	β	α	S(exp.)	S(calc.)[a]	Δ
Benzaldehyde	0.606	0.92	0.44	0	2.80	2.52	−0.28
Benzonitrile	0.590	0.90	0.37	0	2.90	2.62	−0.28
Nitrobenzene	0.631	1.01	0.30	0	2.69	2.96	0.27
Acetophenone	0.690	0.90	0.49	0.04	3.10	2.78	−0.32
Anisole	0.639	0.73	0.32	0	2.88	3.01	0.13
Methyl benzoate	0.736	0.75	0.39	0	3.20	3.27	0.07
N,N-Dimethylaniline	0.752	0.90	0.43	0	3.09	3.21	0.12

[a] $S = (1.09 \pm 0.14) + (4.55 \pm 0.15)v_w/100 - (0.252 \pm 0.13)\pi^* - (2.50 \pm 0.17)\beta + (0.0948 \pm 0.15)\alpha$; $n = 49$; $R = 0.987$; S.D. = 0.156.

TABLE III

VALUES OF SOLVATOCHROMIC PARAMETERS AND COMPARISON OF EXPERIMENTAL S VALUES WITH CALCULATED VALUES FOR VARIOUS COMPOUNDS

Column, Hypersil-ODS; eluent, methanol–water (methanol from 30 to 90%, v/v); phosphate buffer was used when applied to ionizable compounds. Data for S from ref. 15; solvatochromic parameters from ref. 18.

Compound	$v_w/100$	π^*	β	α	S(exp.)	S(calc.)[a]	Δ
4-Nitrophenol	0.676	1.15	0.32	0.82	3.09	3.19	0.10
4-Nitroaniline	0.702	1.25	0.48	0.42	2.78	2.77	−0.01
Benzene	0.491	0.59	0.10	0	2.83	3.03	0.20
Toluene	0.592	0.55	0.11	0	3.27	3.45	0.18
Chlorobenzene	0.581	0.71	0.07	0	3.48	3.41	−0.07
Nitrobenzene	0.631	1.01	0.30	0	2.97	2.92	−0.05
Phenol	0.536	0.72	0.33	0.61	2.64	2.76	0.12
Aniline	0.562	0.73	0.50	0.26	2.28	2.37	0.09
Benzoic acid	0.650	0.74	0.40	0.59	3.13	3.05	−0.08
p-Xylene	0.668	0.51	0.12	0	3.76	3.76	0.0
4-Chlorotoluene	0.679	0.67	0.08	0	3.99	3.82	−0.17
4-Nitrotoluene	0.729	0.97	0.31	0	3.40	3.32	−0.08
p-Cresol	0.634	0.68	0.34	0.58	3.08	3.16	0.08
p-Toluidine	0.660	0.69	0.51	0	2.74	2.71	−0.03
p-Toluic acid	0.748	0.70	0.41	0.59	3.57	3.45	−0.12
1,4-Dichlorobenzene	0.671	0.70	0.03	0	4.04	3.89	−0.15
4-Nitrochlorobenzene	0.721	1.01	0.26	0	3.32	3.39	0.07
4-Chlorophenol	0.626	0.72	0.23	0.67	3.34	3.38	0.04
4-Chloroaniline	0.653	0.73	0.40	0.31	3.06	3.00	−0.06
4-Chlorobenzoic acid	0.740	0.74	0.36	0.63	3.71	3.53	−0.18
1,3,5-Trimethylbenzene	0.769	0.47	0.13	0	4.21	4.17	−0.04
1,2,4,5-Tetramethylbenzene	0.867	0.43	0.15	0	4.48	4.55	0.07
Naphthalene	0.753	0.70	0.15	0	3.98	3.94	−0.08
Phenanthrene	1.015	0.80	0.20	0	4.84	4.85	0.01
Anthracene	1.015	0.80	0.20	0	4.96	4.85	−0.11
Pyrene	1.156	0.90	0.25	0	5.10	5.26	0.16
Perylene	1.415	1.0	0.30	0	6.11	6.17	0.06

[a] $S = (1.55 \pm 0.11) + (4.13 \pm 0.12)v_w/100 - (0.523 \pm 0.14)\pi^* - (2.357 \pm 0.21)\beta + (0.249 \pm 0.10)\alpha$; $n = 27$; $R = 0.993$; S.D. = 0.116.

TABLE IV

COEFFICIENTS OF SP_0, m, d, b AND a ON DIFFERENT COLUMNS PACKED WITH VARIOUS C_{18} PACKING MATERIALS WITH SURFACE COVERAGE RANGING FROM 0.255 TO 0.690 mmol/g

S values for regression taken from refs. 25 and 26. Compounds used for the regression: acetophenone, *p*-cresol, benzyl alcohol, phenol, aniline, benzene, toluene, ethylbenzene, *n*-propylbenzene, *n*-butylbenzene, pentane, hexane, heptane, octane, 1-butanol, 1-pentanol, 1-hexanol.

C_{18} coverage (mmol/g)	SP_0	m	d	b	a	R	n	S.D.
0.255	0.21 (±0.17)	6.25 (±0.24)	−0.43 (±0.11)	−2.87 (±0.21)	−0.16 (±0.16)	0.997	17	0.098
0.335	0.28 (±0.17)	6.21 (±0.24)	−0.53 (±0.11)	−2.71 (±0.22)	−0.10 (±0.16)	0.997	17	0.099
0.499	0.24 (±0.13)	6.15 (±0.18)	−0.41 (±0.08)	−2.63 (±0.16)	−0.22 (±0.12)	0.998	17	0.074
0.690	0.50 (±0.15)	5.76 (±0.21)	−0.44 (±0.09)	−2.64 (±0.19)	−0.25 (±0.14)	0.998	17	0.087

listing the experimental S values and the values calculated on the basis of the relationship between S and the solvatochromic parameters for 27 aromatic compounds.

Table IV gives the coefficients SP_0, m, d, b and a on four different C_{18} packings with surface coverages ranging from 0.255 to 0.699 mmol/g. The variation of S for a specific solute on the four different columns is within ±0.04 [4], and the values of m, d, b and a on the four columns are approximately equal, showing the characteristic constants of the solvents used.

TABLE V

COMPARISON OF EXPERIMENTAL S VALUES [S(exp.)] WITH THOSE CALCULATED [S(calc.)] FROM THE SOLVATOCHROMIC PARAMETERS FOR SOME PAHs

Column, YWG-C_{18}; eluent, methanol–water (methanol from 60 to 90%, v/v). S values taken from ref. 4.

Compound	v_w/100	S(exp.)	S(calc.)[a]	Δ
Benzene	0.49	2.74	2.74	0.00
Naphthalene	0.75	3.60	3.62	0.02
Biphenyl	0.92	4.24	4.20	−0.04
Phenanthrene	1.01	4.44	4.50	0.06
Anthracene	1.01	4.54	4.50	−0.04
Chrysene	1.25	5.24	5.32	0.08
p-Terphenyl	1.38	5.73	5.66	−0.07

[a] $S = (1.14 \pm 0.06) + (3.32 \pm 0.06)v_w/100$; $n = 7$; $R = 0.9996$; S.D. = 0.061.

For non-polar compounds such as polynuclear aromatic hydrocarbons (PAHs), from eqn. 6 we can see that there is a linear relationship between S and the Van der Waals volume of the solute. Table V shows the experimental S value and values calculated from the Van der Waals volume for some PAHs in methanol–water.

For homologous series, as v_w can be written as

$$v_w = n\Delta v_w(CH_2) + n_e\Delta v_w(e) \quad (12)$$

where n and n_e are the number of methylene groups and end-groups, respectively, and $\Delta v_w(CH_2)$ and $\Delta v_w(e)$ are the Van der Waals volume contributed by the methylene groups and end-groups, respectively, then for homologues the insertion of a CH_2 group into a compound should give a constant change in S values, as can be seen from Tables VI and VII. The average contribution of a methylene group to S approaches a constant value. The average contribution of a methylene group to S for alkylbenzenes is defined by

$$\Delta S(CH_2) = [S(n\text{-alkylbenzene}) - S(\text{benzene})]/n \quad (13)$$

where $S(n$-alkylbenzene) is the experimental S value for n-alkylbenzenes and S(benzene) is the experimental S value for benzene. The calculated S values for these alkylbenzenes based on the linear relationship between S and carbon number are also listed in Tables VI and VII.

In conclusion, the S index (the "hydrophilic

TABLE VI

EXPERIMENTAL S VALUES [S(exp.)], $\Delta S(CH_2)$ AND CALCULATED VALUES [S(calc.)] FOR n-ALKYLBENZENES IN METHANOL–WATER SYSTEM

Column, SIL-X-5-C_{18}; eluent, methanol–water (methanol from 60 to 95%, v/v). S values from ref. 16.

Compound	n	S(exp.)	$\Delta S(CH_2)$	S(calc.)[a]	Δ
Benzene	0	2.95	–	2.96	0.01
Toluene	1	3.52	0.57	3.48	−0.04
Ethylbenzene	2	3.96	0.51	4.01	0.05
Propylbenzene	3	4.55	0.53	4.53	−0.02
Butylbenzene	4	5.06	0.53	5.05	−0.01
Hexylbenzene	6	6.10	0.53	6.10	0.00
Octylbenzene	8	7.14	0.52	7.15	0.01
Decylbenzene	10	8.20	0.53	8.20	0.00

[a] $S = (2.96 \pm 0.02) + (0.524 \pm 0.03)n$; $n = 8$; $R = 0.9999$; S.D. = 0.03.

index") in the retention equation $\log k' = \log k'_w - S\varphi$ in RP-HPLC can be calculated by using the solvatochromic parameters. The coefficients in the correlation of the S index with the solvatochromic parameters of the solutes are determined mainly by the properties of the mobile phase. For non-polar compounds, a linear relationship between S and the Van der Waals volume can be used to calculate S values. For homologues, a linear correlation between S and carbon number is strictly observed. Therefore, increasing the volume of the solute results in an increase in S, whereas increasing the dipolarity and hydrogen bonding ability of the solute lead to a dramatic decrease in S when other factors remain the same.

ACKNOWLEDGEMENT

Dr. W. Zhang is thanked for the help with computer programming.

TABLE VII

EXPERIMENTAL S VALUES [S(exp.)], $\Delta S(CH_2)$ AND CALCULATED VALUES [S(calc.)] FOR n-ALKYLBENZENES IN ACETONITRILE–WATER SYSTEM

Column, YMC-phenyl; eluent, acetonitrile–water (acetonitrile from 50 to 80%, v/v). Data recalculated from ref. 17.

Compound	S(exp.)	n	$\Delta S(CH_2)$	S(calc.)[a]	Δ
Benzene	2.21	0	–	2.21	0.00
Toluene	2.41	1	0.20	2.44	0.03
Ethylbenzene	2.69	2	0.24	2.66	−0.03
Propylbenzene	2.88	3	0.22	2.89	0.01
Butylbenzene	3.12	4	0.23	3.11	−0.01
Hexylbenzene	3.57	6	0.23	3.56	−0.01
Heptylbenzene	3.80	7	0.23	3.79	−0.01
Octylbenzene	4.04	8	0.23	4.01	−0.03
Nonylbenzene	4.25	9	0.23	4.24	−0.01
Decylbenzene	4.43	10	0.22	4.47	0.04

[a] $S = (2.21 \pm 0.01) + (0.226 \pm 0.002)n$; $n = 10$, $R = 0.9997$; S.D. = 0.03.

REFERENCES

1 J. W. Dolan, J. R. Gant and L. R. Snyder, *J. Chromatogr.*, 165 (1979) 31.
2 L. R. Snyder, J. W. Dolan and J. R. Gant, *J. Chromatogr.*, 165 (1979) 3.
3 L. R. Snyder, M. A. Quarry and J. L. Glajch, *Chromatographia*, 24 (1987) 33.
4 N. Chen, Y. Zhang and P. Lu, *J. Chromatogr.*, 603 (1992) 35.
5 P. J. Schoenmakers, H. A. H. Billiet and L. de Galan, *J. Chromatogr.*, 218 (1981) 261.
6 W. E. Hammers, G. J. Meurs and C. L. de Ligny, *J. Chromatogr.*, 247 (1982) 1.
7 H. A. Cooper and R. J. Hurtubise, *J. Chromatogr.*, 360 (1986) 313.
8 P. Jandera, *J. Chromatogr.*, 352 (1986) 91.
9 A. Opperhuizen, T. L. Sinnige, J. M. D. van der Steen and O. Hutzinger, *J. Chromatogr.*, 388 (1987) 51.
10 R. Kaliszan, *Quantitative Structure Chromatographic Retention Relationships*, Wiley, New York, 1987.
11 M. A. Quarry, R. L. Grob, L. R. Snyder, J. W. Dolan and M. P. Rigney, *J. Chromatogr.*, 384 (1987) 163.
12 M. A. Stadalius, H. S. Gold and L. R. Snyder, *J. Chromatogr.*, 296 (1984) 31.
13 N. Chen, Y. Zhang and P. Lu, *Chin. J. Chromatogr.*, 6 (1988) 325.
14 H. Zou, Y. Zhang and P. Lu, *J. Chromatogr.*, 522 (1990) 49.
15 T. L. Hafkenscheid and C. Tomlinson, *J. Chromatogr. Sci.*, 24 (1986) 307.
16 M. Harnisch, H. J. Mockel and G. Schulze, *J. Chromatogr.*, 282 (1983) 315.
17 T. Hanai and J. Hubert, *J. Chromatogr.*, 291 (1984) 81.
18 M. J. Kamlet, R. M. Doherty, M. H. Abraham, Y. Marcus and R. W. Taft, *J. Phys. Chem.*, 92 (1988) 5244.
19 J. H. Park, P. W. Carr, M. H. Abraham, R. W. Taft, R. W. Doherty and M. J. Kamlet, *Chromatographia*, 25 (1988) 373.
20 R. W. Taft, M. H. Abraham, G. R. Famini, R. M. Doherty, J. L. M. Abboud and M. J. Kamlet, *J. Pharm. Sci.*, 74 (1985) 807.
21 D. E. Leahy, P. W. Carr, R. S. Pearlman, R. W. Taft and M. J. Kamlet, *Chromatographia*, 21 (1980) 473.
22 P. C. Sadek, P. W. Carr, R. M. Doherty, M. J. Kamlet, R. W. Taft and M. H. Abraham, *Anal. Chem.*, 57 (1985) 2971.
23 P. W. Carr, R. M. Doherty, M. J. Kamlet, R. W. Taft, W. Melander and Cs. Horváth, *Anal. Chem.*, 58 (1986) 2674.
24 A. Bondi, *J. Phys. Chem.*, 68 (1964) 441.
25 S. M. Petrovic and S. Lomic, *J. Liq. Chromatogr.*, 12 (1989) 59.
26 S. M. Petrovic and S. M. Lomic, *Chromatographia*, 27 (1989) 378.

Journal of Chromatography, 606 (1992) 9–17
Elsevier Science Publishers B.V., Amsterdam

CHROM. 24 249

Chiral-bonded silica gel stationary phases obtained from chiral silanes for high-performance liquid chromatography

Comparison of performance with that of stationary phases obtained from γ-aminopropylsilica gel*

Laureano Oliveros

Conservatoire National des Arts et Métiers, Laboratoire de Chimie Générale (CNRS URA 1103), 292 Rue Saint-Martin, 75141 Paris Cédex 03 (France)

Cristina Minguillón

Laboratorio de Química Farmacéutica, Facultad de Farmacia, Universidad de Barcelona, Avd. Diagonal s/n, 08028 Barcelona (Spain)

Bernard Desmazières and Paul-Louis Desbène

CNRS, URA 455, Université Pierre et Marie Curie, Laboratoire de Chimie Organique Structurale, 4 Place Jussieu, 75230 Paris Cédex 05 and Université de Rouen, LASOC, 43 Rue Saint Germain, 27000 Evreux (France)

(First received November 28th, 1991; revised manuscript received February 25th, 1992)

ABSTRACT

Several chiral triethoxysilanes, easily prepared from acidic or basic chiral compounds and aminopropyltriethoxysilane or isocyanatepropyltriethoxysilane were bonded onto silica gel. In the chiral stationary phases thus obtained, only silanol groups and the chiral selector can interact with solutes. To deactivate these silanol groups, an end-capping treatment with hexamethyldisilazane was applied. Unlike chlorotrimethylsilane, this reagent does not destroy the chemically bonded chiral silica gel. The performance of these stationary phases was evaluated and compared with that of bonded silica gel phases with the same chiral selector but fixed on a γ-aminopropylsilica gel. Chiral stationary phases obtained from chiral silanes and an end-capping treatment showed the best resolution and the shortest retention time for most of the compounds tested.

INTRODUCTION

The chiral stationary phases used in high-performance liquid chromatography (HPLC) which belong to the acceptor–donor type are generally prepared by condensation of the chiral compound on silica gel previously treated with a silane bearing, in most instances, a primary amino group [1] or an epoxide [2,3] or, rarely, a sulphide group [4]. These condensations are not quantitative. The chiral stationary phases obtained in this way always have some unreacted groups remaining which are able to interact in a non-stereoselective way with the racemic mixtures to be resolved.

There are various ways of preparing stationary

Correspondence to: Dr. L. Oliveros, Conservatoire National des Arts et Métiers, Laboratoire de Chimie Générale (CNRS URA 1103), 292 Rue Saint-Martin, 75141 Paris Cédex 03, France.

* Presented at the *15th International Symposium on Column Liquid Chromatography, Basle, June 3–7, 1991.* The majority of the papers presented at this symposium have been published in *J. Chromatogr.*, Vol. 592 and 593 (1992).

0021-9673/92/$05.00

phases without using previously functionalized silica gel. Some of these are easy to carry out; for instance, the condensation of an alkoxysilane [5–7] or a chlorosilane [8,9] bearing a chiral radical on the silica gel. Others are rarely used; for instance, the cross-linking or chemically bonding chiral polysiloxanes with Si–H groups linked to the silica gel via silanol groups [10]. All these methods used for the preparation of chiral stationary phases should be able to overcome the disadvantages inherent in the use of previously functionalized silica. The condensation of chiral silanes on silica gel was therefore chosen as a method for the preparation of chiral stationary phases with the aim of obtaining stationary phases able to establish the minimum of achiral interactions with solutes. If the pursued objective is the resolution of racemic compounds, the reduction of achiral interactions contributes to a reduction in the retention time and to an increase in the selectivity factor [11]. The selectivity factor, α, for a racemic mixture is the ratio between the two capacity factors of the two enantiomers. These are a function of the sum of achiral interactions, common to both enantiomers, and chiral interactions, different in each enantiomer. Thus α will increase when achiral interactions become smaller.

The preparation of such stationary phases from chiral silanes provides the opportunity to compare performances with those of stationary phases bearing the same chiral entity but obtained by condensation on a γ-aminopropylsilica gel [12]; both stationary phases are prepared from the same silica gel.

This paper describes the preparation of six chiral silanes, their condensation on silica gel and the evaluation of the chiral stationary phases thus obtained. One of the six chiral selectors used belongs to the π-acceptor type and the others have a π-donor character. The π-acceptor chiral selector is 3,5-dinitrobenzoylphenylalanine, which has been used previously [13,14]. The π-donor chiral selectors chosen previously [12] were N-(3,5-dimethoxybenzoyl), N-(3,5-dimethylbenzoyl) and 3,5-dimethylanilido derivatives of (*S*)-phenylalanine and (*S*)-naproxen (Fig. 1). The last compound has been used by Doyle and co-workers [15,16] to prepare a chiral stationary phase by a different method. Silanes were obtained for this study by the reaction of chiral entities with acidic groups on 3-aminopropyltriethoxysilane and the chiral selector with an amino group on 3-isocyanatopropyltriethoxysilane (Fig. 2). The synthetic scheme for the preparation of chiral stationary phases is given in Fig. 3 and their structures in Fig. 4. Formulae of racemic compounds used as test compounds are given in Fig. 5.

EXPERIMENTAL

NMR spectra were measured using a Brucker AC200 spectrometer. Tetramethylsilane (TMS) was

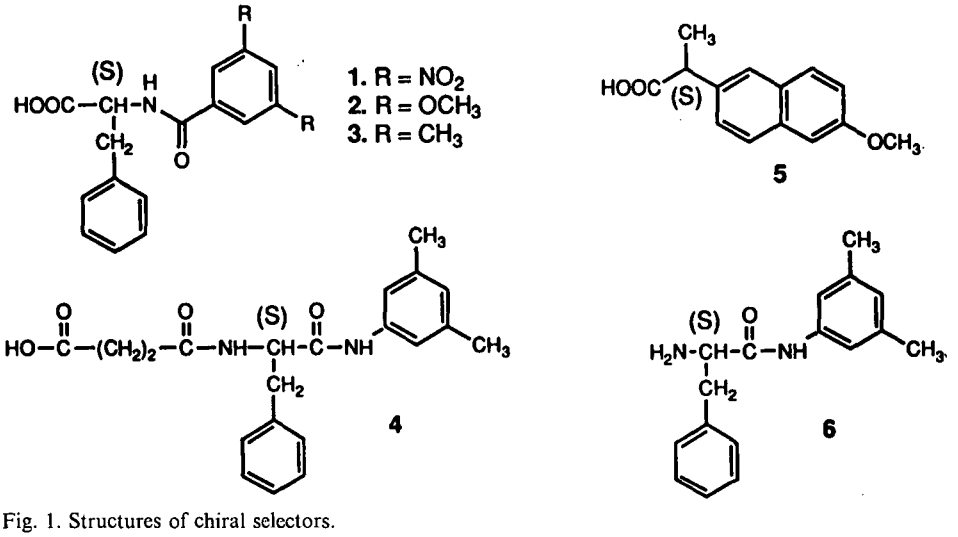

Fig. 1. Structures of chiral selectors.

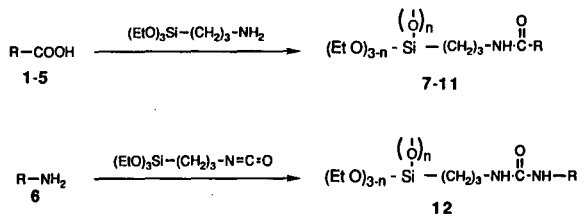

Fig. 2. Synthetic scheme for the preparation of chiral silanes **7** to **12**.

used as the internal standard and the chemical shift, δ, is measured in ppm. Rotatory power was measured with a Perkin-Elmer Model 241 polarimeter. Elemental analyses were performed by the Service Central de Microanalyse du CNRS (Vernaison, France). The chromatographic experiments were carried out on an HP 1090 liquid chromatograph (Hewlett-Packard, Palo Alto, CA, USA) equipped with a PU4020 UV detector (Philips, Cambridge, UK). The chiral stationary phases were packed into stainless-steel tubes (100 × 4.6 mm I.D.) by the slurry method according to Coq *et al.* [17]. The volume of sample injected was 5 μl. The flow-rate of the pump was 1 ml/min. The detection wavelength was 254 nm. The mobile phases consisted of various mixtures of *n*-heptane, chloroform and methanol.

Chemicals and reagents

Compounds **1–4** (Fig. 1) were prepared by the method described previously [12]. Compound **5** was purchased from Fluka. Compounds **13–15** (Fig. 5) were obtained by treating the methyl ester of each amino acid with 3,5-dinitrobenzoyl chloride. Compounds **16** and **17** (Fig. 5) and 3-aminopropyltriethoxysilane were purchased from Aldrich. 3-Isocyanatopropyltriethoxysilane was purchased from Hüls-Petrarch.

To prepare phenylalanyl(3,5-dimethyl)anilide (**6**) (Fig. 1), 27 g (73.3 mmol) of (*S*)-*tert.*-butoxycarbonylphenylalanyl-3,5-dimethylphenylamine, prepared by the method described previously [12], were dissolved in 250 ml of glacial acetic acid and cooled in an ice-bath. Hydrogen chloride was passed through for 45 min and the solution was left to stand at room temperature for 3 h. The solvent was removed *in vacuo* and 350 ml of 1 *M* NaOH were added to the residual white solid. The mixture was extracted with chloroform. Evaporation of the solvent gave 19.4 g (98.6% yield) of **6** as a viscous liquid. ^{1}H NMR (200 MHz): δ (C^2HCl_3) 1.56 (s, 2H, NH_2), 2.32 (s, 6H, CH_3), 2.78 (m, 1H, CH_aAr), 3.35 (m, 1H, CH_bAr), 3.68 (m, 1H, CH), 6.78 (s, 1H, C^4H), 7.27 (m, 7H, aromatics), 9.40 (ba, 1H, NH). ^{13}C NMR (50.3 MHz): δ (C^2HCl_3) 21.3 (CH_3), 40.6 (CH_2), 56.7 (CH), 117.2 (C^2H and C^6H), 125.8 and 126.8 (C^4H and $C^{4'}H$), 128.7 and 128.2 ($C^{2',6'}H$ and $C^{3',5'}H$), 137.5 and 137.7 (C^1 and $C^{1'}$), 138.5 ($C^{3,5}$), 172.3 (CO). $[\alpha]_D^{23} = -61°$ (c = 1.5, pyridine).

The hydrochloride had a melting point of 230°C

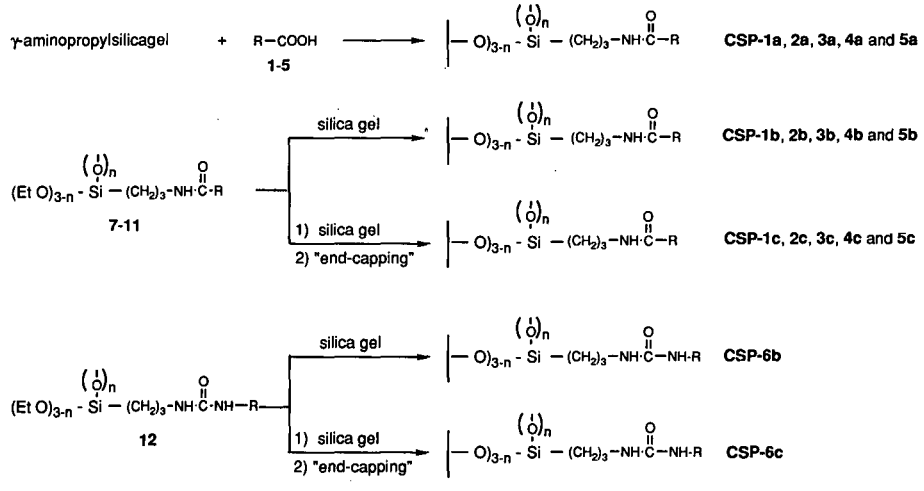

Fig. 3. Synthetic scheme for the preparation of chiral stationary phases.

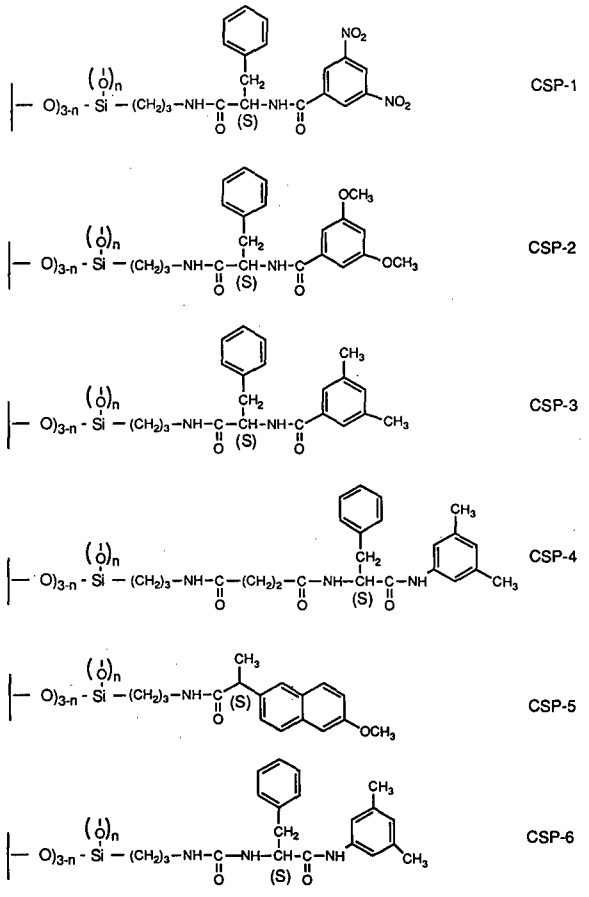

Fig. 4. Structures of chiral stationary phases.

(ethanol absolute). $[\alpha]_D^{23} = +113.5°$ (c = 1.6, ethanol 96°). Analysis: calculated for $C_{17}H_{21}ClN_2O$, C 66.98, H 6.94, Cl 11.68, N 9.19%; found, C 66.89, H 6.86, Cl 11.74, N 9.14%.

N-Acyl-3-aminopropyltriethoxysilane (**7**, **8**, **9**, **10** and **11**) (Fig. 2) was prepared as follows. To a solution of 6 mmol of the appropriate chiral acidic compound (**1–5**) in 18 ml of pyridine, 1.7 ml (7.2 mmol) of 3-aminopropyltriethoxysilane in 12 ml of pyridine were added. The mixture was stirred under reflux for 1.5 h. The solvent and the excess of 3-aminopropyltriethoxysilane were removed under reduced pressure (0.1 mmHg) and the residue was used in the following step without further purification.

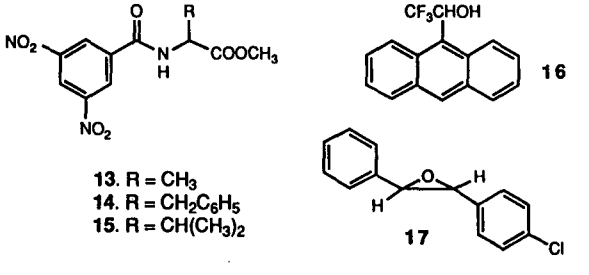

Fig. 5. Structures of test compounds.

When silanes were prepared by heating at reflux temperature a variable loss of ethoxy groups was observed. The extent of this loss depended on the silane and on the time of heating. Silane **12** was the most stable in the series prepared here and silane **8** was the least stable. However, more stable phases can be obtained when these compounds are prepared at high temperatures. These can be explained if a partial polymerization takes place in this step. It was therefore decided to prepare these compounds by heating under the same experimental conditions. (In spite of the difference of stability in silanes, the amount of bonded chiral moiety per gram of stationary phase is almost the same in all comparable stationary phases CSP-1b to 5b.)

*N-[N-(3,5-Dinitrobenzoyl)-(S)-phenylalanyl]-(3-triethoxysilyl)propylamide (**7**).* ^{1}H NMR (200 MHz): δ (C^2HCl_3) 0.64 (t, 2H, CH_2Si), 1.17 (t, 9H, CH_3), 1.77 (m, 2H, $CH_2CH_2CH_2$), 2.87 (t, 2H, CH_2N), 3.21 (m, 2H, CH_2Ar), 3.77 (q, 6H, CH_2O), 4.58 (m, 1H, CH), 6.68 (bb, 1H, NH), 7.13 (m, 5H, C_6H_5), 8.21 (bb, 1H, NH), 8.85 (d, 2H, C^2H and C^6H), 8.98 (d, 1H, C^4H). ^{13}C NMR (50.3 MHz): δ (C^2HCl_3) 7.5 (CH_2Si), 18.2 (CH_3), 21.8 (CH_2), 37.6 (CH_2Ar), 42.0 (CH_2N), 56.8 (CH), 58.6 (CH_2O), 120.7 (C^4H), 126.6 ($C^{4'}H$), 127.4, 128.3 and 129.1 ($C^{2,6}H$, $C^{2',6'}H$ and $C^{3',5'}H$), 137.7 and 138.8 (C^1 and $C^{1'}$), 148.3 ($C^{3,5}$), 162.4 (ArCONH), 176.5 (CONH).

*N-[N-(3,5-Dimethoxybenzoyl)-(S)-phenylalanyl]-(3-triethoxysilyl)propylamide (**8**).* ^{1}H NMR (200 MHz): δ (pyridine-d_5) 0.93 (m, 2H, CH_2Si), 1.24 (t, 9H, CH_3), 1.93 (m, 2H, CH_2), 2.22 (m, 2H, CH_2N), 3.32 (m, 2H, CH_2Ar), 3.72 (s, 6H, CH_3O), 3.89 (q, 6H, CH_2O), 5.35 (m, 1H, CH), 5.61 (bb, 1H, NH), 6.74 (d, 1H, C^4H), 7.16–7.71 (m, 7H, C_6H_5, C^2H and C^6H), 8.32 (bb, 1H, NH). ^{13}C NMR (50.3 MHz): δ (pyridine-d_5) 10.6 (CH_2Si), 19.2 (CH_3CH_2O), 23.7 (CH_2), 38.8 (CH_2Ar), 42.7 (CH_2N), 55.3 (CH_3O), 57.3 (CH_2O), 58.5 (CH), 104.1 (C^4H), 106.2 ($C^{2,6}H$), 126.7 ($C^{4'}H$), 128.7 and

129.9 ($C^{2',6'}H$ and $C^{3',5'}H$), 137.2 and 138.1 (C^1 and $C^{1'}$), 161.2 ($C^{3,5}$), 167.0 (ArCONH), 172.4 (CONH).

*N-[N-(3,5-Dimethylbenzoyl)-(S)-phenylalanyl]-(3-triethoxysilyl)propylamide (**9**).* ^1H NMR (200 MHz): δ (C^2HCl_3) 0.54 (m, 2H, CH_2Si), 1.16 (t, 9H, CH_3), 1.64 (m, 2H, $CH_2CH_2CH_2$), 2.18 (s, 6H, CH_3Ar), 2.67 (m, 2H, CH_2N), 3.21 (m, 2H, CH_2Ar), 3.73 (q, 6H, CH_2O), 4.53 (m, 1H, CH), 6.98 (bb, 1H, NH), 7.11 (m, 10H, aromatics and NH). ^{13}C NMR (50.3 MHz): δ (C^2HCl_3) 7.4 (CH_2Si), 18.2 (CH_3), 20.9 (CH_3Ar), 23.1 (CH_2), 37.6 (CH_2Ar), 42.6 (CH_2N), 56.5 (CH), 58.2 (CH_2O), 124.6 ($C^{2,6}H$), 126.1 ($C^{4'}H$), 127.9 and 129.4 ($C^{2',6'}H$ and $C^{3',5'}H$), 132.7 (C^4H), 137.8 ($C^{3,5}$), 134.3 and 138.2 (C^1 and $C^{1'}$), 167.1 (ArCONH), 176.7 (CONH).

*(S)-N-[1-(3,5-Dimethylphenylaminocarbonyl)-2-phenylethyl]-N'-(3-triethoxysilylpropyl)succinamide (**10**).* ^1H NMR (200 MHz): δ (pyridine-d_5) 0.49 (m, 2H, CH_2Si), 0.91 (t, 9H, CH_3), 1.51 (m, 2H, $CH_2CH_2CH_2$), 1.79 (s, 6H, CH_3Ar), 2.51 (m, 4H, CH_2CO), 2.92 (m, 2H, CH_2N), 3.20 (m, 2H, CH_2Ar), 3.48 (t, 6H, CH_2O), 5.02 (m, 1H, CH), 6.28 (s, 1H, NHAr), 6.6–7.4 (m, 8H, aromatics), 9.15 (bb, 1H, CONH), 10.31 (bb, 1H, CONH). ^{13}C NMR (50.3 MHz): δ (pyridine-d_5) 7.5 (CH_2Si), 18.5 (CH_3), 20.7 (CH_3Ar), 22.8 (CH_2), 33.0 and 33.9 (CH_2CO), 38.3 (CH_2Ar), 42.2 (CH_2N), 55.6 (CH), 56.6 (CH_2O), 117.9 ($C^{2,6}H$), 125.1 and 126.1 (C^4H and $C^{4'}H$), 128.0 and 129.0 ($C^{2',6'}H$ and $C^{3',5'}H$), 137.6 ($C^{3,5}$), 137.6 and 138.8 (C^1 and $C^{1'}$), 170.7, 173.5 and 178.3 (CONH).

*(S)-2-(6-Methoxy-2-naphthyl)propionyl-3-triethoxysilylpropylamide (**11**).* ^1H NMR (200 MHz): δ (pyridine-d_5) 0.49 (m, 2H, CH_2Si), 0.83 (t, 9H, CH_3), 1.37 (d, 3H, CH_3), 1.55 (m, 2H, $CH_2CH_2CH_2$), 3.16 (m, 2H, CH_2N), 3.41 (s, 3H, CH_3O), 3.51 (q, 6H, CH_2O), 6.93 (m, 2H, C^3H and C^7H), 7.46 (m, 4H, C^1H, C^4H, C^5H and C^8H), 8.36 (bb, 1H, CONH). ^{13}C NMR (50.3 MHz): δ (pyridine-d_5) 9.0 (CH_2Si), 18.2 (CH_3CH_2O), 19.3 (CH_3), 23.5 (CH_2), 42.4 (CH_2N), 46.6 (CH), 54.9 (CH_3O), 58.1 (CH_2O), 105.9 and 116.7 (C^7H and C^5H), 126.0, 126.8, 127.5 and 129.2 (C^3H, C^1H, C^4H and C^8H), 129.3, 133.7 and 138.3 (C^{8a}, C^{4a} and C^2), 157.5 (C^6), 174.1 (CO).

(*S*)-N-(3-Triethoxysilyl)propyl-N'-[1-(3,5-dimethylphenyl)aminocarbonyl-2-phenyl]ethylurea (**12**) was prepared as follows. To a solution of 6 mmol (1.6 g)

TABLE I

ELEMENTAL ANALYSES OF CHIRAL STATIONARY PHASES

Chiral stationary phase	Elemental analysis (%)			Ratio of carbon atoms per nitrogen atom		Bonded chiral moieties per gram of stationary phase (mmol)		α_{exp} (μmol/m^2) from %C[a]
	C	H	N	Analytical	Theoretical	From %C	From %N	
CSP-1b	8.35	1.40	2.22	4.39	4.75	0.36	0.39	1.20
CSP-1c	10.36	1.36	2.11	5.73	–	–	0.38	–
CSP-2b	9.74	1.44	1.22	9.31	10.50	0.39	0.44	1.30
CSP-2c	10.79	1.49	1.20	10.43	–	–	0.43	–
CSP-3b	9.74	1.49	1.30	8.74	10.50	0.39	0.46	1.28
CSP-3c	11.12	1.76	1.27	10.22	–	–	0.45	–
CSP-4b	10.93	1.68	1.80	7.08	8.00	0.38	0.43	1.29
CSP-4c	12.27	1.94	1.72	8.32	–	–	0.41	–
CSP-5b	7.32	1.17	0.62	13.77	17.00	0.36	0.44	1.14
CSP-5c	9.48	1.55	0.65	17.20	–	–	0.46	–
CSP-6b	4.70	1.07	0.83	6.45	7.00	0.19	0.20	0.58
CSP-6c	7.15	1.52	0.89	9.37	–	–	0.21	–

Surface concentration of surface-bonded chiral entities, $\alpha_{exp} = \frac{w}{M}\left(\frac{10^6}{S_{BET}(1-w)}\right)$, where w = weight of functional group (grams per gram of adsorbent), M = molar weight of the bonded functional group (g/mol) and S_{BET} = specific surface area of the starting support (m^2/g) [18].

of the amine **6** in 18 ml of pyridine, 7.2 mmol of 3-isocyanatopropyltriethoxysilane in 8 ml of pyridine were added. The mixture was stirred under reflux for 1.5 h. The solvent and the excess of isocyanatopropyltriethoxysilane were removed under reduced pressure (0.1 mmHg) and the residue was used in the next step without further purification. ^{1}H NMR (200 MHz): δ (pyridine-d_5) 0.72 (m, 2H, CH_2Si), 1.17 (t, 9H, CH_3), 1.78 (m, 2H, $CH_2CH_2CH_2$), 2.13 (s, 6H, CH_3), 3.30 (m, 2H, CH_2Ar), 3.41 (m, 2H, CH_2N), 3.81 (q, 6H, CH_2O), 5.18 (s, 2H, NH), 5.37 (m, 1H, CH), 6.8–7.6 (m, 8H, aromatics). ^{13}C NMR (50.3 MHz): δ (pyridine-d_5) 8.1 (CH_2Si), 16.5 (CH_3CH_2O), 21.3 (CH_3), 24.4 (CH_2), 39.7 (CH_2Ar), 43.2 (CH_2N), 56.6 (CH), 58.4 (CH_2O), 118.4 ($C^{2,6}H$), 125.6 and 126.7 (C^4H and $C^{4'}H$), 128.6 and 129.9 ($C^{2',6'}H$ and $C^{3',5'}H$), 138.3 ($C^{3,5}$), 138.5 and 139.5 (C^1 and $C^{1'}$), 159.2 (NHCONH), 172.2 (CONH).

Chiral stationary phases

Chiral stationary phases CSP-1a, -2a, -3a, -4a and -5a were obtained from the appropriate chiral acidic compound (**1–5**) as described previously [12].

Chiral stationary phases CSP-1b, -2b, -3b, -4b, -5b and -6b were prepared as follows. A 6-g mass of spherical silica (5 μm, 100 Å, Nucleosil 100-5; Macherey–Nagel) was slurried with toluene and then the water was removed azeotropically using a Dean-Stark trap. After the complete removal of water, toluene was removed by distillation and a solution of 6 mmol of the appropriate chiral silane (**7–12**) freshly prepared in 50 ml of pyridine was added. The mixture was stirred under reflux for 1.5 h. The resulting bonded silica was collected by filtration and washed exhaustively with pyridine, ethanol, water, ethanol, acetone and diethyl ether, and dried *in vacuo* at room temperature.

Chiral stationary phases CSP-1c, -2c, -3c, -4c, -5c and -6c were obtained by the procedure just described but 3 ml of hexamethyldisilazane were added after the refluxing period and the mixture was allowed to react for an additional hour at reflux temperature. The stationary phases thus obtained were washed as described.

The elemental analyses and the surface concentration of surface-bonded chiral entities (μmol/m^2), according to Unger *et al.* [18], of the new stationary phases are given in Table I.

RESULTS AND DISCUSSION

Chromatographic results are shown in Table II. Results relating to stationary phases obtained from γ-aminopropylsilica gel (CSP-Xa) are from Oliveros *et al.* [12].

Comparison of performance of stationary phases with the same chiral selector obtained either by condensation of a chiral silane on the silica gel (CSP-Xb) or by condensation of the chiral entity on γ-aminopropylsilica gel (CSP-Xa)

In many instances stationary phases obtained by the action of chiral silanes on the silica gel (CSP-Xb) have slightly lower selectivity factors than those of stationary phases obtained by condensation of chiral entities on γ-aminopropylsilica gel (CSP-Xa). The CSP-Xb gels show retention times longer than CSP-Xa in most instances. Although there are no free aminopropyl groups in this kind of stationary phase (these are always present in stationary phases obtained from γ-aminopropylsilica gel), the presence of free silanol groups is possible. Silanol groups may be left over from the silica gel or come from the hydrolysis of unreacted ethoxysilyl groups on the silane. The remaining silanol groups on the stationary phases are considered to be strong adsorption sites [19]. This could be the reason for the increased retention of compounds by stationary phases.

Comparing the elemental analyses of CSP-Xa [12] and CSP-Xb (Table I) the calculated values of the amount (mmol) of chiral selector per gram of stationary phase in CSP-Xb are generally 20% lower than those in CSP-Xa (calculated from the percentage carbon). In the last instance, the presence of free aminopropyl groups has not been considered, but the presence of such groups cannot explain the difference in analytical values. In any case, and although the amount of chiral selector per gram of stationary phase would be the same, the lack of aminopropyl groups on CSP-Xb makes them much more polar than CSP-Xa and increases the retention of test compounds. This inconvenience would be overcome by adding an end-capping step in the preparation of stationary phases.

Comments on the end-capping treatment of silicas obtained from chiral silanes

Taking into account these results and the aim to

TABLE II

CAPACITY FCATORS k' AND SELECTIVITY FACTORS α IN COLUMNS TESTED

Chiral stationary phase	13			14			15			16			17		
	k'_1	k'_2	α	k'_1	k'_2	α	k'_1	k'_2	α	k'_1	k'_2	α	k'_1	k'_2	α
CSP-1a	1.84 (*R*)[a]	2.20	1.19	1.27 (*R*)	1.54	1.21	1.03 (*R*)	1.26	1.22	2.18 (*S*)	2.59	1.19	0.52	0.83	1.60
CSP-1b	2.14 (*R*)	2.62	1.22	1.05 (*R*)	1.26	1.19	0.89 (*R*)	1.05	1.18	3.92 (*S*)	4.66	1.19	0.39	0.60	1.55
CSP-1c	1.32 (*R*)	2.18	1.65	0.90 (*R*)	1.50	1.67	0.84 (*R*)	1.40	1.66	2.94 (*S*)	5.27	1.79	0.40	0.56	1.41
CSP-2a	1.66 (*R*)	3.80	2.29	0.75 (*R*)	1.66	2.21	0.56 (*R*)	1.12	2.00	2.06	2.06	1.00	0.04	0.15	3.33
CSP-2b	3.13 (*R*)	5.34	1.71	4.20 (*R*)	6.69	1.59	1.29 (*R*)	2.20	1.71	2.18	2.18	1.00	0.20	0.38	1.93
CSP-2c	1.38 (*R*)	3.33	2.41	0.68 (*R*)	1.91	2.80	0.61 (*R*)	1.42	2.35	1.86	1.86	1.00	0.17	0.17	1.00
CSP-3a	2.02 (*R*)	3.29	1.63	0.90 (*R*)	1.71	1.90	0.62 (*R*)	1.12	1.81	2.91	2.91	1.00	0.14	0.21	1.50
CSP-3b	3.31 (*R*)	5.15	1.56	1.12 (*R*)	2.35	2.11	0.92 (*R*)	1.71	1.84	2.29	2.29	1.00	0.14	0.24	1.70
CSP-3c	0.79 (*R*)	2.12	2.69	0.44 (*R*)	1.23	2.79	0.38 (*R*)	0.92	2.44	1.98	1.98	1.00	0.10	0.10	1.00
CSP-4a	1.90 (*R*)	4.40	2.32	0.91 (*R*)	1.91	2.10	0.65 (*R*)	1.61	2.47	1.50	1.50	1.00	0.14	0.24	1.70
CSP-4b	3.48 (*R*)	6.86	1.97	1.61 (*R*)	3.10	1.93	1.26 (*R*)	2.55	2.02	2.46	2.46	1.00	0.15	0.32	2.09
CSP-4c	1.82 (*R*)	4.45	2.44	1.13 (*R*)	2.40	2.12	1.00 (*R*)	2.14	2.14	2.21	2.21	1.00	0.12	0.18	1.56
CSP-5a	5.53 (*S*)	7.40	1.34	2.37 (*S*)	3.57	1.51	1.37 (*S*)	2.07	1.51	2.10	2.17	1.03	0.22	0.33	1.50
CSP-5b	9.96 (*S*)	11.34	1.14	2.86 (*S*)	3.42	1.19	2.54 (*S*)	2.97	1.17	2.49	2.49	1.00	0.24	0.50	2.06
CSP-5c	3.00 (*S*)	5.29	1.76	1.29 (*S*)	2.43	1.89	1.00 (*S*)	1.84	1.84	1.51	1.58	1.05	0.12	0.12	1.00
CSP-6b	5.35 (*R*)	7.72	1.44	2.03 (*R*)	3.78	1.86	1.75 (*R*)	2.91	1.67	2.21	2.21	1.00	0.18	0.47	2.57
CSP-6c	0.97 (*R*)	3.35	3.45	0.47 (*R*)	1.53	3.24	0.37 (*R*)	1.13	3.04	1.05	1.05	1.00	0.08	0.08	1.00
Mobile phase chloroform–0.5% methanol/heptane	70:30			70:30			70:30			70:30			25:75		

[a] Absolute configuration of first-eluted enantiomer.

prepare stationary phases able to establish the weakest achiral interactions with solutes, the silanol groups were deactivated. This is a common treatment consisting most often in bonding trimethylsilyl radicals onto the silanol groups. This can be achieved by several reagents [20–22]. Trimethylchlorosilane (TMCS) and hexamethyldisilazane (HMDS) are often used as deactivating reagents. Buszewski [23] has suggested that HMDS liberates ammonia during the end-capping treatment which leads to a partial loss of the bonded silane. The end-capping treatment was therefore carried out first with TMCS, one of the most reactive reagents towards residual silanol groups.

The elemental analyses of the resulting stationary phases showed that this reagent causes the loss of the chiral entity. This degradation has been studied with CSP-1b and CSP-3b, whose chiral selectors are 3,5-dinitrobenzoylphenylalanine and 3,5-dimethylbenzoylphenylalanine, respectively. Elemental analyses after the treatment with TMCS are: C 4.86, H 1.54 and N 1.11% for CSP-1b; and C 4.60, H 1.55 and N 1.10% for CSP-3b. These values are different from those of the same phases before the treatment (Table I), but similar to each other and also similar to those of the γ-aminopropylsilica gel obtained by the action of 3-aminopropyltriethoxysilane on the same silica gel (C 3.10, H 1.05, N 0.90% [13]). This observation suggests that a breakage between the chiral entity and the spacer takes place on the amide group between them.

Methoxytrimethylsilane has also been used as a silylating agent. In this instance degradation of the bonded stationary phases has also been observed, but to a lesser degree than that observed using TMCS.

Finally, the end-capping treatment was carried out using HMDS. As can be seen in Table I, the amount of chiral compound per gram of stationary phase is nearly the same before and after the end-capping. Therefore, there is no noticeable degradation of the stationary phases.

Comparison of stationary phases with CSP-Xc or without CSP-Xb end-capped silanol groups

The consequences of the end-capping treatment on the chromatographic behaviour of stationary phases obtained by condensation of chiral silanes on silica gel are very important.

First, selectivity factors are clearly larger in end-capped stationary phases. Only compound **17**, resolved by CSP-2b, -3b, -5b and -6b, with selectivity factors from 1.70 to 2.57, is not resolved by end-capped chiral stationary phases with the same chiral selector. At present, we cannot explain this loss of selectivity in chiral stationary phases by the end-capping treatment.

Secondly, in general, retention times shown by these silicas are shorter than those shown by silicas which have not been end-capped. CSP-6b and CSP-6c are good examples: the reduction of the retention time of the first eluted enantiomer and the increase in selectivity factors in CSP-6c relating to CSP-6b is remarkable.

Moreover, if the retention time of the last eluted enantiomer is sometimes longer in CSP-Xc than in CSP-Xb, then the selectivity factor is more strongly enhanced in CSP-Xc than in CSP-Xb. Figs. 6 and 7 show these situations. Chromatograms of the resolution of compounds **15** and **16** on the three kinds of stationary phases (CSP-Xa, CSP-Xb and CSP-Xc) can be compared.

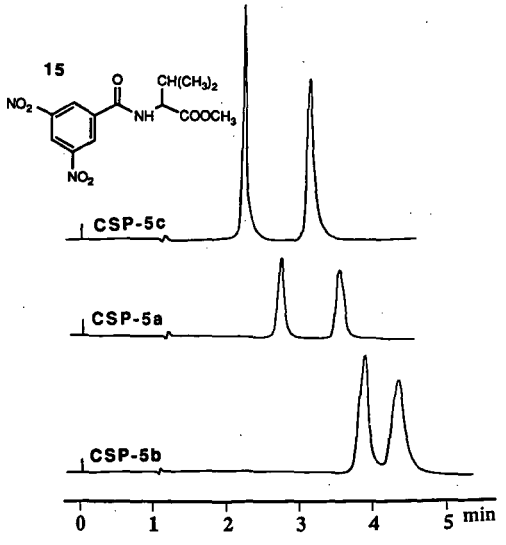

Fig. 6. Chromatograms of resolution of compound **15** on CSP-5a, CSP-5b and CSP-5c. Experimental conditions: column 100 × 4.6 mm I.D.; eluent: chloroform–0.5% methanol/heptane (70:30, v/v); flow-rate 1 ml/min.

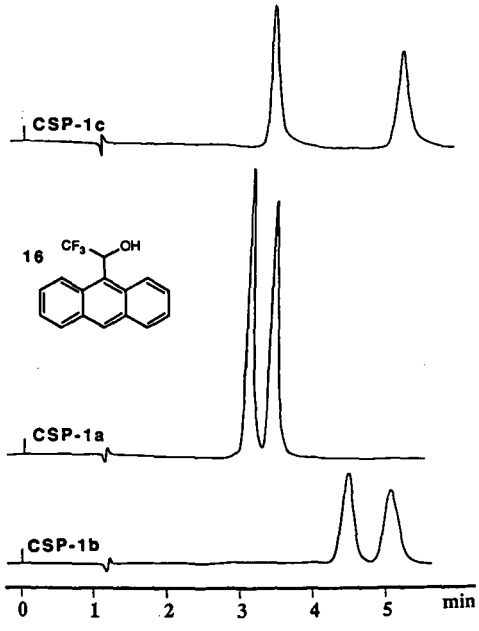

Fig. 7. Chromatograms of resolution of compound **16** on CSP-1a, CSP-1b and CSP-1c. Experimental conditions: column 100 × 4.6 mm I.D.; eluent: chloroform–0.5% methanol/heptane (80:20, v/v); flow-rate 1 ml/min.

Pirkle and Readnour [24] have reported the influence of end-capping treatment with three trimethylsilyl donors on the enantioselectivity of chiral stationary phases obtained by condensation of a chiral triethoxysilane with π-donor character on silica gel. The differences observed by these workers between end-capped silica and silica which has not been end-capped are less remarkable than those observed in this study. In particular, the retention time of the first-eluted enantiomer is almost insensitive to the end-capping treatment when hexamethyldisilazane is used as the silylating reagent.

Certainly, the method of end-capping treatment is not the same in both studies (end-capping before or after packing the column) but, in our opinion, the differences in results cannot be explained in these terms. The cause of these discrepancies may be the diverse origins of the silica gel used in the two studies. Dobashi and Hara [11] have already observed the influence of silanol groups on the reten-

tion time and selectivity factors in a different way, but with stationary phases obtained from the silica gel Nucleosil 100-5 (100 Å, 5 μm). To verify this hypothesis stationary phases analogous to CSP-1b (non-end-capped) and CSP-1c (end-capped) were prepared from Spherisorb S5W (80 Å, 5 μm) (Phase Separations) silica, possibly the same quality of Spherisorb silica gel used by Pirkle *et al.* [25]. The results confirm that the influence of end-capping treatment on the chromatographic behaviour of chiral stationary phases depends on the origin of the silica gel used. Phases obtained from Spherisorb show only minor differences between end-capped and non-end-capped silicas. Thus values $k'_1 = 4.64$ and $\alpha = 1.32$ and $k'_1 = 4.64$ and $\alpha = 1.34$ are obtained for **16** with chiral stationary phases analogous to CSP-1b and CSP-1c, respectively, prepared from Spherisorb S5W.

Stationary phases CSP-1b and CSP-1c obtained from Nucleosil 100-5 have nearly 1.20 μmol of chiral entity per m^2 (Table I). Analogous stationary phases obtained by condensation of the same chiral silane on silica gel Spherisorb S5W have a lower specific surface coverage (1.01 μmol/m^2) of the same chiral entity (C 4.65, H 0.51, N 1.10% before end-capping treatment and C 5.10, H 0.60, N 1.06% after treatment). Differences in the physical properties of silica, *i.e.*, the amount of residual surface silanols, from manufacturer to manufacturer [26] may cause this reduction. However, the lesser influence of end-capping treatment on stationary phases obtained from Spherisorb S5W cannot be explained by the lower amount of chiral entity grafting on this silica. In fact, CSP-6b and -6c have 0.60 μmol of chiral entity per m^2 of stationary phase, but there are large differences in chromatographic behaviour between them.

CONCLUSIONS

The method described here to prepare and condense chiral silanes on silica gel is easy to carry out and leads to chiral stationary phases with a good performance. The decrease in achiral interactions in chiral stationary phases often improves, sometimes significantly, the resolution of racemic compounds. This procedure, condensation of a chiral silane on the silica gel followed by an end-capping treatment, is advantageous compared with the same chiral entity on γ-aminopropylsilica gel.

The influence of end-capping on the selectivity of a chiral stationary phase depends on the origin of the silica gel used to prepare it.

REFERENCES

1 W. H. Pirkle, D. W. House and J. M. Finn, *J. Chromatogr.*, 192 (1980) 143.
2 F. Gasparrini, D. Misiti, C. Villani, F. La Torre and M. Sinibaldi, *J. Chromatogr.*, 457 (1988) 235.
3 R. Däppen, V. R. Meyer and H. Arm, *J. Chromatogr.*, 361 (1986) 93.
4 A. Tambuté, A. Begos, M. Lienne, P. Macaudière, M. Caude and R. Rosset, *New J. Chem.*, 13 (1989) 625.
5 A. Foucault, M. Caude and L. Oliveros, *J. Chromatogr.*, 185 (1979) 345.
6 M. H. Hyun and W. H. Pirkle, *J. Chromatogr.*, 393 (1987) 357.
7 H. Brendt and G. Krüger, *J. Chromatogr.*, 348 (1985) 275.
8 R. Kuropka, B. Müller, H. Höcker and H. Berndt, *J. Chromatogr.*, 481 (1989) 380.
9 A. Dobashi, Y. Dobashi, K. Kinoshita and S. Hara, *Anal. Chem.*, 60 (1988) 1985.
10 F.-J. Ruffing, J. A. Lux, W. Roeder and G. Schomburg, *Chromatographia*, 26 (1988) 19.
11 Y. Dobashi and S. Hara, *J. Org. Chem.*, 52 (1987) 2490.
12 L. Oliveros, C. Minguillón, B. Desmazières and P.-L. Desbène, *J. Chromatogr.*, 589 (1992) 53.
13 L. Oliveros, C. Minguillón, B. Desmazières and P.-L. Desbène, *J. Chromatogr.*, 543 (1991) 277.
14 L. Oliveros and M. Cazau, *J. Chromatogr.*, 409 (1987) 183.
15 T. D. Doyle, in W. J. Lough (Editor), *Chiral Liquid Chromatography*, Blackie, London, 1989, Ch. 6, p. 102.
16 T. D. Doyle, C. A. Brunner and E. Smith, *U.S. Pat.*, 4919803; *C.A.*, 113 (1990) 29390q.
17 B. Coq, C. Gonnet and J. L. Rocca, *J. Chromatogr.*, 106 (1975) 249.
18 K. K. Unger, N. Becker and P. Roumeliotis *J. Chromatogr.*, 125 (1976) 115.
19 M. L. Hair and W. Hertl, *J. Phys. Chem.*, 73 (1969) 4269.
20 L. C. Sander and S. A. Wise, *CRC Crit. Rev. Anal. Chem.*, 18 (1987) 299.
21 K. D. McMurtrey, *J. Liq. Chromatogr.*, 11 (1988) 3375.
22 B. Porsch, *J. Liq. Chromatogr.*, 14 (1991) 71.
23 B. Buszewski, *Chromatographia*, 28 (1989) 574.
24 W. H. Pirkle and R. S. Readnour, *Chromatographia*, 31 (1991) 129.
25 W. H. Pirkle, T. H. Pochapsky, G. S. Mahler, D. E. Corey, D. S. Reno and D. M. Alessi, *J. Org. Chem.*, 51 (1986) 4991.
26 J. Nawrocki, *Chromatographia*, 31 (1991) 193.

Journal of Chromatography, 606 (1992) 19–31
Elsevier Science Publishers B.V., Amsterdam

CHROM. 24 274

Studies of a novel membrane for affinity separations

I. Functionalisation and protein coupling

C. H. Bamford and K. G. Al-Lamee

Department of Clinical Engineering, University of Liverpool, Liverpool L69 3BX (UK)

M. D. Purbrick and T. J. Wear

Kodak Ltd., Headstone Drive, Harrow, Middlesex HA1 4TY (UK)

(First received December 23rd, 1991; revised manuscript received April 7th, 1992)

ABSTRACT

A study is presented of the potentialities of an electrostatically-spun poly(ether–urethane–urea) as an affinity separation membrane. The spinning process produces a fibrous network with a high internal surface area. A variety of chemical methods has been used for functionalising and activating the membrane.

Assessments of the capacities of the activated membranes for covalent coupling of protein A and human immunoglobulin G have given very encouraging data. Non-specific adsorption of both proteins by the inactivated polymer was negligible.

Geometric considerations suggest that the limiting factor determining protein coupling is the accessible surface area rather than the number of coupling sites.

INTRODUCTION

Membrane-based techniques are playing an increasingly important role in affinity separation and, together with fibre-based systems, seem likely to compete successfully with beads as supports for some purposes. Research in membrane technology in Europe, including aspects related to separation systems, is showing a steady increase. The desirable properties in a membrane designed for affinity separation are well-known and include high macroporosity, large internal and external surface areas, high chemical, biological and mechanical stabilities, a degree of hydrophilicity, low non-specific adsorption of bioactive species and the presence of chemical groups which permit suitable functionalisation. Among membranes which are currently available are those based on "hydrophilic" modified polyvinylidene difluoride (Immobilon AV Affinity Membrane) [1], activated nylon *e.g.* Carboxydyne, Aminodyne, Hydroxydyne (Pall) [2], cellulosic polymers (Genex) [3], and "UltraBind" —a mixture of a polysulphone and polyacrolein (Gelman Sciences) [4].

During recent years we have become familiar with the properties of some electrostatically-spun polymers. The poly(ether–urethane–urea) Biomer (**1**) has been studied in these laboratories by Dr. D. Annis [5] in his work on prosthetic vascular grafts, and it occurred to us that the material has most or all of the desirable properties outlined above. Accordingly, we have investigated its application as an affinity membrane and report the results [6] in this paper. Similar membranes may be made from other poly(ether–urethane)s, *e.g.* Pellethane, Tecoflex, Estane.

Correspondence to: Dr. C. H. Bamford, Department of Clinical Engineering, University of Liverpool, Liverpool L69 3BX, UK.

0021-9673/92/$05.00

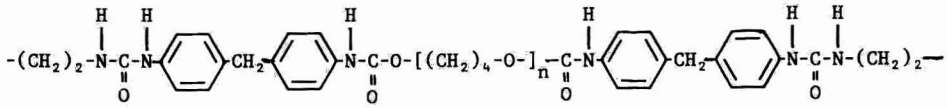

(1) Biomer

EXPERIMENTAL

Materials

The poly(ether–urethane–urea) Biomer was obtained from Ethicon (Somerville, NY, USA) as a 30% solution in N,N-dimethylacetamide (DMAc). The following materials were purchased from Aldrich (Gillingham, UK): poly(ethylene glycol) (PEG), molecular mass 4000, 2-chloroethyl isocyanate and the diisocyanates, Bolton–Hunter reagent, 1,1′-carbonyl diimidazole (CDI), 2-fluoro-1-methylpyridinium toluene-4-sulphonate (FMP), 1-hexanol, 6-aminocaproic acid and rhenium carbonyl. The last was purified by sublimation in vacuum before use. We are indebted to Kodak (Harrow, UK), for a gift of the N-succinimido ester of N-methacrylamido-6-caproate (7); N-acryloxysuccinimide was purchased from Kodak.

2-Isocyanatoethyl methacrylate was bought from Monomer-Polymer and Dajac Labs. (Trevose, PA, USA) and D-glucamine and ethanolamine were obtained from Fluka (Glossop, UK). Protein A (soluble, purified by chromatography) and human immunoglobulin G (IgG) were supplied by Sigma (Poole, UK) and the ^{125}I-labelled proteins by Amersham International (Protein A) (Aylesbury, UK) and NEN Research (human IgG) (DuPont, Stevenage, UK).

Acetonitrile and diethyl ether, dried by refluxing over calcium hydride were distilled before use.

Electrostatic spinning

In this process the spinning solution (polymer solution) is introduced through an appropriate spinneret (*e.g.*, a hypodermic needle) into an electric field to produce filaments which are attracted towards a collecting electrode at a different potential. In our experiments the needle was earthed and the collecting electrode was a stainless-steel rotating mandrel with a diameter in the range 5–10 cm at a potential of −10 kV. The spinning liquid was a solution of Biomer (16%, w/w) in a mixture of N,N-dimethylacetamide and methyl ethyl ketone (1.45:1, w/w). Fibres collected on the mandrel formed a tube which was subsequently removed and opened by cutting to produce a mat or membrane of polymer fibre. Further details are to be found in the paper by Annis *et al.* [5].

Fig. 1 is a typical scanning electron micrograph (SEM) of the spun membrane, which is seen to be essentially a network of very thin fibres of diameter approximately 1 μm. These are melded at many points and enclose irregular holes or pores with a typical dimension in the range 5–10 μm. The pore size and, to a certain extent, the filament diameter, are controllable through the spinning conditions; fibre diameters in the range 0.1–25 μm have been claimed in the patent literature [7,8]. As will appear later, fibres of diameter less than 1 μm and pores smaller than 5 μm could have advantages for present purposes. The overall internal surface area of the membrane is large, 1 g of the material as spun having an area of about 4 m^2; not all of this will be accessible to protein molecules.

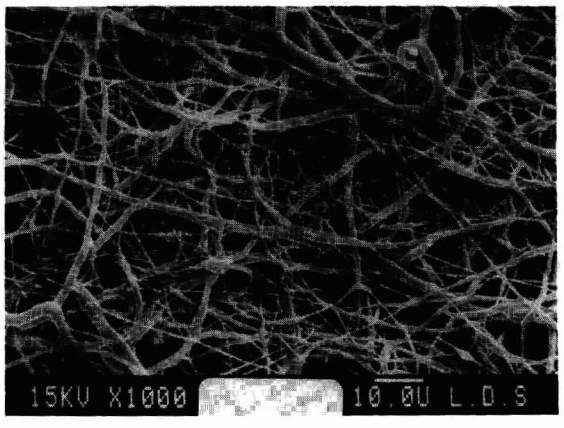

Fig. 1. SEM of electrostatically-spun Biomer membrane.

General procedure

Synthesis of an activated membrane of the type we are considering involves functionalisation of the initial poly(ether–urethane) and activation of the product by attachment of an appropriate active moiety. The general aim is to obtain constructions of the type shown below.

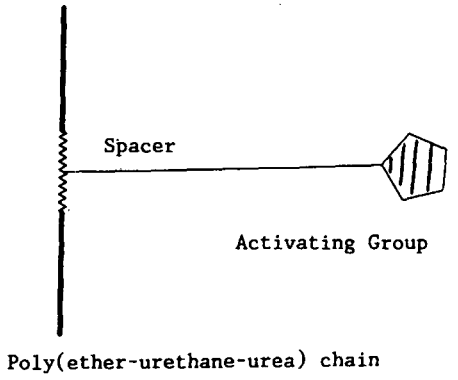

Fig. 2 is a flow-chart for the syntheses of the activated membranes. Functionalisation of Biomer has been carried out both before (a) and after (b) spinning, and satisfactory membranes have been obtained in both cases. Post-spinning activation is preferable and has been employed through-out most of this work; with this technique a larger proportion of the activating groups is accessible and further, the spinning process (best effected at a high relative humidity) can deactivate moisture-sensitive groups.

All processes used for functionalising poly(ether–urethane)s involve isocyanate couplings; subsequent activation may be based on free-radial reactions or direct coupling [9,10]. The following isocyanate derivatives were employed: 2-chloroethyl isocyanate (**2**), 2-isocyanatoethyl methacrylate (**3**), hexamethylene diisocyanate (**4**), 2,4-tolylene diisocyanate (**5**). For activation by free-radial procedures, we used "activated monomers", in which the active group (*e.g.*, succinimidyl) was linked to a polymerisable double bond. These were N-acryloxysuccinimide (**6**) and N-succinimide methylacrylamido-6-caproate (**7**).The activating species used for direct coupling were N-succinimidyl 3-(4-hydroxyphenyl)propionate (Bolton–Hunter reagent) (BH), CDI and FMP. The active moieties so introduced into the polymer react readily with nucleophilic groups (*e.g.*, $-NH_2$, –OH, –SH) in proteins or other biological species so that these become covalently attached to the polymer chains.

Figs. 3–5 set out the reactions employed. Fig. 3 includes the free-radical processes used in activation, leading to the membranes **10**, **11**, **12**; Figs. 4

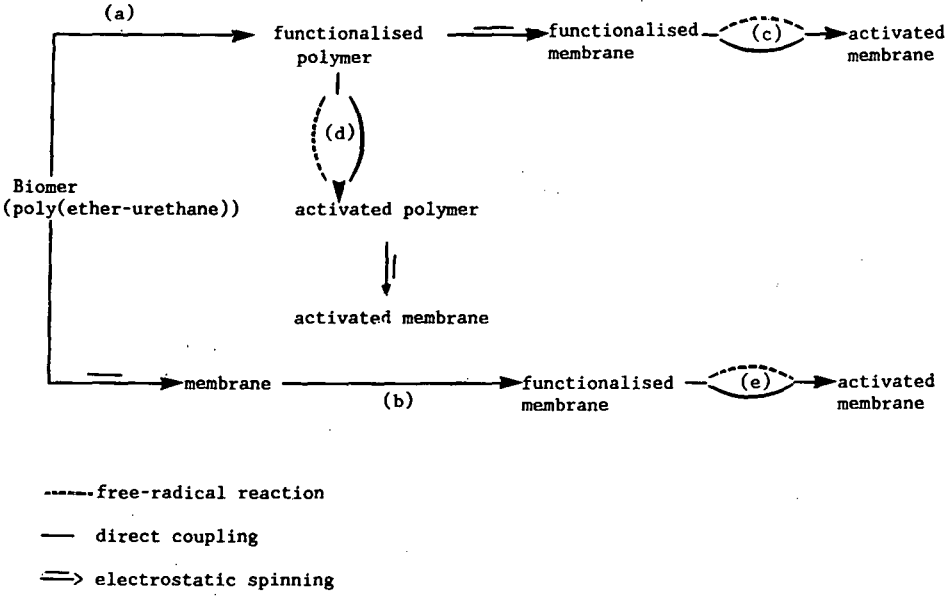

Fig. 2. Flow-chart for preparation of activated membranes.

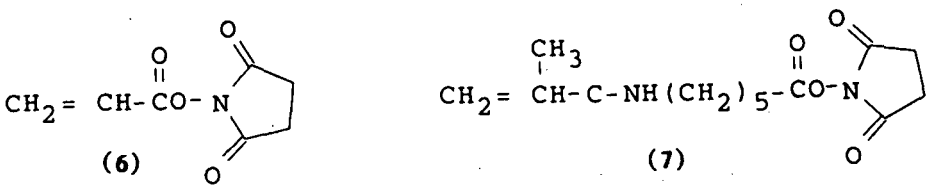

N-acryloxysuccinimide N-succinimide methacrylamido caproate

and 5 refer to activation by direct coupling forming the membranes **14–19** and **21–27**.

Functionalisation

Pre-spinning functionalisation of Biomer [(a) in Fig. 2] was carried out by reaction with **2** (Fig. 3). A 10-g amount of Biomer and 8 g of **2** were dissolved in 100 ml DMAc and allowed to react at 25°C for three days. The resulting adduct (**8**) was precipitated into water, reprecipitated from DMAc and dried in vacuum.

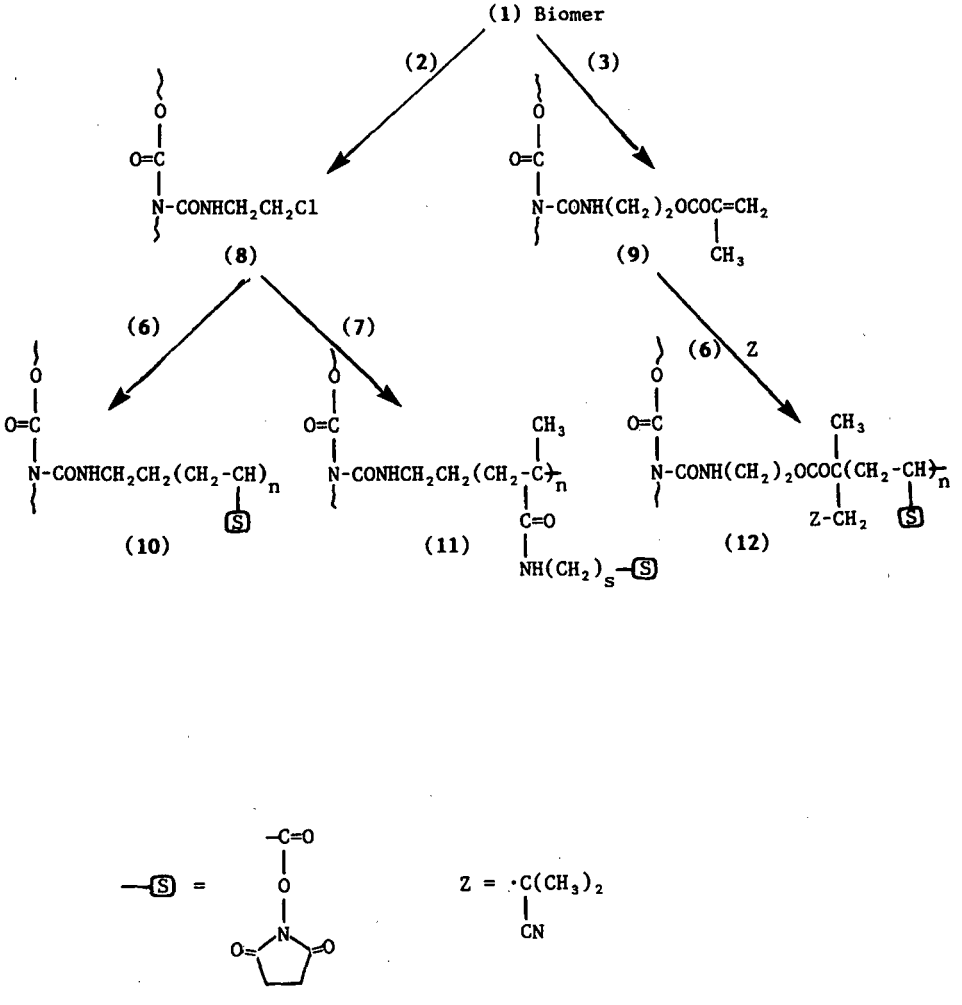

Fig. 3. Activated polymers by free-radical techniques.

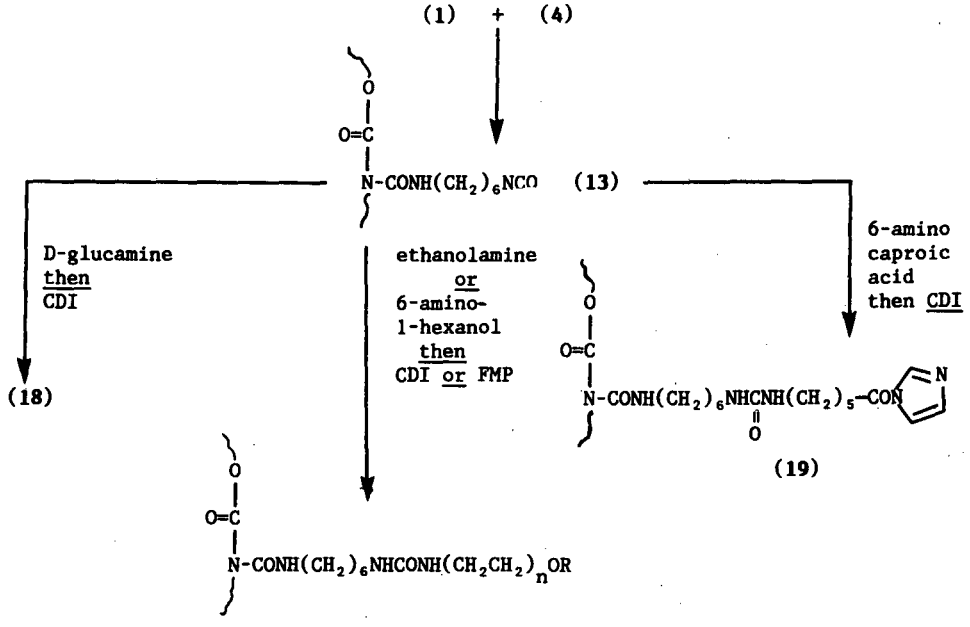

Identification of activated polymers

	Activating Group R	
n	-CON	Tos⁻
1	(14)	
3	(15)	
1		(16)
3		(17)
D-glucamine	(18)	

Fig. 4. Activated polymers by direct coupling.

For post-spinning functionalisation [(b) in Fig. 2] the membranes were allowed to react heterogeneously with isocyanates **2–5** at 25°C to form adducts **8**, **9** (Fig. 3), **13** (Fig. 4), **20** (Fig. 5). Conditions are:

A 4.3-g amount of Biomer membrane was used in each case.
2-Chloroethyl isocyanate: 1 day, hexane solution 8% (w/w), 100 ml.
2-Isocyanatoethyl methacrylate: 5 days, hexane solution 20% (w/w), 100 ml.
Hexamethylene diisocyanate: 4 days, hexane solution 30% (w/w) (excess).
2,4-Toluene diisocyanate: 3 days, bulk (excess).

After reaction the membranes were washed several times with hexane and vacuum-dried.

Activation [(c)–(e) in Fig. 2]

Both free-radical processes and direct coupling were assessed as procedures for attaching active moieties to the polymer.

Free-radical routes. The functionalised polymer **8** (Fig. 3) was used in conjunction with a metal carbonyl to generate "attached" free radicals [11] which propagate through the double bonds in the

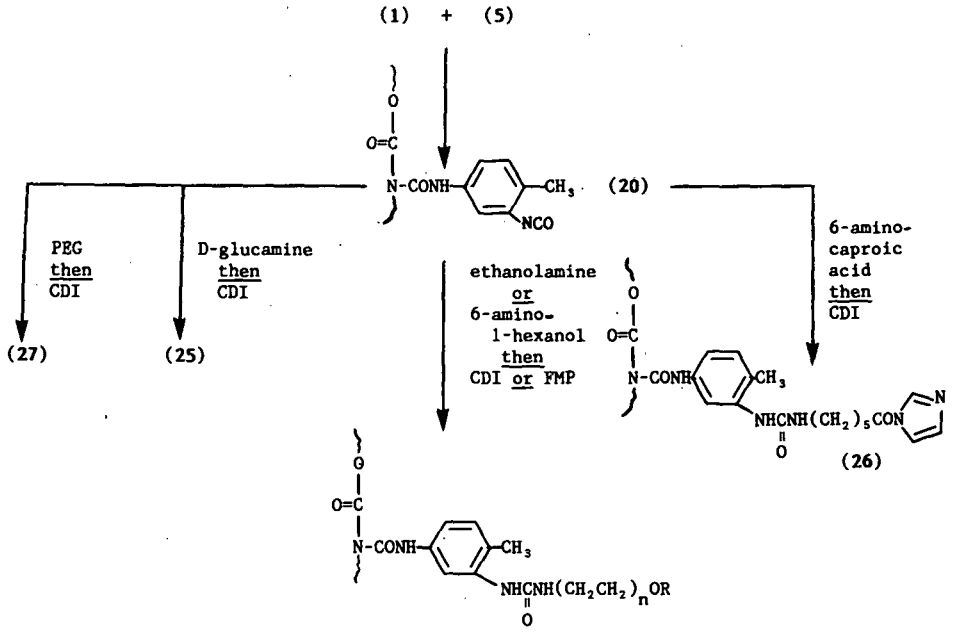

Identification of activated polymers

Activating Group R

n	-CON	Tos⁻
1	(21)	
3	(22)	
1		(23)
3		(24)
D-glucamine	(25)	
PEG	(27)	

Fig. 5. Activated polymers by direct coupling.

active monomers **6** and **7**. Eqn. 1 illustrates the reactions between **8** and **6** in these systems. Manganese and rhenium carbonyls ($Mn_2(CO)_{10}$, $Re_2(CO)_{10}$) are very effective for these reactions at wavelengths of 436 and 365 nm, respectively, while molybdenum carbonyl [$Mo(CO)_6$] may be used as a thermal initiator at 60°C or above [11].

A 14.5-g amount of **8** with 3 g of **6** (or **7**) were dissolved in 160 ml of DMAc: a solution of 0.123 g $Re_2(CO)_{10}$ in 15 ml DMAc was then added and the liquid irradiated with light of wavelength 365 nm

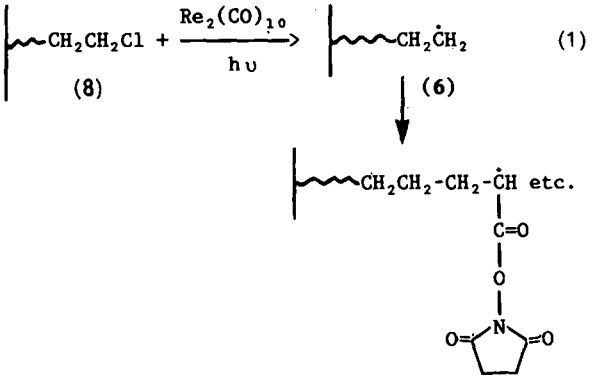

from a 100-W high-pressure mercury arc for 5.5 h.

Polymers for subsequent spinning [(d) in Fig. 2] were precipitated in a mixture of diethyl ether and ethyl acetate (9:1, v/v), filtered off and reprecipitated. The products were **10** and **11** (Fig. 3). If activation had been effected after spinning [(c) or (e) in Fig. 2], the membraness were washed with acetonitrile and dried in vacuum.

In a second type of procedure the macromer **9** (Fig. 3) was copolymerised with active monomer **6** with the aid of a conventional free-radical initiator. A 1.9-g amount of **9** was added to a solution of 0.5 g of **6** and 0.2 g azo-bis-isobutyronitrile in 10 ml acetonitrile. After degassing, the polymerisation was carried out thermally at 60°C for 4 h. The membrane was removed, washed with dry acetonitrile and dried in vacuum. The product was composed of units such as **12** (Fig. 3).

Direct coupling. Figs. 4 and 5 present the reactions by which membranes activated by CDI and FMP were prepared. After functionalisation of the poly(ether–urethane) membrane to give **13** or **20**, the terminal isocyanate residues were converted to hydroxylic forms by reaction with the following series of hydroxyamino compounds or PEG. Reaction conditions are:

In each experiment the weight of isocyanated membrane was 4.2 g.
Ethanolamine: 25°C, 24 h, bulk, 50 ml.
6-Amino-1-hexanol: 25°C, 24 h, 4% (w/v) in dry ether, 80 ml.
PEG, molecular mass *ca.* 4000: 50°C, 72 h, 50% (w/v) in dry acetonitrile, 50 ml.
D-Glucamine: 25°C, 2 h, 8% (w/v) in formamide, 75 ml.

The hydroxylated membranes were washed with dry acetonitrile and dried in vacuum. Activation of the membranes was carried out with CDI in acetonitrile (15%, w/v). The weight of CDI used was 2–3 times that of the polymer. After 48 h at 25°C the membranes were washed extensively with dry acetonitrile and vacuum-dried.

For activation by coupling with FMP, the hydroxylated membranes (4.2 g) were reacted (25°C, 24 h) with FMP in acetonitrile (5%, w/v) in the presence of 1 ml triethylamine, then washed with acetonitrile and dried.

A further series of membranes was prepared by reacting the functionalised polymers **13** and **20** with 6-amino-caproic acid (Figs. 4 and 5). A 5-g amount of the acid dissolved in 50 ml of 0.75 *M* sodium hydroxide was added to 4.2 g of membrane and reacted for 3 h at 25°C. The acidic membranes produced were washed with water, 0.8% HCl and finally water then dried in vacuum. They were activated by reaction with CDI (5 g) in acetonitrile (50 g) for 48 h at 25°C.

The Bolton–Hunter reagent was condensed with the functionalised membranes **13** and **20** to give the activated membranes **28** and **29**, respectively. For this purpose 1.2 g of **13** or **20** were allowed to react with 0.8 g of BH in 40 ml dry acetonitrile for 4 days at 25°C.

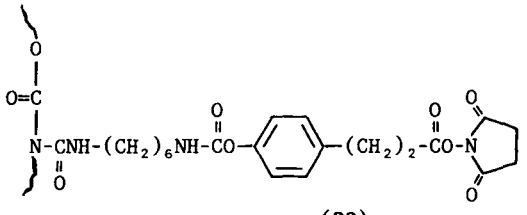

(28)

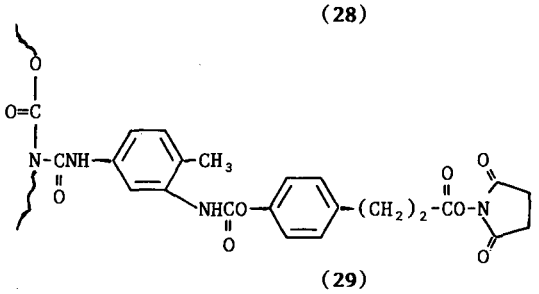

(29)

An aspect of the work (to be discussed later) involved determination of the activating groups in a membrane to establish its influence on the coupling capacity for proteins. This was effected by use of ^{125}I-labelled BH, the coupling experiments being carried out as described above.

Assessments of protein coupling to activated membranes

Discs (diameter 2.54 cm) were cut from sheets of activated membranes (thickness approximately 0.3 mm). For each test one or three such discs were placed in a Millipore Micro-Syringe 25 mm filter holder and a solution of ^{125}I-labelled protein A (1 mg per ml, in 0.1 *M* $NaHCO_3$) was passed through with the aid of a syringe pump at a rate of 1 ml/h. The discs were then washed copiously with 0.1 *M* $NaHCO_3$ followed by deionized water; they were then allowed to stand for 1 h in 2% sodium dodecyl

sulphate solution then washed again with de-ionized water and blotted dry on filter paper.

The protein A contents of the separate discs were determined by counting each in 8 ml of Optiphase scintillant.

All the above procedures were repeated with "unactivated" Biomer (*i.e.*, functionalised but not activated) to determine the non-specific adsorption.

Assessment of the direct coupling of ^{125}I-labelled human IgG to the activated and unactivated polymers was carried out in exactly the same manner as described above.

Assessment of binding of IgG by protein A coupled to activated Biomer membranes

Discs of the activated membranes to which protein A had been coupled were treated with bulk ethanolamine to block unreacted activating residues and washed copiously with deionized water and phosphate-buffered saline (PBS). A 5-ml volume of a solution of ^{125}I-labelled human IgG in 0.15 *M* PBS (2.8 mg per ml) was passed through the discs at a rate of 1 ml/h. The discs were then washed with deionized water and placed in 10 ml of a solution of 0.2% Tween 20 in 0.15 *M* PBS for 1 h to remove non-specifically bound protein. Finally the discs were washed with deionized water, blotted and counted.

RESULTS AND DISCUSSION

Protein A binding

Measurements were made of covalently bound protein A using either one or three discs as described; these are numbered 1, 2 and 3, the order in which they are encountered by the solution. Table I presents total weights of protein A coupled (on all discs); for the purposes of calculation the area is taken as that of one disc.

Table I shows that the non-specific adsorption of protein A by the unactivated membranes is low. As a fraction of the coupling by the corresponding activated membrane it has an average value of 2.0%.

Fig. 6 is an SEM of the membrane of the activated polymer **28**. The fibrous structure resembles that of Fig. 1, indicating that the functionalisation process has not greatly altered the porosity. On the other hand the pore structures of polymers **10** and **12** (Figs. 7 and 8) show considerable changes from those of their precursors **8** and **9** (Fig. 3), respectively. Different techniques were used for activating these polymers. For polymer **28**, which gives the best result of the three (Table I), direct coupling with Bolton–Hunter reagent was employed, while **7** and **9** were synthesised by free-radical reactions through the macroinitiator **8** and macromer **9** (Fig. 3), respectively. The activating group was a succinimido

TABLE I

PROTEIN A COUPLING TO ACTIVATED MEMBRANES

Reference number of activated membrane	Number of discs used	Protein A coupled		Non-specific adsorption of protein A	
		mg/g	μg/cm	mg/g	μg/cm
10	1	1.24, 1.66	27.5	0.037	0.79
12	1	0.61	11.8	0.037	0.79
14	1	6.26	93.2	0.014	0.25
15	3	1.46	88.1	0.020	1.35
16	1	0.66	16.9	0.014	0.25
18	3	2.94	183.2	0.055	3.71
19	3	3.64	221.5	0.022	1.51
21	1	0.63	13.6	0.014	0.25
22	3	1.81	114.2	0.020	1.35
23	1	0.29	6.0	0.014	0.25
25	3	3.04	209.7	0.055	3.71
26	3	4.16	269.3	0.023	1.51
27	3	1.43	85.5	0.008	0.77
28	1	3.17	70.3	0.037	0.79

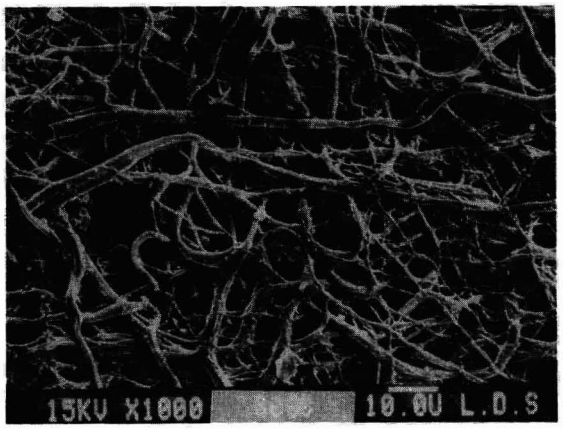

Fig. 6. SEM of membrane **28**, activated with Bolton–Hunter reagent.

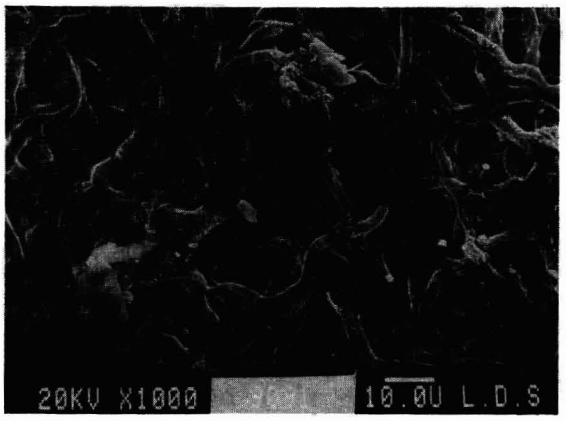

Fig. 8. SEM of membrane **12**, grafted with acryloxysuccinimide by macromer technique.

derivative in each case, and the differences in the capacity for protein coupling are likely to reflect the pore structure. Figs. 7 and 8 show relatively large pores and closely-packed areas; the surface area of the fibres accessible to the proteins is evidently reduced in these structures. Another example of the efficacy of direct coupling is provided by **26** which was activated by CDI (Fig. 5) and has relatively high capacity for protein A. The structure is shown in Fig. 9 and is not very different from those of polymer **29** (Fig. 6) or the original Biomer (Fig. 1). According to these findings direct coupling of the activating group gives more suitable structures than the free-radical methods so later work was focused on the former technique.

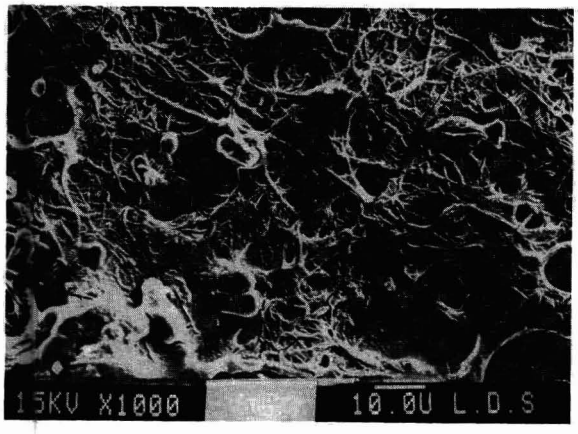

Fig. 7. SEM of membrane **10**, grafted with acryloxy-succinimide by macroinitiator technique.

The choice of activating group is important. It is known that the hydrolysis half-lives at pH 8–9 for N-hydroxysuccinimide ester, imidazole carbamate and 2-fluoro-1-methylpyridinium toluene-4-sulphonate groups attached to a support of cross-linked agarose are of the order: minutes, a few hours and 100 h, respectively. In our experiments (at pH 8) it would seem that for coupling to amino groups (*e.g.* those in protein A) FMP gave relatively low values (polymers **16** and **23**) and CDI high values (polymers **14**, **18**, **19**, **25**, **26**). Although **14** and **18** were both synthesised from **13** the intermediate stages involved the use of ethanolamine and D-glucamine respectively (Fig. 4), while **25** was prepared from **20** with the aid of D-glucamine (Fig. 5). These details may influence the above comparison, which therefore needs further investigation.

The activated membranes **19**, **26** formed from acid membranes (Figs. 4 and 5) are seen from Table I to be very effective. The content of activating groups is probably high in these materials by virtue of the rapid reaction between carboxyl and CDI and the absence of cross-link (carbonate) formation (which is possible with hydroxylic polymers). However, we shall see later that this factor is unlikely to be responsible for the high coupling capacity of the membranes. The combination of properties possessed by the spacers —which are rather hydrophobic and contain about twenty backbone atoms— could be particularly favourable.

Membrane **27**, (prepared from the same precursor **20** as **26**) (Fig. 5) was also activated by CDI and

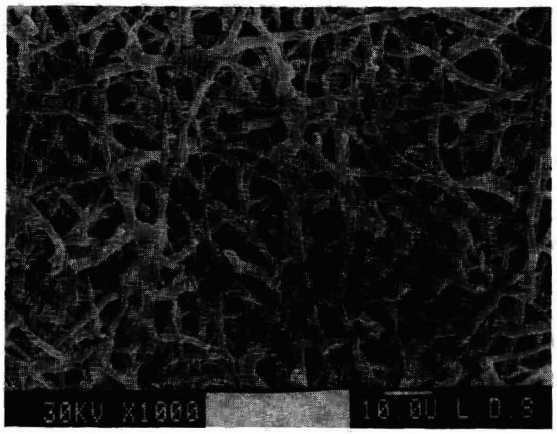

Fig. 9. SEM of acid membrane **26** after direct coupling of CDI.

carried long hydrophilic spacers of PEG having a backbone length of about 270 atoms. These did not confer any marked improvement in capacity (compare Kato and Kito [12] and Phillips *et al.* [13]).

Table II shows the distribution of coupled protein A between the discs.

According to the data in Table II, when three discs are present, the extents of coupling are in the order 1 > 2 > 3. The coupling capacities given in mg/g in Table I for determinations with three discs are therefore underestimates since they are averages based on the total for all three. For example, the maximum capacity for the first disc in polymer **19** calculated from Table II is 8.16 mg/g.

The distribution data lead to interesting conclusions. We assume the three discs of a given polymer are effectively identical in structure. Disc 1 of polymer **26** removes 32.5% of the protein presented to it in the solution so that the average concentration of emerging solution is approximately 67.5% of the initial. Disc 2 might therefore be expected to adsorb 0.675 × 0.976 = 0.659 mg of protein A. Similarly for disc 3 the expected removal is 0.578 mg. These values for discs 2 and 3 are much greater than those observed, 0.247 and 0.141 mg, respectively. The same conclusion may be drawn for polymer **14**. Similar, but smaller effects follow for the polymers **15** and **22**, the expected removals for discs 2 and 3 being 0.184 and 0.175 mg, respectively for **15** and 0.297 and 0.276 mg for **22**. We believe these results reflect the non-uniform nature of the liquid flow through the discs. For instance, they are compatible with a leakage of solution around the edges of the discs, so that some pass through the apparatus virtually unchanged. Inspection of the equipment makes this aspect unlikely. A more probable explanation lies in the range of pore sizes between the

TABLE II

DISTRIBUTION OF PROTEIN A BETWEEN DISCS

(a) = Weight of protein A coupled (mg); (b) = percentage of total coupled protein on each disc; (c) = percentage of total protein initially present in solution removed by disc.

Reference number of activated membrane	Disc 1	Disc 2	Disc 3	Percentage of total protein A in solution which becomes coupled
15 (a)	0.197	0.140	0.112	15.0
(b)	43.9	31.2	24.9	
(c)	6.56	4.66	3.72	
22 (a)	0.335	0.191	0.053	19.3
(b)	57.8	33.0	9.2	
(c)	11.15	6.37	1.77	
19 (a)	0.838	0.198	0.085	37.4
(b)	74.8	17.6	7.6	
(c)	27.94	6.59	2.83	
26 (a)	0.976	0.247	0.141	45.5
(b)	71.5	18.2	10.3	
(c)	32.5	8.24	4.71	

fibres, some pores being sufficiently large to allow solution to pass through them virtually unchanged. Such an effect of large pores is not surprising in view of the small diffusion coefficients of protein molecules. Simple quantification of this model shows that the difference between the expected and actual adsorptions increases with the activity of the membrane in agreement with the above discussion. The above argument assumes a linear relation between weight of protein bound and the solution concentration. If the relation is not linear but has the familiar form with a plateau adsorption the argument is strenghthed.

IgG binding

The coupling of IgG has also been examined. This protein may be bound in two ways: (a) direct to the activated membrane, as described for protein A, and (b) to protein A coupled to the membrane. Data for the two procedures are given in Table III.

Since the coupling values in Table III are given for three discs together, they are unlikely to represent maximum capacities.

As with protein A, the non-specific adsorption of IgG is low, amounting, on average, to approximately 0.64% of the coupling to the activated membrane. The corresponding value given in ref. 14 for "Quenched Immobilon" membrane is about 2%.

A simple geometric model for estimating the capacity for protein adsorption by electrostatically spun fibres

The present system readily lends itself to idealisation in the form of a model suitable for these estimates. The simplest model consists of a single fibre of which the surface is fully covered by adsorbed protein. Estimation of the maximum weight of protein adsorbed is therefore made in terms of relative areas, on the assumption that there is always an excess of activated groups present. It will appear later that the latter supposition is normally true for our membranes. This model naturally tends to over-estimate the maximum capacity, for, as we have mentioned earlier, the whole of the surface area is not accessible to the protein.

If D and ρ are the diameter and density of the

TABLE III

IgG COUPLING

Reference number of activated membrane	Direct coupling of IgG		Coupling of IgG to protein A on membrane		Non-specific adsorption of IgG	
	mg BH/g	μg/cm²	mg/g	μg/cm²	mg/g	μg/cm²
28	5.65	266.3	2.68	152.0	0.02	1.43
29	5.70	206.2	3.96	290	0.02	1.00

TABLE IV

CONCENTRATIONS OF FREE AND OCCUPIED ACTIVE SITES IN MEMBRANES

S = mol of active sites per g Biomer; S_{occ} = mol of active sites per g Biomer coupled to IgG assuming one bond per protein molecule. Estimated from data in Table III.

Reference number of activated membrane	Active sites present in 1 g Biomer		$10^8\ S_{occ}$ mol/g	S/S_{occ}
	mg BH/g	$10^5\ S$ mol/g		
28′	28.2	10.7	3.77	2838
29′	138	52.4	3.80	13815

fibre, respectively, the length L of fibre weighing 1 g is

$$L = \frac{4}{\pi\rho D^2}\,\mathrm{cm/g} \tag{2}$$

and the surface area per gram A is

$$A = \frac{4}{\rho D}\,\mathrm{cm^2/g} \tag{3}$$

The volume of the constituent chains in a protein molecule of molecular mass M is M/ρ_p cm^3/mol or $M/N\rho_p$ cm^3/molecule, where N is the Avogadro number and ρ_p is the density of the chains. For estimating the packing of the molecules we consider each as a sphere; the volume of this sphere will clearly be greater than $M/N\rho_p$ cm^3 and we may write it was $FM/\mathrm{N}\rho$ cm^3, F being a factor probably in the range 1–10. The radius r of this sphere is given by:

$$r = \left(\frac{3FM}{4\pi N\rho_p}\right)^{1/3}\,\mathrm{cm} \tag{4}$$

A closely packed monolayer of such spheres would have the centres of neighbours separated by a distance $2r$ so that each sphere in the layer occupies an area $2\sqrt{3}r^2$. From eqns. 3 and 4 we see that the maximum number of protein molecules n which can be accommodated on 1 g of fibre is therefore

$$n = \frac{\mathrm{A}}{2\sqrt{3}r^2} = \frac{2}{\sqrt{3}\rho D}\left(\frac{4\pi\rho_p N}{3FM}\right)^{2/3} \tag{5}$$

Thus the weight of protein bound to 1 g of fibre W is given by

$$W = \frac{nM}{N} = \frac{2}{\sqrt{3}\rho D}\left(\frac{M}{N}\right)^{1/3}\left(\frac{4\pi\rho_p}{3F}\right)^{2/3} \tag{6}$$

The following extreme values of the coupling capacities for the two proteins studied may be deduced from eqn. 6. They are based on $F = 1$ and $F = 10$, with $\rho = 1.0$, $\rho_p = 1.3$ g/cm and $D = 10^{-4}$ cm in each case.

$$\begin{aligned} &\text{Protein A, } M = 42\,000; && W_{max} = 14.7\ \mathrm{mg/g} \\ &&& W_{min} = 3.16\,\mathrm{mg/g} \\ &\text{IgG, } M = 150\,000; && W_{max} = 22.4\ \mathrm{mg/g} \\ &&& W_{min} = 4.85\,\mathrm{mg/g} \end{aligned} \tag{7}$$

The coupling capacities mentioned earlier lie within the limits in both cases, suggesting that the maximum covering corresponds to a monomolecular layer.

Further evidence supporting this conclusion may be adduced from considerations of the number of activated groups introduced into the sample. We determined the content of such groups as described for two samples of polymer: these, like **28** and **29**, were synthesised from the functionalised polymers **13** and **20** by direct coupling of ^{125}I-labelled Bolton–Hunter reagent. The activated products are designated **28′** and **29′**. We assume that as far as protein coupling is concerned **28′** and **29′** behave similarly to **28** and **29**, respectively.

Data are presented in Table IV.

Two considerations follow: (i) the considerable difference in the site number per gram in the two polymers is not reflected in the IgG capacities (Table III) and (ii) the number of sites greatly exceeds the number of protein molecules bound. Clearly in these samples the initial site density is not a limiting factor determining the protein adsorption, in agreement with our hypothesis.

The data presented allow estimation of the mean area per active site a_s, assuming all sites lie on the fibre surface. This is given by

$$a_s = \frac{4}{\rho DSN} \tag{8}$$

From Table IV, $a_s = 6.2$ Å^2 for **28′** and 1.3 Å^2 for **29′**. Both areas are unacceptably small, indicating that all the active groups cannot be accommodated on the fibre surface. We therefore believe that in the activating process, fibre swelling allows the reaction to proceed to a limited extent beneath the surface. Groups introduced in this way, unlike those lying on the surface, would not be accessible to a protein.

We are currently concerned with optimisation and further exploration of this promising system.

REFERENCES

1 A. J. Weiss and L. A. Blankstein, *Am. Clin. Prod. Rev.*, 6 (1987) 8–19.
2 P. J. Degen, J. Martin, J. Schriefer and B. Shirley, *US Pat.*, 4 693 985 (1987).
3 S. R. Fahnestock, P. A. Alexander, J. Nagle and D. Filpula, *J. Bacteriol.*, 167 (1986) 870–880.
4 K. P. W. Pemawansa, M. D. Heisler and M. A. Kraus, *US Pat.*, 4 961 852 (1990).
5 D. Annis, A. Bornat, R. O. Edwards, A. Higham, B. Loveday and J. Wilson, *Trans. Am. Soc. Artif. Intern. Organs*, 24 (1978) 209–214.

6 C. H. Bamford, K. G. Al-Lamee, M. D. Purbrick, S. A. Jones and T. J. Wear, *GB Pat. Appl.*, 91 0.17 277 (1991).
7 G. E. Martin, I. D. Cockshott and F. J. T. Fildes, *GB Pat.*, 1 530 990 (1974).
8 C. I. Derek and F. J. T. Fildes, *US Pat.*, 4 044 404 (1977).
9 C. H. Bamford, I. P. Middleton, K. G. Al-Lamee and J. Paprotny, *Brit. Polym. J.*, 19 (1987) 269–274.
10 C. H. Bamford, K. G. Al-Lamee, I. P. Middleton, J. Paprotny and R. Carr, *Bull. Soc. Chim. Belges*, 99 (1990) 919–930.
11 C. H. Bamford, in A. D. Jenkins and A. Ledwith (Editors), *Reactivity, Mechanism and Structure in Polymer Chemistry*, Wiley, New York, 1974, p. 52.
12 Y. Kato and T. Kito, *New Functionality Materials —Design, Preparation and Control, Part B, Report of Priority Area Research Program, Japan, 1987–1989*, Ministry of Education, Science and Culture, 1990, p. 231.
13 D. J. Phillips, B. Bell-Alden, M. Cava, E. R. Grover, W. H. Mandeville, R. Mastico, W. Sawlivich, G. Vella and A. Weston, *J. Chromatogr.*, 536 (1991) 95–106.
14 L. A. Blankstein and L. Dohrman, *Clin. Prod. Rev.*, 4 (1985) 33–41.

Journal of Chromatography, 606 (1992) 33–42
Elsevier Science Publishers B.V., Amsterdam

CHROM. 24 268

Chromatographic behaviour of bis(2,2′-bipyridine)ruthenium(II) complexes containing alaninato, phenylalaninato and tyrosinato ligands

Takashi Nagai

Laboratory of Chemistry, Nippon Medical School, Kosugi, Nakahara-ku, Kawasaki 211 (Japan)

(First received December 24th, 1991; revised manuscript received April 13th, 1992)

ABSTRACT

Diastereoisomeric resolutions of aminoacidatobis(2,2′-bipyridine)ruthenium(II) complexes, $[Ru(S\text{-am})(bpy)_2]^+$ [am = alaninate (Ala), phenylalaninate (Phe) and tyrosinate anion (Tyr); bpy = 2,2′-bipyridine], were carried out by high-performance liquid chromatography (HPLC) using columns of C_8-bonded silica gel, tartaric acid-immobilizing silica gel and silica gel and by liquid column chromatography using ion exchangers (SP- and CM-Sephadex and SE-Toyopearl). The *Δ-S* isomer was eluted faster than the *Λ-S* isomer on the ion exchangers, whereas the reverse order was found on stationary phases based on silica gel. In the latter instance, adsorption was the major mode of separation. ^1H NMR spectroscopy showed that the aromatic side-chain of the aminoacidato ligand oriented toward the intramolecular amino group bound to ruthenium both in water and in methanol. The results demonstrate that the isomers are distinguished primarily through asymmetric hydrogen bonding between silanolate and the amine proton, which is sterically hindered by the aromatic ring. Sephadex ion exchanger showed enantioselectivity in the elution of $[Ru(RS\text{-Phe})(bpy)_2]Br$.

INTRODUCTION

The photochemical and thermochemical properties of $[Ru(S\text{-am})(bpy)_2]X_n$ (am = aminoacidate anion) have been studied in the last few years [1–6]. Complexes of this kind possess two diastereoisomers, *Δ*-$[Ru(S\text{-am})(bpy)_2]^{n+}$ (*Δ-S*) and *Λ*-$[Ru(S\text{-am})(bpy)_2]^{n+}$ (*Λ-S*), which were partially resolved by liquid chromatography (LC) with SP-Sephadex cation exchanger by Vagg and Williams [1]. In addition, we completely resolved the complex coordinating *S*-Phe or *S*-Tyr anion by LC using SE-Toyopearl cation exchanger [6]. However, there are no reports of the use of high-performance liquid chromatography (HPLC) in the separation of these complexes.

HPLC with a cation-exchange column has been reported to be effective in separating complexes of the type $[RuXY(bpy)_2]^{n+}$ having different XY ligands but the same charge [7,8]. The separation of *cis*- and *trans*-isomers of this type of complex by reversed-phase HPLC has also been reported [9]. Further, optical resolution on a DNA–hydroxyapatite column has been examined for racemic solutions of this kind of complex [10]. These studies have provided useful information, but mechanisms for distinguishing the isomers have not been explained in detail.

We report here a diastereoisomeric separation of bis(2,2′-bipyridine)ruthenium(II) complexes coordinating (*S*)-Ala, (*S*)-Phe and (*S*)-Tyr anions (abbreviated to *S*-Ala, *S*-Phe and *S*-Tyr complexes, respectively) by the use of various stationary phases, and discuss the mechanisms of the separation.

Correspondence to: Dr. T. Nagai, Laboratory of Chemistry, Nippon Medical School, Kosugi, Nakahara-ku, Kawasaki 211, Japan.

0021-9673/92/$05.00

EXPERIMENTAL

Chemicals and reagents

All materials were of analytical reagent or HPLC grade and used as received. *Δ*- and *Λ*-[Ru(*S*-am)$(bpy)_2]ClO_4$ (am = Ala, Phe and Tyr) and [Ru(*RS*-Phe)$(bpy)_2$]Br were prepared by methods reported previously [6]. The (*S*)-aminoacidato complexes resolved were used as references to identify the chromatographic peaks in HPLC.

^1H NMR measurement

The ^1H NMR spectra of the complexes in ^2H_2O and $C^2H_3O^2H$ were obtained using a JEOL GX270 Fourier transform NMR spectrometer. Chemical shifts (δ) are reported in parts per million relative to sodium 2,2-dimethyl-2-silapentane-5-sulphonate (DSS) (0.015 ppm) as an internal standard. Amine proton signals were assigned in accordance with Vagg and Williams's report [2].

Tartaric acid-immobilizing silica gel (TA-sil)

Four grams of silica gel (Unisil Q30-5) were dried at 110°C for 6 h and suspended in 40 ml of an aqueous solution in which 25 g of (*R,R*)- or (*S,S*)-tartaric acid were dissolved. The solution was stirred moderately for 4 days, then diluted with the same amount of water. The gel in the solution was filtered off with glass-fibre filter (0.5-μm pore size), dried by heating and dehydrated at 180°C for 3 h in a stream of nitrogen. The yellowish powder was washed with a large amount of water by stirring and decantation several times until it became colourless, then filtered off. All the procedures were repeated twice. The almost white gel obtained was washed with methanol and dried at 80°C.

Measurement of adsorption capacity of silica gel

A 200-mg amount of the gel stored in a silica gel desiccator was packed in a stainless-steel column (5 cm × 4 mm I.D.) by the slurry method [11] using methanol–water–dichloromethane (6:2:2, v/v/v) as solvent. While the solvent flowed at a rate of 1 ml min^{-1}, an excess of the complex solution containing [Ru(*S*-Phe)$(bpy)_2]ClO_4$ or [Ru(*S*-Ala)$(bpy)_2]ClO_4$ was loaded on the column, which was then washed until no absorption due to the complex was detected in the eluate. The solvent was changed to a solution containing 0.005 mol dm^{-3} lithium chloride so that the complex adsorbed came out of the column. All the eluate containing the complex was collected and evaporated to dryness at 45°C by blowing nitrogen gas. The residue on evaporation was dissolved in 50 ml of water and the absorption at 492 nm was measured (ε = 9040 and 9250 for *S*-Ala and *S*-Phe complexes, respectively). The amounts of the complexes determined are shown in Table I as the adsorption capacity.

TABLE I

ADSORPTION CAPACITIES

Complex	Adsorption capacity (μmol g^{-1} gel)	
	TA-sil	Silica gel
[Ru(*S*-Phe)$(bpy)_2]ClO_4$	6 ± 2	2 ± 0
[Ru(*S*-Ala)$(bpy)_2]ClO_4$	8 ± 2	2 ± 0

HPLC

The HPLC system consisted of a Hitachi Model 638-30 system and a Hitachi L-4200 variable-wavelength spectrophotometric detector with a 17.7-μl flow cell. The packings used were silica gel (Unisil Q30-5, GL Science), tartaric acid-immobilizing silica gel and two kinds of C_8-bonded silica gel (Nucleosil $10C_8$, Macherey–Nagel, and Inertsil C_8-packed column, 25 cm × 4.6 mm I.D., GL Science). In a typical experiment, the gel was packed in a stainless-steel column (25 cm × 4 mm I.D.) by the viscosity method [12] and chromatography was carried out using methanol–water–dichloromethane containing lithium chloride as the mobile phase at a flow-rate of 1 ml min^{-1}. A volume of aqueous solution of the complex (10^{-4}–10^{-5} mol dm^{-3}) less than 20 μl was taken and injected on to the column. The retention time increased with increasing proportion of water in the mobile phase above about 30%. The complexes were irreversibly adsorbed by the gel when a salt such as lithium chloride was not present in the mobile phase.

Liquid chromatography using ion exchangers

The ion exchangers employed were SP- and CM-Sephadex C-25 (Pharmacia) and SE-Toyopearl, which was prepared according to ref. 13. All of the elutions took place in the dark to prevent inversion between the *Δ*- and *Λ*-forms by exposure to light. In

a typical experiment, the exchanger was packed in a glass column (50 cm × 1.0 cm I.D.) equipped with thermostated jacket to keep the temperature at 30.0 ± 0.1°C. The elution curve was recorded at 492 nm, where the absorption maximum of the complexes was observed, and the eluate was collected fractionally if necessary. The closed peaks on the chromatogram were analysed by means of the least-squares method.

RESULTS AND DISCUSSION

Diastereoisomeric resolution of [Ru(S-am)-(bpy)$_2$]ClO$_4$

Typical chromatograms are shown in Fig. 1[a] and the chromatographic data are listed in Table II. In all of the elutions, the *Λ-S* form was eluted faster than the *Δ-S* form.

The Inertsil C_8 column, in which residual silanols were appreciably reduced on the surface of the gel, was also used under the same conditions as with the Nucleosil C_8 column. In this instance, the narrow peak of the complex overlapped with the solvent peak, indicating little interaction between the stationary phase and the complex. Further, when lithium chloride was not added to the mobile phase, Nucleosil C_8 showed irreversible adsorption of the complex, but only a weak interaction was observed on Inertsil C_8, although tailing occurred after the narrow peak. These phenomena seem to be explainable in terms of the amounts of residual silanols on the surface of the gel.

On elution using silica gel (Unisil), irreversible adsorption also occurred using methanol, ethanol, acetonitrile, acetone, chloroform and toluene that did not contain any salt such as lithium chloride[b]. For methanolic solvents, the retention time of each isomer decreased with increasing concentration of LiCl. Including the elution order of the isomers, these trends were similar to those for elution on

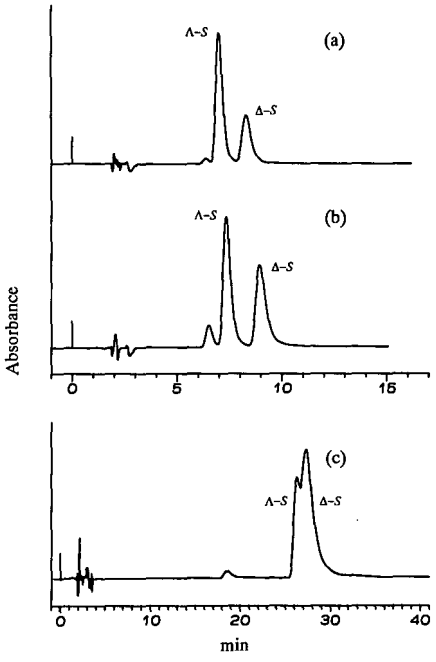

Fig. 1. Chromatograms of (a) [Ru(*S*-Tyr)(bpy)$_2$]ClO$_4$ and (b) [Ru(*S*-Phe)(bpy)$_2$]ClO$_4$ obtained by HPLC on silica gel using as eluent methanol–water–dichloromethane (6:2:2) containing 0.005 mol dm^{-3} of LiCl and (c) [Ru(*S*-Ala)(bpy)$_2$]ClO$_4$ on (*R*)-TA-sil using a 6:1:3 eluent containing 0.01 mol dm^{-3} of LiCl. Flow-rate, 1 ml min^{-1}.

Nucleosil C_8, in spite of the fact that the surfaces of the two gels possess opposite polarities.

It has been reported that a neutral complex, [Ru(CN)$_2$(bpy)$_2$]°, was developed by methanol alone on a silica gel thin-layer plate, and the appropriate adsorption was explained by the dipole moment of the complex [14]. Hence it is suggested that the irreversible adsorption of the aminoacidato complexes occurs on silica gel in elution with methanol alone because of the aminoacidato ligand and/or the overall charge of the complexes. In preliminary experiments, it was found that an acidic solvent reduced the adsorption ability of the complex toward silica gel without changing α as compared with a neutral solvent containing lithium chloride. The adsorbent used was Unisil Q30. When the *S*-Phe complex was eluted with mobile phase (6:2:2) (Table II) solution containing 0.005 mol dm^{-3} lithium chloride, $k'_1 = 2.1$, HETP = 360 μm, $R_s = 1.1$ and $\alpha = 1.28$; with a solution containing 0.005 mol dm^{-3} hydrochloric acid, $k'_1 = 1.4$, HETP = 420 μm, R_s

[a] A peak preceding the peak of *Λ*-S seems to be that of a decomposition product, which is not discussed in this paper.

[b] To obtain appropriate elution conditions, LiCl, LiClO$_4$, NaCl, NaClO$_4$, NaI and Na$_2$(R,R)-tart or acetic acid were used as additives. Of these, Na$_2$(R,R)-tart showed the largest R_s value but long tailing peaks, whereas LiCl and LiClO$_4$ showed sharper and more clearly separated peaks.

TABLE II

DATA FOR THE CHROMATOGRAPHIC SEPARATION OF THE DIASTEREOISOMERS BY HPLC[a]

Separation factor (α), resolution (R_s) and height equivalent to a theoretical plate (HETP) are obtained by the following equations:
$\alpha = (V_{R2}\text{-}V_O)/(V_{R1}\text{-}V_O)$
$R_s = 1.18\,(V_{R2}\text{-}V_{R1})/(W_1 + W_2)$
$\text{HETP} = L/[5.54(V_{R1}/W_1)^2]$
where V_{R1} and W_1 represent retention volume and peak half-width of an earlier eluted peak, respectively, and V_{R2} and W_2 those of a later eluted peak, L is the height of the column and V_O is the void volume, which was approximated by the retention volume of the solvent peak in HPLC and by the column bed volume in LC on ion exchangers.

Complex[b]	Adsorbent	Mobile phase[c]		k'_1[d]	HETP (μm)	R_s	α[e]
S-Phe	Nucleosil C_8[f]	A (7:3)	0.017 *M* LiCl	1.1	270	0.85[g]	1.18
	Unisil[h]	A (8:2)	0.03 *M* LiCl	4.2	130	2.4	1.31
			0.03 *M* $LiClO_4$	3.4	140	1.9	1.27
		B (6:2:2)	0.005 *M* LiCl	3.6	170	1.9	1.29
		B (6:1:3)	0.003 *M* $LiClO_4$	3.5	170	2.1	1.32
			0.005 *M* LiCl	2.5	280	1.5	1.33
		C (6:2:2)	0.03 *M* LiCl	2.1	170	2.8	1.50
	(*R*)-TA-sil[i]	B (6:2:2)	0.01 *M* LiCl	2.4	86	2.5	1.31
		B (6:1:3)	0.01 *M* LiCl	3.7	81	2.7	1.28
	(*S*)-TA-sil	B (6:1:3)	0.01 *M* LiCl	3.1	93	2.7	1.30
S-Tyr	Nucleosil C_8	A (65:35)	0.024 *M* LiCl	0.67	250	1.1[g]	1.28
	Unisil	A (8:2)	0.03 *M* LiCl	2.8	130	2.1	1.35
		A (6:4)	0.05 *M* LiCl	5.2	100	2.6	1.27
		A (5:5)	0.05 *M* LiCl	5.5	140	2.4	1.32
		B (6:2:2)	0.005 *M* LiCl	2.6	170	1.6	1.27
		B (6:1:3)	0.005 *M* LiCl	2.6	280	1.3	1.28
		C (6:2:2)	0.03 *M* LiCl	2.0	150	2.6	1.45
	(*R*)-TA-sil	B (6:2:2)	0.01 *M* LiCl	2.3	86	2.1	1.25
		B (6:1:3)	0.01 *M* LiCl	2.5	89	2.1	1.22
	(*S*)-TA-sil	B (6:1:3)	0.01 *M* LiCl	3.3	89	2.2	1.24
S-Ala	Unisil	B (6:2:2)	0.01 *M* LiCl	5.7	250	0.4	1.05
		B (6:1:3)	0.004 *M* LiCl	9.2	250	0.5	1.07
	(*R*)-TA-sil	B (6:2:2)	0.01 *M* LiCl	7.3	80	0.4	1.03
		B (6:1:3)	0.01 *M* LiCl	13	80	0.4	1.03
	(*S*)-TA-sil	B (6:1:3)	0.01 *M* LiCl	9.0	100	0.6	1.06

[a] *A*-*S* was eluted early.
[b] *S*-am represents $[Ru(S\text{-am})(bpy)_2]ClO_4$.
[c] A = methanol–water; B = methanol–water–dichloromethane; C = ethanol–water–dichloromethane. The volumetric proportion of the components are given in parentheses. 1 *M* = 1 mol dm^{-3}.
[d] Capacity factor of *A*-*S* peak.
[e] Deviation of α was roughly estimated to be ± 0.04.
[f] C_8-bonded silica gel.
[g] Column height was 500 mm.
[h] Silica gel.
[i] (*R*)-TA-sil represents the silica gel immobilizing (*R*,*R*)-tartaric acid.

= 0.9 and α = 1.29. When *S*-Tyr complex was eluted with 0.005 mol dm^{-3} lithium chloride solution, k'_1 = 1.7, HETP = 380 μm, R_s = 0.9 and α = 1.24; with 0.005 mol dm^{-3} hydrochloric acid, k'_1 = 1.1 and the other parameters were not measurable, as the two peaks were very close. This can be attributed to the extent of dissociation of surface silanols. All of the observations mentioned above imply the presence of a direct interaction between the complex and surface silanols, and hence that normal-phase adsorption is the major separation mode in the present chromatography with silica gel. The occurrence of peak tailing also supports this conclusion (Fig. 1).

Table II shows that the separation factor α for each complex is approximately constant and is not much affected by the adsorbents and the composition of the solvents, except ethanolic solvents. It was also independent of the concentration of lithium chloride in the mobile phase, within experimental error. The values for the *S*-Ala complex were smaller than those of the other complexes. The α value can be regarded as the ratio of distribution coefficients for the two isomers. It is therefore suggested that differences in the eluent conditions hardly changed the fundamental distinction mechanism, which determines the value of α. For the *S*-Phe complex, the resolution R_s increased in the order C_8-bonded silica gel < silica gel < TA-sil, whereas the height equivalent to a theoretical plate (HETP) tended to become shorter in this order. Similar trends were also observed for *S*-Tyr and *S*-Ala complexes.

The main reason why high resolutions were found for TA-sil was not stereospecific interaction with tartaric acid on the gel, but the increase in the number of theoretical plates caused by immobilization of tartaric acid, as the effect of TA-sil appeared markedly in HETP but scarcely in α. This is also supported by the data in Table I, where the adsorption capacity increases three to four times for TA-sil in comparison with silica gel.

Chromatographic separations using ion exchangers were examined for the eluents involving $K_2(R,R)$-tart and $K_2[Sb_2(R,R)\text{-tart}_2]$, which are representative anionic selectors [15], as listed in Table III. The elution order of the diastereoisomers was the opposite to that using adsorbents based on silica gel; *Δ-S* moved faster than *Λ-S* on the ion exchangers. For the elution of *S*-Phe complex on a CM-Sephadex column, the R_s values were 0.50, 0.63 and 0.80 for eluents containing KCl, $K_2(R,R)$-tart and $K_2[Sb_2(R,R)\text{-tart}_2]$, respectively. Nevertheless, the corresponding α values were the same, although HETP decreased keeping the same elution order. Moreover, it was shown that R_s or α took the same values when using either (*R,R*)- or (*S,S*)-tartrate salt as an eluting agent. The elution on SP-Sephadex also showed almost the same α values as with CM-Sephadex, giving a higher resolution and shorter HETP. However, in aqueous media, the α value for SE-Toyopearl was different from those for CM- and SP-Sephadex. It seems that the complexes interacted more weakly with such anions than with

TABLE III

DATA FOR THE CHROMATOGRAPHIC SEPARATION OF THE DIASTEREOISOMERS ON ION EXCHANGERS

Complex[a]	Ion exchanger	Eluent[b]	Retention volume (bed volumes)		HETP (μm)	R_s	α[c]
			Δ-S	*Λ-S*			
S-Phe	CM-Sephadex	0.01 *M* $K_2[Sb_2(R,R)\text{-tart}_2]$	22.3	25.1	670	0.80	1.13
		0.01 *M* $K_2(R,R)$-tart	6.6	7.3	840	0.63	1.12
		0.01 *M* $K_2(S,S)$-tart	6.9	7.6	910	0.61	1.12
		0.02 *M* KCl	10.7	11.8	1400	0.50	1.12
	SP-Sephadex	0.05 *M* $Na_2(R,R)$-tart	4.3	4.9	630	1.5	1.15
	SE-Toyopearl	0.05 *M* $Na_2(R,R)$-tart	13.3	17.4	220	2.6	1.33
		0.1 *M* KCl	11.3	14.7	160	2.6	1.33
		Methanol–0.02 *M* LiCl	11.8	16.0	350	1.8	1.39
	HW-40[d]	0.01 *M* KCl	8.0	9.5	387	1.0	1.22
		Methanol–water (9:1)	65.4	65.4	650	0.0	1.00
S-Ala	CM-Sephadex	0.008 *M* $Na_2(R,R)$-tart	23.4	24.1	200	0.5	1.05
	SP-Sephadex	0.04 *M* $Na_2(R,R)$-tart	4.1	4.2	580	0.62	1.05

[a] *S*-Phe and *S*-Ala represent $[Ru(S\text{-Phe})(bpy)_2]ClO_4$ and $[Ru(S\text{-Ala})(bpy)_2]ClO_4$, respectively.

[b] Aqueous solution. 1 *M* = 1 mol dm^{-3}.

[c] Deviation of α was roughly estimated to be ± 0.04.

[d] TSK-GEL Toyopearl HW-40F (Toyo Soda).

the ion-exchange resin. In other words, these observations indicate that the stereospecific character of $[(R,R)\text{-tart}]^{2-}$ and $[Sb_2(R,R)\text{-tart}_2]^{2-}$ anions in the eluents did not exert an intrinsic effect for discrimination of the isomers. A similar situation was also observed when TA-sil was used as an adsorbent.

We define a value A which is the ratio of distribution coefficients of the two isomers, as follows:

$$A = K_{\Delta}/K_{\Lambda}$$

where K_{Δ} is the distribution coefficient of the Δ-S isomer,

$$K_{\Delta} = [\Delta\text{-}S]_{\text{stationary}}/[\Delta\text{-}S]_{\text{mobile}}$$

and K_{Λ} similarly that of the Λ-S isomer. A has the same significance as α when Λ-S elutes faster than Δ-S, but for the contrary case $A = 1/\alpha$. The A values obtained for each adsorbent are listed in Table IV. A is transformed as

$$A = Ks_s/Ks_m$$

where $Ks_s = [\Delta\text{-}S]_{\text{stationary}}/[\Lambda\text{-}S]_{\text{stationary}}$ and $Ks_m = [\Delta\text{-}S]_{\text{mobile}}/[\Lambda\text{-}S]_{\text{mobile}}$. For instance, when A is less than unity, Ks_s becomes smaller than Ks_m, which means that the stationary phase prefers Λ-S to Δ-S in comparison with the mobile phase. Table IV therefore shows that a more effective interaction occurred on Λ-S with the ion exchangers and on Δ-S with the adsorbents based on silica gel. This trend was unchanged even if the components of the eluent were modified to some extent.

With elution on silica gel, hydrogen bonding, charge transfer, π–π, dipole–dipole and Van der Waals interactions and steric effects would be expected in the adsorption of the complexes in the present experiments. The elution of the $[RuCl_2(bpy)_2]Cl$ complex on silica gel gave a peak at a capacity factor $k' = 0.6$, whereas peaks were found at 2.05 for Λ-S and 2.68 for Δ-S of the S-Phe complex under the same elution conditions. The dichloro complex dissolved in dichloromethane was injected on to the column of Unisil Q30-5. Methanol–water–dichloromethane (6:1:3) containing 0.005 mol dm^{-3} of lithium chloride was used as the mobile phase. The peak at $k' = 0.6$ showed extensive tailing and a shoulder appeared at $k' = 1.4$ on the tailing peak. The latter peak grew strongly when a methanol solution of the complex was used, and was larger than the peak at $k' = 0.6$ when an aqueous solution was injected. It is known that the complex is easily hydrolysed in water. Hence the peak at $k' = 1.4$ seemed to be one of the hydrolysis products of the complex. The fact that the small k' value was derived from chloro ligands implies that a significant interaction was accomplished by hydrophilic groups of the aminoacidato ligand. The aminoacidato complex would interact with silica gel mainly through three forces: hydrogen bonding, dipole–di-

TABLE IV

VALUES OF A OBTAINED FOR EACH ADSORBENT IN METHANOL–WATER SYSTEM

$A = K_{\Delta}/K_{\Lambda}$, where $K_{\Delta} = [\Delta\text{-}S]_{\text{stationary}}/[\Delta\text{-}S]_{\text{mobile}}$ and K_{Λ} similarly that of Λ-S.

Adsorbent	Component[a]	A	Solvent
SE-Toyopearl	Polyvinyl derivative containing OH groups (sulphoethyl groups)	0.76 (0.72)[b]	Water
CM-, SP-Sephadex	Dextran (carboxymethyl or sulphopropyl groups)	0.87–0.89	
HW-40	Polyvinyl derivative containing OH groups	0.82 (1.0)[b]	
Nucleosil C_8	C_8-bonded silica gel	1.2	Methanol–water–dichloromethane
Unisil	Silica gel	1.2–1.3	
TA-sil	Tartaric acid-immobilizing silica gel	1.2–1.3	

[a] Ion-exchange group is given in parentheses.

[b] Methanol as solvent.

pole and weak ion–ion interactions. Considering an ion-exchange process, hydrogen bonding would reinforce the weak ion–ion interaction. For the aminoacidato complex cation, one of the amine protons would be able to approach a silanolate to form a hydrogen bond, the surface of the gel being electrically neutralized. On the other hand, no available hydrogen is present in the dichloro complex, which therefore cannot form any effective hydrogen bond.

Vagg and Williams [2] reported the ^1H NMR spectra of the *S*-Ala complex in ^2H_2O. Significant low-field shifts were observed on the resonance peaks of amine protons of the *S*-Ala ligand, and were explained in terms of asymmetric solvation of the coordinated NH_2 group through hydrogen bonding (asymmetric hydrogen bonding). Further, deuterium exchange rates of the protons were measured, and it was clarified that H_a (Fig. 2) in the *Δ-S* form was exchanged faster than H_b in the *Λ-S* form between the two less sterically hindered protons, which were accessible to the solvent to interact with it through asymmetric hydrogen bonding in each isomer. In our NMR measurements, similar chemical shifts were observed for the *S*-Phe and *S*-Tyr complexes, as shown in Table V, and it was confirmed that asymmetric hydrogen bonding also occurred on the two complexes in a similar manner.

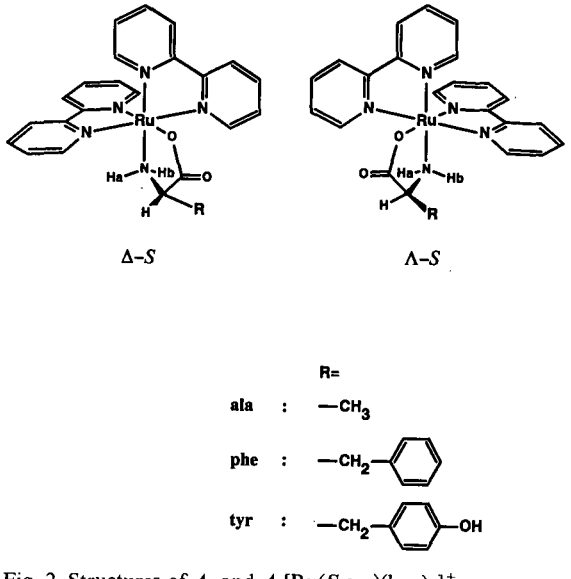

Fig. 2. Structures of *Δ*- and *Λ*-[Ru(*S*-am)(bpy)$_2$]$^+$.

TABLE V

CHEMICAL SHIFTS OF AMINE PROTONS OF AMINOACIDATO LIGAND

^2H_2O was used as a solvent.

Ligand[a]	δ (ppm)			
	Δ-S		*Λ-S*	
	H_a	H_b	H_a	H_b
S-Ala	4.4	4.1	3.6	5.2
S-Phe	4.3	3.5	2.8	5.2
S-Tyr	4.3	3.5	2.7	5.2

[a] *S*-am represents [Ru(*S*-am)(bpy)$_2$]ClO$_4$.

This is not inconsistent with the fact that the *Δ-S* isomer of the *S*-Phe complex was more soluble than the *Λ-S* isomer in water (the solubilities of the *Δ-S*-Phe and *Λ-S*-Phe complexes were 1100 and 830 mg, respectively, in 100 ml of water at 45°C). Considering asymmetric hydrogen bonding with silica gel, the interaction would be stronger for the *Δ-S* than for the *Λ-S* isomer. This trend accounts for the elution order of the isomers in HPLC using silica gel, but cannot solely explain the difference in α between *S*-Ala and the other two complexes.

The NMR spectra in the resonance region of phenol ring protons were obtained for the *S*-Tyr complex as shown in Fig. 3. The resonance peaks of phenol protons in *Δ-S* appeared at almost the same positions as those in free tyrosine, whereas the corresponding peaks of *Λ-S* shifted to higher field. Considering a model in which the phenol ring orients to an intramolecular amino group as shown in Fig. 4, the upfield shift was explainable in terms of the shielding effect induced by the ring current on the pyridine ring that faced on the phenol ring in the *Λ-S* isomer. A similar orientation of the aromatic ring was expected in *Δ-S*, as not much difference was observed between the isomers in the coupling constants of methylene protons bound to the carbon that adjoined the aromatic ring ($^3J_{HH_1}$, $^3J_{HH_2}$ = 2.7, 5.5 Hz for *Λ-S*-Tyr, 2.4, 5.7 Hz for *Δ-S*-Tyr, 4.4, 5.1 Hz for *Λ-S*-Phe and 3.4, 5.6 Hz for *Δ-S*-Phe). The peaks of the phenol protons of *Λ-S* in $C^2H_3O^2H$ showed similar upfield shifts, which reflected that the aromatic group retained the orientation even in the methanolic solvent. The point to

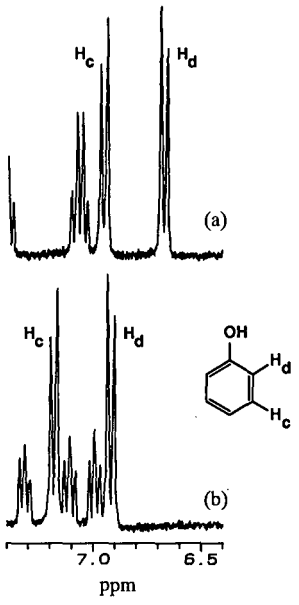

Fig. 3. Proton NMR spectra in the range δ 6.4–7.4 ppm: (a) Λ-[Ru(*S*-Tyr)(bpy)$_2$]ClO$_4$ and (b) Δ-[Ru(*S*-Tyr)(bpy)$_2$]ClO$_4$, dissolved in ^2H_2O.

be emphasized is that the aromatic ring orients toward not the carboxyl group but the amino group in the *S*-Tyr and, probably, *S*-Phe ligands. Because of this orientation, steric interference would be expected to act against the asymmetric hydrogen bonding between amine protons and the surface silanolates on the silica gel. This consideration is supported by the fact that the retention times of both the *S*-Tyr and *S*-Phe complexes were shorter than that of the *S*-Ala complex, being about 6–10 min for the former complexes and about 15–20 min for the latter in typical elutions on Unisil.

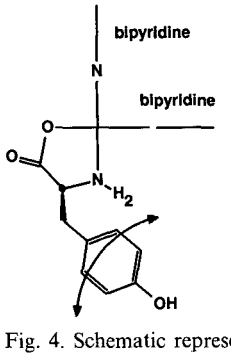

Fig. 4. Schematic representation of the orientation of the aromatic ring of the *S*-Tyr ligand in Λ-[Ru(*S*-Tyr)(bpy)$_2$]$^+$.

Table V shows that, for the *S*-Ala complex, the difference in the chemical shifts between H_a and H_b in Λ-*S* ($\Delta\delta$ = 1.6) is larger than that in Δ-*S* ($\Delta\delta$ = 0.3). Further, for the *S*-Phe and *S*-Tyr complexes, the difference in Λ-*S* ($\Delta\delta$ = 2.5) becomes even larger than that in Δ-*S* ($\Delta\delta$ = 0.8). The effect of the aromatic ring appears more marked in Λ-*S* than in Δ-*S*, suggesting that the aromatic ring is located closer to the amine protons in Λ-*S* than in Δ-*S*. The amine protons in Λ-*S* would, therefore, be less accessible to the surface silanolate. This situation can provide the possibility of distinguishing the isomers, and enhance the discrimination by the asymmetric hydrogen bonding in the diastereoisomeric separation observed for the *S*-Ala complex. Large α values for the *S*-Tyr and *S*-Phe complexes can be explained reasonably also in terms of these effects.

On the other hand, with elution on the ion exchangers, it was found that the complex isomers did not interact distinctively with the anionic selectors. In aqueous media, elution on SE-Toyopearl showed that the *S*-Ala complex was eluted earlier than the *S*-Phe complex. This can be explained by hydrophobic interactions between the complex and the framework of the exchanger.

Noteworthy α values were observed in elution on HW-40 (Table III). HW-40 is the parent gel of SE-Toyopearl, and consists of a polyvinyl derivative containing hydroxyl groups and having no ion-exchange group. HW-40 showed irreversible adsorption of the complex in elution with water alone, but with aqueous potassium chloride solution it gave sufficient α values to resolve the isomers, which were eluted in the same order as with the ion exchangers. It is obvious that matrix effects contributed significantly to elution on the ion exchangers. As with silica gel, it was expected that the complex would interact with surface hydroxyl groups, but the interaction would be weak owing to the low acidity of the C–OH hydroxyl group [16]. Instead of this, hydrophobic interactions would be effective because of the low polarity of the framework of HW-40. Elutions with methanol alone or methanol–water (9:1) showed reversible adsorption of the complex, indicating a decrease in adsorption ability. This could be explained by the idea that the hydrophobic interaction with the stationary phase was diminished owing to low polarity of methanol. Hence the system of HW-40 with a methanolic sol-

vent showed no selectivity for the diastereoisomers.

Sephadex G-10, which is the parent gel of Sephadex ion exchangers, also revealed irreversible adsorption in water containing no salt, but the adsorption ability was substantially decreased when a small amount of potassium chloride was dissolved in the mobile phase. Of the Λ- and Δ-*S* isomers, Λ-*S* would be more hydrophobic than Δ-*S*, as the amine proton in Λ-*S* is less accessible to water as described above. The elution order of the isomers can therefore be explained by hydrophobic interaction with the ion exchangers. The difference in A values between Toyopearl and Sephadex may be due to matrix effects, but further discussion is not possible owing to a lack of information on the structure of HW-40.

It is interesting that, among the elutions on the ion exchangers, the largest α value was observed in elution where a methanolic solution of lithium chloride was used on SE-Toyopearl (Table III). In this elution, the mobile phase reduced the adsorption ability of the complex, and the retention time of the *S*-Ala complex became the same as that of the *S*-Phe complex. From the results of elution on HW-40 with methanol–water (9:1), it is likely that the hydrophobic effect on the matrix is almost cancelled by the methanolic solvents. In this instance it is necessary to consider a different mechanism such as ion-pair chromatography, but it could not be elucidated solely from the present data.

In these experiments, primarily hydrogen bonding explained the chromatography on silica gel and hydrophobic interaction that on ion exchangers. These interactions apply in substantially opposite directions but have the same implication, as the complexes would interact with the mobile phase through hydrophobic moieties in HPLC on silica gel and through hydrogen bonding in LC on ion exchangers. It is reasonable to deduce that the opposite relationship causes the reversed order in the elution of the diastereoisomers between the two kinds of chromatography, and this implication is demonstrated by the α values, which are roughly comparable to each other for the corresponding complexes in Tables II and III.

Enantiomeric resolution of [Ru(RS-Phe)(bpy)$_2$]Br

Sephadex ion exchangers showed enantioselectivity when [Ru(*RS*-Phe)(bpy)$_2$]Br was eluted with an aqueous solution. In addition to Δ-*S* and Λ-*S* isomers, Λ-*R* and Δ-*R* isomers exist in this complex. The four isomers were partially resolved by CM-Sephadex column chromatography using $K_2[Sb_2(R,R)\text{-tart}_2]$ as an eluting agent. The elution curve is shown in Fig. 5, together with the curve for [Ru(*S*-Phe)(bpy)$_2$]ClO$_4$ eluted under the same conditions. From absorption and circular dichroism measurements on the fraction of the eluate, it was found that the order of elution of the isomers was Δ-*S* > Λ-*R* ≈ Δ-*R* > Λ-*S*. The same elution order and α values were obtained on elution with $K_2(R,R)$-tart instead of $K_2[Sb_2(R,R)\text{-tart}_2]$. It is interesting that Λ-*R* and Δ-*R* isomers containing an *R*-Phe ligand were hardly resolved. This indicates that the ability for diastereoisomeric discrimination was cancelled by that for enantiomeric discrimination and that the two kinds of discrimination mechanisms are energetically comparable.

It has been reported that for both $[Ru(bpy)_3]^{2+}$ and $[Ru(bpy)_2(\text{di-2-pyridylamine})]^{2+}$ complex ions, the Δ form was eluted faster than the Λ form in SP-Sephadex column chromatography with the use of either $Na_2[Sb_2(R,R)\text{-tart}_2]$, $Na_2(R,R)$-tart or NaCl as eluting agent [17]. This order accorded with the results of the elutions in the present experiments.

As regards SE-Toyopearl, elution of [Ru(*RS*-Phe)(bpy)$_2$]Br with $Na_2(R,R)$-tart showed no enantioselectivity, giving two completely resolved peaks, the faster consisting of Δ-*S* and Λ-*R* and the later one Λ-*S* and Δ-*R* [6]. Moreover, two peaks were

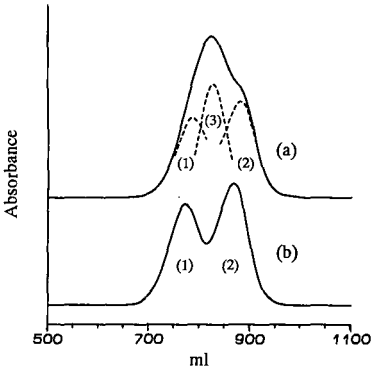

Fig. 5. Chromatograms of (a) [Ru(*RS*-Phe)(bpy)$_2$]Br and (b) [Ru(*S*-Phe)(bpy)$_2$]ClO$_4$ obtained by LC on CM-Sephadex C-25 (column, 43 cm × 1 cm I.D.) with 0.01 mol dm^{-3} aqueous $K_2[Sb_2(R,R)\text{-tart}_2]$ as eluent. Peak 1 = Δ-*S*-isomer, peak 2 = Λ-*S* isomer and peak 3 = Λ- and Δ-*R* isomers.

also obtained in HPLC on silica gel or TA-sil, but the faster peak consisted of *Λ*-*S* and *Δ*-*R* and the later one *Δ*-*S* and *Λ*-*R*.

The enantioselectivity shown by Sephadex ion exchangers in these experiments can be explained in terms of its characteristic asymmetric framework. Also in the diastereoisomeric resolution, the difference in the frameworks of Sephadex and Toyopearl was reflected in the *A* values (Table IV). It is certain that some interactions occur between the complexes and the framework of the resin. However, as there is not a particular interaction with the aminoacidato complexes, it would be necessary to obtain data for other monovalent cationic bis(2,2′-bipyridine)ruthenium(II) complexes.

REFERENCES

1 R. S. Vagg and P. A. Williams, *Inorg. Chim. Acta*, 51 (1981) 61.
2 R. S. Vagg and P. A. Williams, *Inorg. Chem.*, 22 (1983) 355.
3 F. S. Stephens, R. S. Vagg and P. A. Williams, *Inorg. Chim. Acta*, 72 (1983) 253.
4 T. J. Goodwin, P. A. Williams and R. S. Vagg, *Inorg. Chim. Acta*, 83 (1984) 1.
5 R. S. Vagg, *J. Proc. R. Soc. N. S. W.*, 117 (1984) 99.
6 T. Nagai, *Bull. Chem. Soc. Jpn.*, 62 (1989) 2897.
7 B. E. Buchanan, E. McGovern, P. Harkin and J. G. Vos, *Inorg. Chim. Acta*, 154 (1988) 1.
8 B. E. Buchanan, R. Wang, J. G. Vos, R. Hage, J. G. Haasnoot and J. Reedijk, *Inorg. Chem.*, 29 (1990) 3263.
9 R. Kroener, M. J. Heeg and E. Deutsch, *Inorg. Chem.*, 27 (1988) 558.
10 A. D. Baker, R. J. Morgan and T. C. Strekas, *J. Am. Chem. Soc.*, 113 (1991) 1411.
11 C. D. Scott and N. E. Lee, *J. Chromatogr.*, 42 (1969) 263.
12 C. J. Little, A. D. Dale, D. A. Ord and T. R. Marten, *Anal. Chem.*, 49 (1977) 1311.
13 M. Fujita, Y. Yoshikawa and H. Yamatera, *Chem. Lett.*, (1982) 437, and references cited therein.
14 J. N. Demas, T. F. Turner and G. A. Crosby, *Inorg. Chem.*, 8 (1969) 674.
15 T. Yukimoto and H. Yoneda, *J. Chromatogr.*, 210 (1981) 477.
16 R. E. Majors, *J. Chromatogr. Sci.*, 18 (1980) 488.
17 T. Fukuchi, N. Nagao, E. Miki, K. Mizumachi and T. Ishimori, *Bull. Chem. Soc. Jpn.*, 62 (1989) 2076.

Journal of Chromatography, 606 (1992) 43–48
Elsevier Science Publishers B.V., Amsterdam

CHROM. 24 264

Determination of the unusual amino acid hypusine at the lower picomole level by derivatization with 4-dimethylaminoazobenzene-4′-sulphonyl chloride and reversed-phase high-performance or medium-pressure liquid chromatography

Dirk Bartig and Friedrich Klink

Institut für Biochemie, Universität Kiel, Olshausenstrasse 40–60, 2300 Kiel (Germany)

(Received February 7th, 1992)

ABSTRACT

Hypusine, an unusual amino acid formed by post-translational modification of lysine, is normally determined by specific metabolic labelling followed by measurement of released radioactivity after protein hydrolysis. This paper describes a sensitive non-radioactive method for the determination of hypusine, involving complete protein hydrolysis and precolumn derivatization of the released amino acids with 4-dimethylaminoazobenzene-4′-sulphonyl chloride, followed by reversed-phase high-performance or medium-pressure liquid chromatography of the dabsylated derivatives. The detection limit of hypusine was about 500 fmol. Additionally, the hypusine-containing protein from the archaebacterium *Sulfolobus acidocaldarius* was purified. By applying the dabsylation method to the analysis of tryptic peptides derived from this protein, it was possible to determine the correct positioning of the hypusine residue in the amino acid sequence, which was not possible by the amino acid sequencing procedure alone.

INTRODUCTION

The post-translationally formed amino acid hypusine [N^{ε}-(4-amino-2-hydroxybutyl)lysine] occurs specifically in the eukaryotic initiation factor eIF-5A (formerly eIF-4D) [1]. The biosynthesis of this amino acid is performed in two steps. Firstly, in a transferase reaction, the aminobutyl moiety of spermidine is coupled to the ε-amino group of a specific lysine residue [2]. The second step consists in the hydroxylation of the newly formed deoxyhypusine by an unusual type of dioxygenase [3]. Until a few years ago, the occurrence of hypusine was considered to be a specific feature of the eukaryotic kingdom [4]. However, it was recently demonstrated that the synthesis of deoxyhypusine and hypusine is also common to all archaebacterial species so far investigated, but not to eubacteria [5,6]. In contrast to the eukaryotic hypusine-containing protein (HP), attempts to label specifically the archaebacterial HP by various *in vivo* [4,5] or *in vitro* [7] methods have not been successful until now. Considering this and the fact that there is as yet no functional test for the archaebacterial HP, we developed a sensitive non-radioactive method for the determination of hypusine, thus allowing the purification and analysis of the archaebacterial HP from *Sulfolobus acidocaldarius*. The details of the purification procedure and other results will be published elsewhere [8]. In this paper we report a procedure for the determination of picomole amounts of the HP by a precolumn derivatization method with 4-dimethylaminoazobenzene-4′-sulphonyl chloride (DABS-Cl). The de-

Correspondence to: Dirk Bartig, Institut für Biochemie, Universität Kiel, Olshausenstrasse 40–60, 2300 Kiel, Germany.

0021-9673/92/$05.00

tection limit of this method, its applicability in high-performance (HPLC) and medium-pressure liquid chromatographic (MPLC) systems and its use for the analysis of a hypusine-containing tryptic peptide is described.

EXPERIMENTAL

Materials

DABS-Cl was purchased from Fluka (Neu-Ulm, Germany) and recrystallized from boiling acetone as described [9]. Trifluoroacetic acid (TFA) and constant-boiling (c.b.) hydrochloric acid were obtained from Sigma (Deisenhofen, Germany), Amberlite CG 120 II (200–400 mesh) from Serva (Heidelberg, Germany), acetonitrile, isopropanol and water (all of HPLC grade) from Biomol (Hamburg, Germany) and trypsin (sequencing grade) from Boehringer (Mannheim, Germany). All other chemicals (analytical-reagent grade quality) were obtained from Merck (Darmstadt, Germany). Synthetic hypusine was a kind gift from T. Shiba, Osaka University, Japan.

Chromatographic equipment

The HPLC system consisted of a Model 2248 pump, a Model 2252 controller, a Rheodyne Model 7125 injection valve, a UV-M II detector (Pharmacia–LKB, Freiburg, Germany), an ERC 7215 UV detector and an ERC 3522 degasser (ERC, Alteglofsheim, Germany).

The MPLC system included two P-500 FPLC pumps, an LCC-500 controller, an MV-7 injection valve and a UV-M detector (Pharmacia–LKB). The column used for peptide chromatography was Hypersil C_{18}, 5-μm particle size (120 × 2 mm I.D.). A Spherisorb C_{18}, 5-μm particle size column (100 × 4.2 mm I.D., plus guard column) was employed in the separation of DABS derivatives.

Analysis of tryptic peptides derived from HP

Purified HP from *S. acidocaldarius* was dissolved in 100 μl of 100 m*M* NH_4HCO_3–0.02% Tween 20 (pH 7.3) and trypsin was added in a weight ratio of 1:50 (trypsin:substrate). The reaction was performed at 37°C for 6 h and was stopped by the addition of formic acid. The peptide mixture was separated by reversed-phase HPLC using a 70-min linear gradient from 5 to 80% acetonitrile in 0.1% TFA at a flow-rate of 0.4 ml/min. The absorbance of the eluate was measured at 214 nm and peaks were collected manually.

Hydrolysis procedures

Protein amounts of more than 20 μg were hydrolysed in small flame-sealed glass tubes (60 × 4 mm I.D.) after adding 30–50 μl of c.b. HCl. Aliquots of pure HP or tryptic peptides were pipetted into the bottom of small glass tubes, dried under vacuum and then subjected to gas-phase hydrolysis in a vacuum hydrolysis vessel (Waters, Eschborn, Germany) after addition of 300 μl of c.b. HCl and applying a vacuum of $\leqslant$0.2 mbar. All hydrolyses were carried out at 110°C for 24 h.

Prepurification of hypusine

Because of the large amounts of other amino acids ($\geqslant$300-fold excess) in hydrolysates, the direct determination of hypusine required the incorporation of a prepurification step. This procedure was performed on a small Amberlite CG 120 II column (4 ml of resin, NH_4^+ form). The protein hydrolysate was bound to the resin previously equilibrated with water and eluted stepwise with 7 ml of 0.5 *M* NH_4^+ and 5 ml of 1.5 *M* NH_4^+. The eluate from the last step was collected in fractions of 0.5 ml and lyophilized.

Dabsylation procedure

The derivatization reaction was carried out in a small glass tubes (40 × 4 mm I.D.) previously pyrolysed overnight at 500°C in a muffle oven. A 4 m*M* stock solution of DABS-Cl in acetonitrile was always prepared freshly. Dried aliquots of samples or standard amino acids (2 nmol) were dissolved in 10 μl of 100 m*M* $NaHCO_3$ (pH 8.4) and 20 μl of DABS-Cl solution were added. The reaction mixture was shaken carefully, stoppered with a silicone-rubber plug and allowed to react for 10 min at 70°C. After cooling to room temperature, the solution was diluted by adding 50 m*M* phosphate (pH 7.0)–ethanol (1:1, v/v) [11,14].

Analysis of DABS derivatives

DABS–hypusine (DABS–Hpu) was separated from all other DABS derivatives using an elution system of 25 m*M* sodium acetate (pH 6.5) (buffer A) and acetonitrile (buffer B). For analysis of the hydrolysed tryptic peptides, the elution system con-

sisted of 33 m*M* sodium acetate (pH 6.3) (buffer A) and acetonitrile–isopropanol (4:1) (buffer B). DABS derivatives were detected by measuring the absorbance at 436 nm and concentrations were calculated by integration of peak areas.

RESULTS AND DISCUSSION

Reversed-phase HPLC and MPLC of DABS–Hpu

As shown in Fig. 1 DABS–Hpu is separated by reversed-phase HPLC within 25 min from all other DABS derivatives, specially from DABS–Lys, the only remaining basic amino acid after prepurification of the hydrolysates with a similar retention time to DABS–Hpu. Although the elution positions are not shown in Fig. 1, both DABS–His and DABS–Ty r would elute shortly after DABS–Lys, but still before DABS–Hpu, so that it is possible to analyse directly a hydrolysate of pure HP using this gradient system.

The determination of DABS–Hpu using a reversed-phase MPLC system is presented in Fig. 2 Owing to the lower pressure limit of the MPLC apparatus, the flow-rate had to be reduced to 0.3 ml/min, thus allowing the application of the same buffer–column system as used in reversed-phase HPLC. The disadvantage of the MPLC system is a comparatively noisy baseline, resulting in a detection limit poorer than 1 pmol of DABS–Hpu, and a much longer analysis time. However, it has been clearly demonstrated that the dabsylation method

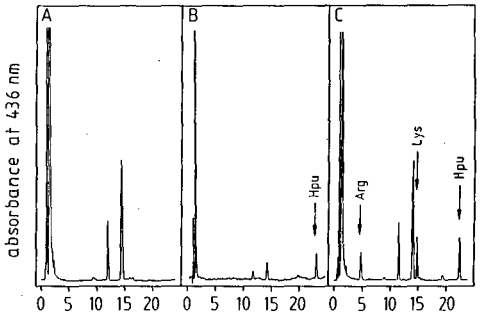

Fig. 1. Reversed-phase HPLC determination of DABS–Hpu on a Spherisorb ODS column. The column (100 × 4.2 mm I.D. plus guard column) was eluted with a 24-min linear gradient from 30–58% acetonitrile (buffer B) in 25 m*M* sodium acetate (pH 6.5) (buffer A) at a flow-rate of 1 ml/min and room temperature. (A) Blank; (B) 1 pmol of DABS–Hpu; (C) Amberlite CG 120 II prepurified protein hydrolysate.

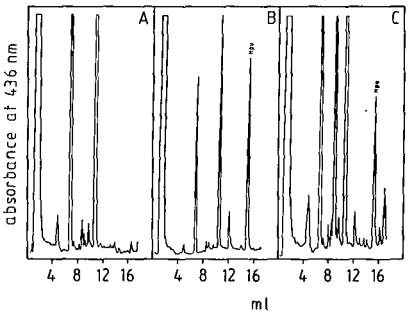

Fig. 2. Reversed-phase MPLC determination of DABS–Hpu on a Spherisorb ODS column. Column and buffers as in Fig. 1; flow-rate, 0.3 ml/min. The gradient shape was 2 ml isocratic at 35% B and then linear from 35 to 60% B in 15 ml. (A) Blank, (B) 4 pmol of DABS-Hpu; (C) Amberlite CG 120 II prepurified protein hydrolysate.

for the sensitive determination of hypusine is applicable using short HPLC columns in a system working in the medium pressure range.

Detection limit

The detection limit for DABS–Hpu in the HPLC system using the "fast" gradient run (Fig. 1) is 500 fmol of hypusine standard with an acceptable signal-to-noise ratio. This method is about 800 times more sensitive than the previously used ninhydrin system in a Biotronik LC 5001 amino acid analyser [5,6] and a ten-fold improvement on the most sensitive non-radioactive method described so far [10]. Owing to the low flow-rate resulting in a more unstable baseline, the sensitivity of the MPLC system was only half that of the HPLC system, although amounts of $\geqslant 1$ pmol DABS–Hpu could be readily determined. The overall detection limit for the determination of hypusine in a hydrolysate originating from pure HP or hypusine-containing peptides was about ten times lower in relation to hypusine standard as a maximum of 10% of the reaction mixture should be injected for analysis. Injections of larger amounts of reaction mixture impaired the resolution owing to the presence of interfering by-products.

The relationship between the amount of DABS–Hpu injected and the resulting peak area was linear over a broad range (Fig. 3). The detector response showed good reproducibility, with a maximum relative standard deviation of 2.4% ($n = 3$). The

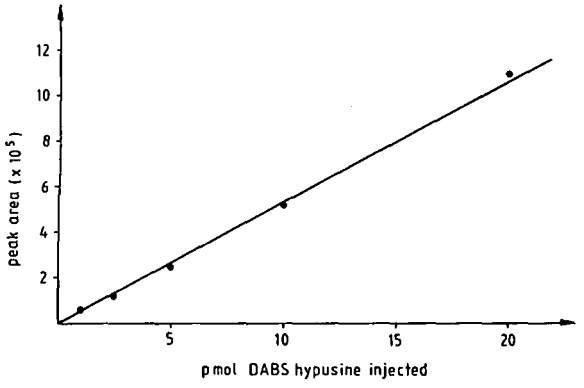

Fig. 3. Concentration–peak area relationship for different amounts of injected DABS–Hpu.

relative standard deviation for the retention time of DABS–Hpu was 0.26% (n = 12).

Discussing the detection limit of the hypusine determination in hydrolysates deriving from a mixture of proteins, the influence of the necessary prepurification step must also be considered. This prepurification procedure for hydrolysates was unavoidable if hypusine was present in only trace amounts compared with the other amino acids in the reaction mixture. Molar ratios above 1:300 (hypusine to other amino acids) resulted in incomplete derivatization of hypusine and other amino acids, because a critical excess of reagent over derivatizable groups is necessary in order to avoid artefact peaks in the reversed-phase chromatogram. On the other hand, large amounts of reagent in the injected sample gave rise to an unstable baseline, thus disturbing the determination of picomole amounts of hypusine. To solve this problem, the bulk of contaminating amino acids was eliminated by chromatography on a small Amberlite CG 120 II ion-exchange column. Most amino acids were eluted by the first step (0.5 M NH_4^+). Because of its basic properties, hypusine was bound very tightly to the resin and could be separated from all other amino acids by increasing the NH_4^+ concentration in the second elution step. Only minor amounts of the basic amino acids lysine and arginine were found in the hypusine-containing fraction(s). The use of this prepurification step was limited by the fact that the chromatography of very small amounts of hypusine on the Amberlite column resulted in loss of hypusine, probably caused by irreversible binding of hypusine to the resin or by dilution effects during elution. Lowering the volume of the column to minimize this problem resulted in a decrease in resolving power. The system described here can therefore be used in the purification of a minimum of 20 pmol of hypusine (equivalent to the same amount of HP) if the hydrolysate has to be prepurified. Screening other ion-exchange materials for the prepurification step may lead to the possibility of chromatographing smaller amounts of hypusine, thus enabling more advantage to be taken of the detection limit of the reversed-phase HPLC system.

Analysis of the hypusine-containing tryptic peptide.

As hypusine is formed by post-translational modification of a lysine residue, sequencing of the HP-gene can only reveal the position of the codon for the potential hypusine precursor. Moreover, direct amino acid sequencing yielded no signal for released hypusine, owing to the strong hydrophobicity of the PTH–hypusine [12]. Hence, the only way to verify the correct position of hypusine in the sequence is by comparison of sequence data with amino acid composition of defined short peptides (including the hypusine residue) resulting from chemical or enzymatic cleavage of HP.

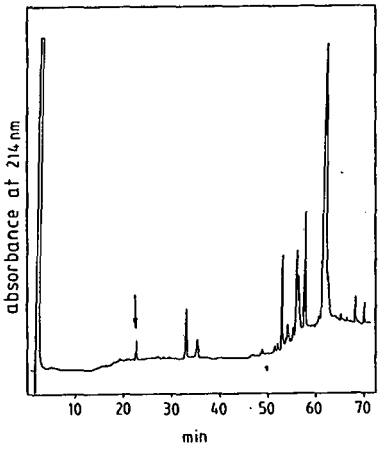

Fig. 4. Reversed-phase HPLC of tryptic peptides derived from HP of *S. acidocaldarius*. The fragments resulting from a tryptic digest of 10 μg of HP were separated on a Hypersil C_{18} column (120 × 2 mm I.D.) with a linear 70-min gradient from 5 to 80% acetonitrile in 0.1% TFA at a flow-rate of 0.4 ml/min. Peaks were collected manually. The tryptic peptide containing hypusine is marked with an arrow.

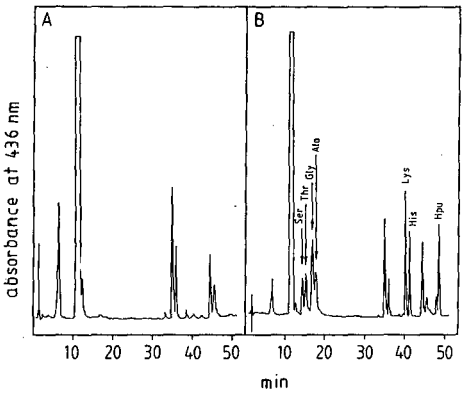

Fig. 5. Reversed-phase HPLC of DABS–amino acids resulting from the hypusine-containing tryptic peptide. The separated tryptic fragments (see Fig. 4) were lyophilized, gas-phase hydrolysed and dabsylated. The DABS derivatives were determined using a Spherisorb C_{18} column with an elution system of 33 m*M* sodium acetate (pH 6.3) (buffer A) and acetonitrile–isopropanol (4:1) (buffer B). The gradient was 2 min at 15% B, 3 min from 15 to 22% B, 9 min from 22 to 23% B, 1 min at 23% B, 5 min from 23 to 24% B, 20 min from 24 to 62% B and 2 min at 62% B at a flow-rate of 1 ml/min at room temperature. (A) Blank; (B) analysis of the hypusine-containing tryptic peptide.

Fig. 4 illustrates the separation of the hypusine-containing tryptic peptide. It can be seen that the hypusine-containing fragment was eluted in the earlier part of the gradient, thus suggesting a very hydrophilic composition of this peptide. This conclusion was confirmed by analysis of the DABS derivatives resulting from gas-phase hydrolysis of the isolated peptide. The determination of the amino acid composition of the tryptic hypusine-containing peptide is shown in Fig. 5 and Table I. The resulting sequence, after comparison of the data obtained with this method and those obtained from direct sequencing, is shown in Table II.

For the complete separation and determination of all amino acids derived from this peptide, the buffer composition and gradient shape in reversed-phase HPLC had to be altered. Because of their very similar elution behaviour in reverse-phase systems, DABS–Gly and DABS–Ala are not fully resolved, probably owing to the use of a short column. Several other workers have demonstrated the complete baseline separation of all proteinogenic DABS–amino acids using a longer column or higher column

TABLE I

AMINO ACID COMPOSITION OF THE HYPUSINE-CONTAINING TRYPTIC PEPTIDE FROM *S. ACIDOCALDARIUS*

Amino acid	Amount (pmol)	Residues
Ala	203	1
Gly	523	2
His	225	1
Lys	246	1
Ser	208	1
Thr	264	1
Hpu	220	1
Total	1889	8

TABLE II

COMPARISON OF HYPUSINE-CONTAINING TRYPTIC PEPTIDES FROM ARCHAEBACTERIA AND EUKARYOTES

Tryptic peptides derived from the HP of *S. acidocaldarius* were sequenced by direct amino acid sequencing [12] and by analysis of the amino acid composition after dabsylation. For comparison, the sequence of the corresponding eukaryotic tryptic peptide from human red blood cells is aligned (data taken from ref. 13).

Sequence[a]	Position of amino acid							
	1	2	3	4	5	6	7	8
A	Thr	Gly	Xaa[b]	His	Gly	Ser	Ala	Lys
B	Thr	Gly	Hpu	His	Gly	Ser	Ala	Lys
C	Thr	Gly	Hpu	His	Gly	His	Ala	Lys

[a] A = Sequence resulting from direct amino acid sequencing of the tryptic peptide from *S. acidocaldarius*. B = Sequence resulting from comparison of (A) with amino acid composition after analysis of DABS derivatives from this peptide (see Table I). C = Sequence of the corresponding eukaryotic peptide.

[b] Xaa = No signal during sequencing procedure.

temperatures [11,14–17]. It should thus be possible to combine and adapt these methods for the simultaneous determination of the common amino acids and hypusine, as the elution conditions can always be adjusted such that DABS–Hpu elutes after the last common DABS derivative (DABS–Tyr).

CONCLUSIONS

Use of the DABS-Cl precolumn derivatization method followed by reversed-phase HPLC or MPLC for the determination of hypusine can replace the need for radioactive labelling of HP and hypusine. This allows the isolation and characterization of further HPs from other archaebacteria on an analytical scale, as only picomole amounts of HP are needed for the determination of hypusine. In combination with narrow-bore reversed-phase HPLC, tryptic peptides from nanogram amounts of different HPs can be analysed for amino acid composition and compared with reference to the conservation of the special hypusine-surrounding sequence.

ACKNOWLEDGEMENTS

We thank Dr. F. Lottspeich, MPI, Martinsried, Germany, for amino acid sequencing of the tryptic peptide. This work was supported by a grant from the Deutsche Forschungsgemeinschaft.

REFERENCES

1 H. C. Cooper, H. M. Park, J. E. Folk, B. Safer and R. Braverman, *Proc. Natl. Acad. Sci. U.S.A.*, 80 (1983) 1854.
2 E. Wolff, M. H. Park and J. E. Folk, *J. Biol. Chem.*, 265 (1990) 4793.
3 A. Abbruzzese, M. H. Park and J. E. Folk, *J. Biol. Chem.*, 261 (1986) 3085.
4 E. D. Gordon, R. Mora, S. C. Meredith, C. Lee and S. C. Lindquist, *J. Biol. Chem.*, 262 (1987) 1658.
5 H. Schümann and F. Klink, *System. Appl. Microbiol.*, 11 (1989) 103.
6 D. Bartig, H. Schümann and F. Klink, *System. Appl. Microbiol.*, 13 (1990) 112.
7 D. Bartig, unpublished results.
8 D. Bartig, K. Lemkemeier, J. Frank, F. Lottspeich and F. Klink, *Eur. J. Biochem.*, 204 (1992) 751.
9 J.-Y. Chang, R. Knecht and D. Braun, *Methods Enzymol.*, 91 (1983) 41.
10 S. Beninati, A. Abbruzzese and J. E. Folk, *Anal. Biochem.*, 184 (1990) 16.
11 G. Hughes, S. Frutiger and C. Fonck, *J. Chromatogr.*, 389 (1987) 327.
12 F. Lottspeich, personal communication.
13 M. H. Park, T.-Y. Liu, S. H. Neece and W. J. Swiggard, *J. Biol. Chem.*, 261 (1986) 14515.
14 H. J. Schneider, *Chromatographia*, 28 (1989) 45.
15 U. Stocchi, C. Cucchionini, G. Piccoli and M. Magnani, *J. Chromatogr.*, 349 (1985) 77.
16 J. Vendrell and F. X. Avilés, *J. Chromatogr.*, 358 (1986) 401.
17 R. Knecht and J.-Y. Chang, *Anal. Chem.*, 58 (1986) 2375.

Journal of Chromatography, 606 (1992) 49–53
Elsevier Science Publishers B.V., Amsterdam

CHROM. 24 259

Determination of peroxycarboxylic acids by high-performance liquid chromatography with electrochemical detection

Ole Kirk, Ture Damhus and Morten Würtz Christensen

Novo Nordisk A/S, Novo Allé, DK-2880 Bagsvaerd (Denmark)

(First received January 8th, 1992; revised manuscript received April 10th, 1992)

ABSTRACT

A sensitive high-performance liquid chromatographic method employing reversed-phase chromatography and amperometric detection of low levels of peroxycarboxylic acids is described. Detection limits of 0.1–0.6 μM and linear dynamic ranges of at least 0.05–5 mM were obtained. As a consequence of the high sensitivity and selectivity provided by the electrochemical detector, the method is well suited for detection of various peroxycarboxylic acids even in the complex matrices represented by detergent solutions. As an illustration of the applicability of the system developed, the levels of various peroxycarboxylic acids were monitored in the course of a washing cycle performed with some commercially available detergents.

INTRODUCTION

Systems that generate peroxycarboxylic acids have become an important component in detergents over the last few decades as these highly oxidizing chemicals provide effective bleaching of a broad range of stains at low temperatures, without damaging coloured fabrics [1,2]. Owing to their aggressive nature and poor storage stability, the peroxycarboxylic acids are preferably formed *in situ* by perhydrolysis of bleach activators, *i.e.* by lysis of activated acyl compounds with hydrogen peroxide, the latter provided by peroxy salts, *e.g.* sodium perborates. The most frequently used bleach activators are tetraacetylethylenediamine (TAED) and sodium nonanoyloxybenzenesulphonate (NOBS) (Fig. 1), which form peroxyacetic and peroxynonanoic acid, respectively, upon perhydrolysis.

As bleach activators have found their way into detergents, the need for analytical methods capable of monitoring peroxycarboxylic acids in the presence of a large excess of hydrogen peroxide has emerged. The levels to be detected are in the low millimolar range and occur in the rather complex matrix of a detergent solution, comprising surfactants, builders (phosphates, zeolites), enzymes and various other components.

The analytical methods that have been described so far are largely based upon either titration or spectrophotometry. Hydrogen peroxide may be titrated initially with cerium(IV) sulphate followed by determination of the remaining peroxyacid by

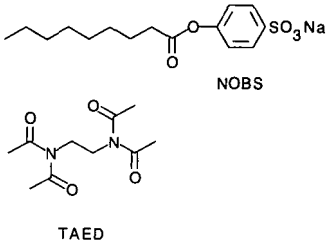

Fig. 1. Structures of TAED and NOBS.

Correspondence to: Dr. Ole Kirk, Diabetes Research, Novo Nordisk A/S, 2880 Bagsvaerd, Denmark.

0021-9673/92/$05.00

iodometry [3]. In another approach, the much higher reactivity of iodide with peroxyacids compared with hydrogen peroxide is utilized and liberated iodine is titrated with thiosulphate [4]. Alternatively, the liberated iodine can be determined photometrically [5]. Recently, the different rate of oxidation of methyl phenyl sulphoxide by peroxyacids and hydrogen peroxide has been utilized in a gas–liquid chromatographic method [6].

The above methods share several disadvantages. First of all, no method reported so far has been able distinguish between various peroxycarboxylic acids, which would be relevant if, for example, TAED and NOBS were combined in a detergent formulation. Second, the methods described are rather time-consuming and suffer from quite high detection limits. The aim of this study was to develop a fast and sensitive high-performance liquid chromatographic (HPLC) method allowing selective detection of various peroxycarboxylic acids and, preferably, also hydrogen peroxide, directly in washing liquors.

EXPERIMENTAL

Chemicals

All chemicals were of analytical grade and most were purchased from Merck (Darmstadt, Germany). Hydrogen peroxide was obtained either as a 30% (w/w) solution (Merck) or as a 60% (w/v) solution (BDH, UK). Peroxyacetic acid was obtained as Proxitane 4002, a solution determined to be 6.7 *M* with respect to peroxyacetic acid, 8.4 *M* with respect to acetic acid and 1.2 *M* with respect to hydrogen peroxide (and also containing, presumably, traces of strongly acidic catalyst), from Peroxide-Chemie (Germany). The surface-active agents Berol 08 and Nansa 1127 were obtained from Berol (Sweden) and Albright & Wilson (UK), respectively. The experimental lipase preparation was made in house (Novo Nordisk, Denmark). All solvents for HPLC were purchased from Rathburn (Walkerburn, UK).

Reference detergent

As a reference detergent without bleaching agents, we used a heavy-duty powder detergent with phosphate builder, containing the following ingredients (%, w/w): sodium triphosphate (36.7), sodium sulphate (42.0), sodium metasilicate (8.4), carboxymethylcellulose (1.0), EDTA (0.2), fatty alcohol ethoxylate (Berol 08, 3.8), linear alkylbenzenesulphonate (Nansa 1127, 7.8) and an experimental detergent–lipase preparation (0.1). Solutions were made by dosing 5 g/l of the detergent.

Peroxycarboxylic acid standards

Long-chain crystalline peroxycarboxylic acids were synthesized according to Parker *et al.* [7] by oxidation of the parent carboxylic acid with 60% (w/v) hydrogen peroxide, using sulphuric acid as catalyst. The content of active peroxyacid in the preparations was determined by iodometry in a 3:2 (v/v) mixture of glacial acetic acid and chloroform, performed under nitrogen to exclude air. The contents of peroxyacetic acid and acetic acid in the above-mentioned Proxitane preparation were determined by titration with sodium hydroxide and the content of hydrogen peroxide by cerimetry. UV spectra were recorded on an 8452A diode-array spectrophotometer (Hewlett-Packard, USA).

Experiments with commercial detergents

The experiments in which the peroxycarboxylic acid evolution was followed in commercial detergents were all performed at 40°C. The detergents were dosed according to the manufacturers [5 g/l for the European detergents OMO Micro (Unilever) and Ariel Ultra (Procter & Gamble), and 1.2 g/l for the American detergent Tide With Bleach (Procter & Gamble)]. The experiments were performed in open beakers using tap water (5 l, of a total hardness equivalent to approximately 3.2 m*M* Ca^{2+}) and magnetic stirring (500 rpm). The levels of peroxyacids and hydrogen peroxide were expressed as the mean value of five repeated experiments.

Chromatographic apparatus and conditions

The chromatographic apparatus consisted of an LC-6A HPLC pump (Shimadzu, Japan) equipped with an additional external pulse damper (Shimadzu) and a Type 7125 injection valve (Rheodyne, Cotati, CA, USA). Solvents were degassed using a Type ERC-3110 degasser (Erma Optical Work, Japan). A LiChrosorb RP-18 (10 μm) reversed-phase column (250 × 4.6 mm I.D.) was used with a LiChroCART RP-18 (10 μm) guard column, both supplied by Merck. As the mobile phase, 100 m*M* phosphate buffer (adjusted to pH 6) was used for the

detection of peroxyacetic acid or 15 m*M* phosphate buffer (adjusted to pH 6)–methanol (30:70, v/v) for the detection of long-chain peroxycarboxylic acids. Sodium chloride was further added to a concentration of 5 m*M*. The mobile phases were filtered prior to use. The flow-rate was 1.5 ml/min.

The HPLC system was connected to an AMOR amperometric detector (Spark Holland, Netherlands) equipped with a platinum working electrode and a Ag/AgCl reference electrode. Cleaning of the working electrode was done either by wiping it off with a tissue moistened in acetone or ethanol or, after more severe loss in activity, by polishing it according to the manufacturer's guidelines. Of various potential settings tested, a potential of −0.27 V *versus* the reference electrode was found to be suitable for the detection of both peroxycarboxylic acids and hydrogen peroxide. At this potential the compensation current was typically 100–200 nA. In front of the amperometric detector an SPD-6A UV detector (Shimadzu) was inserted. Both detectors were linked to a Shimadzu C-R5A two-channel integrator. Peak areas were taken to represent analyte concentrations. All chromatography and detection was carried out at ambient temperature. However, the AMOR detector comprises an insulated chamber in which the amperometric cell as well as the column are mounted to reduce the influence of temperature fluctuations.

Sample preparation

Pure solutions of reference compounds were injected directly into the HPLC system. Detergent solutions were, however, filtered on a 0.45-μm Minisart disposable filter (Sartorius, Germany) prior to injection. A 20-μl injection volume was used in all experiments.

RESULTS AND DISCUSSION

Initially, we attempted to develop an HPLC system using UV detection. Peroxycarboxylic acids were found to have maximum UV absorbance at 206 nm. Accordingly, using this wavelength and the conditions described above, the detection limit was found to be around 50 μ*M* (*e.g.* 0.17 μg of peroxynonanoic acid) at a signal-to-noise ratio of 3 when analysing solutions of pure preformed peroxycarboxylic acids. However, as illustrated in Fig. 2A, when analysing a 0.2 m*M* solution of peroxyacetic acid (made from a commercial preparation further containing acetic acid, hydrogen peroxide and traces of strongly acidic catalyst), the peroxyacid proved difficult to separate from the other components even though the mobile phase was buffered at pH 6, which should keep the peroxyacid protonated (pK_a of peroxyacetic acid is *ca.* 8.3 as determined from the base titration) while dissociating other acids, *e.g.* acetic acid. Furthermore, addition of 5 g/l of the reference detergent without bleaching agent described above made detection of even higher concentrations of peroxyacetic acid impossible owing to huge absorptions of the various other components in the complex matrix (Fig. 2B).

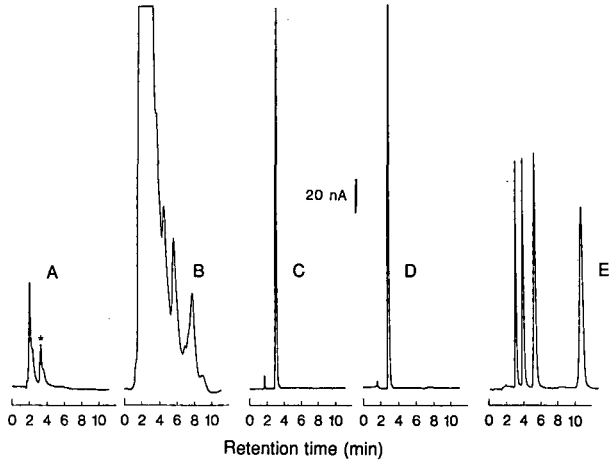

Fig. 2. Chromatograms of 0.2 m*M* solutions of peroxyacetic acid (✳): (A) reference solution, UV detection; (B) detergent solution, UV detection; (C) reference solution, electrochemical detection; (D) detergent solution, electrochemical detection; (E) chromatogram of a 0.1 m*M* solution of peroxyoctanoic, peroxynonanoic, peroxydecanoic and peroxydodecanoic acids (eluted in the order given). Integrator attenuation used: UV detector, 2^2; electrochemical detector, 2^4.

To overcome the interference from other components in a detergent solution, reductive electrochemical detection was attempted as an alternative. This detection principle has previously been applied advantageously for detection of various organic hydroperoxides [8]. Using a platinum electrode and the conditions described above, amperometric detection fulfilled all demands with respect to sensitivity and selectivity, as illustrated by the chromato-

grams obtained when analysing the same solutions of peroxyacetic acid as described above (Fig. 2C and D). Evidently, only the peroxyacid and hydrogen peroxide (in the front of the chromatogram) are detected by the electrochemical system. Examining the chromatogram obtained after addition of the reference detergent, an identical response was found in the case of peroxyacetic acid while the signal originating from hydrogen peroxide was markedly reduced. This effect was found to be the result of decomposition caused by catalase present in the lipase preparation added to the reference detergent used.

Detection of various peroxycarboxylic acids

As gradient elution is poorly compatible with electrochemical detection, different mobile phases were applied for the detection of various peroxycarboxylic acids. The chromatogram obtained when analysing a mixture of peroxyoctanoic, peroxynonanoic, peroxydecanoic and peroxydodecanoic acids using a mobile phase containing 70% (v/v) methanol is illustrated in Fig. 2E. Obviously, hydrogen peroxide has no retention in a reversed-phase chromatographic system and is eluted in the front of a chromatogram. The system described is, accordingly, in principle not suitable for quantification of hydrogen peroxide levels. However, as the bleaching agents, as indicated in Fig. 2, are the only compounds giving detector response in a typical detergent matrix, the area of the signal in the front of the chromatogram was found to be applicable as a rough indicator of the hydrogen peroxide level in a sample, provided the concentration was in the range 1–10 m*M*.

Detection limits, linearity and repeatability of the system

The detector response was optimized by varying the potential of the working electrode *versus* the reference electrode. Fig. 3 shows the peak area–voltage curves for peroxydecanoic and peroxyacetic acids as well as hydrogen peroxide. Based on the curves, a potential of −0.27 V was chosen as a compromise. Although higher potentials would increase the detector signal, which would be particularly desirable in the case of hydrogen peroxide, this would also increase the background noise owing to deterioration of the mobile phase, indicated by the dramatic increase in compensation current on the figure. The pH dependency of the amperometric reaction was not studied in detail. However, an almost similar response was observed when analysing peroxyacetic acid using a 100 m*M* acetic buffer with a pH of 4 as mobile phase.

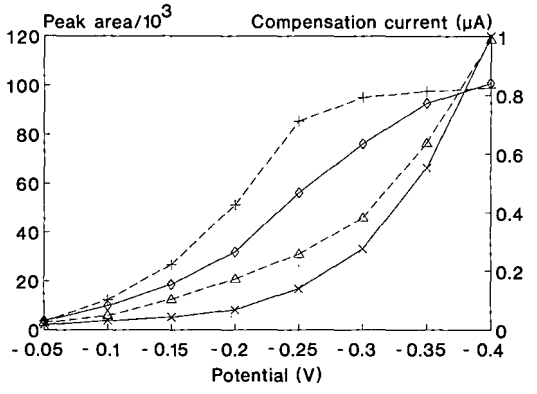

Fig. 3. Peak area–voltage curves for 0.1 m*M* peroxydecanoic acid (+), 0.1 m*M* peroxyacetic acid (◇) and 2 m*M* hydrogen peroxide (△). Compensation current of detector when measuring peroxyacetic acid or hydrogen peroxide (right *y*-axis, ×).

Using a potential of −0.27 V, the detection limit was determined to be 0.1 μ*M* (0.15 ng) in the case of peroxyacetic acid (signal-to-noise ratio of 3) and the calibration graph was linear at least in the range 0.05–5 m*M* (r^2 = 0.9999, n = 4). Using the methanol-containing mobile phase the detection limit was determined to be 0.6 μ*M* in the case of peroxynonanoic acid and a linear calibration graph was observed in the range 0.05–5 m*M* (r^2 = 0.9998, n = 4).

The repeatability of the system was found to be satisfactory as the relative standard deviation on ten analyses performed on the same day using a 0.5 m*M* solution (chosen to represent a typical concentration in a detergent solution) of peroxynonanoic acid was determined to be only 1.6%. Wear of the working electrode was very moderate under the conditions described and the system was, normally, used for several weeks without cleaning the electrode. As outlined above, the system was also used to indicate levels of hydrogen peroxide. The standard deviation on ten analyses performed on the same day using a 2.5 m*M* solution of hydrogen peroxide was found to be 2.7%. Estimation of hydrogen peroxide levels was, however, not reliable below a level of 1 m*M*

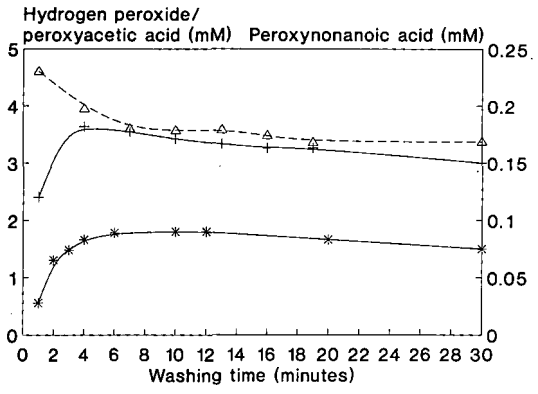

Fig. 4. Hydrogen peroxide level (△) and formation of peroxyacetic acid (+) in a washing liquor containing OMO Micro and formation of peroxynonanoic acid (*) in a washing liquor containing Tide With Bleach.

while a linear calibration curve was obtained in the range 1–10 mM (r^2 = 0.9992, n = 4).

Applicability of the method

The system is used routinely in our laboratory to study the peroxycarboxylic acid formation in the course of a washing cycle when employing various detergents. As an illustration of the applicability of the system, Fig. 4 shows the observed level of hydrogen peroxide and the formation of peroxyacetic acid in a washing liquor made using the TAED-containing detergent OMO Micro (left y-axis) and formation of peroxynonanoic acid in a solution of the NOBS-containing detergent Tide With Bleach (right y-axis). Hydrogen peroxide levels are not illustrated in the case of Tide With Bleach as they were found to be beyond the detection limit of 1 mM. Analysing a second TAED-containing detergent, Ariel Ultra, the peroxyacid formation was found to resemble closely that of OMO Micro, but reaching only roughly 2 mM peroxyacetic acid (results not shown).

CONCLUSION

Compared with the methods described previously in the literature for detecting peroxycarboxylic acids, the HPLC system developed provides a fast, highly sensitive and selective system which, furthermore, is capable of distinguishing between various peroxycarboxylic acids. However, the development of a single chromatographic system capable of detecting a broader range of peroxycarboxylic acids simultaneously could still be desirable.

ACKNOWLEDGEMENT

The skillful experimental work of Ole F. Pedersen is highly appreciated.

REFERENCES

1 K. Grime and A. Clauss, *Chem. Ind.*, (1990) 647.
2 T. A. B. M. Bolsman, R. Kok and A. D. Vreugdenhil, *J. Am. Oil Chem. Soc.*, 65 (1988) 1211.
3 F. P. Greenspan and D. G. Mackellar, *Ann. Chem.*, 20 (1948) 1061.
4 B. D. Sully and P. L. Williams, *Analyst (London)*, 87 (1962) 653.
5 M. D. Davies and M. E. Deary, *Analyst (London)*, 113 (1988) 1477.
6 F. Di Furia, M. Prato, U. Quintily, S. Salvagno and G. Scorrano, *Analyst (London)*, 109 (1984) 985.
7 W. E. Parker, C. Ricciuti, C. L. Ogg and D. Swern, *J. Am. Chem. Soc.*, 77 (1955) 3037.
8 M. O. Funk, Jr. and W. J. Baker, *J. Liq. Chromatogr.*, 8 (1985) 633.

Journal of Chromatography, 606 (1992) 55–64
Elsevier Science Publishers B.V., Amsterdam

CHROM. 24 253

Affinity partitioning of enzymes in aqueous two-phase systems containing dyes and their copper(II) complexes bound to poly(ethylene glycol)

Vilius Žutautas, Birutė Baškevičiūtė and Henrikas Pesliakas

Department of Biotechnology, Institute of Applied Enzymology, Fermentas, Fermentu 8, Vilnius 232028 (Lithuania)

(First received December 30th, 1991; revised manuscript received March 23rd, 1992)

ABSTRACT

Affinity partitioning of lactate dehydrogenase from rabbit muscle was studied in aqueous two-phase systems containing many dyes bound to poly(ethylene glycol), and partitioning of lactate dehydrogenase and yeast glucose-6-phosphate dehydrogenase was studied with PEG derivatives containing Cu(II) complexes of the Red-Violet 2KT, Red-Brown 2KT and Claret 4CT. It was established that lactate dehydrogenase showed a higher affinity when it interacted with dyes without Cu^{2+} ions in their structure. Investigation of the partitioning of enzymes when sodium chloride, nucleotide ligands or chelating agents were introduced into two-phase systems showed that with the Cu(II) complex of Red-Brown 2KT the presence of Cu^{2+} ions in the dye resulted in partial loss of the specificity of its interaction with lactate dehydrogenase. In contrast to lactate dehydrogenase, the Cu(II) complex of this dye showed selectivity to glucose-6-phosphate dehydrogenase from yeast.

INTRODUCTION

Aqueous phase systems composed of poly(ethylene glycol) (PEG) and dextran or of PEG and salts have been successfully used for the extraction and purification of biomacromolecules [1–3]. Affinity partitioning of enzymes and proteins is a particular case of the partitioning technique. This technique is based on specific interaction of biomacromolecules with an affinity ligand covalently coupled to one of the phase system forming polymer. Consequently, a protein or an enzyme is preferentially concentrated in the phase containing the covalently attached ligand. Various fatty acids [4,5], alcohols [6], coenzymes [7] and triazine dyes [7–14] are useful as affinity ligands. Phase systems containing dyes as specific ligands are widely applied in the investigation of the affinity of biomacromolecules to triazine dyes [4,10,13,14].

Previously, we used the affinity partitioning technique for the comparative study of the interaction of the alcohol dehydrogenases (ADH) from yeast and horse liver with various dyes [15]. It was found that affinity partitioning of both ADH in two-phase systems containing dyes was most effective using Cu (II) complexes of the dyes Light Resistant Yellow 2KT, Red-Violet 2KT and Red-Brown 2KT (horse liver ADH). It was concluded [15] that the interaction of horse liver ADH with some dyes was also dependent on the presence of Cu^{2+} ions, and it was also assumed that the binding of enzyme to dyes might occur through the formation of the mixed Cu(II) complexes involving donor groups of the dyes and amino acid residues of the enzyme in a similar manner to yeast ADH. However, investigation of the interaction of yeast ADH and lactate dehydrogenase (LDH) from rabbit muscle with some dyes, *i.e.*, Yellow 2KT, Orange 5K and Light Resistant Yellow 2KT, in solution by differential

Correspondence to: Dr. H. Pesliakas, Department of Biotechnology, Institute of Applied Enzymology, Fermentas, Fermentu 8, Vilnius 232028, Lithuania.

0021-9673/92/$05.00

and induced circular dichroism spectroscopy and chromatography on dye–adsorbents showed [16] that LDH interacted more specifically with dyes containing no metal ions.

In this work, the interaction of LDH from rabbit muscle with a range of dyes and dye–Cu(II) complexes was studied more thoroughly. Affinity partitioning of yeast glucose-6-phosphate dehydrogenase (G6PDH) in two-phase systems containing Cu (II) complexes of Red-Violet 2KT, Red-Brown 2KT and Claret 4CT attached to PEG was also studied for elucidation of the Cu^{2+} ions role.

EXPERIMENTAL

Chemicals

Lactate dehydrogenase from rabbit muscle and glucose-6-phosphate dehydrogenase from yeast were purchased from Serva (Heidelberg, Germany). Poly(ethylene glycol) PEG 6000 (mol. wt. 6000–7500) was obtained from Serva or Fluka (Basle, Switzerland) and dextran 60 000 (mol. wt. 60 000 ± 10 000 from the Factory of Clinical Preparations (Krasnojarsk, Russia). Tris, NADH, pyruvic acid, imidazole, adenine and glycylglycine were obtained from Sigma (St. Louis, MO, USA) and NADP and glucose-6-phosphoric acid disodium salt from Reanal (Budapest, Hungary). Reactive dyes were of local production, or obtained from Serva or Sigma [15]. All other chemicals were of analytical-reagent or high-purity grade.

Synthesis of dye–PEG derivatives

The dye-liganded PEGs were synthesized according to the method of Johansson and Joelsson [13] modified in such a manner that dye–PEGs were extracted supplementarily with chloroform before the chromatographic purification steps. After extraction, the dye–PEG derivatives were purified on columns of DEAE-cellulose DE-52 (Whatman, Maidstone, UK), and isolated by chloroform extraction. Cu^{2+} ions were removed from the PEG–Light Resistant Yellow 2KT,–Red-violet 2KT and –Red-Brown 2KT conjugates by washing these conjugates adsorbed on an anion exchanger (DEAE-cellulose or macroporous silica supports possessing anion-exchange groups) with 0.1 *M* EDTA solution. Dye–PEG derivatives were eluted with salts or acetone and finally the products were isolated by chloroform extraction [13,15]. Dye–PEG conjugates with the amount of dye as indicated earlier [15] were used.

Enzyme assays

The enzyme activities were determined spectrophotometrically at 340 nm at 30°C. Lactate dehydrogenase (E.C. 1.1.1.27) was determined according to Worthington [17] and glucose-6-phosphate dehydrogenase (E.C. 1.1.1.49) as described previously [18].

Two-phase systems

Two-phase systems (4 g) were prepared by weighing from stock solution of 20–50% (w/w) PEG, 20–30 (w/w) dextran and 0.1 *M* Tris–HCl buffer (pH 7.0) containing 5 m*M* EDTA for LDH and 0.2 *M* Tris–HCl buffer (pH 7.5) containing 5 m*M* Mg $(NO_3)_2 \cdot 6H_2O$, 10 m*M* EDTA, 5 m*M* 2-mercaptoethanol and 5% glycerine for G6PDH. A two-phase system composed of 6.5% (w/w) PEG 6000 and 10% (w/w) dextran in 10 m*M* Tris–HCl buffer (pH 7.0) containing 0.5 m*M* EDTA was used for LDH and a system composed of 7.0% (w/w) PEG 6000 and 10% (w/w) dextran in 20 m*M* Tris–HCl buffer (pH 7.5) containing 5 m*M* $Mg(NO_3)_2 \cdot 6H_2O$, 1.0 m*M* EDTA, 0.5 m*M* 2-mercaptoethanol and 0.5% glycerine for G6PDH. The amount of dye–PEG derivative is given as a percentage of the total mass of PEG present in the system or expressed as dye concentration (μM/kg) per kg of two-phase system.

Affinity partitioning of enzymes

After 2–20 units of LDH or 2–8 units of G6PDH had been introduced into the two-phase systems, the mixture was shaken gently for about 15 s, kept for 5 min and then centrifuged at 2000 *g* for about 2 min at 4°C to complete the phase separation. Samples of known volume were withdrawn from each phase and analysed for enzyme activity. The partition coefficient of the enzyme, *K*, defined as the ratio of enzyme concentration in the upper and lower phases, was calculated. The change in enzyme partition coefficients, $\Delta \log K$, was defined as the difference between the logarithmic partition coefficients of enzymes in the presence (K) and in the absence (K_0) of dye ($\Delta \log K = \log K - \log K_0$).

All the affinity partition curves of the enzymes

were linearized in double reciprocal plots of $\Delta\log K$ *vs.* dye concentration, treated by regression analysis and the due concentration which is required for the half-saturation point of the enzyme partition curve calculated according to Kopperschläger *et al.* [10]. The change in the enzyme partition coefficients when different selected agents were introduced into two-phase systems was expressed as a percentage of the initial value of $\Delta\log K$ in the presence of the dye and the absence of the agent. A decrease in $\Delta\log K$ by 100% was taken as $\Delta\log K = 0$.

RESULTS

Partitioning of LDH

The affinity of an enzyme to dye–PEG derivatives can advantageously be studied when the enzyme is concentrated in the lower phase of the dye–PEG-free two-phase system. Using a two-phase system consisting of 6.5% PEG 6000 and 10% dextran 60 000, the partition coefficient of LDH from rabbit muscle is 0.0088 ± 0.0008, *i.e.*, it exceeds 99% of the LDH introduced into the system in the bottom dextran-rich phase. Replacement of a portion of PEG with increasing portions of dye–PEG leads to changes in the enzyme logarithmic partition coefficients, rising to a maximum value $\Delta\log K_{max}$, which was regarded as a measure of the enzyme partitioning effect.

As seen from Table I, LDH is effectively transferred into the dye–PEG-containing upper phase when PEG derivatives with dyes from Procion Blue SP-3R ($\Delta\log K_{max} = 2.80$) to Claret 4CT–Cu(II) (1.93) were present in the system. Less extraction of the enzyme into the upper phase occurs in the presence of the PEG conjugates with Light Resistant Yellow 2KT–Cu(II) ($\Delta\log K_{max} = 1.40$), Red-Violet 2KT–Cu(II) (1.50) and Bright Yellow 2KT (0.88). The relative affinities of the enzyme to the dyes, calculated as the concentration required to yield $0.5\Delta\log K_{max}$, decrease in the order Procion Green H-4G (2.6 μM/kg of two-phase system), Orange 5K (35.0), Cibacron Blue F3G-A (47.0), Bright Yellow 53 (58.0) and Procion Blue MX-R (76.0). The affinity of other dyes was lower and the concentration of dyes yielding $0.5\Delta\log K_{max}$ was in the range 127–205 μM/kg.

It is noticeable that the LDH extraction power

TABLE I

INFLUENCE OF DIFFERENT PEG–DYE DERIVATIVES ON THE AFFINITY PARTITIONING OF RABBIT MUSCLE LACTATE DEHYDROGENASE

Two-phase system (4 g) composition: 6.5% (w/w) PEG 6000, 10% (w/w) dextran 60 000, 10 mM Tris–HCl buffer (pH 7.0), 0.5 mM EDTA.

Dye–PEG	$\Delta\log K_{max}$	Dye yielding $0.5\Delta\log K_{max}$ (μM/kg)
Light Resistant Yellow 2KT–Cu(II)	1.40 (1.10)[a]	205
Red-Violet 2KT–Cu(II)	1.50 (1.10)[a]	127
Procion Blue SP-3R	2.80	n.d.[b]
Cibacron Blue F3G-A	2.78	47
Procion Yellow H-3R	2.60	n.d.
Bright Red 6C	2.35	153
Procion Blue MX-R	2.40	76
Red-Brown 2KT–Cu(II)	2.64 (2.23)[a]	128
Red-Brown 2K	2.50	n.d.
Procion Green H-4G	2.65	2.6
Orange 5K	2.75	35
Bright Yellow 53	2.54	58
Claret 4CT–Cu(II)	1.93	201
Bright Yellow 2KT	0.88	n.d.

[a] Dye–PEG derivatives without Cu^{2+} ions.
[b] n.d. = Not determined.

($\Delta\log K_{max}$) and the relative affinity of dye to the enzyme with Cibacron Blue F3G-A (Table I) agree with the results obtained by Kirchberger *et al.* [19].

It may be concluded from the data in Table I that generally, LDH exhibits a higher affinity and is more effectively extracted into the upper phases containing dyes with no metal ions in their structure and interacts more weakly with dye–PEG derivatives containing coordinated Cu^{2+} ions. However, in the latter instance some difference in the interaction of the dye–Cu(II) complexes with the enzyme should be noted. For example, more effective extraction of LDH into the upper phase was observed with the Cu(II) complexes of Claret 4CT ($\Delta\log K_{max}$ = 1.93) and Red-Brown 2KT (2.64) in comparison with Cu(II) complexes of Light Resistant Yellow 2KT and Red-Violet 2KT ($\Delta\log K_{max}$ = 1.40–1.50).

A comparative study of the partitioning of LDH in the presence of the Cu(II) complexes of dye–PEG derivatives and their analogues after Cu^{2+} ions had been removed is summarized in Table II. It is obvious that the contribution of the Cu^{2+} ions is greater in the interaction of LDH with Red-Brown 2KT and Claret 4CT. Removal of the Cu^{2+} ions from these dyes resulted in a decrease in $\Delta\log K$ of LDH by 46% when equal concentrations of dye with no Cu^{2+} and dye–Cu(II) complex were participating in the system. For Light Resistant Yellow 2KT and Red-Violet 2KT the decrease in $\Delta\log K$ of the enzyme reached 29–31%. These data contrast with the results reported previously [15] by determiningg the role of Cu^{2+} ions in the interaction of dyes with yeast and horse liver ADH. It was found [15] that the affinity extraction of both ADH into the upper phases was greater with Cu(II) complexes of Light Resistant Yellow 2KT, Red-Violet 2KT (yeast ADH) and additionally Red-Brown 2KT (horse liver ADH) than partitioning in the presence of PEG–dyes containing no metal ions as cited in Table I. It was determined [15] that the removal of Cu^{2+} ions from PEG–Light Resistant Yellow 2KT–Cu(II) caused a decrease in $\Delta\log K$ of yeast ADH by 93%. For horse liver ADH and PEG conjugates with Light Resistant Yellow 2KT, Red-Violet 2KT and Red-Brown 2KT after the removal of Cu^{2+} ions from the latter the decrease in $\Delta\log K$ reached 77, 78, and 76%, respectively. Comparison of these findings clearly demonstrates that the contribution of Cu^{2+} is smaller in the formation of LDH complexes with the above-mentioned dyes than for yeast and horse liver ADH.

Partitioning of LDH in the presence of selected agents

The evaluation of the specificity of dyes to LDH, the character and the nature of the forces of the binding of dyes to the enzyme were studied by affinity partitioning of the enzyme in the presence of NaCl, NADH and chelating agents (imidazole, adenine and EDTA). The compounds were selected based on previously reported data [16] by studying the eluting capacity of various agents in yeast ADH affinity chromatography on an adsorbent with an immobilized Cu(II) complex of Light Resistant Yellow 2KT and the ability of the agents to participate in the formation of mixed Cu(II) complexes with

TABLE II

INFLUENCE OF Cu^{2+} IONS ON THE AFFINITY PARTITIONING OF LACTATE DEHYDROGENASE

System composition as in Table I.

Dye–PEG	Concentration of dye (μM/kg)	$\Delta\log K$		Decrease in $\Delta\log K$ in the presence of dye–PEG without Cu^{2+} (%)
		Cu^{2+}	–	
Light Resistant Yellow 2KT	400	1.36	0.96	29
Red-Violet 2KT	450	1.42	0.98	31
Claret 4CT	200	1.30	0.70	46
Red-Brown 2KT	350	2.60	1.40	46

this dye, and as a result their ability to displace the enzyme from the coordination sphere of the Cu^{2+} ions.

Table III shows that 1 m*M* NADH, as a specific agent of LDH, introduced in a PEG–dye system with no metal ions could reduce the value of $\Delta\log K$ by 85–105%. This leads to the assumption that this group of dyes might be expected to interact with enzyme specifically at the nucleotide ligand binding domain. A similar conclusions was made by studying the effect of structural variations of Procion Red HE-3B on the affinity and specificity of the ligand LDH interaction [19].

Addition of NaCl and an increase in its concentration in the phase systems up to 0.6 *M* caused a decrease in $\Delta\log K$ by 52–88% in the presence of the same group of PEG–dyes. This could indicate that electrostatic binding forces were involved and dominated over other forces in the formation of the dye-LDH complexes.

The effects of NADH and NaCl on the changes in $\Delta\log K$ for the studied PEG–dye–Cu(II) complexes differ greatly (Table III, Fig. 1). Low concentrations of NADH (1 m*M*) or NaCl (0.2 *M*) had resulted in the reduction of $\Delta\log K$ by 100 and 57–72%, respectively, in the cases of PEG–Light Resistant Yellow 2KT–Cu(II) and PEG–Red-Violet 2KT–Cu (II). Hence it may be concluded that Cu(II) complexes of both dyes behaved towards the enzyme similarly to a group of dyes containing no metal ions. However, the $\Delta\log K$-reducing capacity of the analogous concentration of NADH and NaCl by 26 and 5%, respectively, seemed insufficient in the case of PEG–Red-Brown 2KT–Cu(II). Such a change in $\Delta\log K$ in the latter instance correlates with the data in Table II. As indicated, the contribution of Cu(II) ions in the interaction between Red-Brown 2KT and LDH had been more important in comparison with Light Resistant Yellow 2KT and Red-Violet 2KT and, as a result, the low concentrations of NADH and NaCl were not capable of destroying the LDH–Red-Brown 2KT–Cu(II) complex.

Previously, we determined [15] that for the disruption of complexes formed by ADH and PEG–dyes with coordinated Cu^{2+} ions the concentration of selected agents added to two-phase systems should increase as the strength of the interaction of the dye–Cu(II) complexes with enzymes did. This is also valid for systems containing PEG–Red-Brown 2KT–Cu(II) in the presence of NADH. An increase in its concentration to 5 m*M* increased the $\Delta\log K$ reduction to 82%. However, an increase in the concentration of NaCl to 0.6 *M* had no appreciable effect on the change in $\Delta\log K$. The effect of chelat-

TABLE III

DEPENDENCE OF THE AFFINITY PARTITION EFFECT ($\Delta\log K$) OF RABBIT MUSCLE LACTATE DEHYDROGENASE ON THE CONCENTRATION OF NaCl AND NADH

System composition as in Table I.

Dye–PEG	Concentration of dye (μ*M*/kg)	Decrease in $\Delta\log K$ (%)				
		NADH (m*M*)			NaCl (*M*)	
		0.5	1.0	5.0	0.2	0.6
Orange 5K	250	70	89	115	63	85
Procion Green H-4G	80	92	104	125	66	88
Procion Blue SP-3R	1%	95	96	105	29	52
Cibacron Blue F3G-A	200	58	92	114	61	85
Procion Blue MX-R	320	100	105	126	55	82
Procion Yellow H-3R	1%	88	102	117	n.d.	n.d.
Bright Red 6C	350	88	95	100	72	85
Bright Yellow 53	250	74	85	95	58	88
Light Resistant Yellow 2KT–Cu(II)	280	74	100	152	57	48
Red-Violet 2KT–Cu(II)	380	86	100	114	72	76
Red-Brown 2KT–Cu(II)	250	15	26	82	5	20
Red-Brown 2KT	250	108	108	114	79	85

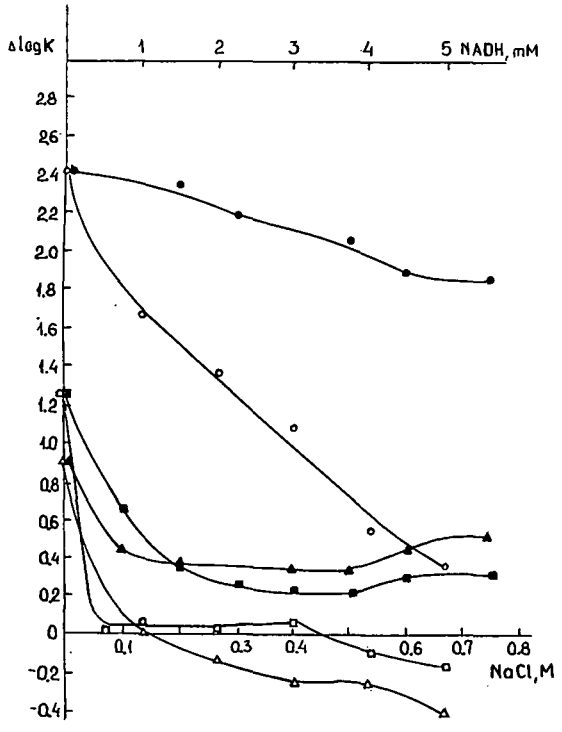

Fig. 1. Partitioning of lactate dehydrogenase in systems containing increasing concentrations of NADH and NaCl in the presence of dye–Cu(II) complexes. System composition as in Table I, dye–PEG concentrations as in Table III. Dye–PEG: ○, ● = Red-Brown 2KT–Cu(II); □, ■ = Red-Violet 2KT–Cu(II); △, ▲ = Light Resistant Yellow 2KT–Cu(II). Open symbols for systems containing NADH, closed symbols for NaCl.

ing agents on the affinity partitioning of LDH was studied in the presence of PEG conjugates with Light Resistant Yellow 2KT–Cu(II) and Red-Brown 2KT–Cu(II) as cases differing in the contribution of Cu^{2+} ions to the formation of dye–LDH complexes. Fig. 2 and Table IV show that of the chelating agents used, *i.e.*, EDTA, adenine and imidazole, the last is the most effective for the destruction of the LDH–PEG–Red-Brown 2KT–Cu(II) complex. For example, 0.5 m*M* imidazole caused a decrease in $\Delta\log K$ of 68%, whereas the same concentration of NADH gave only a 15% decrease. In contrast, the effect of 0.5 m*M* imidazole on the decrease in $\Delta\log K$ is smaller in the presence of PEG–Light Resistant Yellow 2KT–Cu(II), whereas 0.5 m*M* NADH reduced $\Delta\log K$ of LDH by 74% (Table III).

These data serve as a further confirmation that Cu^{2+} ions play a more important role in the interaction of Red-Brown 2KT–Cu(II) with LDH. It is worth noting that chelating agents in concentrations up to 5 m*M* reduced $\Delta\log K$ insignificantly (by 16–45%) when the PEG conjugate with Red-Brown 2KT after the removal of Cu^{2+} ions was used (Fig. 3), whereas 1.0 m*M* NADH or 0.2 *M* NaCl effectively destroyed this dye–LDH complex (Table III). According to these data, it is evident that Red-Brown 2KT becomes more specific to LDH after Cu^{2+} ions have been removed and could interact with enzymes similarly to the group of dyes containing no metal ions.

Partitioning of yeast glucose-6-phosphate dehydrogenase in the presence of selected agents

Partitioning data for the enzyme, in the presence of PEG conjugates with Cu(II) complexes of Red-Brown 2KT, Red-Violet 2KT and Claret 4CT when NaCl, NADP or chelating agents were introduced into the phase systems, are summarized in Table V. It is obvious that in all the cases studied the specific

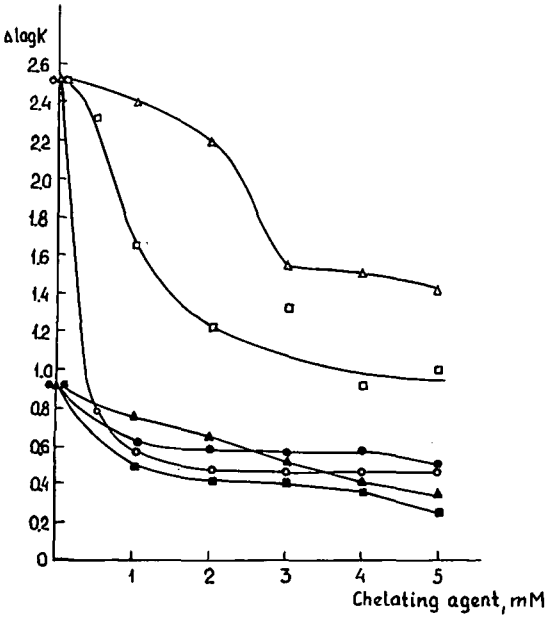

Fig. 2. Partitioning of lactate dehydrogenase in systems containing increasing concentrations of chelating agents in the presence of PEG–Light Resistant Yellow 2KT–Cu(II) and PEG–Red-Brown 2KT–Cu(II). System composition and dye–PEG concentrations as in Table III. ○ = Imidazole; □ = adenine; △ = EDTA; Open symbols for PEG–Red-Brown 2KT–Cu(II), closed symbols for PEG–Light Resistant Yellow 2KT–Cu(II).

TABLE IV

DEPENDENCE OF THE AFFINITY PARTITION EFFECT (Δlog K) OF RABBIT MUSCLE LACTATE DEHYDROGENASE ON THE CONCENTRATION OF CHELATING AGENTS

System composition and dye–PEG concentration as in Table III.

Agent	Concentration (mM)	Decrease in Δlog K (%)		
		Red-Brown 2KT–Cu(II)	Light Resistant Yellow 2KT–Cu(II)	Red-Brown 2KT
Imidazole	0.5	68	23	10
	5.0	81	44	16
Adenine	0.5	8	27	19
	5.0	63	74	36
EDTA	0.5	1	7	21
	5.0	43	63	45

agent NADP, at concentrations up to 1 mM, was capable of destroying the enzyme–dye complexes and this led to the assumption that the tested dye–Cu(II) complexes probably interacted with the enzyme at nucleotide ligand binding sites. The non-specific agent NaCl influenced the change in the enzyme partition coefficient by a different mode. At 0.2 M NaCl Δlog K of the enzyme was reduced by 46, 66 and 113%, respectively, in the cases of PEG conjugates with Red-Brown 2KT–Cu(II), Red-Violet 2KT–Cu(II) and Claret 4CT–Cu(II). A further increase in the concentration of NaCl (up to 0.4 M) resulted in decreases Δlog K by 87% and 107% with

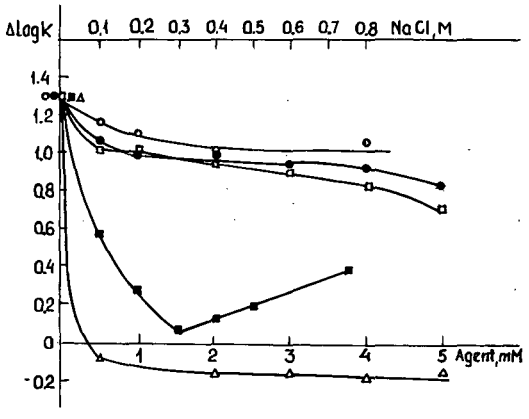

Fig. 3. Partitioning of lactate dehydrogenase in systems containing increasing concentrations of various agents in the presence of Red-Brown 2KT wihtout Cu^{2+}ions. Systems composition and dye–PEG concentration as in Table III. ○ = Imidazole; ● = adenine; □ = EDTA; ■ = NaCl; △ = NADH.

PEG–Red-Brown 2KT–CU(II) and Red-Violet 2KT–Cu(II), respectively. The different effects of the same concentration of NaCl on the decrease in Δlog K over the range of dye–Cu(II) complexes (from Red-Brown 2KT to Claret 4CT) could be attributed to the participation of a different part of the Cu^{2+} coordination bonds in the formation of the enzyme–dye complexes. This is confirmed by the enzyme partitioning in the presence of chelating agents such as imidazole and adenine. It is seen (Table V) that low concentrations of these agents decreased Δlog K most efficiently in the case of PEG–Red-Brown 2 KT–Cu(II). As 1 mM NADP also caused an effective decrease in Δlog K, it could be concluded that the Cu(II) complex of Red-Brown 2KT is more specific to yeast G6PDH, in contract to LDH from rabbit muscle. Probably, it will be able to participate in the formation of highly selective ternary complexes involving G6PDH, Cu^{2+}ions and dye similarly to the yeast ADH–Cu (II) complex of Light Resistant Yellow 2KT studied previously [29].

DISCUSSION

The technique of affinity partitioning of LDH from rabbit muscle [19–24] and G6PDH from yeast [21,25–27] in aqueous two-phase systems containing dye-liganded polymers has been applied to the screening of dyes with respect to their affinity to the enzymes. The possibilities of rapid purification of

TABLE V

DEPENDENCE OF THE AFFINITY PARTITION EFFECT (Δlog K) OF YEAST GLUCOSE-6-PHOSPHATE DEHYDROGENASE ON THE CONCENTRATION OF NaCl, NADP AND CHELATING AGENTS

Two-phase system (4 g) contained 7% (w/w) PEG 6000, 10% (w/w) dextran 60 000, 20 mM Tris–HCl buffer (pH 7.0), 5.0 mM $Mg(NO)_3 \cdot 6H_2O$, 1.0 mM EDTA, 0.5 mM 2-mercaptoethanol and 0.5% (v/v) glycerine.

Agent	Concentration (mM)	Decrease in Δlog K (%)		
		Red-Brown 2KT–Cu(II) (357 μM/kg)	Claret 4CT–Cu(II) (425 μM/kg)	Red-Violet 2KT–Cu(II) (510 μM/kg)
NaCl	200	46	113	66
NADP	1.0	138	90	Δlog K = 0
Imidazole	1.0	77	20	20
	2.5	94	32	48
Adenine	1.0	61	14	26
	2.5	87	52	52

enzymes using affinity partitioning have also been demonstrated on medium [28] and large scales [23].

It was shown [20] that the dye Procion Yellow HE-3G interacted strongly with LDH from rabbit muscle, and various polymers as dye carriers were compared [22]. Finally, this dye was used as a conjugate with PEG for the large-scale affinity extraction of the enzyme using a PEG–Aquaphase PPT two-phase system [23]. Recently, Kirchberger and co-workers studied the binding behaviour of LDH [19] and its isoenzymes [24] to different triazine dyes covalently coupled to PEG, and showed a high relative affinity of Procion Red HE-3B to LDH and its isoenzymes. With the aid of Procion Yellow HE-3G coupled to various polymers, yeast G6PDH could be effectively extracted, as has been demonstrated [21,25,27].

Based on the data presented (Tables I and III), it may be concluded that some of the dyes studied in this work could also act as relatively high affinity ligands for LDH from rabbit muscle and probably other NAD(H)-dependent dehydrogenases. This is confirmed by the fact that adsorbents carrying Orange 5K and Bright Yellow 5Z have been used successfully as highly specific materials for the large-scale purification of some dehydrogenases, including LDH from rabbit muscle (data not shown).

Some of the dyes studied, Light Resistant Yellow 2KT, Red-Brown 2KT, Red-Violet 2KT and Claret 4CT, exsist as Cu(II) complexes in which the coordination of the Cu^{2+} ions involves an azo bond and two adjacent hydroxyl moieties of the dyes. The remaining coordination site could be occupied by appropriate protein donor groups. Therefore, these structures are useful as a means for the investigation of metal ion-promoted binding of proteins to dyes including also the technique of affinity partitioning [15].

Metal ion-dependent interactions between dyes and proteins are well documented [15,16,29–37]. It has been shown [29,30,33,34,38] that metal ions could enhance the binding of dyes to proteins by lowering the dissociation constant for the dye–enzyme interaction. The dye–enzyme complexes produced could be broken by selected competing effectors [16,30,31,35] or appropriate chelating agents [15,16,32,35,39]. Recently [37], metal–EDTA–sugar complexes were proposed as efficient specific enzyme-desorbing eluents.

It has been shown [32] that the influence of different metal ions differs depending on the nature of the dye and protein studied and that the immobilized and free dyes do not show the same mechanism towards the metal ion-mediated dye–enzyme association–dissociation [35] (ref. 37, p. 216). Further studies to elucidate the nature of transition metal ion-mediated binding of dyes to enzymes are necessary.

It was assumed [30] that the orientation of the dye–metal ion complex may be slightly different than that of the dye alone or the dye conformation could be stabilized owing to its coordination with metal ions in such a manner that the dye–metal ion complex becomes acceptable to the complementary protein [32]. This could lead to the formation of a highly selective ternary complex involving dye, metal ion and the enzyme at the active site region of the enzyme [33,34]. An analogous assumption has been made for the interaction of yeast alcohol dehydrogenase with the Cu(II) complex of Light Resistant Yellow 2KT [16,29]. Interaction of the free dye with the enzyme modified by diethyl pyrocarbonate, studied by means of differential and induced circular dichroism spectroscopy, confirmed the proposed assumption that the formation of a specific ternary complex involving dye, Cu^{2+}ions and histidine residue of yeast ADH analogous to His^{51} in horse liver ADH may be possible. The metal ion-promoted specific interaction of some dyes with yeast ADH has been confirmed by the results of enzyme partitioning in aqueous two-phase systems and this technique has enabled us to show [15] that the interaction of horse liver enzyme with some dyes depends also on the presence of Cu^{2+}ions. However, the results reported here show that the presence of Cu^{2+}ions in the structure of the dye could have an inverse action by lowering the specificity of the dye to the enzyme. This is supported by lactate dehydrogenase affinity partitioning in the presence of PEG conjugates with the Cu(II) complex of Red-Brown 2KT and its analogue with no metal ion when chelating agents and nucleotide ligand participated in two-phase systems (Tables III and IV, Figs. 1–3).

One can assume that the studied Cu(II) complexes of Light Resistant Yellow 2KT, Red-Violet 2KT in the case of LDH and Cu(II) complexes of Red-Brown 2KT, Claret 4CT and Red-Violet 2KT in the case of yeast G6PDH may interact predominantly at the coenzyme binding domains of the enzymes studied. This proposal is supported by the fact that the $\Delta \log K$ values of the enzymes are effectively decreased by low concentrations (up to 1 m*M*) of nucleotide ligands (Tables III and V). The same may be valid for the interaction of Red-Brown 2KT–Cu (II) after Cu^{2+}ions had been removed wih LDH (Fig. 3, Table III). If it is assumed that the same donor ligand from a nucleotide binding site was involved in the coordination with Cu^{2+}ions of dyes, it seems likely that the differences in the contribution involved in the binding with the enzyme coordination bonds are determined by the differences in the spatial structures of the dye–Cu(II) complexes. It is conceivable that the steric accessibility of Cu^{2+}ions coordinated with dyes determines the contribution of coordination bonds involved in the interaction with accessible donor groups of the enzyme.

It is well established that the accessibility of surface-exposed histidine residues in proteins governs the binding strength of immobilized metal chelates to proteins [40] and increases the partition coefficients of proteins in the presence of Cu(II) iminodiacetate (IDA)-derivatized poly(ethylene glycol) in PEG–dextran two-phase system [41,42]. As was mentioned above, such a coordination of histidine residue from yeast ADH with the Cu(II) complex of Light Resistant Yellow 2KT was supported by us. Unfortunately, at present we do not have exact information about the possibility of participation in coordination with metal ions of exposed histidine residue of LDH and G6PDH. With G6PDH, such participation of histidine residue is possible in view of the fact indicated by Kopperschläger and Lorez [26] that the imidazole residue of the enzyme could be involved in the interaction of Procion Navy HE-R-PEG with the enzyme. Earlier we concluded [16] that the differences in the interaction of LDH from rabbit muscle and yeast ADH with Light Resistant Yellow 2KT–Cu(II) may be due to the fact that in contrast to ADH a histidine residue with the same function is not observed at the nucleotide binding site of LDH. This conclusion agrees with the recent observation of Kirchberger *et al.* [24] that the hydrophobic nicotinamide pocket and arginine residue of the substrate binding site of LDH are probably involved in the binding with dyes such as Cibacron Blue F3G-A and Procion Red HE-3B.

As the coordination of the dye with metal ions could stabilize its conformation and limit conformation freedom, preference should be given to the differences in the conformational states of the studied dyes–Cu(II) complexes in their interaction with the enzyme. According to this, one could assume that the coordination of Red-Brown 2KT with Cu^{2+} may result in a dye conformation that would be expected to be spatially unfavourable for the spe-

cific interaction with LDH from rabbit muscle.

Further studies are necessary to support these assumptions but it is fairly clear that the direct confirmation of such interactions could be obtained by X-ray studies, as was determined [43] for the binding of Cibacron Blue F3GA to liver alcohol dehydrogenase.

REFERENCES

1 P.-Å. Albertsson, *Partition of Cell Particles and Macromolecules*, Wiley, New York, 3rd ed., 1986.
2 M.-R. Kula, K. H. Kroner and H. Hustedt, *Adv. Biochem. Bioeng.*, 24 (1982) 74.
3 G. Johansson, in H. Walter, D. E. Brooks and D. Fisher (Editors), *Partitioning in Aqueous Two-Phase Systems: Theory, Methods, Uses, and Applications to Biotechnology*, Academic Press, Orlando, FL, 1985, pp. 161–226.
4 G. Johansson and V. P. Shanbhag, *J. Chromatogr.*, 284 (1984) 63.
5 G. Johansson, M. Joelsson, B. Olde and V. P. Shanbhag, *J. Chromatogr.*, 331 (1985) 11.
6 G. Johansson, *J. Chromatogr.*, 368 (1986) 309.
7 M.-R. Kula, G. Johansson and A. F. Bückman, *Biochem. Soc. Trans.*, 7 (1979) 1.
8 K. H. Kroner, A. Cordes, A. Schelper, M. Morr, A. F. Bückmann and M.-R. Kula, in T. J. C. Gribnau, J. Visser and R. J. F. Nivard (Editors), *Affinity Chromatography and Related Techniques*, Elsevier, Amsterdam, 1982, p. 491.
9 G. Johansson, G. Kopperschläger and P.-Å. Albertsson, *Eur. J. Biochem.*, 131 (1983) 589.
10 G. Kopperschläger, G. Lorenz and E. Usbeck, *J. Chromatogr.*, 259 (1983) 97.
11 G. Kopperschläger and G. Johansson, *Anal. Biochem.*, 124 (1982) 117.
12 J. Schiemann and G. Kopperschläger, *Plant Sci. Lett.*, 36 (1984) 205.
13 G. Johansson and M. Joelsson, *Biotechnol. Bioeng.*, 27 (1985) 621.
14 G. Kopperschläger, J. Kirchberger and T. Kriegel, *Makromol. Chem., Macromol. Symp.*, 17 (1988) 373.
15 J.-H. J. Pesliakas, V. D. Žutautas and A. A. Glemža, *Chromatographia*, 26 (1986) 85.
16 S. S. Flaksaitė, O. F. Sūdžiuvienė, J.-H. J. Pesliakas and A. A. Glemža, *Biokhimiya*, 52 (1987) 73.
17 Worthington, in *Enzymes and Related Biochemicals*, Millipore, Bedford, MA, 1979, p. 109.
18 V. A. Kaduševičius, O. F. Sūdžiuvienė and J. J. Pesliakas, *Bioorg. Khim.*, 9 (1983) 1128.
19 J. Kirchberger, F. Cadelis, G. Kopperschläger and M. A. Vijayalakshmi, *J. Chromatogr.*, 483 (1989) 289.
20 G. Johansson and M. Joelsson, *Appl. Biochem. Biotechnol.*, 13 (1986) 15.
21 G. Johansson and M. Joelsson, *J. Chromatogr.*, 393 (1987) 195.
22 G. Johansson and M. Joelsson, *J. Chromatogr.*, 411 (1987) 161.
23 F. Tjerneld, G. Johansson and M. Joelsson, *Biotechnol. Bioeng.*, 30 (1987) 809.
24 J. Kirchberger, G. Kopperschläger and M. A. Vijayalakshmi, *J. Chromatogr.*, 557 (1991) 325.
25 G. Johansson and M. Andersson, *J. Chromatogr.*, 303 (1984) 39.
26 G. Kopperschläger and G. Lorenz, *Biomed. Biochim. Acta*, 44 (1985) 517.
27 F. Tjerneld, S. Berner, A. Cajarville and G. Johansson, *Enzyme Microb. Technol.*, 8 (1986) 417.
28 G. Johansson and M. Joelsson, *Enzyme Microb. Technol.*, 7 (1985) 629.
29 S. S. Flaksaitė, O. F. Sūdžiuvienė, J.-H. J. Pesliakas and A. A. Glemža, *Bioorg. Khim.*, 13 (1987) 293.
30 Y. D. Clonis, M. J. Goldfinch and C. R. Lowe, *Biochem. J.*, 197 (1981) 203.
31 D. A. P. Small, T. Atkinson and C. R. Lowe, *J. Chromatogr.*, 216 (1981) 175.
32 P. Hughes, C. R. Lowe and R. F. Sherwood, *Biochim. Biophys Acta*, 700 (1982) 90.
33 P. Hughes, R. F. Sherwood and C. R. Lowe, *Biochem. J.*, 205 (1982) 453.
34 P. Hughes, R. F. Sherwood and C. R. Lowe, *Eur. J. Biochem.*, 144 (1984) 135.
35 S. Rajgopal and M. A. Vijayalakshmi, *Enzyme Microb. Technol.*, 6 (1984) 555.
36 S. Rajgopal and M. A. Vijayalakshmi, *J. Chromatogr.*, 315 (1984) 175.
37 M. A. Vijayalakshmi and O. Bertrand (Editors), *Protein–Dye Interaction: Developments and Applications*, Elsevier Applied Science, Barking, 1988, Ch. 5.
38 S. S. Flaksaitė, O. F. Sūdžiuvienė, J.-H. J. Pesliakas and A. A. Glemža, *Bioorg. Khim.*, 10 (1984) 25.
39 R. F. Sherwood, R. G. Melton, S. M. Alvan and P. Hughes, *Eur. J. Biochem.*, 148 (1985) 447.
40 E. S. Hemdan, Y.-J. Zhao, E. Sulkowski and J. Porath, *Proc. Natl. Acad. Sci. U.S.A.*, 86 (1989) 1811.
41 S.-S. Suh and F. H. Arnold, *Biotechnol. Bioeng.*, 35 (1990) 682.
42 F. H. Arnold, *Bio/Technology*, 9 (1991) 151.
43 J. F. Biellman, J. P. Samama, C. I. Branden and H. Eklund, *Eur. J. Biochem.*, 102 (1979) 107.

Journal of Chromatography, 606 (1992) 65–71
Elsevier Science Publishers B.V., Amsterdam

CHROM. 24 266

Quantification of intermediates involved in the cyclic 2,3-diphosphoglycerate metabolism of methanogenic bacteria by ion-exchange chromatography

Gert-Jan W. M. van Alebeek, John M. H. Hermans, Jan T. Keltjens and Godfried D. Vogels

Department of Microbiology, Faculty of Science, University of Nijmegen, Toernooiveld, NL-6525 ED Nijmegen (Netherlands)

(First received January 22nd, 1992; revised manuscript received April 10th, 1992)

ABSTRACT

A novel method was developed to quantify the intermediates involved in cyclic 2,3-diphosphoglycerate metabolism, *i.e.* cyclic 2,3-diphosphoglycerate, 2,3-bisphosphoglycerate, 2-phosphoglycerate, 3-phosphoglycerate, phosphoenolpyruvate, pyruvate and phosphate. The method consists of an ion-chromatographic separation followed by conductivity and ultraviolet detection. In a single run (41 min) all compounds were readily resolved, except for 2- and 3-phosphoglycerate. Concentrations down to 10–20 μM and up to 1.0–1.5 mM can be accurately determined. The method was suitable for the analysis of cell-free extract and for the determination of enzymic conversions of the compounds involved. It was found to be reliable and faster than isotachophoresis or enzymic determination.

INTRODUCTION

Cyclic 2,3-diphosphoglycerate (cDPG) is a 2,3-bisphosphoglycerate (2,3-BPG) derivative in which both phosphate groups are connected by a phosphoric anhydride binding [1–3]. The occurrence of cDPG in nature is restricted to methanogenic bacteria belonging to the genera *Methanobacterium, Methanobrevibacter, Methanothermus, Methanosarcina* and *Methanosphaera* [4–6]. In these organisms the compound may be present in concentrations from 2 mM to as high as 1.5 M [3,7–10]. The function of cDPG is not completely clear, and the compound is suggested to act in storage of energy [1,11,12], phosphorus [2] or cell carbon [7,13]. As the *in vivo* counter ion of potassium, cDPG may also play a role in thermostabilization of proteins in extreme thermophilic organisms [4]. cDPG is synthesized and degraded as shown in Fig. 1 [12,14].

To come to a better understanding of cDPG metabolism and its potential regulation, suitable analysis techniques are required for cDPG and its cellular precursors and metabolites. After acid hydrolysis of cDPG into 2,3-BPG, the compound may be analysed enzymically [3]. Enzymic methods are also

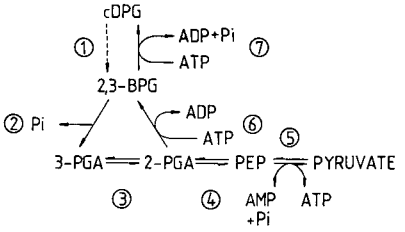

Fig. 1. cDPG biosynthesis and degradation related on the intermediate cell carbon (C_3) metabolism in *M. thermoautotrophicum* [12]. The numbers refer to the following enzymes: 1 = cyclic 2,3-diphosphoglycerate hydrolase; 2 = 2,3-biphosphoglycerate phosphatase; 3 = phosphoglycerate mutase; 4 = enolase; 5 = phosphoenolpyruvate synthetase; 6 = 2-phosphoglycerate kinase; 7 = cyclic 2,3-diphosphoglycerate synthetase.

Correspondence to: Dr. Gert-Jan W. M. van Alebeek, Department of Microbiology, Faculty of Science, University of Nijmegen, Toernooiveld, NL-6525 ED Nijmegen, Netherlands.

0021-9673/92/$05.00

available for the other compounds shown in Fig. 1. However, the methods are laborious and time-consuming; each component requires a separate analysis. A number of these drawbacks may be overcome by isotachophoresis [11,12], which enables the simultaneous analysis of the relevant compounds. This technique, however, still may be slow and is tedious to handle. As an alternative, this paper describes the use of ion-exchange chromatography connected to a background suppressor system for the identification and quantification of the compounds involved in the cDPG metabolism.

EXPERIMENTAL

Chemicals

ATP was purchased from Boehringer (Mannheim, Germany). N-tris(hydroxymethyl)methyl-2-aminoethanesulphonate] (TES), 2,3-bisphosphoglycerate (2,3-BPG), 2-phosphoglycerate (2-PGA), 3-phosphoglycerate (3-PGA) and phosphoenolpyruvate (PEP) were obtained from Sigma (St. Louis, MO, USA). Tris(hydroxymethyl)aminomethane] (Tris), potassium chloride, magnesium chloride, oxalate and pyruvate were from Merck (Darmstadt, Germany). Dipotassium hydrogenphosphate, sodium hydroxide (analysed reagent) and sulphuric acid (instra-analysed reagent) were purchased from J. T. Baker (Deventer, Netherlands). cDPG was purified as described previously [11]. The concentration was determined after acid hydrolysis into 2,3-BPG and subsequent enzymic analysis [3]. Gases were from Hoek-Loos (Schiedam, Netherlands) and were made oxygen-free by passage over a prereduced BASF R3-11 catalyst at 150°C or a BASF R0-20 catalyst at ambient temperature for hydrogen-free and hydrogen-containing gases, respectively. The catalysts were a gift from BASF (Ludwigshafen, Germany).

Ion-exchange chromatography

Separation and quantification of cDPG, 2,3-BPG, 2-PGA (and 3-PGA), PEP, pyruvate and inorganic orthophosphate (P_i) was performed with an HP 1050 Ti automated gradient system consisting of a gradient pump, an autosampler, a UV detector and an analog-to-digital converter (interface 35900), which translated the signal of the pulsed electrochemical detector (conductivity mode; Dionex) to the computer. The system was controlled with a high-performance liquid chromatographic (HPLC) ChemStation (DOS series).

Samples (20 μl) were injected by means of an autosampler on an Ionpac AG5A-5μ guard column (Dionex P/N 037134; 50 mm × 4 mm I.D.) connected to an Ionpac AS5A-5μ anion-exchange analytical column (Dionex P/N 037131; 250 mm × 4 mm I.D.). The column material (capacity, 35 μequiv.) contains an alkanol quaternary amine functional group linked to a latex (polyacrylate) matrix. Elution was performed at ambient temperature; the elution rate was 1 ml/min. Separation took place by a linear gradient in 23 min of 0.75 m*M* sodium hydroxide (pH 10.67) to 120.75 m*M* sodium hydroxide (pH 13.07). Thereafter, sodium hydroxide was kept at 120.75 m*M* for 5 min. Following a 0.1-min gradient to 0.75 m*M* sodium hydroxide and a 13-min equilibration at 0.75 m*M* sodium hydroxide, the next sample could be injected. Eluents were passed through an anion trap column (ATC-1, P/N 037151) placed before the injector to remove carbonate from the buffer. The compounds to be analysed were detected with a Dionex conductivity detector set at 30 μS full scale and with a UV detector set at a wavelength of 215 nm. The conductivity caused by OH^- was suppressed by means of an anion micromembrane suppressor (AMMS, P/N 038019) with a 25 m*M* sulphuric acid regenerant set at a flow-rate of 20 ml/min.

Standard solutions in the range of 0.05–1.5 m*M* were prepared in water and contained 0.5 m*M* oxalate as an internal standard. Samples of 20 μl were injected on the column. Calibration graphs were constructed by plotting the area against the amount (external standard) or by plotting the area response ratio against the amount ratio (internal standard).

Organism and enzyme preparation

Methanobacterium thermoautotrophicum (strain ΔH) (DSM 1053) was cultured on a defined medium [15] under 80% hydrogen–20% carbon dioxide in a 300-l fermenter as documented previously [16]. Cells were harvested under nitrogen with a Sharples continuous centrifuge and stored at −70°C. The preparation of cell-free extract was undertaken under strictly anaerobic conditions as described previously [12]. The dry weight of cell-free extracts was 76 mg/ml. A cofactor-free extract was obtained by

ultracentrifugation of a cell-free extract (36 ml) at 135 000 *g* for 1 h at 4°C. The pellet was washed with anoxic 100 m*M* TES/K^+ buffer (pH 7) and the first and the second supernatants were combined, extensively washed on a Amicon PM-30 filter (cut-off 30 000 dalton) with 100 m*M* TES/K^+ buffer and added to the pellet fraction.

Protein was determined with the Bio-Rad method using γ-globulin as a standard.

Cyclic 2,3-diphosphoglycerate synthetase

The activity of cyclic 2,3-diphosphoglycerate synthetase was determined in 50 m*M* Tris (pH 7). Reaction mixtures (200 μl) prepared in 10-ml serum vials placed inside an anaerobic glove box contained 18 m*M* magnesium chloride, 20 m*M* ATP, 0.5 *M* potassium chloride, 10 m*M* 2,3-BPG and 50 μl of cofactor-free extract (2.07 mg of protein); incubations took place under a hydrogen atmosphere. The reactions were started by placing the vials in a

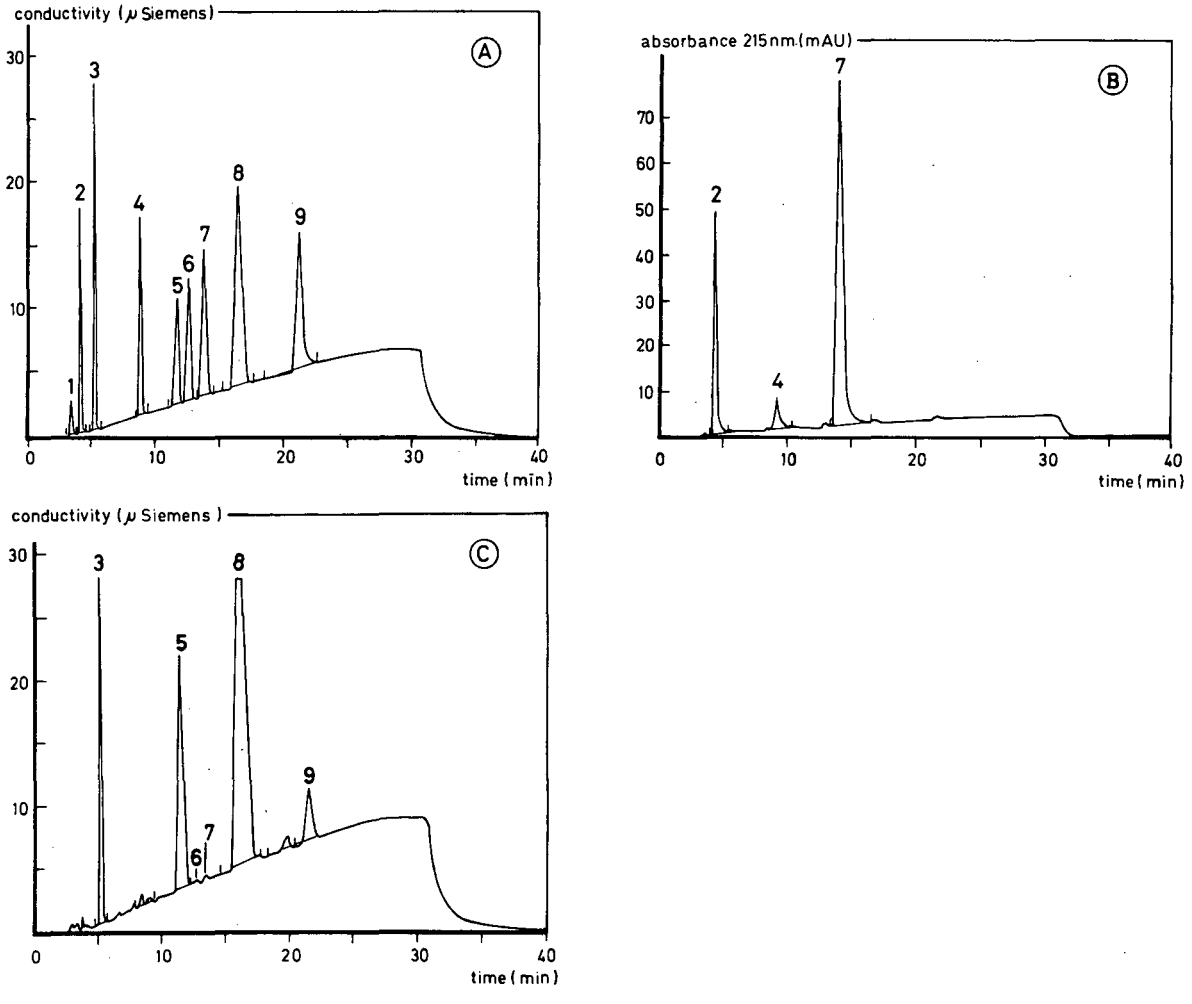

Fig. 2. Ion chromatograms of a standard mixture (A and B) and of a cell-free extract of *M. thermoautotrophicum* (C). Separation was performed as described in the Experimental section; detection took place by conductivity (A and C) or by UV (215 nm) absorption (B). Peaks: 1 = acetate; 2 = pyruvate; 3 = chloride; 4 = oxalate; 5 = phosphate; 6 = 2-phosphoglycerate; 7 = phosphoenolpyruvate; 8 = cyclic 2,3-diphosphoglycerate; 9 = 2,3-bisphosphoglycerate. Standards were present at a concentration of 0.5 m*M* (20 μl injection volume) except chloride and acetate. Cell-free extract was diluted 40-fold and heat-denatured as described in the Experimental section. No internal standard was added in C.

waterbath at 60°C. After an appropriate incubation period the reaction was stopped by placing the vials on ice. Thereafter, the vials were opened, diluted with 750 μl of Milli-Q water and boiled for 30 min. After 10 min of cooling on ice, 50 μl of oxalate (10 m*M*) were added as internal standard and the samples were centrifuged at 12 000 *g* for 10 min at 4°C to remove the denaturated protein. Aliquots of 20 μl of the supernatant were used for analysis on ion-exchange chromatography as described above.

RESULTS

Ion chromatography

The HPLC chromatogram of a mixture of pure compounds obtained by anion-exchange chromatography and conductivity detection is illustrated in Fig. 2A. Pyruvate, oxalate and PEP could also be detected by UV absorption at 215 nm (Fig. 2B). As expected for an anion exchanger, retention of the individual compounds tended to increase with increasing charge of the anions at the pH (10.67–12.04) used during the separation. With the exception of 2-PGA and 3-PGA, the compounds of interest were readily resolved. The retention times of the individual compounds were rather constant, though they decreased somewhat when increasing concentrations were injected. This effect is more pronounced for compounds with higher retention times. Calibration graphs obtained by conductivity and UV detection are shown in Fig. 3A and B, respectively. In Fig. 3C the response and concentration ratios with respect to the internal standard (oxalate) are plotted. Linear regression coefficients of the standard curves were $\geqslant 0.999$ in Fig. 3A and B and varied between 0.993 and 0.999 in Fig. 3C. Hence, up to at least 20–30 nmol of the various compounds can be accurately determined. The sensitivity of the individual compounds towards conductivity detection increased with increasing negative charge; however, 3-PGA and cDPG are exceptions to this (Fig. 2). Detection limits were of the order of 1–2 nmol, which equals 50–100 μ*M* in the sample when 20 μl are injected. Since the injection volume can be varied from 1 to 100 μl, concentrations down to 10–20 μ*M* may be quantified. Retention times and the (relative) response factors are compiled in Table I.

Analysis of cell-free extract of Methanobacterium thermoautotrophicum

Fig. 2C shows the ion-chromatographic conduc-

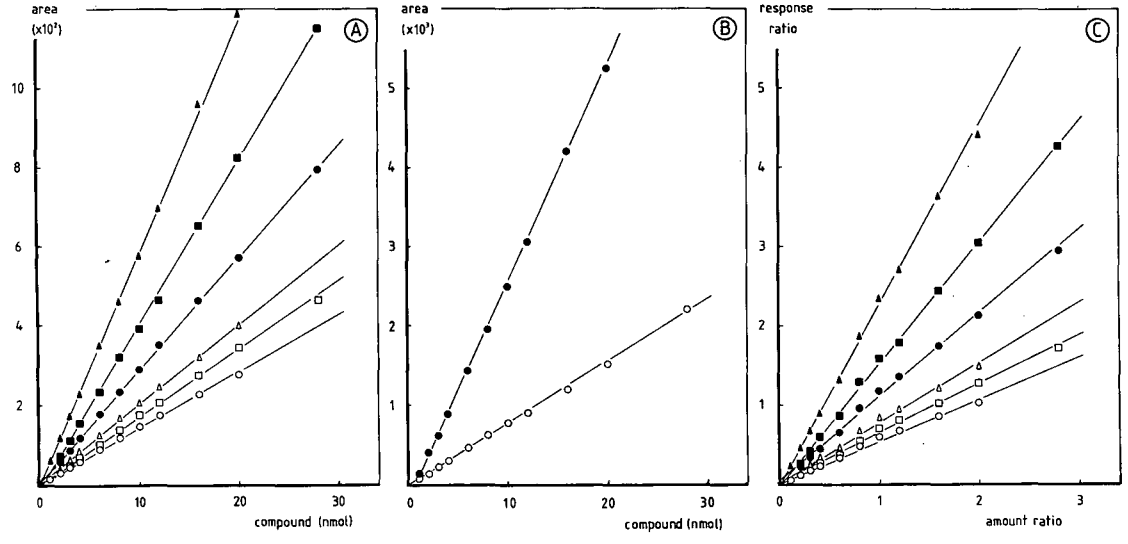

Fig. 3. Calibration graphs of standard compounds detected by conductivity (A) and UV absorption (B). Standards include (○) pyruvate, (□) phosphate, (△) 2-phosphoglycerate, (●) phosphoenolpyruvate, (■) 2,3-BPG and (▲) cDPG. In (C) the response ratio of the compounds with respect to the internal standard (10 nmol of oxalate) is plotted against the amount ratio; detection took place by conductivity. Solid lines are linear regression curves.

TABLE I

HPLC CHARACTERIZATION OF INTERMEDIATES INVOLVED IN THE cDPG METABOLISM SEPARATED ON AN IONPAC AS5A-5μ ANION-EXCHANGE COLUMN

N.D. = Not determined.

Compound[a]	Retention time (min)	Response factor[b]
Pyruvate	4.00–4.01	0.072 (1.92)
	4.36	0.013
Oxalate	8.71	N.D. (–)
	9.13	N.D.
Phosphate	11.33–11.80	0.060 (1.61)
3-PGA	12.29–12.71	0.036 (0.92)
2-PGA	12.30–12.73	0.050 (1.35)
PEP	13.34–13.97	0.035 (0.95)
	13.75–14.37	0.0036
cDPG	16.03–16.80	0.017 (0.45)
2,3-BPG	20.67–21.61	0.024 (0.65)

[a] The compounds were measured by conductivity detection; a second set of data refers to UV (215 nm) detection.

[b] Response factor is the reciprocal of the linear regression coefficients of the standard curves shown in Fig. 3A and B. The values between parentheses represent the relative response factor, *viz.* the reciprocal of the linear regression coefficients of the curves shown in Fig. 3C.

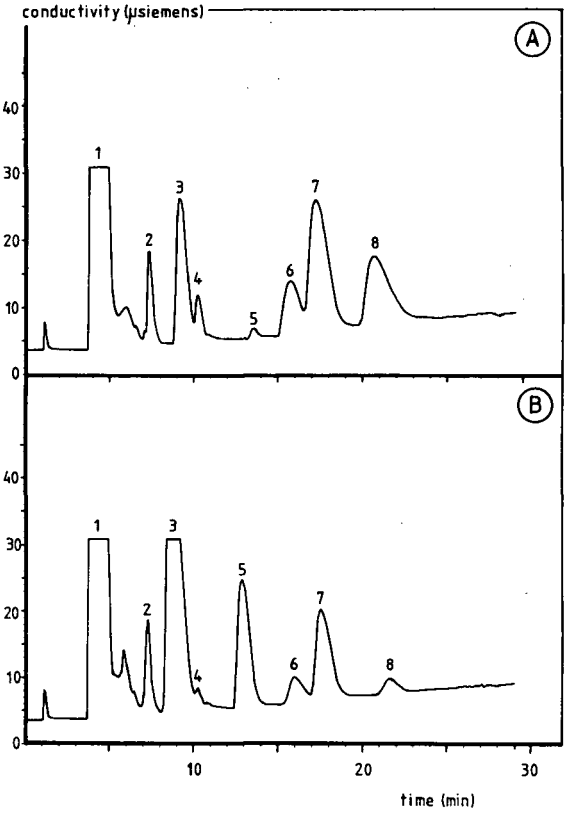

tivity elution profile of cell-free extract from *M. thermoautotrophicum*. The presence of chloride, phosphate, cDPG and 2,3-BPG, identified on the basis of their retention times (Fig. 2A), is evident. None of these or other compounds were detected by UV absorption (not shown). The amounts of phosphate, cDPG and 2,3-BPG were determined to be 398, 306 and 36.3 μmol/g dry weight, respectively. If one assumes an intracellular volume of the cells of 1.8 ml per g dry weigth of cells [17], the internal concentrations of phosphate, cDPG and 2,3-BPG amount to 221, 170 and 20 m*M*, respectively. The last two values correspond nicely to 170 m*M* cDPG and 22 m*M* 2,3-BPG previously measured by isotachophoretic analysis [11].

Enzymic conversion of 2,3-BPG

To test the application of the method, the ATP-dependent synthesis of cDPG from 2,3-BPG was investigated with a cofactor-free extract of *M. thermoautotrophicum*. Reaction mixtures were prepared and analysed as described in the Experimental section; the results are shown in Fig. 4. From Fig. 4C it

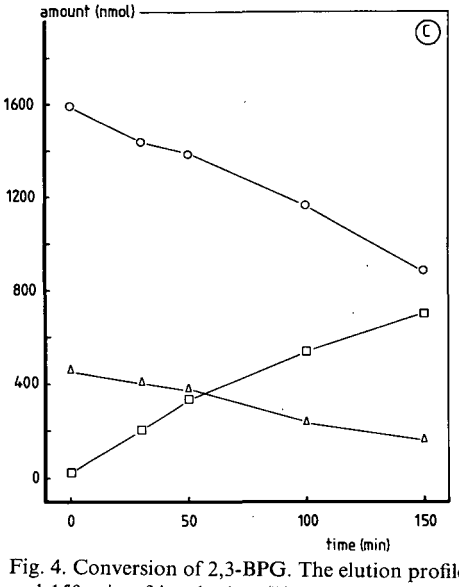

Fig. 4. Conversion of 2,3-BPG. The elution profiles at 0 min (A) and 150 min of incubation (B) are shown. The numbers correspond to chloride (1), oxalate (2), phosphate (3), phosphoglycerate (4), cDPG (5), ADP (6), 2,3-BPG (7) and ATP (8). In (C) the amount of (○) 2,3-BPG, (△) PGA and (□) cDPG are plotted against time.

can be calculated that starting from $t = 0$ min 2,3-DPG decreased at a rate of 4.6 nmol/min (2.2 nmol/min · mg protein). Concomitantly, cDPG was produced at a rate of 4.5 nmol/min (2.2 nmol/min · mg protein). The amounts of 2,3-BPG converted equalled the amounts of cDPG produced. No cDPG was formed when ATP was omitted (not shown). From Fig. 4A and B it can be seen that ADP and phosphate were produced at the expense of ATP. This conversion, however, cannot be solely attributed to cDPG synthesis, since ATP was also converted in the absence of 2,3-BPG owing to the presence of ATPase and adenylate kinase activities in the crude enzyme preparations. In addition, at $t = 0$ min about 400 nmol of PGA and 1600 nmol of 2,3-BPG were present (reaction mixtures were prepared with 2000 nmol of 2,3-BPG); thereafter, PGA slowly decreased. These events also took place when either 2,3-BPG or PGA was incubated in the absence of ATP (not shown) and are the result of 2,3-BPG and PGA phosphatase activities in the extract. None of the above reactions were observed when cell extract was omitted from the assays.

The example shows that the HPLC method developed in this paper may be used for analysis of reaction mixtures that contain high concentrations of proteins (10 mg/ml) and where complex reactions simultaneously take place.

DISCUSSION

Ion-exchange chromatography can be used for the determination of anionic compounds. Separation occurs on the basis of charge and conformation and a compound can be identified by its retention time in the chromatogram. We used this technique to quantify the phosphate-containing metabolites present in methanogenic bacteria, *i.e.* cDPG, 2,3-BPG, P_i, 2-PGA, 3-PGA, PEP and pyruvate. With the exception of 2-PGA and 3-PGA, these compounds are readily resolved and may be simultaneously analysed within a single run. Quantification of cDPG and 2,3-BPG in a cell-free extract of *M. thermoautotrophicum* yielded values that were in good agreement with the literature [11]. Application of the method described was demonstrated by the enzymic ATP-dependent conversion of 2,3-BPG into cDPG. The specific activity of cyclic 2,3-diphosphoglycerate synthetase in cell-free extract of *M. thermoautotrophicum* amounted to 2.2 nmol/min · mg protein, which is about ten-fold lower than in *Methanothermus fervidus* [14]. The sensitivity and accuracy of ion-exchange chromatography are of the same order or even better than to enzymic determination [3] or isotachophoretic analysis [12] of the compounds of interest. Enzymic analysis suffers from the disadvantage that each compound must be determined separately and therefore may be elaborate and time-consuming. By isotachophoresis the various compounds also can be measured simultaneously [12]. However, separation of the individual compounds is easily disturbed and a cleaning operation is required every three or four runs. Moreover, automation has not yet been realized. A definite advantage of ion-exchange chromatography is that it is automated, which decreases the operating time: analyses can be performed 24 h a day.

ACKNOWLEDGEMENTS

The research of G. J. W. M. v. A. was supported by the Foundation for Fundamental Biological Research (BION), subsidized by the Netherlands Organization of Pure Research (NWO); the work of J. T. K. has been made possible by a senior fellowship of the Royal Netherlands Academy of Arts and Sciences (KNAW).

REFERENCES

1 S. Kanodia and M. F. Roberts, *Proc. Natl. Acad. Sci. USA*, 80 (1983) 5217–5221.
2 R. J. Seely and D. E. Fahrney, *J. Biol. Chem.*, 258 (1983) 10835–10838.
3 R. J. Seely and D. E. Fahrney, *Curr. Microbiol.*, 10 (1984) 85–88.
4 R. Hensel and H. König, *FEMS Microbiol. Lett.*, 49 (1988) 75–79.
5 C. J. Tolman, S. Kanodia, M. F. Roberts and L. Daniels, *Biochim. Biophys. Acta*, 886 (1986) 345–352.
6 L. G. M. Gorris, J. Korteland, P. Kaesler, C. van der Drift and G. D. Vogels, unpublished results.
7 R. J. Seely and D. E. Fahrney, *J. Bacteriol.*, 16 (1984) 50–54.
8 R. D. Krueger, S. H. Harper, J. W. Campbell and D. E. Fahrney, *J. Bacteriol.*, 167 (1986) 49–56.
9 R. D. Krueger, R. J. Seely and D. E. Fahrney, *Syst. Appl. Microbiol.*, 7 (1986) 388–392.
10 H. Rudnick, S. Hendrich, U. Pilatus and K.-H. Blotevogel, *Arch. Microbiol.*, 154 (1990) 584–588.
11 L. G. M. Gorris, J. Korteland, R. J. A. M. Derksen, C. van der Drift and G. D. Vogels, *J. Chromatogr.*, 504 (1990) 421–428.

12 G. J. W. M. van Alebeek, C. Klaassen, J. T. Keltjens, C. van der Drift and G. D. Vogels, *Arch. Microbiol.*, 156 (1991) 491–496.
13 J. N. S. Evans, C. J. Tolman, S. Kanodia and M. F. Roberts, *Biochemistry*, 24 (1985) 5693–5698.
14 A. Lehmacher, A.-B. Vogt and R. Hensel, *FEBS Lett.*, 272 (1990) 94–98.
15 P. Schönheit, J. Moll and R. K. Thauer, *Arch. Microbiol.*, 123 (1979) 105–107.
16 P. van Beelen, W. J. Geerts, A. Pol and G. D. Vogels, *Anal. Biochem.*, 131 (1983) 285–290.
17 P. Schönheit and H. J. Perski, *FEMS Microbiol. Lett.*, 20 (1983) 263–267.

Journal of Chromatography, 606 (1992) 73–86
Elsevier Science Publishers B.V., Amsterdam

CHROM. 24 283

Inter-elemental selectivity, spectra and computer-generated specificity of some main-group elements in the flame photometric detector☆

Walter A. Aue, Xun-Yun Sun and Brian Millier

Department of Chemistry, Dalhousie University, Halifax, Nova Scotia B3H 4J3 (Canada)

(First received January 8th, 1992; revised manuscript received April 21st, 1992)

ABSTRACT

Inter-elemental selectivities (ratios of emission intensities) of some important main-group elements —B, Ge, Sn, Pb, N, P, As, Sb, S and Se— have been measured in a filter-less flame photometric detector (FPD) under one common set of conditions. In cases of unknown, unassigned or doubtful spectral distributions —*e.g.* from B, Pb, N and Sb— luminescences were recorded directly from the detector under analytical operating conditions. Despite the detector's dependence on broad, low-resolution spectra that frequently overlap, a computer algorithm using dual-channel data allowed specific (= infinitely selective) chromatograms to be recorded for any FPD-active element. The spectral requirements of this method, which is based on the conditional access (CONDAC) of slope ratios, were minimal: one optical filter permitted a single computer-stored run to produce several CONDAC chromatograms. Each of these was specific in the sense that it showed only the peaks of one particular element.

INTRODUCTION

A variety of factors have contributed to the ever-increasing presence of complex, multi-element chromatograms in the analytical laboratory. Some factors are task-related, such as the prevailing trend toward environmental and biochemical samples. Others are technique-related, such as the ready availability of high-resolution chromatographies for both volatile and non-volatile organics, and the improvements in sensitivity and scope of various gas chromatography (GC) detectors.

The flame photometric detector (FPD) provides a case in point. The only elements to which it was once considered sensitive were phosphorus and sulphur; and its function was restricted to *gas* chromatographic effluents [1]. In the years since its commercial introduction [2], some twenty elements have been shown to respond in the FPD, and the detector has been used with separation methods for *non*-volatile analytes such as micro-high-performance liquid chromatography and supercritical fluid chromatography. The FPD is often used for surveys —particularly for the presence of compounds containing P, S and Sn— in chromatograms that contain hundreds of peaks.

In such cases it is important to recognize those compounds that contain FPD-active elements, since these are more likely to exhibit biological activity and, consequently, represent the analytes of interest. Beyond the mere recognition that *some* hetero-atom is present in a particular peak, its identity has to be established. This means that inter-elemental selectivity and, if attainable, element-specific response become crucial quality parameters.

We have recently studied comparative FPD spectra as well as FPD selectivity ratios of various *transition* elements from conventional (interference-fil-

Correspondence to: Dr. Walter A. Aue, Department of Chemistry, Dalhousie University, Halifax, Nova Scotia B3H 4J3, Canada.

☆ Part of doctoral thesis of X.-Y. S.

0021-9673/92/$05.00

ter equipped) and open (filterless) detector channels [3,4]. We have also suggested dual-channel methods to improve that selectivity for compounds of Mn, Ni, Fe, Ru, Os, etc. [4–6]. In the present study we intend to explore selectivity among *main-group* elements, and to devise approaches of increasing their selectivity to apparent specificity. Note that the terms "selectivity" and "specificity" retain here their original analytical meaning, *i.e.* "specificity" indicates infinite selectivity and, derived from that, "apparent specificity" refers to a situation where compounds of only one particular element appear on the chromatogram.

While specificity, thus defined, is a simple and unambiguous term, the term "selectivity" can have several meanings. Traditionally, selectivity ratios in flame photometric detection of GC effluents have been used to compare the response of a particular analyte element within a narrow wavelength range (typically a 10-nm interference filter bandpass) to that of a hydrocarbon. Comparison with another FPD-active element was rare. Not surprisingly, then, the detector conditions of these literature measurements were most often those at which the element of primary interest exhibited the highest signal/noise ratio (rather than, say, the conditions at which it displayed the largest discrimination against some other species).

Current interest in *multi*-element mixtures suggests the determination of inter-elemental selectivity ratios at conditions that are deliberately not optimized for one particular element, but that suit as many elements as possible. Among the earlier investigated transition metals, individually optimized flame conditions did not differ excessively from one element to the other [3]. Also, the luminescence of many elements did spread out over most of the photomultiplier's spectral range, thereby severely curtailing attempts to improve selectivity by spectral means alone. In fact, the selectivity among transition metals proved to be much more a function of their comparative overall emission intensities ("innate" sensitivities) than a function of the —however carefully chosen— wavelengths of the various interference filters deployed to monitor each metal individually. The increase in various selectivity ratios from a channel that is open to the full spectrum, to one that is restricted to a narrow bandpass, was usually less than ten. In contrast, the comparative luminescence yields of the transition elements varied by several *powers* of ten [5].

Main-group elements could be expected to behave likewise. Spectra from different elements do differ by several orders of magnitude in intensity. And, more often than not, their wavelength ranges overlap severely. As a historical example, the interference of S_2 bands —which stretch over and beyond the HPO emission range— caused the earliest interference problem in the FPD. Even at that time, its solution involved a *dual*-channel approach [7] (*cf.* ref. 8). For any method that relies on two or more simultaneous chromatograms being obtained under different optical circumstances, spectra valid *at the analytical operating conditions* of the detector are needed for a rational choice of wavelengths to monitor. Only a few of the more prominent emissions —S_2, Se_2, HPO, SnH, SnOH and the like— have been obtained from a conventionally operating FPD.

A complete account of interelemental selectivity, even at one and the same set of conditions, can only be provided by the full ranges of all calibration curves. If single-number selectivity ratios are to serve instead —as they are often asked to do, for instance in this report— the data must at least be taken from within the linear range of *both* elements. To illustrate: deceptively high metal/carbon selectivity ratios have resulted when hydrocarbon standards were used in amounts beyond their linear range.

Selectivity ratios (of linearly responding elements) are traditionally defined as ratios of response produced by injecting *equal amounts* of elements (or compounds). Alternatively, selectivity ratios are defined as those ratios of injected amounts that produce *equal response*. These definitions correspond, of course, directly to the vertical and horizontal distances between calibration curves plotted in log–log format. Since luminescence intensities cover several orders of magnitude (*i.e.* more orders than the typical linear range), the latter mode of measurement is called for. Also, "mol of element per second" data are used here for analytical convenience.

Beyond the necessary mapping of "innate" selectivities, we were interested in upgrading these selectivities to apparent specificities. This proved possible by letting a computer decide which dual-chan-

nel signals did and which did not originate from a particular element — and directing it to report only the latter. This "conditional acceptance" or "conditional access" (CONDAC) chromatography has been used before [6], although then focused on transition elements and hampered by a still awkward computational procedure. The present study retains the basic principle but uses a direct, simple and more convenient CONDAC-type algorithm on main-group elements.

Now, the conditional acceptance of a particular chromatographic peak is based on the agreement of its ratio of response from the two channels with the "true" value determined previously from an appropriate standard. Thus, if R_A and R_B be the responses (signals, peaks) and S_A and S_B their slopes (first differentials, changes in signal with respect to time) in channels A and B, data pairs are accepted on condition that

$$(S_A - f \cdot S_A) < S_B \cdot SR < (S_A + f \cdot S_A)$$

wherein f is a (user-selectable) factor defining the allowable deviation from the "true" slope ratio SR (ratio of emission intensity changes in the two channels during elution of the hetero-element standard). To be accepted into the CONDAC chromatogram, each peak has to contain a certain percentage (typically 50 to 90%) of data pairs already accepted by the above algorithm. These pairs must stretch over a reasonable time interval (typically 1 to 4 standard deviations of the average Gaussian peak), besides conforming to certain obvious criteria like starting with an increase in positive slope. The data pairs of an accepted peak can be averaged

$$R = (R_A + R_B \cdot SR)/2$$

but the choice of either one or the other single channel is also available to the analyst. All three response modes can be plotted directly or after multiplication by a user-selected scaling factor for convenient recorder display. A "zero" (= "no information") line obtains for data pair sequences failing to gain access.

This approach requires prior knowledge of the slope ratio SR. So far, its value has been determined, very roughly, from peak heights —or, much more precisely but also much more slowly, from an operator-adjudicated iterative matching of peak shapes [4,6]. In this study, the slope ratio average is determined from a "standard peak" on the screen, whose beginning and end (its calculation limits) are defined by the operator through the use of vertical cursors.

The "standard peak", from which the slope ratio is to be determined, can be introduced internally or externally. As an internal standard, the peak is a constituent of the chromatogram under investigation; as an external standard, it has been measured earlier. As is generally the case for chromatographic standards —*e.g.* those of retention or calibration— *spectral* standards, too, provide better analytical performance when used internally than externally. The more demanding and variable the chromatographic circumstances, the more important and decisive the role of the internal standard. It may be mentioned that slope ratios, their "true" value notwithstanding, can be adjusted in their error-band to provide maximum protection against interference from other hetero-elements.

The obvious questions to be answered in regard to the new algorithms are how reliable and convenient they work, how well they suit main-group elements, and how sophisticated the optical discrimination of the dual-channel FPD system has to become in order to result in specific chromatograms.

The objective here is to show that even the simplest of spectral differences between the channels (one channel being used with, the other without, a filter) is enough to allow CONDAC chromatograms for several main-group elements to be obtained from a single chromatographic run. In other words: the objective is to demonstrate that apparent specificity can indeed be extracted from an experimental situation of very limited selectivity. Necessary for achieving and assessing success in this venture is, of course, a thorough knowledge of the analytically relevant spectra and their comparative intensities. Even beyond CONDAC chromatograms, these should be of basic interest to both spectroscopists and analytical chemists.

EXPERIMENTAL

The program used to process the inputs from the dual-channel FPD, and to produce element-specific chromatograms, was assembled for this study by building on the relevant sections of three existing programs. The first, named CHROM, is a laborato-

ry-developed, general-purpose, high-resolution program for the acquisition and manipulation of dual-channel data [4]. From it were taken the input/output functions and the zoom and digital-filtering modes, plus statistical diagnostics that define noise in Gaussian terms for determination of detection limits (*cf.* ref. 3). The second program, BC, had originally been adopted from the common domain and provides a cubic-spline manual baseline correction useable on CHROM data. The third program, CORR, is a laboratory-developed, special-purpose correlation algorithm designed to compare amplitude-matched two-channel peaks for conformity of the first and second differentials [6]; it was further adjusted and augmented by the new routines described in the Introduction.

The dual-channel data, as received from the (modified) Shimadzu electrometers, were converted to digital pulse trains by a laboratory-made interface [4] and, after counting at 0.1-s intervals, were processed by a 12 mHz AT-compatible computer equipped with 1 megabyte of memory, 40 megabyte hard disk, 80287 math coprocessor, VGA display adapter and Multi-Sync monitor.

The gas chromatograph, a Shimadzu Model GC-4BMPF, was used with a short packed column (100 · 0.3 cm I.D. glass, 5% OV-101 on Chromosorb W, 100–120 mesh) under a nitrogen flow of 20 ml/min and temperature-programmed conditions. The Shimadzu dual-channel FPD (with its quartz chimney normally left in place, in contrast to earlier work with transition metals [3,4]; and with its flame shield down for viewing the unshielded flame) was run at the "*common*" conditions of *200 ml/min hydrogen and 45 ml/min air* (unless otherwise indicated) under an efficient exhaust duct. The two photomultipliers were both Hamamatsu R-374 tubes. These have a nominal 180–850 nm range with maximum yield at 420 nm; and were run with a roughly signal/noise ratio-optimized supply voltage (for instance, *ca.* 550 V for the comparatively large light input of an open, *i.e.* full-spectrum channel). For the acquisition of spectra, two types of instruments were used depending on the light level available from the typical FPD operating conditions. Both the quarter-meter grating monochromator (Jarrell-Ash Model 82-415) and the variable interference filter (Oriel Model 7155 "filter monochromator") employed a Hamamatsu R-1104 (180–850 nm, 420 nm maximum) photomultiplier tube. Interference filters were mostly Ditric stock items; where their optical specifications are relevant they are indicated in the legends.

The compounds used for the determination of innate sensitivities/selectivities are listed in Table I; they were used without further purification and in amounts commensurate with their linear range in the FPD.

RESULTS AND DISCUSSION

Our choice of particular main-group elements for this study is, to a certain extent, arbitrary. Some main-group elements have never been seriously tested for response in the FPD. Others are known to respond —*e.g.* In, Bi, Te— but are excluded here for lack of general importance or analytical interest, or for the commercial scarcity or premature decomposition of the compounds supposed to carry them through the GC system. Still others —*e.g.* Cl, Br, I— are disregarded here because they respond adequately only in the presence of another metal (Cu, In, etc.). Of the remaining elements, the ones slated for present scrutiny are primarily those that do hold (or could hold) wider interest, that do occur (or could occur) in environmental samples, and that —most important for us— are inexpensive to acquire, easy to handle, and convenient to test.

Our choice of conditions, too, is somewhat arbitrary. Different elements do respond best at *differ-*

TABLE I

COMPOUNDS USED FOR DETERMINATION OF SELECTIVITY RATIOS

Note: The calculation uses moles of *element*, not moles of *compound* (*cf.* S, Se, B, C).

Sn	*n*-Tetrabutyltin	$(n\text{-}C_4H_9)_4Sn$
Ge	Tetraethylgermanium	$(C_2H_5)_4Ge$
P	Triethylphosphate	$(C_2H_5O)_3PO$
S	*tert.*-Butyldisulphide	$(tert.\text{-}C_4H_9)_2S_2$
As	Triphenylarsine	$(C_6H_5)_3As$
Se	Dimethyldiselenide	$(CH_3)_2Se_2$
Sb	Triphenylantimony	$(C_6H_5)_3Sb$
Pb	Tetraethyllead	$(C_2H_5)_4Pb$
B	*o*-Carborane	$1,2\text{-}H_2C_2B_{10}H_{10}$
N	*n*-Tributylamine	$(n\text{-}C_4H_9)_3N$
C	*n*-Hexadecane	$n\text{-}C_{16}H_{34}$

ent flow settings. (In addition, absolute and relative elemental responses depend on the construction of the detector.) However, since response variations with flow are rarely exorbitant, and since inter-element selectivity properly comes into play only if two or more FPD-active elements are to be considered, we felt that using a *common* set of conditions was both more realistic and of greater value to the analyst than comparing data that were separately optimized for each particular element. Still, in an experimental detour we did indeed optimize performance for individual elements, but only to ascertain that their optimized settings did not differ drastically from the "common" conditions (see Experimental) selected to accommodate all of them.

In this context two special groups of elements need to be mentioned. Tin (also germanium) can produce a blue luminescence on the surface of quartz [9]. This luminescence is far more intense than the SnOH and SnH (or GeOH and GeH) emissions, and it is easy to obtain from an HCl- or HBr-doped chromatographic system [10]. In a recent study involving butyltins in a mussel sample, for instance, the surface emission proved about a hundred times more sensitive than the commonly used hydride band [11]. However, the surface emission requires for maximum presence the careful adjustment of conditions, and the absence of (larger amounts of) elements such as phosphorus that "poison" the quartz surface. These circumstances were not compatible with our testing protocol. The more sensitive blue emissions of tin and germanium were therefore deliberately minimized in this study, primarily so by removing the quartz chimney.

Certain elements (*e.g.* boron and arsenic) noticeably increase in signal and, more importantly, also in signal/noise ratio as the air flow increases toward stoichiometric. If such conditions were chosen for a multi-element analysis, the selectivity ratios would change significantly (for instance, B and As response would become stronger while P, S, and Sn response would become weaker). It should be mentioned in this context that arsenic can produce a vastly superior response in a special detector configuration [12].

Solely for this study it would not have been necessary to check and, in some cases, to chart the actual spectra. Yet, knowing these made the task of wavelength selection so much easier —and, beyond this study, such knowledge can be extremely helpful for designing solutions to various FPD selectivity problems. Also, certain spectral features, by virtue of not having been reported before, may attract the interest of the spectroscopist. As discussed earlier [3], analytically reliable spectra should originate from the same detector as used in the actual analysis, running at the same operating conditions. Some such spectra —HPO, S_2, etc.— have been amply documented in the literature and will not be reproduced here. However, for purpose of discussion we need to record the luminescences generated in the FPD by compounds of boron, lead, nitrogen and antimony. Note that the following spectra were obtained by repeatedly injecting the analyte while manually advancing the monochromator's wavelength drive; they are hence free of flame background emissions.

Spectra

Boron. The green flame bands of boron have been studied for over one-and-a-half centuries, and much analytical work has been done with them [13]. Boron spectra are included here only because of the analytically as well as spectroscopically relevant presence in the FPD of *two* emitters; and because the relative contributions of the latter, not surprisingly so, do change with the air flow. The two analytical studies [14,15] closest related to the present context both mention the *ca.* 546 nm emission (and interference filters with central wavelengths of 550 and 546 nm, respectively); they attribute the band to BO. It is interesting to note that Braman and Gordon's "borane monitor" ran with a flame that was air-rich and much larger than that of a typical FPD. For sensitivity reasons, the monitor seems to have actually used a green glass filter [14] (the text is ambiguous on that point). Sowinski and Suffet's work on the Melpar FPD preferred an interference filter; their smaller flame (as judged by the conditions given for the calibration curve) was hydrogen-rich but just barely so [15]. Neither study shows a spectrum. Pearse and Gaydon [16], with some historically justified hesitation (*cf.* ref. 17), list the 546-nm band under "boric acid fluctuation bands, BO_2". They note that "BO bands are usually present as well" (the closest bands of the BO α system occur at 551 and 555 nm [16]).

Indeed, the spectrum taken at our "common"

FPD conditions (Fig. 1, upper part) represents a mixture of systems. If the flame is changed to consume more air, almost up to stoichiometry, the spectrum (Fig. 1, lower part) takes on the appearance of a single system whose bands coincide with those listed for BO_2 [16], $A^2\Pi_u$–$X^2\Pi_g$. The additional spectrum present in the upper part of Fig. 1 is the α system of BO, $A^2\Pi$–$X^2\Sigma^+$. A comparison of the two scans shown in Fig. 1 provides an instructive example of the strong influence FPD flame conditions exert on the spectral distribution, hence the choice of wavelength (or *vice versa*, depending on the optimization mode). This is important not only for spectroscopic assignments but also for the objectives of *this* study: spectra representing more than one emitter alert the analyst to a likely change in the dual-channel slope ratio with a change in detector gas flows.

Lead. Fig. 2 shows the luminescence obtained from injections of tetraethyllead, at the "common" conditions of this study. Some bands are superimposed on a continuum (whose relative contribution grows as the air flow is lowered —*i.e.* under those filterless conditions that produce the maximum signal/noise ratio). The presence or absence of the quartz chimney seems to be of no importance. There is little if any evidence of the 405.8 nm line (*cf.* ref. 3 for energy considerations) that has been used in the photometric detection of lead in gasolines samples fed to an oxyhydrogen flame [18]. The response of lead in a typical FPD has been mentioned before in the literature [19]; however, no spectral data were given there.

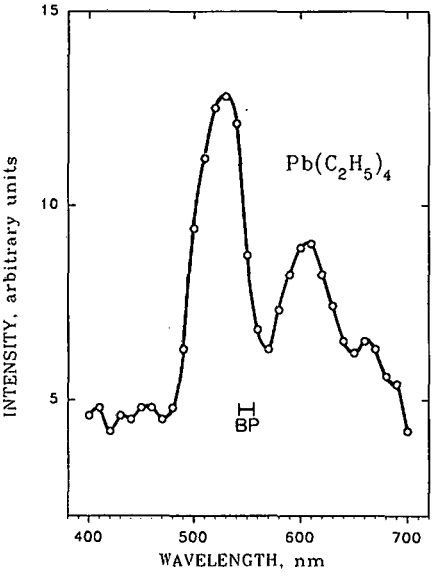

Fig. 2. Spectrum from tetraethyllead at "common" conditions. Filter monochromator with R-1104 PMT. BP = Bandpass (as per Oriel specification).

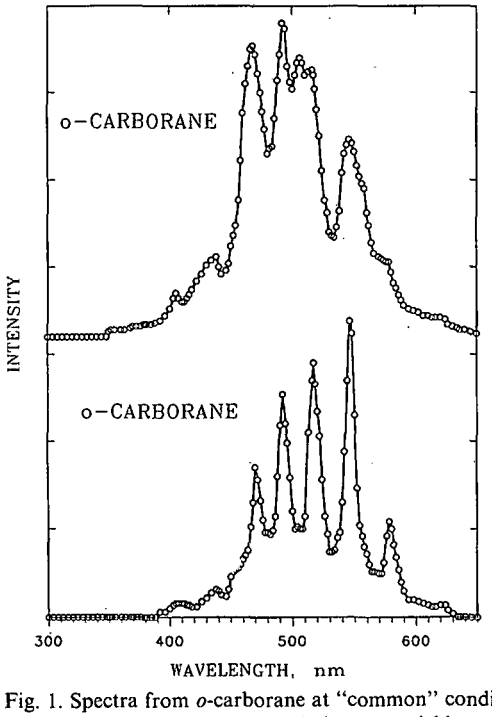

Fig. 1. Spectra from *o*-carborane at "common" conditions (upper part; bandpass 6–7 nm); and close to stoichiometric conditions (lower part; hydrogen 47, air 100, nitrogen 20 ml/min; bandpass 1.6 mm). Grating monochromator, Hamamatsu R-1104 photomultiplier tube.

The low light level (consequently the poor resolution) prevents a possible spectroscopic assignment. The PbH bands could be involved, but the B system of PbO also occurs in that region [16]. Analytically (not spectroscopically) interesting may be the fact that the maximum luminescence of lead is located very close to that of phosphorus, which is conventionally monitored as HPO at 526 nm.

Nitrogen. Fig. 3 shows the flame luminescence due to the introduction of indole. There is no significant difference in the spectra taken with and without the quartz chimney. That this weak luminescence does not originate from the carbon part of the molecule is obvious from the fact that it can also be

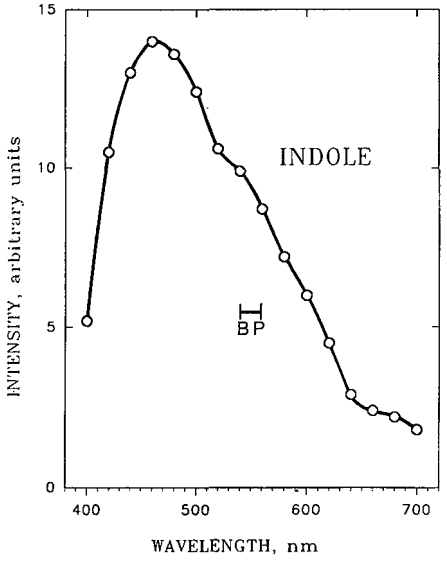

Fig. 3. Spectrum from indole at "common" conditions. Filter monochromator.

obtained from N_2O. The low intensity of organo-nitrogen response is probably the reason that, to our knowledge, it is not described by any detailed report in the FPD literature, despite the fact that nitrogen compounds are ubiquitous constituents of environmental and biological samples.

For the history of direct and indirect nitrogen emissions in flames, Gilbert's detailed account [13] should be consulted; we shall cite here only information that is of particular relevance to the FPD. The interference of nitrogen compounds in the "borane monitor" (a device related to the FPD) was attributed to the NH_2 α bands [14], and a later paper by the same author contains a spectrum and a comparison of the response of nitrogenous *vs.* carbonaceous compounds. The spectrum presented there for triethylamine [20] shows a certain similarity with the luminescence envelope of Fig. 3; however, it is clearly located farther toward the red. The same is true of the spectrum shown for ammonia in a hydrogen-nitrogen diffusion flame [21]; and of the "bright, white" emission in the molecular emission cavity analysis (MECA) oxy-cavity tentatively attributed to the NO–O continuum and monitored for analytical purposes at 500 nm [22]. Interestingly enough, the same study also contains the spectrum of a "faint blue" emission [22, Fig. 1A], which was obtained in the absence of additional oxygen and closely resembles the one obtained by us in the FPD (see Fig. 3). In a hydrogen–nitrogen diffusion flame —where the 336-nm NH band was most prominent and was therefore used for the detection of ammonia— "the wavelength of maximum emission for the NH_2 band varied between 425 and 575 nm". Viewed on a long-slot burner, "a persistent blue emission" was observed at the base of the flame and (with larger amounts of ammonia) a "yellow emission" appeared above it [23].

Note that all these literature flames were oxygen (air) rich; and that, with the possible exception of the regular MECA cavity, they were much hotter than the puny, strongly hydrogen-rich flame of the FPD. Under the "common" conditions of this study, the highest temperature of the FPD flame, as suggested by the response of a thin-wire thermocouple, remained below 550°C. Different emission behaviour is thus to be expected, although both hydrogen-rich and air-rich types of diffusion flames do, of course, contain all three of hydrogen-rich, stoichiometric and air-rich zones. Furthermore, the spectral distribution (wavelength of maximum emission) is likely to vary if two or more chemiluminescent emitters of roughly comparable strength are present.

It may be reasonably assumed that the weaker *blue* emissions referred to in refs. 22 and 23 came from cooler and more hydrogen-rich flame zones and hence were more likely to correspond to the emission shown in Fig. 3. Equally reasonable is the assumption that more than one excited species contributed to the luminescence in the 400–600 nm region, particularly so in the hotter flames of the literature. In several of our own experiments, in which constant doping levels of N_2O entered a variety of FPD flames monitored by a grating monochromator, we, too, found slightly shifting spectral envelopes. The relative and absolute hydrogen and air flows of these FPD flames varied from very hydrogen rich up to almost stoichiometric; and their temperatures from very low to moderately high. At larger air flows and hence hotter conditions, the slight shoulder around 550 nm (see Fig. 3) became more pronounced and, as a consequence, the emission maximum appeared to shift slightly toward the red. This is consistent with the literature behaviour of various types of much hotter flames [14, 21-24], for which visible nitrogen emission occurs at clearly

longer wavelengths than in the conventional FPD.

Neither the NH_2 bands [16] nor any of the other nitrogen emissions commonly found in high-energy sources [13, 16] could be clearly attributed to the FPD luminescence shown in Fig. 3. The 300–400 nm region (which, in typical spectroscopic flames, contains CN and NH bands) was scanned in separate experiments but contained little radiation short of some flame background (OH). Although the presence of NH_2 and/or NO_2 [16] emissions cannot be excluded, we prefer to characterize nitrogen response in the FPD as still being of *unknown* (and possibly mixed) origin. Since the spectral range happens to overlap the emission regions of several important elements —though with low intensity— nitrogenous analytes should be considered capable of causing false positives in various types of FPD-based analyses.

Antimony. Fig. 4 shows the spectrum derived from the luminescent response of triphenylstibine. From a low-temperature hydrogen diffusion flame, a similar spectrum was obtained [25] and attributed to the A system of SbO, particularly $A^2\Pi_{3/2}$–$X^2\Pi_{3/2}$ [16].

For comparison only, we are including in Fig. 4 the spectrum derived from triphenylarsine. It appears to be the long-known "arsenic continuum" [13], similar to the emissions recorded from a laboratory-made FPD [12] and a low-temperature hydrogen diffusion flame [25]. The emitter is generally considered to be unknown (although in some places it is referred to as AsO). We also attempted to check triphenylbismuthine (*cf.* ref. 19) but, encountering problems of reproducibility and contamination, soon gave up.

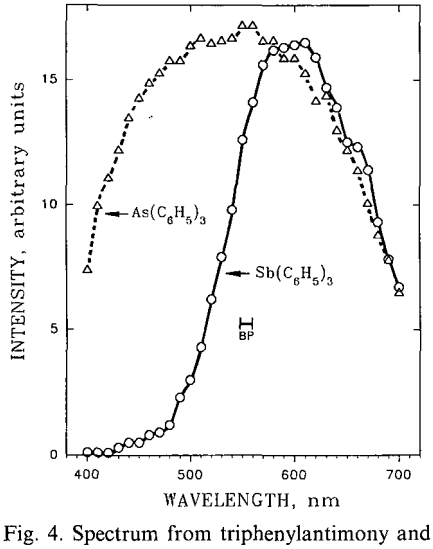

Fig. 4. Spectrum from triphenylantimony and triphenylarsenic at "common" conditions. Filter monochromator.

Selectivity ratios

Table II presents a listing of "innate" selectivity ratios, *i.e.* the ratios of luminescence intensity from an "open" (filter-less) channel. The data describe how much more light the (red-extended) phototube picks up per atom of a particular element (listed vertically) than per atom of another element (listed horizontally). (Sulphur and selenium are included here even though their calibration curves are non-linear, hence inadequately characterized by a single-number selectivity ratio. To compensate in a minor way, their injected amounts are listed in a Table II footnote.)

No untoward surprises lurk in Table II. Clearly, different flow conditions would have lead to a somewhat different set of numbers. Such numbers are valuable for predicting relative elemental responses from a multi-element sample monitored by a *filterless* FPD channel. Given, in a particular case, knowledge of the prevailing spectra on one hand and specifications of interference filters and photomultiplier tubes on the other, the numbers of Table II could be further extended to estimate detector performance from a *spectrally selective* channel. (As will become apparent later, the difference between a channel that is equipped with an interference filter and one that is not, is often quite small.)

Although our measurements and calculations used a minimum of two significant digits, only one digit is shown in the final result. This is meant to remind the reader of further aspects that influence such numbers. Some are obvious, such as the construction or contamination of the detector, and the response profile of the chosen photomultiplier tube. Others are less obvious, such as the question whether some of the chosen test compounds perhaps suffered from premature decomposition; or whether different compounds of the same element would have given different results. For instance, it is well known that aliphatic carbon responds less strongly than aromatic carbon; and the debate whether the

TABLE II

INTER-ELEMENT FULL-SPECTRUM FPD SELECTIVITIES OF MAIN-GROUP ELEMENTS UNDER COMMON CONDITIONS

Molar response of element A (column) over molar response element B (row); both within linear range. "Common" conditions as cited in Experimental section.

Element A	Element B										
	Sn[a]	Ge[a]	P	S[b]	As	Se[b]	Sb	Pb	B	N	C[c]
Sn[a]	"1"	6	$4 \cdot 10^1$	$(9 \cdot 10^1)$	$6 \cdot 10^2$	$(6 \cdot 10^2)$	$2 \cdot 10^3$	$6 \cdot 10^3$	$2 \cdot 10^4$	$3 \cdot 10^4$	$9 \cdot 10^6$
Ge[a]		"1"	8	$(2 \cdot 10^1)$	$1 \cdot 10^2$	$(1 \cdot 10^2)$	$4 \cdot 10^2$	$1 \cdot 10^3$	$4 \cdot 10^3$	$6 \cdot 10^3$	$2 \cdot 10^6$
P			"1"	(2)	$1 \cdot 10^1$	$(1 \cdot 10^1)$	$6 \cdot 10^1$	$1 \cdot 10^2$	$6 \cdot 10^2$	$7 \cdot 10^2$	$2 \cdot 10^5$
S[b]				"1"	(7)	7	$(3 \cdot 10^1)$	$(6 \cdot 10^1)$	$(2 \cdot 10^2)$	$(3 \cdot 10^2)$	$(1 \cdot 10^5)$
As					"1"	(1)	4	$1 \cdot 10^1$	$4 \cdot 10^1$	$5 \cdot 10^1$	$2 \cdot 10^4$
Se[b]						"1"	(4)	$(1 \cdot 10^1)$	$(4 \cdot 10^1)$	$(5 \cdot 10^1)$	$(2 \cdot 10^4)$
Sb							"1"	2	$1 \cdot 10^1$	$1 \cdot 10^1$	$4 \cdot 10^3$
Pb								"1"	4	5	$2 \cdot 10^3$
B									"1"	1	$4 \cdot 10^2$
N										"1"	$3 \cdot 10^2$
C[c]											"1"

[a] Mainly Sn. H and SnH: or GeOH and GeH emissions: the more sensitive blue surface luminescence on quartz is deliberately held to a minimum.

[b] Sulphur and selenium have mostly quadratic calibration curves. For this reason, their values are given in parentheses; they refer to $9 \cdot 10^{-12}$ or $1 \cdot 10^{-10}$ mol/s of S or Se, respectively.

[c] Hydrocarbons produce negative response (inverted peaks) at the chosen conditions with a red-extended phototube.

response of sulphur does indeed vary with the nature of its functional group, has not yet subsided. Beyond these elements, though, we are not aware of any other glaring case where an element's FPD response would strongly depend on its original valence state and/or molecular surroundings. (A reviewer of this manuscript pointed out a report to the contrary, which describes the behaviour of nitrogen in ammonia as opposed to amines [26]).

Apparent elemental specificity

CONDAC chromatograms can perform a variety of tasks. One of the easiest is to distinguish between two congener elements whose spectra overlap (*e.g.* S and Se, As and Sb, etc.), or between two emitters whose low-resolution spectral envelopes closely resemble each other (*e.g.*, surprisingly, Se_2 and GeOH). Once the relevant FPD spectra are known, the choice of wavelength becomes trivial. Incidentally, this type of analytical situation can also be handled —though to different ends— by *non*-conditional dual-channel FPD algorithms [4]. Being fairly obvious, it needs no further belaboring.

Somewhat more interesting for us (and, we hope, more revealing for the reader) are situations in which several hetero-atoms appear at different positions in the chromatogram; and in which only one gas chromatographic injection, *i.e.* only one spectral setting, is used. (Should multiple injections be permitted, optical changes be possible, and spectral distributions be known, the task of distinguishing among the elements simply reduces to repeats of the process suggested in the preceding paragraph.)

Particularly in the case of samples that are not only in short supply (so that every injection counts) but that are also undefined in regard to the elemental composition of their components (so that a survey-type analysis is called for), the smallest reasonable extent of optical discrimination can ensure that none of the possibly present FPD-active elements is overlooked. Typical for such a low-resolution mode is the combination of one channel without filter (an "open" channel) with another one using only a wide-band or a long- (or short-)pass filter. Another reasonable mode (checked out but not reduced to a figure here) is the combination of a long-pass with a short-pass filter, whose transmission ranges may overlap to a major or minor degree. Even the use of

stable colour glass filters would seem quite suited to the purpose (as long as sharp cut-offs are not required for a particular analytical task). Because such configurations are spectrally much less discriminating than, say, two channels equipped with two narrow-band interference filters, they should help to demonstrate how far the optical conditions can be relaxed in the CONDAC approach. Modes that make use of longer sections of the available wavelength range can also produce higher sensitivity for a larger number of elements. Both of these considerations are reflected in the protocol for the CONDAC demonstration experiments of this study. A further consideration was to use not just one but several peaks containing the *same* hetero-element. This tests the reliability of the CONDAC algorithm: all of the peaks that contain the target element (but none of the peaks that do not) must be present in a *bona fide* "element-specific" chromatogram.

Analyte mixtures and spectral conditions designed along these lines are involved in the following three figures. In each case will the pictorial sequence first show the open (filterless) channel; then the wavelength-selective channel; then the sequence of (vertically off-set) CONDAC chromatograms derived by the computer from the two original inputs displayed on top.

Fig. 5 shows a temperature-programmed separation of standard compounds identified by the FPD-active hetero-atom they contain, *i.e.* nitrogen or phosphorus or selenium. Note that the differences in relative peak size between the open and the 40 nm wide-band channel are small (a *narrow*-band filter centered on the main HPO emission, while increasing selectivity and decreasing sensitivity, would not have changed these correlations by much). That the presence of an interference filter —as compared to its absence in an open channel— brings about only small improvements in selectivity, does not represent the exception but, rather, the rule among FPD-active elements (compare the following figures as well as refs. 4 and 6).

For the CONDAC algorithm to work best, the slope ratios for all peaks of a particular hetero-element should be precisely the same. This, unfortunately, may not always be the case. A variety of reasons could be responsible for a deviation in slope ratio, the most obvious being random error. In an

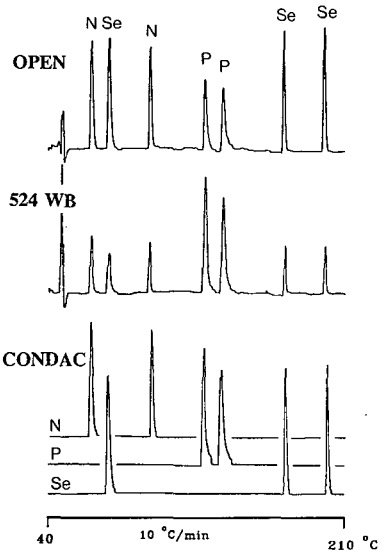

Fig. 5. Two-channel and CONDAC chromatograms from a temperature-programmed separation of (in order of elution) 300 ng triallylamine, 22 ng dimethyldiselenide, 500 ng *n*-butylamine, 1.0 ng trimethylphosphate, 0.6 ng triethylphosphate, 18 ng methylbenzselenazole, and 20 ng diphenylselenide. One channel open, the other fitted with a 524 nm wide-band (WB) interference filter (Ditric, 40 nm bandpass).

effort to demonstrate applicability to trace analysis, the amounts of the substances used here had been kept deliberately low so that the two baselines, even after some digital filtering, still carried noise. Obviously, a similar band of noise distorts the necessary slope measurements on the peaks (this is not visually apparent in the figures due to a sluggish recorder pen climbing up and down steep slopes, but it can be easily ascertained from time-extended analog or digital computer representations). Of course, there are also basic chemical rather than random statistical processes that could cause the slope ratio to vary among compounds of the same element (see below).

Despite the relatively small amounts of analyte in our experimental mixtures, the noise-induced variation of slope ratios was not large enough to prevent the CONDAC algorithm from identifying all three FPD-active hetero-elements. To demonstrate this, the individual CONDAC chromatograms for nitrogen, phosphorus and selenium are stacked up in the lower part of Fig. 5. Apparent specificity has been successfully achieved.

Chromatographers may find the principle of a CONDAC chromatogram logically convincing but its appearance strangely surprising. It is for graphical expediency that the recorder (really: the computer) draws a "zero" line during the absence of acceptable peaks. This zero line may usurp the role of a conventional baseline —yet it is only an impostor devoid of true chromatographic credentials.

Another aspect that may make Figs. 5–7 confusing to the perceptive reader, concerns the heights of CONDAC peaks when compared to those of their parent peaks. The explanation of certain size discrepancies is simple: the CONDAC algorithm accepts or rejects peaks but, having two channels at its disposal, allows the operator to choose which version of the accepted peak to send to the recorder (*i.e.* the peak from channel 1, or from channel 2, or from their average —either in original intensity or after multiplication by a convenient scaling factor). In many cases it made sense for us to select the "better" channel, *i.e.* the one in which the particular element displayed the larger signal/noise ratio.

Providing yet another cause for possible confusion, close inspection of any CONDAC chromatogram reveals that the very start and end of most peaks is characterized by a vertical jump of the recorder pen —a jump that forms the visual connection of the "zero" (= no information) line with the first and then the last datum of an algorithmically accepted stretch of signals. (Actually, the operator *does* have the option of extending that stretch beyond computer acceptance limits in a subroutine called "skirting", but this expedient had been designed for other purposes and was deliberately not invoked in this study). A *short* vertical trace normally reflects the position of the signal in relation to the "true" chromatographic baseline. A *long* vertical trace, on the other hand, indicates that the algorithm has rejected a significant part of the peak itself, usually because that part happens to overlap the peak of another FPD-active hetero-element. (To deal analytically with such a problem, a subtraction chromatogram [4] can be obtained from the computer.) The short vertical artifacts do not prevent proper quantitation; however, a full discussion of analytical performance as related to the CONDAC algorithm is beyond the scope of this qualitatively-minded manuscript.

Fig. 6 presents a situation similar to that of Fig. 5, except that the FPD-active hetero-elements are now sulphur, arsenic, boron and selenium. (It must be admitted that we experienced some difficulties in coming up with convincing test mixtures: of certain elements there are few suitable representatives commercially available and, occasionally, chromatographic overlap or chemical reactions rendered them unfit for the task.)

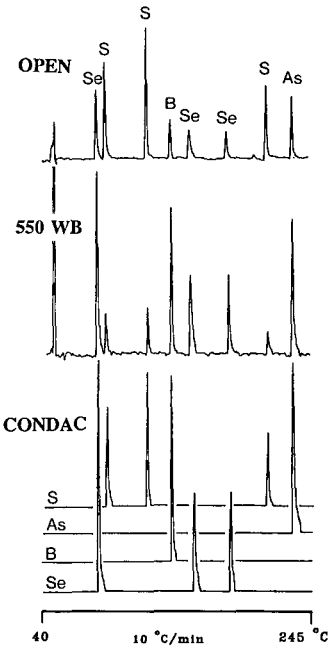

Fig. 6. Two-channel and CONDAC chromatograms of (in order of elution) 14 ng dimethyldiselenide, 1.0 ng diethyldisulphide, 1.6 ng di-*tert.*-butyldisulphide, 100 ng *o*-carborane, 20 ng methylbenzselenazole, 15 ng diphenylselenide, 1.0 ng thianthrene, and 10 ng triphenylarsine.

As demonstrated in the bottom half of Fig. 6, the CONDAC algorithm is able to distinguish among all four hetero-atoms and provide chromatograms of apparent elemental specificity for each. It should be noted that this is achieved with one wide-band filter as the lone wavelength-selective device present in the system. The choice of the filter's optical characteristics is reasonable but not crucial: several other wavelengths or filter types could have been used as well.

While the slope ratios of all peaks carrying the same hetero-atom were close enough to allow the CONDAC algorithm to succeed, it is interesting to speculate why the *SR* value of just one particular

peak happened to be significantly different from those of its congeners. That peak was the second in elution order, *i.e.* the peak of diethyldisulphide. It followed close on the heels of the first-eluting peak, dimethyldiselenide. Some selenium likely remained in the gas phase due to the proximity of the two peaks (note also that selenium —even more so than sulphur— is prone to form residues adhering to, and eluting only very slowly from, the GC system). Thus, the luminescence forming the diethyldisulfide peak probably included the interchalcogen emitter SeS (*cf.* ref. 27) in addition to the predominant S_2. This would have effectively changed the spectral envelope and hence the slope ratio.

It may be argued that such effects could make the use of the CONDAC algorithm a risky business. We prefer to look at it the other way around: it is the CONDAC algorithm that warns the analyst of a potentially risky situation. After all, the same effects must occur in conventional use of the FPD. While the FPD, in our opinion, is one of the most reliable of all the selective GC detectors, the presence of such an interference, and its effect on quantitation, could go unrecognized in everyday analysis. Perhaps the routine use of comparative slope ratios would lead to more reliable analyses; as well as to a better understanding of the processes in, and limitations of, the FPD and other dual-channel detection devices? The concurrence of the slope ratio (in addition to the concurrence of the retention time) between a sample analyte and its calibration standard can certainly reassure the analyst that the two are indeed identical. Caution is, of course, always called for: the FPD (and certain other detectors) are not just simple optical or electrical transducers. Rather, their signals portray dynamically complex, transient chemical systems with individual memories and inhibitions.

Fig. 7 uses CONDAC algorithms on some more main-group elements; namely lead, antimony, germanium and tin. The only spectrally selective device in this configuration is a 540 nm long-pass (LP) filter. Again, the CONDAC algorithm successfully separates/identifies the hetero-elements present.

While the numerical slope ratios of the two germanium peaks were practically identical, those of the two tin peaks were slightly different. This may simply be due to experimental noise, but more basic spectrochemical interferences cannot be ruled out.

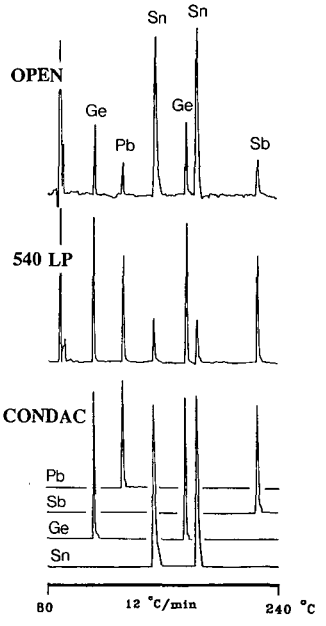

Fig. 7. Two-channel and CONDAC chromatograms of (in order of elution) 1.8 ng tetraethylgermanium, 12 ng tetraethyllead, 0.20 ng tetra-*n*-propyltin, 4.8 ng tetra-*n*-butylgermanium, 0.20 ng tetra-*n*-butyltin and 24 ng triphenylantimony.

For instance, despite our best efforts at suppressing it, some residual surface luminescence of Sn (or Ge) may have been present on, say, the quartz windows shielding the filters/photomultipliers. That type of luminescence is known to be subject to protracted quenching by a variety of elements. If the blue luminescence happened to be present (together with the usual green SnOH and red SnH gas-phase emissions [9]) the potential for changes in slope ratio among tin compounds —eluting at different positions in a temperature-programmed chromatogram and/or following compounds that contain different hetero-elements— cannot be ruled out. Fortunately, the repetitive nature of samples as well as the controlled conditions in a typical analytical laboratory will usually be able to prevent or circumvent such potential errors.

In the past few paragraphs we have drawn considerable, perhaps even undue, attention to certain hypothetical problems that could beset the dealings of CONDAC algorithms with S/Se and Sn/Ge containing samples. This was done for a purpose: by these speculations we wanted to illustrate two *general* types of processes, which can cause variations

in slope ratio among peaks containing the same hetero-atom: *contamination* and *multiple spectra*. It should be noted that the extent of both effects may depend, *inter alia*, on the concentration of the analyte, or on the temperature, or on the concentration of other species in the gas phase (the temperature program alone causes significant changes in carrier flow and column bleed). A variety of other interferences could be surmised even from what little we know about the basic chemistry and chemiluminescent spectroscopy of various FPD-active elements in hydrogen-rich, low-energy flames. Fortunately, the demonstration mixtures of this study were literally more colourful, and the resulting chromatograms hence visually more alarming, than the proverbial "real-life" sample.

It is now obvious that by judicious selection of wavelength in the two channels, the compounds of *any* selected element can be granted exclusive access to, hence sole presence on, the computer-drawn CONDAC chromatograms. Still, it remains the perceptionally most surprising aspect of this rather primitive algorithm that its output is element-*specific*. Somehow it just does not seem right that a device like the FPD —which monitors broad, usually overlapping molecular bands at low resolution— should be capable of infinitely selective response.

While the chromatograms do indeed appear specific for any selected element, they are also subject to obvious limitations. The CONDAC version of specificity is neither intrinsic nor inclusive; rather, it is created by computer and confined by circumstances. For instance, the CONDAC chromatogram may exclude part or all of a peak (despite the fact that the latter does contain the targeted element) if the peak of a different element overlaps it. This implies that the algorithm can successfully operate only on (at least partially) separated peaks. And compounds that, in addition to the targeted element, contain one of similar or higher radiative power, may not show up on the chromatogram at all: only the predominant emitter gains access. As an extreme example, a CONDAC scan set for carbon compounds will not recognize the carbon matrix of an organophosphate.

Such extreme situations aside, it is astonishing how well the CONDAC approach works in practice — particularly in light of the fact that *several* chromatograms of apparent elemental specificity can be derived from the *same* injection (*i.e.* from the same set of weak optical discriminants and the same set of stored data). CONDAC could be dismissed as a gimmick from the computer, or be misused as an oracle from the black box. We hope that it will neither, but that it will simply permit faster and firmer analyses.

ACKNOWLEDGEMENTS

We are thankful to our referees for their well-informed and well-reasoned contributions. In particular, the chapter on the nitrogen spectrum has been enriched by their comments.

We also appreciate greatly the crucial support by NSERC operating grant A-9604.

REFERENCES

1 M. Dressler, *Selective Gas Chromatographic Detectors* (*Journal of Chromatography Library*, Vol. 36) Elsevier, Amsterdam, 1986.
2 S. S. Brody and J. E. Chaney, *J. Gas Chromatogr.*, 4 (1966) 42.
3 X.-Y. Sun, B. Millier and W. A. Aue, *Can. J. Chem.*, in press.
4 W. A. Aue, B. Millier and X.-Y. Sun, *Can. J. Chem.*, in press.
5 W. A. Aue, B. Millier and X.-Y. Sun, *Anal. Chem.*, 62 (1990) 2453.
6 W. A. Aue, B. Millier and X.-Y. Sun, *Anal. Chem.*, 63 (1991) 2951.
7 V. A. Joonson and E. P. Loog, *J. Chromatogr.*, 120 (1976) 285.
8 M. C. Bowman and M. Beroza, *Anal. Chem.*, 40 (1968) 1448.
9 C. G. Flinn and W. A. Aue, *Can. J. Spectr.*, 25 (1980) 141.
10 W. A. Aue, B. J. Flinn, C. G. Flinn, V. Paramasigamani and K. A. Russell, *Can. J. Chem.*, 67 (1989) 402.
11 G. B. Jiang, P. S. Maxwell, K. W. M. Siu, V. T. Luong and S. S. Berman, *Anal. Chem.*, 63 (1991) 1506.
12 S. Kapila and C. R. Vogt, *J. Chromatogr. Sci.*, 17 (1979) 327.
13 P. T. Gilbert, in R. Mavrodineanu (Editor), *Analytical Flame Spectroscopy*, Philips Technical Library/Macmillan, 1969, p. 181.
14 R. S. Braman and E. S. Gordon, *Proc. Ann. Inst. Autom. Conf. Exhibit*, 17 (1962) 13; *C.A.*, (1964) 4754c.
15 E. J. Sowinski and I. H. Suffet, *J. Chromatogr. Sci.*, 9(1971) 632; *Anal. Chem.*, 46 (1974) 1218.
16 R. W. B. Pearse and A. G. Gaydon, *The Identification of Molecular Spectra*, Chapman and Hall, London, 4th ed., 1976.
17 W. E. Kaskan and R. C. Milliken, *J. Chem. Phys.*, 32(1960) 1273.
18 G. W. Smith and A. K. Palmby, *Anal. Chem.*, 31 (1959) 1798.
19 W. A. Aue and C. R. Hastings, *J. Chromatogr.*, 87 (1973) 232.

20 R. S. Braman, *Anal. Chem.*, 38 (1966) 735.
21 R. M. Dagnall, D. J. Smith, K. C. Thompson and T. S. West, *Analyst (London)*, 94 (1969) 871.
22 R. Belcher, S. L. Bogdanski, A. C. Calokerinos and A. Townshend, *Analyst (London)*, 106 (1981) 625.
23 J. M. S. Butcher and G. F. Kirkbright, *Analyst (London)*, 103 (1978) 1104.
24 W. A. Aue, presented at the *Ohio Valley Chromatography Symposium, Hueston Woods, OH*, June 1989.
25 R. M. Dagnall, B. Fleet, T. H. Risby and D. R. Deans, *Talanta*, 18 (1971) 155.
26 W. K. Fowler, *Anal. Chem.*, 63 (1991) 2798.
27 W. A. Aue and C. G. Flinn, *J. Chromatogr.*, 158 (1978) 161.

Journal of Chromatography, 606 (1992) 87–94
Elsevier Science Publishers B.V., Amsterdam

CHROM. 24 284

Simultaneous distillation–extraction under static vacuum: isolation of volatile compounds at room temperature

L. Maignial, P. Pibarot, G. Bonetti, A. Chaintreau and J. P. Marion

Nestle Research Centre, Food Flavour & Quality/Aromatec, NESTEC Ltd., P.O. Box 44, Vers-chez-les-Blanc, 1000 Lausanne 26 (Switzerland)

(First received January 20th, 1992; revised manuscript received April 22nd, 1992)

ABSTRACT

The simultaneous distillation–extraction (SDE) system developed by Likens and Nickerson (ASBC Proceedings, 1964, p. 5) and modified by Godefroot, Sandra and Verzele [*J. Chromatogr.*, 203 (1981) 325] is one of the most popular methods currently used to isolate volatile components from a matrix prior to gas chromatographic analysis. Since it leads to a thermal generation of artefacts, the device has been improved in the present work to allow isolation between 20 and 40°C under vacuum. The system was closed and made airtight by means of a valve under static vacuum to avoid volatile losses. These conditions require the use of solvents with a boiling point close to that of water and the temperature must be electronically regulated. The absence of artefact generation was tested with linalyl acetate, honey and a Maillard model reaction. The recovery yields of classical SDE and SDE under vacuum were found to be similar.

INTRODUCTION

The analyses of flavours and fragrances require the isolation of the volatile fraction from the matrix prior to gas chromatography (GC): direct extraction with a solvent (soxhlet, liquid–liquid extraction, supercritical fluid extraction) co-solubilizes non-volatile components which contaminate the injectors and limit the possibility of concentration.

Direct vacuum distillation followed by solvent extraction and concentration is tedious because of the high volume to be handled and the different steps which are time-consuming and affect the yields.

Since Likens and Nickerson [1] published the first paper concerning simultaneous distillation–extraction (SDE), this method has become very popular in all flavour and fragrance analytical laboratories for the isolation of volatile components from a matrix. The improvement by Godefroot, Sandra and Verzele [2] allowed quantitative determination following extraction for 1 h using a microapparatus without any prior concentration before gas chromatographic analysis. Starting from a fat-containing matrix in which volatiles exhibit a high affinity, Au-Yeung and MacLeod [3] confirmed these high recovery yields (80%).

SDE has also been found to be applicable to the isolation of nitrosamines [4] and pesticides [5] from non-volatile matrices.

However, SDE suffers from a major disadvantage: because of the temperature of the water boiler (105°C), numerous artefacts are generated. The use of antioxidants and an oxygen-free atmosphere decreases oxidative degradations [6] since it is well known that steam distillation produces a lot of thermal reactions [7]. Hence the composition of SDE extracts must be compared with that of essential oils since they both involve steam distillation. On the other hand, SDE is not applicable to heat sensitive products such as food media or flower scents which undergo Maillard reactions, hydrolyses, rearrangements, etc.

Correspondence to: Dr. A. Chaintreau, Nestle Research Centre, Food Flavour & Quality/Aromatic, NESTEC Ltd., P.O. Box 44, Vers-chez-les-Blanc, 1000 Lausanne 26, Switzerland.

0021-9673/92/$05.00

To lower the temperature of the boilers, several authors have proposed working at reduced pressure. Picardi and Issenberg [8] and Seifert and King [9] managed to maintain a sample temperature of between 45 and 50°C. However, no yields were given and volatile components were probably further lost during the continuous vacuum pumping.

Surprisingly, Schultz *et al.* [10] claimed quantitative recoveries under similar conditions (100 Torr), but 52°C in the vapour phase suggests a higher temperature in the boiler, leading to possible thermal reactions. Furthermore, our own experiences showed that significant losses of solvent would be expected when using hexane under continuous pumping.

To minimize these losses Charpentier *et al.* [11] used a three-stage condenser under 200 Torr allowing a sample temperature of 67°C but requiring the control of five different temperatures.

Therefore the aim of this work was to develop an easy-to-use device to isolate volatile components without losses, at room temperature, in a reasonable time, on a microscale and with a high concentration factor.

EXPERIMENTAL

Gas chromatography

For all chromatographic analyses, a Hewlett-Packard 5890 gas chromatograph equipped with either a flame ionization detector or a mass spectrometer was used. Two columns were used, a polar column and a non-polar column. The polar column, 60 m × 0.25 mm I.D., 0.25 μm film thickness, was a fused-silica column coated with cross-linked polyethylene glycol (Supelcowax TM10, Supelco) the non-polar column, 50 m × 0.2 mm I.D., 0.5 μm thickness, was a fused-silica column coated with cross-linked methylsilicone (Pona1, Hewlett-Packard).

The oven temperature was held at 20°C for 0.5 min, ballistically increased to 60°C, and programmed at 4°C/min, up to 250°C for the non-polar phase and 220°C for the polar phase. The programme was then held isothermally until the end of the run.

The injector temperature was 250°C, and 1 μl was injected in splitless mode. Detector temperatures were 275°C for the flame ionization detector and 220°C for the mass spectrometer. Linear indices were calculated from the injection of *n*-alkanes (C_5–C_{28}) [12] and compared with the indices reported in the literature or with those of our own libraries determined from authentic samples.

Mass spectrometry

Electron ionization mass spectrometry was performed on a Hewlett-Packard 5995 instrument with the capillary column directly connected into the ionization source operating at 70 eV ionization energy. The mass spectra of the compounds detected were compared with those in our own libraries.

SDE at atmospheric pressure

The Godefroot–Sandra–Verzele device was used. Typical experiments were run for 1 h with 3 ml of dichloromethane (purity 99.7%) as extracting solvent and with 200 ml of sample solution. The temperature of the sample boiler and of the cooler was held at 105°C and −5°C, respectively.

For quantitation, 3 mg of 1-undecanol was added as internal standard to the solvent flask just before the SDE run. The sample flask initially contained 3 mg of each component listed in Table III.

SDE under vacuum

The Godefroot–Sandra–Verzele device was modified as shown in Fig. 1. The two flasks were connected to the extractor with spherical joint (Rotulex) and Viton toric seals. Before heating, the system was pumped with a water pump and closed under vacuum (extended-tip PTFE valve, Kontes, Switzerland) for the duration of the experiment. The cooler temperature was −5°C.

For a typical run, 200 ml of an aqueous solution or a slurry were heated in the sample flask at 37 ± 0.5°C. The solvent flask (3 ml of isooctane; purity 99.5%) was held at 20 ± 0.5°C. Both were vigorously magnetically stirred. Quantitations were performed as described for the atmospheric experiments.

Linalyl acetate extraction

A 2-mg aliquot of linalyl acetate (Fluka, Switzerland) in 200 ml of water was SDE-extracted for 1 h at atmospheric pressure and under vacuum. The organic extracts were injected into the gas chromatograph without prior concentration.

TABLE I

MAIN VOLATILES PRODUCED WITH SDE AT 105°C STARTING FROM GLUCOSE AND LEUCINE

Peak	Compound	Experimental indices	
		Polar[a]	Non-polar[b]
1	Butan-2,3-dione	968	558
2	Pentan-2,3-dione	1054	681
3	2-Methyltetrahydrofuran-3-one	1268	774
4	Hydroxypropanone	1310	625
5	4-Hydroxy-4-methyl-pentan-2-one	1366	812
6	2-Butoxyethanol	1399	887
7	Furfural	1471	804
8	2-Hydroxymethylfuran	1655	823
9	2-Acetylpyrrole	1983	1030

[a] Indices on Supelcowax TM10 (programmed temperature).
[b] Indices on Ponal (programmed temperature).

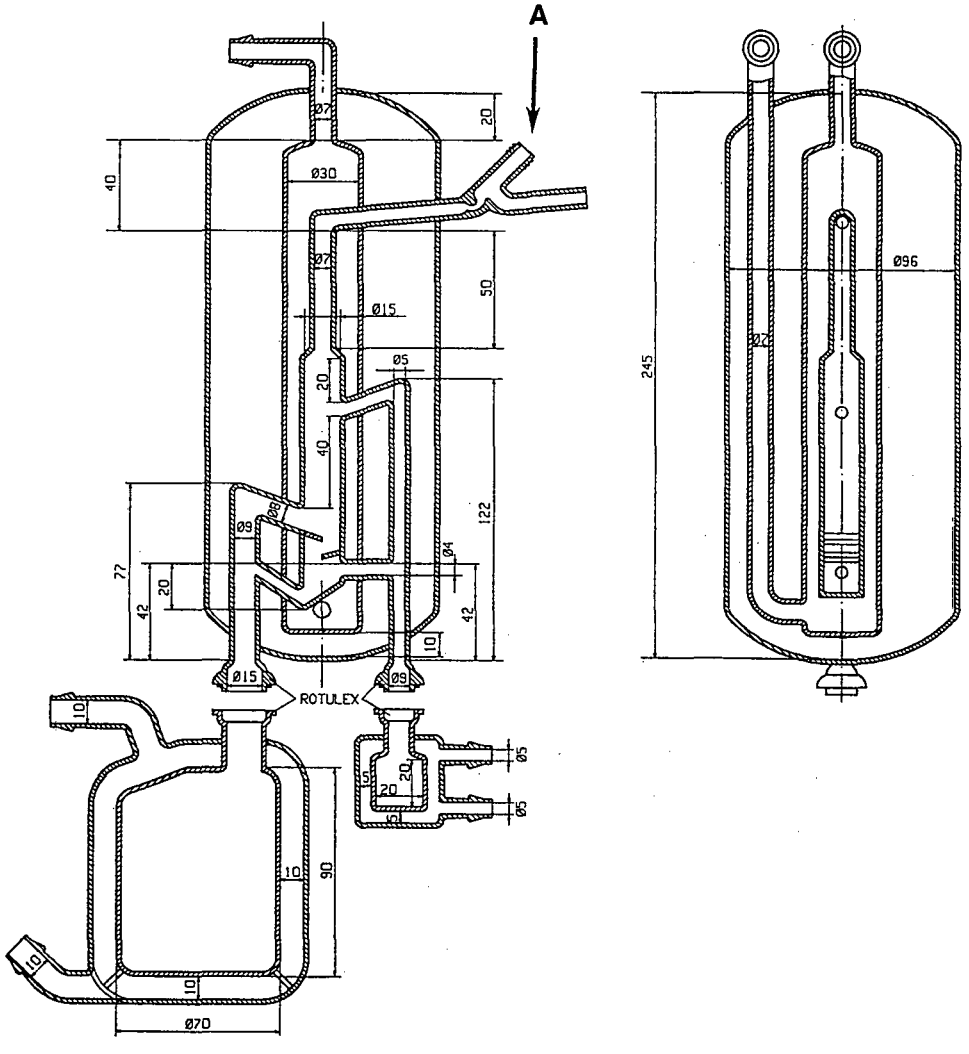

Fig. 1. Modified, static-vacuum, simultaneous steam distillation–extraction apparatus. A = PTFE valve; ∅ = diameter; all sizes in mm.

Honey extraction

An 80-g aliquot of honey diluted to 250 ml with distilled water was SDE-extracted either with dichloromethane for 2 h at atmospheric pressure, or with isooctane for 2 h under vacuum. Organic extracts were analysed by GC after a 100-fold concentration under a gentle stream of nitrogen at room temperature.

Maillard reaction

A 1-g aliquot of L-leucine (Merck, Germany) and 1 g of D-glucose (Fluka, Switzerland) diluted in 200 ml of water were extracted for 6 h for vacuum and atmospheric experiments. Organic extracts were concentrated 100-fold at room temperature under a gentle stream of nitrogen prior to GC–mass spectrometric analysis.

Quantitative assay

The sample flask contained 200 ml of water and 3 mg of each component listed in Table III. 1-Undecanol (3 mg) was used as internal standard in the solvent flask and the extraction was run as described above for vacuum and atmospheric experiments. SDE runs were performed triplicate, and each organic extract was analysed by GC in duplicate without prior concentration, using an autosampler.

RESULTS AND DISCUSSION

Vacuum conditions

In order to avoid losses of volatiles mentioned in the Introduction as well as sophisticated cooler systems, the extractor was equipped with a PTFE valve to maintain a static vacuum during the run. A blank experiment indicated that the Viton rings of the flasks allowed a stable pressure for more than 6 h without giving rise to artefacts.

Device modifications

Compared with the Godefroot–Sandra–Verzele device the main modifications were as follows:

(1) Enlargement of the steam arm diameter from 4 to 8 mm to increase the distillation rate of water. This enables extractions of up to 200 ml of sample and only 1–3 ml of solvent.

(2) An external double-jacket cooler which gives a higher condensation area than the cold finger of the original apparatus and avoids vaporization of the liquids in the phase separator.

(3) A third jacket to insulate the distillation arms and to avoid condensation of the atmospheric moisture on the cold parts while the strength of the glassware was enhanced.

(4) Double-jacketed flasks and electronic control of the thermostatic fluid.

(5) Rotulex joints and a PTFE valve allowing maintenance of a stable static vacuum.

The modified device is commercially available from Trabold (Bern, Switzerland).

Solvent choice

Low-boiling point solvents (*e.g.* dichloromethane, pentane and diethyl ether) are commonly used for atmospheric SDE because they possess good extractive properties, they elute rapidly in GC and they are easily evaporated to concentrate the extract. Their condensation under vacuum requires a very low cooler temperature (about −40°C) with subsequent ice formation in the system. A compromise was found by choosing solvents with boiling points close to that of water and with low retention indices.

Table II summarizes the parameters obtained with *n*-hexane, *n*-heptane, 2,2,4-trimethylpentane, *n*-octane, toluene and 3-pentanone.

The high value of the retention indices on the polar column of toluene and 2-pentanone (1050 and 920, respectively) could mask the early-eluting peaks of the extract during GC. However, their polarity and/or their polarizability [14] offered better extractive properties than the non-polar alkanes. Since the indices on the apolar column are low, they were a viable compromise between the SDE and GC requirements.

The use of *n*-octane (and other higher-boiling-point solvents) provides for a reduction of the sample temperature to 19°C. On the other hand, the solvent flask must be held at 26°C, which decreases the suitability of this solvent unless a lower pressure can be used.

In spite of their higher boiling points than hexane or dichloromethane, the solvents used for vacuum SDE were easily removed at room temperature under a gentle stream of pure nitrogen within less than 30 min. Alkanes were more suitable for sensory evaluation of the extract because of a much weaker

TABLE II

PARAMETERS OF SEVERAL SOLVENTS FOR VACUUM SDE

Solvent	B.p. (γ)	Retention Index		Vacuum (mbar)	Sample temperature	Solvent temperature	Solvent odour
		Polar[a]	Non-polar[b]				
Iso-octane	99	698	691	49	37	20	Weak
Heptane	99	700	700	35	30	17	Weak
2-Pentanone	102	920	677	31	25	17	Unpleasant
Toluene	111	1050	744	37	32	26	Unpleasant
Hexane	69	600	600	115	50	22	Weak
Octane	125	800	800	20	19	26	Weak

[a] Indices on Supelcowax TM10 (programmed temperature).
[b] Indices on Ponal (programmed temperature).

odour than toluene and 2-pentanone. They quickly evaporated when the extract was sniffed on paper strips.

Artefact decrease

Linalyl acetate is known to be hydrolysed during the steam distillation of various plants [7]. A comparative experiment was run (Fig. 2): almost half of the ester was transformed under the atmospheric SDE conditions, whereas it was not modified under vacuum.

Maillard reactions. Since food media contain amino acids and reducing sugars which are subject to Maillard reactions, it is compulsory to reduce this reaction if one wants to identify the components which are really responsible for the authentic taste. For this purpose, a model Maillard mixture of leucine and glucose was used [13].

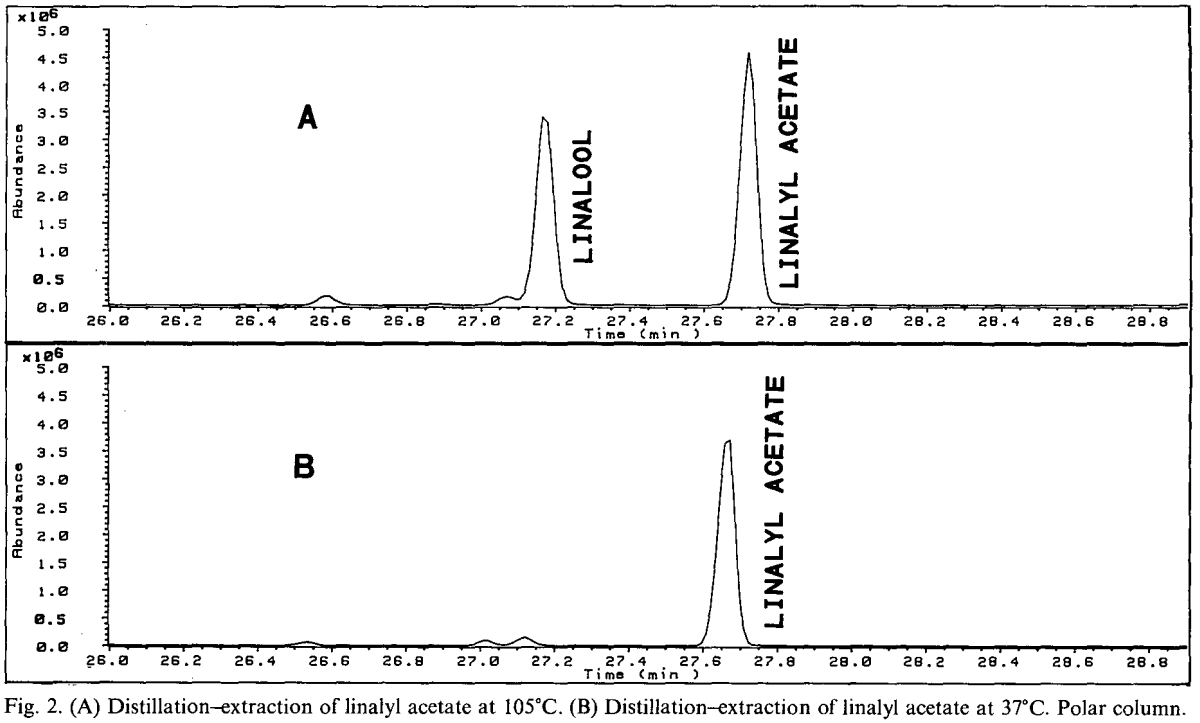

Fig. 2. (A) Distillation–extraction of linalyl acetate at 105°C. (B) Distillation–extraction of linalyl acetate at 37°C. Polar column.

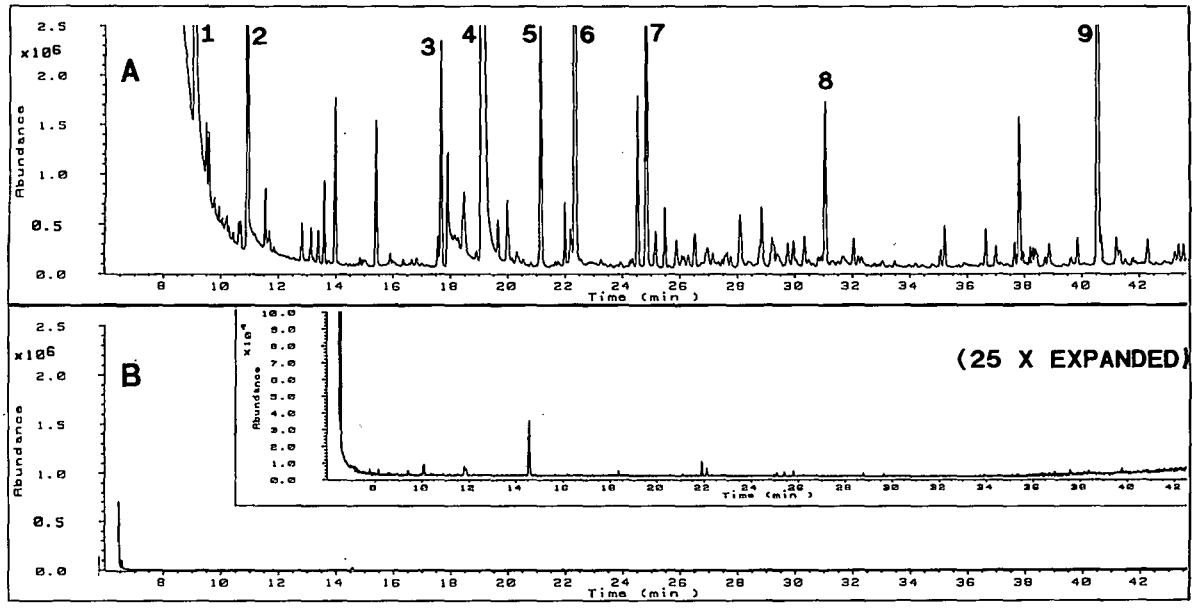

Fig. 3. (A) Distillation–extraction of glucose and leucine at 105°C. (B) Distillation–extraction of glucose and leucine at 37°C. Polar column. For peak identification see Table I.

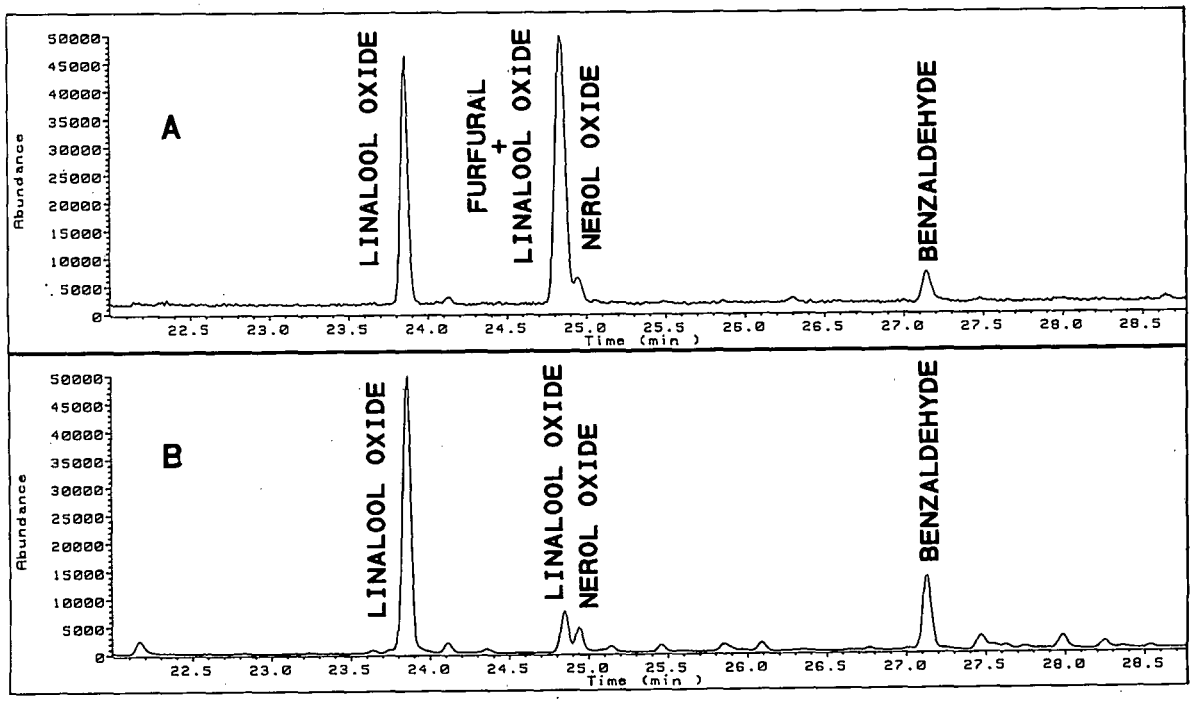

Fig. 4. (A) Distillation–extraction of honey at 105°C. (B) Distillation–extraction of honey at 37°C. Polar column.

TABLE III

RECOVERY YIELDS FOR DIFFERENT COMPOUNDS

Compound	Atmospheric SDE		Vacuum SDE	
	Recovery (%)	Confidence[a]	Recovery (%)	Confidence[a]
Ethyl butyrate	118	13	92	13
Limonene	109	2	103	2
2-Hexenal (*E*)	91	3	76	4
Pyrazine	55	2	44	2
Anethol (*E*)	102	2	92	2
Dodecanol	97	2	92	2

[a] 95% confidence range.

Fig. 3 indicates that the reaction did not occur in our modified system whereas the classical conditions generated numerous reaction products (Table I). Furthermore, the browning reaction observed during the atmospheric extraction was suppressed under vacuum.

Honey extraction. Atmospheric SDE produces a cooked honey flavour, similar to the taste of honey candies. The main components formed during the extraction were observed to be furfural and 5-methylfurfural.

The vacuum experiment gave a furfural-free extract (Fig. 4) with a fresh honey note. The corresponding chromatogram exhibits a small peak of linalool oxide, which was completely hidden by the furfural in the atmospheric experiments. No colour change was noticed under vacuum, unlike with classical SDE.

Quantitative trial

The modified system was tested for its quantitative recovery using six pure synthetic compounds commonly found as flavourings and representing different functional groups. The results summarized in Table III indicate that similar recoveries can be expected when quantitative yields are obtained at atmospheric pressure, whereas they are slightly lower for the less SDE-extractable components. The recovery should be improved by increasing the run time since the sample is not subjected to thermal degradations, unlike atmospheric experiments.

CONCLUSIONS

Classical SDE offers a good selectivity based on the volatility of the molecules responsible for the odour and flavour, however, its applicability is limited because of the formation of thermal artefacts.

On the other hand, dynamic headspace is rather dedicated to the very volatile fraction and gives high concentration factors without allowing easy quantitative measurements.

Thus vacuum SDE would appear to be a valuable method which avoids thermal degradations as well as heavy-component extraction, while it remains quantitative. However, very volatile molecules are masked by the solvent.

Hence vacuum SDE and dynamic headspace appear to be complementary methods for sample preparation in gas chromatography.

ACKNOWLEDGEMENT

We gratefully acknowledge Mr. Trabold for his kind assistance during the development of the extractor prototypes.

REFERENCES

1 S. T. Likens and G. B. Nickerson, *ASBC Proceedings (1964)*, 1964, p. 5.
2 M. Godefroot, P. Sandra and M. Verzele, *J. Chromatogr.*, 203 (1981) 325.
3 C. Y. Au-Yeung and A. MacLeod, *J. Agric. Food Chem.*, 29 (1981) 502.

4 M. Gavinelli, L. Airoldi and R. Fanelli, *J. High Resolut. Chromatogr. Chromatogr. Commun.*, 9 (1986) 257.
5 F. E. Figuerola and T. Shibamoto, *Agric. Biol. Chem.*, 47 (1983) 2933.
6 A. S. MacGill and R. Hardy, *J. Sci. Food Agric.*, 28 (1977) 89.
7 M. J. Garnero, *Parfums Cosmet. Arômes*, 14 (1977) 31.
8 M. Picardi and P. Issenberg, *J. Agric. Food Chem.*, 21 (1973) 959.
9 R. M. Seifert and A. Douglas King, *J. Agric. Food Chem.*, 30 (1982) 686.
10 T. H. Schultz, R. A. Flath, T. R. Mon, S. Eggling and R. Teranishi, *J. Agric. Food Chem.*, 25 (1977) 446.
11 B. A. Charpentier, M. R. Sevenants and R. A. Sanders, in G. Charalambous (Editor), *Proceedings of the 4th International Flavor Conference, Rhodes, July 1985*, Elsevier, Amsterdam, 1986, p. 413.
12 H. van den Dool and P. D. Kratz, *J. Chromatogr.*, 11 (1963) 463.
13 M. J. Garnero, *Parfums Cosmet. Arômes*, 34 (1980) 51.
14 J. Li, Y. Zhang, A. J. Dallas and P. W. Carr, *J. Chromatogr.*, 550 (1991) 101.

Journal of Chromatography, 606 (1992) 95–102
Elsevier Science Publishers B.V., Amsterdam

CHROM. 24 262

Unsteady heat transfer in capillary zone electrophoresis

I. A mathematical model

Michael S. Bello* and Pier Giorgio Righetti

Department of Biomedical Sciences and Technologies, University of Milan, Via Celoria 2, Milan 20133 (Italy)

(First received January 7th, 1992; revised manuscript received April 13th, 1992)

ABSTRACT

A solution to the problem of unsteady heat transfer in capillary zone electrophoresis is presented. A general set of partial differential equations for conjugated heat transfer in a capillary is formulated. An approximate analytical solution is obtained for a limiting case of a "thin-walled" capillary and for different regimes of a power supply (voltage-stabilized, power-stabilized or current-stabilized). An exact analytical solution is derived for transient times in the voltage-stabilized regime. It is shown that temperature evolution in a capillary can be described by the only eigenfunction with a corresponding exponential factor.

INTRODUCTION

Steady-state heat transfer in capillary zone electrophoresis (CZE) has been the subject of a number of publications [1–5]. However, unsteady phenomena such as transition of temperature and electric current to a steady-state were not considered previously. Experimental observations have shown that an increase in the power generation within a capillary and/or an increase in capillary radius lead to an increase in the time necessary to achieve stationary current values. Under certain conditions, current and temperature can increase substantially [4,5]. In order to study theoretically the transient heat transfer in a capillary, we formulated a set of partial non-linear integro-differential equations for unsteady heat transfer in a capillary cross-section taking into account the temperature dependence of electric conductivity [6].

In this paper an equation and its solution are derived for the average temperature in the capillary lumen. The exact solution of the equations for the case of the voltage-stabilized regime is obtained by using an expansion in eigenfunction series.

GOVERNING EQUATIONS

We consider a cross-section of a cylindrical structure consisting of an inner cylindrical lumen that contains an electrolyte solution (buffer), its wall, having different thermal properties, and the outer wall coating, with properties different from those of the electrolyte solution and the wall.

The temperature in the domain is governed by a set of equations [6] which can be represented in dimensionless form as follows:

$$\frac{\partial \vartheta}{\partial t} = \frac{1}{r} \cdot \frac{\partial}{\partial r}\left(r \cdot \frac{\partial \vartheta}{\partial r}\right) + F \qquad 0 \leqslant r < 1 \qquad (1)$$

$$\frac{\partial \vartheta}{\partial t} = \kappa_{WL} \cdot \frac{1}{r} \cdot \frac{\partial}{\partial r}\left(r \cdot \frac{\partial \vartheta}{\partial r}\right) \qquad 1 \leqslant r < r_W \qquad (2)$$

Correspondence to: Professor Pier Giorgio Righetti, Department of Biomedical Sciences and Technologies, University of Milan, Via Celoria 2, Milan 20133, Italy.

* Permanent address: Institute of Macromolecular Compounds, Academy of Sciences, Bolshoi pr. 31, St. Petersburg 199004, Russia.

0021-9673/92/$05.00

$$\frac{\partial \vartheta}{\partial t} = \kappa_{PL} \cdot \frac{1}{r} \cdot \frac{\partial}{\partial r}\left(r \cdot \frac{\partial \vartheta}{\partial r}\right) \qquad r_W \leqslant r < r_P \qquad (3)$$

$$\vartheta = \text{finite at } r = 0 \qquad (4a)$$

$$\vartheta^- = \vartheta^+, \frac{\partial \vartheta^-}{\partial r} = \beta_{WL} \cdot \frac{\partial \vartheta^+}{\partial r} \text{ at } r = 1 \qquad (4b)$$

$$\vartheta^- = \vartheta^+, \frac{\partial \vartheta^-}{\partial r} = \beta_{PW} \cdot \frac{\partial \vartheta^+}{\partial r} \text{ at } r = r_W \qquad (4c)$$

$$-\beta_{PL} \cdot \frac{\partial \vartheta}{\partial r} = Bi(\vartheta - \vartheta_C) \text{ at } r = r_P \qquad (4d)$$

$$\vartheta(r, t = 0) = \vartheta_C \qquad (5)$$

where r is the dimensionless radius measured in units of inner capillary diameter, ϑ is the dimensionless temperature, F the dimensionless heat source, t the dimensionless time, Bi the Biot number, κ_{WL} and κ_{PL} are the relative thermal diffusivities (temperature conductivities) of the wall and coat measured in units of the electrolyte thermal diffusivity and $\beta_{WL} = \chi_W/\chi_L$, $\beta_{PW} = \chi_P/\chi_W$, $\beta_{PL} = \chi_P/\chi_L$ are the relative thermal conductivities (χ_L, χ_W and χ_P being the thermal conductivities of the electrolyte, wall and coating, respectively).

The dimensionless heat source term (volumetric power generation) is represented as follows:

$$F = 1 + k^2\vartheta \qquad (6a)$$

for the voltage-stabilized mode of operation,

$$F = (1 + k^2\vartheta)/(1 + k^2\bar{\vartheta})^2 \qquad (6b)$$

for the current-stabilized mode and

$$F = (1 + k^2\vartheta)/(1 + k^2\bar{\vartheta}) \qquad (6c)$$

for the power-stabilized mode, where $\bar{\vartheta}$ is the average dimensionless temperature, given by

$$\bar{\vartheta} = 2\int_0^1 \vartheta r dr \qquad (6d)$$

and k^2 is the autothermal parameter defined in ref. 6.

The average temperature of the buffer $\bar{\vartheta}$ is of great importance for CZE, as it influences the characteristics of an analyte and the buffer electric conductivity. The dimensionless electric current i is related to $\bar{\vartheta}$ as follows:

$$i = I/I_0 = 1 + k^2\bar{\vartheta} \qquad (6e)$$

where I is the electric current at time t and I_0 is its initial value.

APPROXIMATE SOLUTION FOR AVERAGE TEMPERATURE

In this part we shall derive an approximate equation for the average temperature of the buffer and its solution in an analytical form.

We are mainly interested in the case of poor cooling conditions, as we assume the Biot number to be small in comparison with unity:

$$Bi \ll 1$$

This assumption allows us to assume that the temperature profile within the capillary is flat and close to a constant. In this case the possibility of finding an average temperature would be enough to describe the heat-conduction process. For deriving an equation for the average buffer temperature defined by eqn. 6d, we multiply eqn. 1 by $2r$ and integrate it from 0 to 1. The result is

$$\frac{\partial \bar{\vartheta}}{\partial t} = 2 \cdot \frac{\partial \vartheta}{\partial r}\Big|_{r=1} + \bar{F} \qquad (7)$$

$$\bar{F} = 2\int_0^1 Fr dr \qquad (8)$$

By substituting eqns. 6a–c in eqn. 8, one obtains

$$\bar{F} = 1 + k^2\bar{\vartheta} \qquad (8a)$$

for the voltage-stabilized mode of operation and

$$\bar{F} = 1/(1 + k^2\bar{\vartheta}) \qquad (8b)$$

for the current-stabilized mode. For the power-stabilized mode, the integration gives

$$\bar{F} = 1 \qquad (8c)$$

For deriving the approximate equation, we assume the capillary wall and coating to be thin in the sense that the characteristic times of temperature conduction through the wall and coating are much shorter than the characteristic time of temperature conduction in the lumen. This means validity of the following relationships:

$$p_W \equiv r_W(r_W - 1)/\kappa_{WL} \ll 1;$$

$$p_P \equiv r_P(r_P - r_W)/\kappa_{PL} \ll 1 \qquad (9)$$

where p_W and p_P are dimensionless parameters representing ratios of the characteristic times for temperature conduction in the wall and coating to the characteristic time of the lumen temperature conduction.

Assumption 9 allows us to neglect temporal derivatives on the left-hand sides of eqns. 2 and 3 and to consider them as quasi-steady. By seeking their solutions in the form

$$\begin{aligned} \vartheta &= B\ln(r) + C \qquad 1 \leqslant r < r_W \\ \vartheta &= D\ln(r) + E \qquad r_W \leqslant r < r_P \end{aligned} \tag{10}$$

where B, C, D and E are constants, and by applying boundary conditions 4b–d, one obtains

$$-\frac{\partial\vartheta}{\partial r}\Big|_{r=1} = Bi_{OA}(\bar{\vartheta} - \vartheta_C) \tag{11}$$

$$Bi_{OA} = \beta_{WL}\left\{\ln(r_W) + \frac{1}{\beta_{PW}}\left[\ln(r_P/r_W) + \frac{\beta_{PL}}{r_P\, Bi}\right]\right\}^{-1} \tag{12}$$

By substituting eqn. 11 into eqn. 7 we can derive an approximate equation for the average temperature $\bar{\vartheta}$:

$$\frac{d\bar{\vartheta}}{dt} = -2Bi_{OA}(\bar{\vartheta} - \vartheta_C) + \bar{F} \tag{13}$$

Note that the coefficient Bi_{OA} given by eqn. 12 is exactly the overall Biot number [4].

The initial condition for eqn. 13 follows directly from eqn. 5:

$$\bar{\vartheta}(t = 0) = \vartheta_C \tag{14}$$

If the autothermal parameter k^2 is small (or, more strictly, $k^2\bar{\vartheta} \ll 1$), eqn. 8b, representing the heat source term for the current-stabilized mode, can be linearized as follows:

$$\bar{F} = 1 - k^2\bar{\vartheta} \tag{15}$$

and the governing equation for the average temperature of the buffer for all the modes of operation can be written in the following general form:

$$\frac{\partial\bar{\vartheta}}{\partial t} = -2Bi_{OA}(\bar{\vartheta} - \vartheta_C) + 1 + fk^2\bar{\vartheta} \tag{16}$$

where the factor f is

$$f = \begin{cases} 1 \text{ for the voltage-stabilized mode} \\ -1 \text{ for the current-stabilized mode} \\ 0 \text{ for the power-stabilized mode} \end{cases}$$

The solution of eqn. 16 with initial condition 14 is given by

$$\bar{\vartheta} = \bar{\vartheta}_s + [\vartheta_C - \bar{\vartheta}_s]\exp(-t/\tau) \tag{17}$$

$$\bar{\vartheta}_s = \frac{2Bi_{OA}\vartheta_C + 1}{2Bi_{OA} - fk^2} \tag{17a}$$

$$\tau = (2Bi_{OA} - fk^2)^{-1} \tag{17b}$$

where $\bar{\vartheta}_s$ is the steady-state (*i.e.*, independent of time) part of the solution and τ is the characteristic time of the transient process.

The linearization 15 of the heat source 8b is used only to show clearly the difference between the three modes of power supply operation. The exact solution of eqn. 13 with eqn. 8b can be obtained as this is an ordinary differential equation of first order with separable variables. The solution has the following form:

$$G(\bar{\vartheta}) - G(\vartheta_C) = -t \tag{18}$$

$$G(x) = \frac{1}{4Bi_{OA}} \cdot \ln(X) + d^{-1}\left(1 - \frac{b}{4Bi_{OA}}\right)\ln\left(\frac{2cx + b - d}{2cx + b + d}\right)$$

$X = a + bx + cx^2$, $a = -\vartheta_C - 1$, $b = 2Bi_{OA} - \vartheta_C k^2$, $c = 2Bi_{OA}k^2$, $d = 4c + (2Bi_{OA} + \vartheta_C k^2)^2$.

Solution 18 is not restricted by the condition $k^2\bar{\vartheta} \ll 1$ as is eqn. 15 but it is too complex; therefore, we shall use eqns. 17–17b wherever possible.

SOLUTION FOR THE EQUATION OF UNSTEADY HEAT TRANSFER

This part aims at finding a solution of eqns. 1–5 for the case of the voltage-stabilized mode of operation.

The solution of eqns. 1–5 can be represented as the sum of the temperature-independent function $\vartheta_s(r)$ (steady-state) and the function $\vartheta_u(r,t)$, the latter vanishing as time increases:

$$\vartheta(r,t) = \vartheta_s(r) + \vartheta_u(r,t) \tag{19}$$

The solution for $\vartheta_s(r)$ is straightforward (see ref. 7). In Appendix I we present this solution in our notation and for $\vartheta_C \neq 0$.

The solution for ϑ_u is found in the following form [8]:

$$\vartheta_u = \sum_{n=1}^{\infty} a_n \exp(-\lambda_n^2 t)\, g_n(r) \tag{20}$$

where a_n are constants and λ_n and $g_n(r)$ are the nth eigenvalue and eigenfunction of the differential operator $\boldsymbol{L}$ defined by the right-hand sides of eqns. 1–4 and the appropriate boundary conditions.

The operator $\boldsymbol{L}$ is given by

$$\boldsymbol{L}y = \begin{cases} \boldsymbol{L}_r y + k^2 y & 0 \leqslant r < 1 \\ \dfrac{\partial y^-}{\partial r} = \beta_{WL} \cdot \dfrac{\partial y^+}{\partial r}, \quad y^- = y^+, & r = 1 \\ \kappa_{WL}\, \boldsymbol{L}_r y & 1 < r < r_W \\ \dfrac{\partial y^-}{\partial r} = \beta_{PW} \cdot \dfrac{\partial y^+}{\partial r}, \quad y^- = y^+, & r = r_W \\ \kappa_{PL}\, \boldsymbol{L}_r y & 1 < r < r_W \\ -\beta_{PL} \cdot \dfrac{\partial y}{\partial r} = Biy & r = r_P \end{cases} \quad (21)$$

where $\boldsymbol{L}_r \equiv \dfrac{1}{r} \cdot \dfrac{\partial}{\partial r}\left(r \cdot \dfrac{\partial}{\partial r}\right)$ is the radial part of the Laplace operator in the cylindrical coordinates.

The details of the solution for eigenvalues and eigenfunctions are given in Appendix II. The characteristic times of decay of the exponents 20 and, therefore, of the transition to the steady-state are given by

$$\tau_i = 1/\lambda_n^2 \quad (22)$$

where $\tau_1 > \tau_2 > \ldots > \tau_n$.

It is worth noting that if $\tau_1 \gg \tau_n$ and $a_1 \gg a_n$ then the temporal behaviour of the process is determined by τ_1, which should be considered as the transient time in general. It will be shown below that this is indeed the case.

CALCULATIONS OF TRANSIENT TIMES AND IMPROVEMENT OF THE APPROXIMATE SOLUTION FOR AVERAGE TEMPERATURE

In the following calculations we shall use the dimensionless parameters listed in Table I. These parameters correspond to physical parameters of the buffer, fused silica and polyimide [6].

The ratio of two first characteristic times τ_1/τ_2 as a function of the Biot number *Bi* is shown in Fig. 1 for $r_W = 2.125$, $r_P = 2.28$ and $k^2 = 0.05$. It can be seen that the first characteristic time τ_1 is considerably greater than the second. This allows us to leave in the expansion 20 only the first term and to describe approximately the evolution of the temperature of the buffer by the following equation:

$$\vartheta(r,t) = \vartheta_s(r) + a_1 J_0(\sqrt{\lambda_1^2 + k^2}\, r) \exp(-t\lambda_1^2) \quad (23)$$

where $J_0(x)$ is the Bessel function of the zeroth order of the first kind and a_1 and λ_1^2 are given by the procedure described in Appendix II. These results also permit the identification of the characteristic time of the heat transfer process with the time τ_1.

By substituting eqn. 23 into eqn. 6d and inte-

TABLE I

DIMENSIONLESS PARAMETERS USED FOR COMPUTER SIMULATIONS

Parameter	Value	Parameter	Value
κ_{WL}[a]	4.78	β_{PL}	0.262
κ_{PL}	0.71	β_{PW}	0.107
β_{WL}[b]	2.46		

[a] Relative thermal diffusivity.
[b] Relative thermal conductivity.

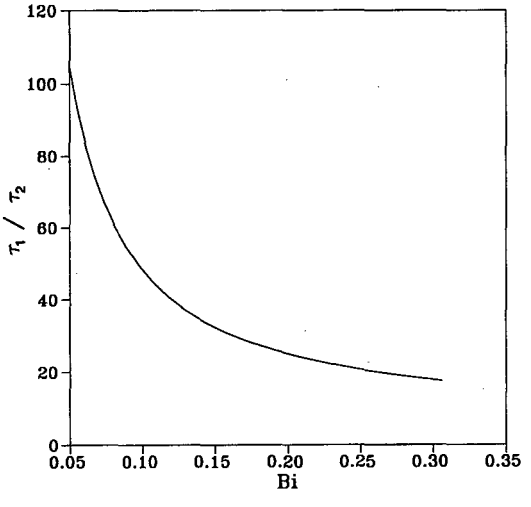

Fig. 1. Ratio of two first characteristic times τ_1/τ_2 as a function of the Biot number; $r_W = 2.125$, $r_P = 2.28$, $k^2 = 0.05$. Note that the Biot number represents the ratio between the thermal conductivity of the wall (in this case the fused-silica capillary) and the product of the thermal conductivity of the liquid contained therein times its dimensionless thickness. The relevant equations for the Biot number are given in Part II (eqns. 4e and 7e).

grating the Bessel function [9], one obtains for the average temperature $\bar{\vartheta}$

$$\bar{\vartheta} = \bar{\vartheta}_s + 2a_1 \cdot \frac{J_1(\sqrt{\lambda_1^2 + k^2})}{\sqrt{\lambda_1^2 + k^2}} \exp(-t/\tau_1) \quad (24a)$$

$$\bar{\vartheta}_s = 2A \cdot \frac{J_1(k)}{k} - 1/k^2 \quad (24b)$$

where $J_1(x)$ is the Bessel function of the first order of the first kind and the coefficient A is given by eqn. A1.5b.

The use of eqns. 23 and 24 instead of the series given by eqn. 20 leads to an error at the very beginning of the transient process, at times of the order of τ_2 which are much less then the duration of the transient process as a whole. With the same degree of accuracy we can simplify eqn. 24a as follows:

$$\bar{\vartheta} = \bar{\vartheta}_s[1 - \exp(-t/\tau_1)] \quad (25)$$

Fig. 2 compares the exact characteristic time τ_1 and approximate solution given by eqn. 17b for $p_W = p_P = 0.1, k^2 = 0.1$ ($r_W = 1.353, r_P = 1.404$). It can be seen that the approximate and exact characteristic times agree qualitatively. Our calculations show that for smaller values of p_W and p_P the agreement is better, in accord with assumption 9.

A comparison of the exact (eqn. 24b) and approximate (eqn. 17a) average stationary temperatures

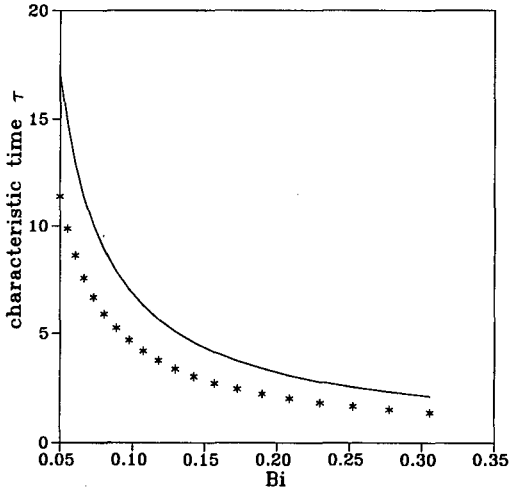

Fig. 2. Comparison of an exact characteristic time τ_1 (solid line) and the approximate solution (symbols) given by eqn. 17b, $p_W = p_P = 0.1$, $k^2 = 0.1$ ($r_W = 1.353$, $r_P = 1.404$).

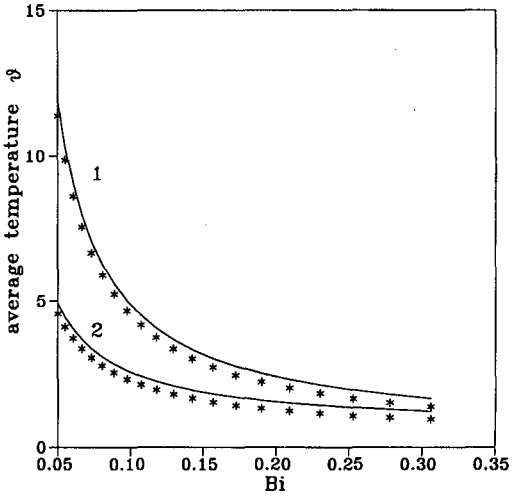

Fig. 3. Comparison of the exact average stationary (solid lines) (eqn. 24b) and approximate (symbols) (eqn. 17a) temperatures; $p_W = p_P = 0.1, k^2 = 0.05$ (curves 1); $p_W = p_P = 1, k^2 = 0.05$ (curves 2).

is given in Fig. 3 for $p_W = p_P = 0.1$, $k^2 = 0.05$ (curves 1) and for $p_W = p_P = 1, k^2 = 0.05$ (curves 2). It is seen from Fig. 3 that the curves corresponding to the approximate and exact solutions are in good agreement for different Biot numbers. Therefore, it is possible to use a simple approximate expression for temperature evaluation (eqn. 17a). By substituting eqn. 17a into eqn. 6e, one obtains for a stationary electric current in the voltage-stabilized mode

$$i_s = \frac{2Bi_{OA}(\vartheta_C k^2 + 1)}{2Bi_{OA} - k^2} \quad (26)$$

This equation can be used for estimations of the overall Biot number of a given capillary and cooling system or, otherwise, to determine the properties of the buffer.

DISCUSSION

A solution of unsteady heat transfer in CZE has been given for the general case of capillary and cooling conditions and approximate equations and their solutions for average temperature have been derived for different modes of power supply operation. The temporal behaviour of temperature in CZE can be described by an exponent for small Biot

numbers (poor cooling). A procedure has been given for finding the characteristic time of an unsteady process from a solution of an eigenvalue problem for conjugated heat transfer. The approximate equation for the characteristic time is valid for "thin-walled" capillaries. The approximate equations for stationary temperature and current can be used instead of exact equations for small Biot numbers.

The problem of heat evolution in electrophoretic techniques is not a trivial one. In the particular case of CZE, where this problem has been extensively studied both theoretically and experimentally, the following general conclusions can be drawn.

According to the original equation proposed by Jorgenson [10], the plate number N is directly proportional to the applied voltage gradient (E). In their experiments, N increased linearly with E with a tendency for plateauing at high E values. There is now a general consensus [4,11,12] that this is not the case: at high field strengths (varying according to several experimental parameters, such as molarity of background electrolyte and capillary radius, but in general above 200 V/cm) there exists a maximum in the experimental dependence of N *vs.* E, explained in terms of joule heat.

According to Jones *et al.* [13], at increasing applied potentials, the slope of the peak variance *versus* time plot increases in magnitude. If only molecular diffusion were causing this time-dependent variance, there should be a negligible slope change over the experimental range of applied voltages, as the calculated temperature increase was less than 1°C. According to Jones *et al.*, at high field strengths joule heating is approximately twice as significant than any other "non-ideal" flow contribution to solute band spreading.

As will be indicated in the accompanying Part II, a way to minimize temperature gradients would be to resort to narrow-bore capillaries and/or lower the conductivity of the background electrolyte. However, by decreasing the concentration of the operative buffer one could obtain highly skewed peaks due to a mismatch of the respective conductivities of analyte and buffer. In addition, in very narrow bore capillaries (*e.g.*, 25 μm diameter) zone detection could be problematic.

Perhaps, as suggested by Jansson *et al.* [14], a good solution would be to adopt rectangular cross-section capillaries. When the aspect ratio is increased from 1 (cylindrical) to 25 (highly flattened) capillaries, owing to the strongly increased heat dissipation in the rectangular conduit, the temperature increase is negligible even at E values well above 1000 V/cm. Moreover, if detection is made through the long side of the rectangle, sensitivity is increased even at progressively decreasing channel heights. Jansson *et al.* also proposed the use of rectangular silicon capillaries, as silicon has a *ca.* 100 times higher heat conductivity than fused silica.

According to a recent study [15], the overall column temperature could have a profound impact on protein separation and analysis. For example, on going from 20 to 45°C, myoglobin showed a progressive reduction from the Fe^{3+} form to the Fe^{2+} form. In the same temperature range, α-lactalbumin demonstrated a conformational transition that resulted in asymmetric peaks and sigmoidal mobility *vs.* temperature plots. Hence the importance of cooling the capillary, even below room temperature (at 2–4°C), as is customarily done in other electrophoretic techniques [16], for protein analysis, cannot be over-emphasized.

Another important aspect of operating at varying column temperatures is that the sample volume injected (*e.g.*, by pressure loading) could also vary substantially. Rush *et al.* [15] calculated that in the column temperature range 15–50°C, there will be a 70% increase in the sample volume injected.

SYMBOLS (PARTS I AND II)

a	Temperature coefficient of electric conductivity
β_{PL}	Relative thermal conductivity of polyimide coating
β_{WL}	Relative thermal conductivity of fused-silica wall
Bi	Biot number
C_L	Specific heat capacity of liquid (buffer inside the capillary)
C_P	Specific heat capacity of the capillary polyimide coating
C_W	Specific heat capacity of the capillary fused-silica wall
E	Electric field strength
$\bar{\vartheta}$	Average dimensionless temperature
F	Volumetric power generation
h	Coefficient of external heat transfer

i Dimensionless electric current
I Electric current
J_0 Bessel function of the zeroth order of the first kind
k^2 Autothermal parameter
k_{PL} Relative thermal diffusivity of polyimide coating
k_{WL} Relative thermal diffusivity of fused-silica wall
Nu Nusselt number
Pr Prandtl number
q_0 Initial dissipated power per unit volume
q Joule heat generation
ρ_L Density of the buffer inside the capillary
ρ_P Density of the capillary polyimide coating
ρ_W Density of the capillary fused-silica wall
Ra Rayleigh number
Re Reynolds number
R_L Radius of the capillary lumen
R_P Radius of the capillary polyimide coating
R_W Radius of the capillary fused-silica wall
r Dimensionless radius (in units of inner capillary diameter)
σ Buffer electric conductivity
t Dimensionless time
T_c Temperature of coolant
τ Time of a transient process
Y_0 Bessel function of the zeroth order of the second kind

ACKNOWLEDGEMENTS

M.S.B. thanks the European Space Agency (ESA) for a fellowship enabling him to carry out this work at the University of Milan. P.G.R. thanks ESA, ASI (Agenzia Spaziale Italiana) and Progetto Finalizzato Chimica Fine II (CNR, Rome) for funding these studies.

APPENDIX I

Steady-state radial temperature distribution

By substituting $\vartheta_s(r)$ in eqns. 8–14a, one obtains

$$\frac{1}{r}\cdot\frac{\partial}{\partial r}\left(r\cdot\frac{\partial\vartheta_s}{\partial r}\right)+1+k^2\vartheta_s=0 \quad 0\leqslant r<1 \quad \text{(A1.1)}$$

$$\frac{1}{r}\cdot\frac{\partial}{\partial r}\left(r\cdot\frac{\partial\vartheta_s}{\partial r}\right)=0 \quad 1\leqslant r<r_P \quad \text{(A1.2)}$$

$$\vartheta_s = \text{finite at } r=0 \quad \text{(A1.3a)}$$

$$\vartheta_s^- = \vartheta_s^+,\ \frac{\partial\vartheta_s^-}{\partial r}=\beta_{WL}\cdot\frac{\partial\vartheta_s^+}{\partial r} \text{ at } r=1 \quad \text{(A1.3b)}$$

$$\vartheta_s^- = \vartheta_s^+,\ \frac{\partial\vartheta_s^-}{\partial r}=\beta_{PW}\cdot\frac{\partial\vartheta_s^+}{\partial r} \text{ at } r=r_W \quad \text{(A1.3c)}$$

$$-\beta_{PL}\cdot\frac{\partial\vartheta_s}{\partial r}=Bi(\vartheta_s-\vartheta_C) \text{ at } r=r_P \quad \text{(A1.3d)}$$

We seek the solution in the form

$$\vartheta_s = AJ_0(kr)-\frac{1}{k^2} \qquad 0\leqslant r<1 \quad \text{(A1.4)}$$

$$\vartheta_s = B\ln(r)+C \qquad 1\leqslant r<r_W$$

$$\vartheta_s = D\ln(r)+E \qquad r_W\leqslant r<r_P$$

where $J_0(x)$ is the Bessel function of the zeroth order of the first kind. The five constants A, B, C, D and E should be determined from the boundary conditions (eqns. A1.3b–d). Substitution of eqn. A1.4 into eqns. A1.3b–d gives the following set of equations for the constants:

$$AJ_0(k)-\frac{1}{k^2}=C$$

$$-AkJ_1(k)=\beta_{WL}B$$

$$B\ln(r_W)+C=D\ln(r_W)+E \quad \text{(A1.5a)}$$

$$B=\beta_{PW}D$$

$$-\beta_{PL}\cdot\frac{D}{r_P}=Bi[D\ln(r_P)+E-\vartheta_C]$$

where $J_1(x)$ is the Bessel function of the first-order of the first kind.

Solving this set of equations, one obtains

$$A=\frac{Bi_{OA}(1+k^2\vartheta_C)}{Bi_{OA}J_0(k)-kJ_1(k)} \quad \text{(A1.5b)}$$

where

$$Bi_{OA}=\beta_{WL}\left\{\ln(r_W)+\frac{1}{\beta_{PW}}\left[\ln(r_P/r_W)+\frac{\beta_{PL}}{r_P\,Bi}\right]\right\}^{-1} \quad \text{(A1.6)}$$

is the dimensionless coefficient of proportionality of the heat flux from the inner surface of the lumen to the temperature difference between the inner surface and the coolant.

APPENDIX II

Calculation of eigenvalues, eigenfunctions and coefficients for the unsteady solution.

We seek an eigenfunction of the operator $\boldsymbol{L}$ in the following form:

$$g_\lambda(r) = \begin{cases} AJ_0(r\sqrt{\lambda^2+k^2}) & 0 \leqslant r < 1 \\ BJ_0(\lambda r/\sqrt{\kappa_{WL}}) + CY_0(\lambda r/\sqrt{\kappa_{WL}}) & 1 < r < r_W \\ DJ_0(\lambda r/\sqrt{\kappa_{PL}}) + EY_0(\lambda r/\sqrt{\kappa_{PL}}) & 1 < r < r_W \end{cases} \quad \text{(A2.1)}$$

where $Y_0(x)$ is the Bessel function of the zeroth order of the second kind.

Substitution of eqn. A2.1 into the boundary conditions included in the definition of the operator $\boldsymbol{L}$ leads to the set of equations for the determination of unknown constants A, B, C, D and E:

$$\begin{aligned} &AJ_0(\sqrt{\lambda^2+k^2}) - BJ_0(\lambda/\sqrt{\kappa_{WL}}) - CY_0(\lambda/\sqrt{\kappa_{WL}}) = 0 \\ &A\sqrt{\lambda^2+k^2}J_1(\sqrt{\lambda^2+k^2}) - B\sqrt{\beta_{WL}}\lambda J_1(\lambda/\sqrt{\kappa_{WL}})/\sqrt{\kappa_{WL}} - C\sqrt{\beta_{WL}}\lambda Y_1(\lambda/\sqrt{\kappa_{WL}})/\sqrt{\kappa_{WL}} = 0 \\ &BJ_0(\lambda r_W/\sqrt{\kappa_{WL}}) + CY_0(\lambda r_W/\sqrt{\kappa_{WL}}) - DJ_0(\lambda r_W/\sqrt{\kappa_{PL}}) - EY_0(\lambda r_W/\sqrt{\kappa_{PL}}) = 0 \\ &\frac{1}{\sqrt{\kappa_{WL}}}[BJ_1(\lambda r_W/\sqrt{\kappa_{WL}}) + CY_1(\lambda r_W/\sqrt{\kappa_{WL}})] - \frac{\beta_{PW}}{\sqrt{\kappa_{PL}}}[DJ_1(\lambda r_W/\sqrt{\kappa_{PL}}) + EY_1(\lambda r_W/\sqrt{\kappa_{PL}})] = 0 \\ &\lambda\beta_{PL}[DJ_1(\lambda r_P/\sqrt{\kappa_{PL}}) + EY_1(\lambda r_P/\sqrt{\kappa_{PL}})]/\sqrt{\kappa_{WL}} - Bi[DJ_0(\lambda r_P/\sqrt{\kappa_{PL}}) + EY_0(\lambda r_P/\sqrt{\kappa_{PL}})] = 0 \end{aligned} \quad \text{(A2.2)}$$

The linear uniform system of eqns. A2.2 has a non-trivial solution when the determinant of the system is equal to zero. This condition gives an equation for eigenvalues the solution of which is obtained numerically. The Bessel functions are computed by using programs from ref. 17. For calculating the eigenfunctions corresponding to the found eigenvalues, the coefficient A is set equal to 1 and the remaining coefficients are determined from the set of equations obtained from eqns. A2.2 by setting $A = 1$ and omitting the last equation.

In order to find the coefficients a_n we substitute eqns. 19 and 20 into the initial condition 5, thus obtaining

$$\vartheta_C - \vartheta_s = \sum_{n=1}^{N} a_n g_n(r) \quad \text{(A2.3)}$$

where N is the number of eigenfunction used in the expansion. Multiplying eqn. A2.3 by $rg_m(r)$ ($m = 1, \ldots, N$) and integrating with respect to r, one obtains a set of N linear algebraic equations for N unknowns a_n:

$$\sum_{n=1}^{N} a_n(g_n g_m) = \vartheta_m, \quad m = 1, \ldots, N \quad \text{(A2.4)}$$

$$(g_n g_m) = \int_0^{r_P} g_n g_m r\mathrm{d}r, \quad \vartheta_m = -\int_0^{r_P} \vartheta_s g_m r\mathrm{d}r$$

The set of eqns. A2.4 was solved by Gauss–Jordan elimination with pivoting [17].

REFERENCES

1 A. E. Jones and E. Grushka, *J. Chromatogr.*, 466 (1989) 219–225.
2 A. Vinther and H. Søberg, *J. Chromatogr.*, 559 (1991) 3–26.
3 R. J. Nelson, A. Paulus, A. S. Cohen, A. Guttman and B. L. Karger, *J. Chromatogr.*, 480 (1989) 111–127.
4 W. A. Gobie and C. F. Ivory, *J. Chromatogr.*, 516 (1990) 191–200.
5 H. J. Issaq, I. Z. Atamna, G. M. Muschik and G. M. Janni, *Chromatographia*, 32 (1991) 155–161.
6 M. S. Bello and P. G. Righetti, *J. Chromatogr.*, 606 (1992) 103–111.
7 H. S. Carslaw and J. C. Jaeger, *Conduction of Heat in Solids*, Clarendon Press, Oxford, 2nd ed., 1959.
8 G. Arfken, *Mathematical Methods for Physicists*, Academic Press, New York, 2nd ed., 1970.
9 E. Jahnke and F. Emde, *Tables of Functions*, Dover, New York, 1945.
10 J. W. Jorgenson, in J. W. Jorgenson and M. Phillips (Editors), *New Directions in Electrophoresis Methods (ACS Symposium Series*, Vol. 335), American Chemical Society, Washington, DC, 1987, pp. 182–198.
11 H. T. Rasmussen and H. M. McNair, *J. Chromatogr.*, 516 (1990) 223–231.
12 F. Foret, M. Deml and P. Bocek, *J. Chromatogr.*, 452 (1988) 601–613.
13 H. K. Jones, N. T. Nguyen and R. D. Smith, *J. Chromatogr.*, 504 (1990) 1–19.
14 M. Jansson, A. Emmer and J. Roerade, *J. High Resolut. Chromatogr.*, 12 (1989) 797–801.
15 R. S. Rush, A. S. Cohen and B. L. Karger, *Anal. Chem.*, 63 (1991) 1346–1350.
16 P. G. Righetti, *Isoelectric Focusing: Theory, Methodology and Applications*, Elsevier, Amsterdam, 1983.
17 W. H. Press, B. P. Flannery, S. A. Teukolsky and W. T. Vetterling, *Numerical Recipes in C, The Art of Scientific Computing*, Cambridge University Press, Cambridge, 1988.

Journal of Chromatography, 606 (1992) 103–111
Elsevier Science Publishers B.V., Amsterdam

CHROM. 24 263

Unsteady heat transfer in capillary zone electrophoresis

II. Computer simulations

Michael S. Bello* and Pier Giorgio Righetti

Department of Biomedical Sciences and Technologies, University of Milan, Via Celoria 2, Milan 20133 (Italy)

(First received January 7th, 1992; revised manuscript received April 13th, 1992)

ABSTRACT

Unsteady heat transfer in capillary zone electrophoresis in considered. Equations are derived that allow the calculation of the temperature evolution of the buffer under three different modes of electrophoresis: current-, voltage- or power-stabilized. In the power-stabilized mode, the temperature increase is intermediate between those in the current- (lowest) and voltage-stabilized (highest) modes. As the shortest transient time and the smallest temperature rise correspond to the current-stabilized mode of operation, this regime is recommended for temperature-sensitive separations and evaluations of the capillary heat-transfer coefficient, especially in the case of instrumentation-lacking forced cooling.

INTRODUCTION

Any electrophoresis process, whenever it occurs, is accompanied by internal heat generation caused by a dissipation of energy of moving ions. Heat exchange of the electrolyte solution with the outer medium is possible only through the surface of the electrophoresis cell. This inevitably leads to the appearance of temperature gradients within the solution and to a rise in the average temperature of the buffer. Changes in the buffer temperature affect its conductivity, dissociation constants (pK and hence pH), the wall ζ-potential and the mobilities of the separated particles and, as a result, influence the electrophoretic separation.

The importance of the heat-transfer process in capillary electrophoresis was realized a long time ago. However, systematic theoretical and experimental studies of temperature fields in the capillary, conditions of cooling and the like have been published only recently [1–7].

Experimental investigations have shown a non-linear dependence of the electric current on the applied voltage [1–3], high sensitivity of the electric current to variations of cooling conditions [1] and a decrease in the theoretical plate height due to inadequate cooling [1]. The advantages of forced or Peltier cooling have been demonstrated by Nelson *et al.* [1]. It has also been reported that at high currents the electrophoresis process becomes unstable [1].

Theoretical papers mostly deal with the radial temperature distribution within the capillary. Gobie and Ivory [2] unambiguously explained the deviations from Ohm's law by the temperature dependence of the conductivity. They considered the steady-state temperature distribution within the capillary by taking into account the temperature

Correspondence to: Professor Pier Giorgio Righetti, Department of Biomedical Sciences and Technologies, University of Milan, Via Celoria 2, Milan 20133, Italy.

* Permanent address: Institute of Macromolecular Compounds, Academy of Sciences, Bolshoi pr. 31, St. Petersburg 199004, Russia.

0021-9673/92/$05.00

dependence of the buffer conductivity[a]. They predicted and experimentally verified a situation in which the temperature increases infinitely. For this case they introduced the term "autothermal runaway". We accept this term and will use it below, but the mathematical treatment in ref. 2 and the equations therein do not consider time-dependent processes.

The aim of this study was to consider the transient process of establishing the steady-state temperature distribution. The following arguments justifying the significance of this problem can be provided: (1) such an unsteady process exists, it has been observed experimentally [1] and, therefore, it should be studied; (2) the heat transfer during electrophoresis under stacking conditions [6], when the electric conductivity of the sample zone differs from that of the buffer is, in fact, an unsteady process; and (3) it can be assumed that the process of micelle formation in micellar electrokinetic chromatography [8] depends not only on the resulting temperature but also on the transient temperature regime.

Below we formulate equations of unsteady heat transfer in the capillary. The approximate solution of these equations allows us to calculate a time dependence of the electric current in the capillary after a voltage has been applied for different operating modes from a power supply (voltage-, current- or power-stabilized mode). A transient time (*i.e.*, the time necessary to achieve a steady state) is calculated as a function of the capillary parameters and also parameters of the electrophoretic process.

THEORY

This part presents the general equations of unsteady heat transfer and boundary conditions in both dimensional and dimensionless forms and sets the problem in mathematical terms.

We consider the same system dealt with by others [2,6], consisting of a lumen, a fused-silica wall and a polyimide coat (Fig. 1). The electric conductivity of the buffer is assumed to be linearly dependent on

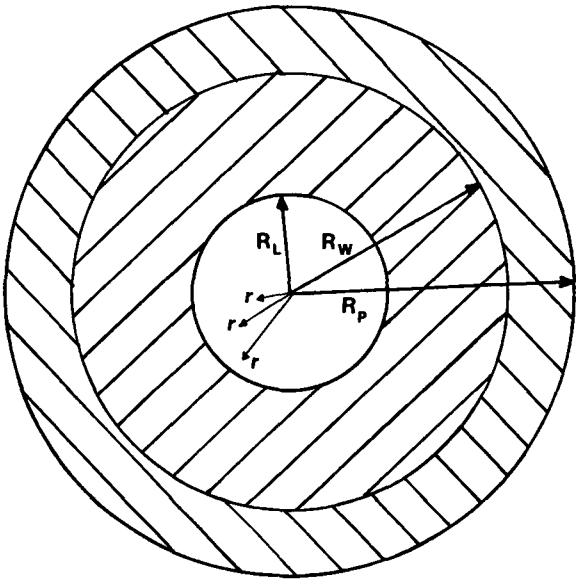

Fig. 1. Schematic representation of the capillary cross-section. R_L, R_W and R_P = radii of the lumen, wall and polyimide coat, respectively; r = distance between the centre of the capillary and any point of the cross-section (modified from Gobie and Ivory [2]).

temperature [2]. The difference between previous studies and this work is that we consider the development of the temperature field not only in space but also in time. The behaviour of the temperature field in the lumen, in the wall and in the coat is governed by the equations of unsteady heat transfer[b] [9]:

$$\rho_L C_{pL} \cdot \frac{\partial T}{\partial t} = \chi_L \cdot \frac{1}{r} \cdot \frac{\partial}{\partial r}\left(r \cdot \frac{\partial T}{\partial r}\right) + q \quad 0 \leqslant r < R_L \quad (1)$$

$$\rho_W C_{pW} \cdot \frac{\partial T}{\partial t} = \chi_W \cdot \frac{1}{r} \cdot \frac{\partial}{\partial r}\left(r \cdot \frac{\partial T}{\partial r}\right) \quad R_L \leqslant r < R_W \quad (2)$$

$$\rho_P C_{pP} \cdot \frac{\partial T}{\partial t} = \chi_P \cdot \frac{1}{r} \cdot \frac{\partial}{\partial r}\left(r \cdot \frac{\partial T}{\partial r}\right) \quad R_W \leqslant r < R_P \quad (3)$$

where T is the temperature, t the time, r the radius, ρ_L, ρ_W and ρ_P are the densities of the buffer, wall and the polyimide, respectively, C_L, C_W and C_P are their specific heat capacities, χ_L, χ_W and χ_P are their thermal conductivities, R_L, R_W and R_P are the radii of the lumen, wall and the polyimide coat, respec-

[a] A heat-transfer process is called "steady" if the temperature field does not vary with time, otherwise it is called "unsteady". These terms are used in order to avoid using "equilibrium" and "non-equilibrium", because a process of heat transfer is non-equilibrium in its nature.

[b] For symbols, see Part I [11].

tively, and q is the Joule heat generation (quantity of energy dissipated in unit volume per unit time).

The boundary conditions for eqns. 1–3 specify the finiteness of the temperature at the origin $r = 0$, the continuity of the temperature and the heat flux at the lumen–wall and wall–coat interfaces and the heat balance at the external surface of the capillary. These boundary conditions are expressed as follows:

$$T = \text{finite at } r = 0 \tag{4a}$$

$$T^- = T^+,\ \chi_L \cdot \frac{\partial T}{\partial r} = \chi_W \cdot \frac{\partial T^+}{\partial r} \text{ at } r = R_L \tag{4b}$$

$$T^- = T^+,\ \chi_W \cdot \frac{\partial T^-}{\partial r} = \chi_P \cdot \frac{\partial T^+}{\partial r} \text{ at } r = R_W \tag{4c}$$

$$-\chi_P \cdot \frac{\partial T}{\partial r} = h(T - T_C) \text{ at } r = R_P \tag{4d}$$

where the superscripts $^-$ and $^+$ indicate left and right values of the temperature and its derivative with respect to a boundary, h is the coefficient of the external heat transfer and T_C is the temperature of the coolant.

The heat-transfer coefficient depends on cooling conditions and for the case of forced cooling can be represented as follows:

$$h = Nu\chi_C/(2R_P) \tag{4e}$$

where χ_C is the thermal conductivity of the coolant and Nu is the Nusselt number, which is given by

$$Nu = 0.76Re^{0.4}Pr^{0.37} \tag{4f}$$

for the case of forced cooling and by

$$Nu = \left\{0.6 + \frac{0.387Ra^{1/6}}{[1 + (0.559/Pr)^{9/16}]^{8/27}}\right\}^2 \tag{4g}$$

for the case of lack of forced cooling [10], Re, Pr and Ra are the Reynolds, Prandtl and Rayleigh numbers, respectively, whose definition can be found also in ref. 8.

The initial condition for eqns. 1–3 is set in the following form:

$$T(r, t = 0) = T_C \tag{5}$$

An explicit expression for q appearing on the right-hand side of eqn. 1 depends on the mode in which the power supply is used. We shall distinguish three modes by which Joule heat is produced, outlined below.

Voltage-stabilized mode (E = constant)

$$q = \sigma E^2 = q_0[1 + \alpha(T - T_0)] \tag{6a}$$

$$\sigma = \sigma_0[1 + \alpha(T - T_0)] \tag{6b}$$

where σ is the electric conductivity of the buffer at temperature T, σ_0 the electric conductivity of the buffer measured at temperature T_0, α the temperature coefficient of the electric conductivity, E the electric field strength and q_0 the initial dissipated power per unit volume. In this mode the power and the electric current are time dependent.

Current-stabilized mode (I = constant)

By introducing the average electric conductivity as

$$\bar{\sigma} = 2\pi \int_0^{R_L} r\,\sigma dr/S \tag{6c}$$

where $S = \pi R_L^2$ is the area of the lumen cross-section, one obtains for E and q the following equations:

$$E = I_0/(S\bar{\sigma}) \tag{6d}$$

$$q = \sigma[I_0/(S\bar{\sigma})]^2 = q_0\sigma_0^2[1 + \alpha(T - T_0)]/\bar{\sigma}^2 \tag{6e}$$

where I_0 is the value of the current which is maintained stable. It was taken into account, when deriving eqns. 6d and e, that the electric field strength may vary with time but not in radius. In the current-stabilized mode the power and the electric field (voltage) are time dependent.

Power-stabilized mode (Q = constant)

In analogy with the previous case, one obtains for q

$$q = q_0\sigma/\bar{\sigma} \tag{6f}$$

In this mode the electric field and the electric current are time dependent. In all instances we neglected the transient times of the power supply.

It is useful for further analysis to introduce several dimensionless variables. We shall use the lumen radius R_L as a length scale, the characteristic temperature difference:

$$\Delta T_{ref} = q_0R_L^2/\chi_L \tag{7a}$$

as the temperature scale and the characteristic time of thermal diffusivity:

$$\tau_c = R_L^2 \cdot \frac{\rho_L C_{pL}}{\chi_L} \quad (7b)$$

as the time scale.

The autothermal parameter k^2 is defined as follows:

$$k^2 = \alpha \Delta T_{ref} \quad (7c)$$

the dimensionless temperatures are

$$\vartheta = (T - T_0)/\Delta T_{ref},\ \vartheta_C = (T_C - T_0)/\Delta T_{ref} \quad (7d)$$

and the Biot number is defined by

$$Bi = hR_L/\chi_L \quad (7e)$$

The average dimensionless temperature $\bar{\vartheta}$ is given by

$$\bar{\vartheta} = \frac{2}{R_L^2} \int_0^{R_L} \vartheta r dr \quad (8)$$

Eqns. 1–6 form a set of non-linear integro-differential equations of conjugated heat transfer. In the particular case of the voltage-stabilized mode of operation, this system becomes linear and merely differential. This case is the most common in capillary electrophoresis practice and will be studied in detail below. However, we shall consider in a simplified form all modes of operation listed above.

APPROXIMATE ANALYSIS OF THE UNSTEADY HEAT TRANSFER

In this part we shall use approximate solutions for the buffer average temperature for different modes of power supply (see also Part I [11]). Although not quantitative, such results are useful for a better understanding of the physical nature of the unsteady process.

The approximate solution for the average buffer temperature in the case of good cooling conditions (see Part I [11]) is given by

$$\bar{\vartheta}_a = \bar{\vartheta}_{a_s} + [\vartheta_C - \bar{\vartheta}_{a_s}] \exp(-t/\tau) \quad (9)$$

$$\bar{\vartheta}_{a_s} = \frac{2Bi_{0A}\vartheta_C + 1}{2Bi_{0A} - fk^2} \quad (9a)$$

$$\tau = (2Bi_{0A} - fk^2)^{-1} \quad (9b)$$

where the factor f is

$$f = \begin{cases} 1 \text{ for the voltage-stabilized mode} \\ -1 \text{ for the current-stabilized mode} \\ 0 \text{ for the power-stabilized mode,} \end{cases}$$

$\bar{\vartheta}_a$ is the approximate average temperature, Bi_{0A} is the overall Biot number defined below, $\bar{\vartheta}_{a_s}$ is the steady-state (*i.e.*, independent of time) part of the solution and τ is the characteristic time of the transient process.

The overall Biot number used by Gobie and Ivory [2] in our notation has the following form:

$$Bi_{0A} = \beta_{WL}\left\{\ln(R_W/R_L) + \frac{1}{\beta_{PW}}\left[\ln(R_P/R_W) + \frac{R_L\beta_{PL}}{R_P Bi}\right]\right\}^{-1} \quad (10)$$

The solution, as seen from eqn. 9, consists of two parts, one of which is the steady-state temperature and the other is the transient part vanishing in time. During a period of time equal to τ, the unsteady part of the temperature decreases e times. We shall define the transient time of the process τ_{tr} as the time necessary for decrease in the unsteady part of e^4 times ($1/e^4 = 1.8\%$):

$$\tau_{tr} = 4\tau \quad (9c)$$

The dependences of the dimensionless average temperature $\bar{\vartheta}_a$ on the dimensionless time calculated using eqns. 9 for three modes of operation are shown in Fig. 2. The curves corresponding to different

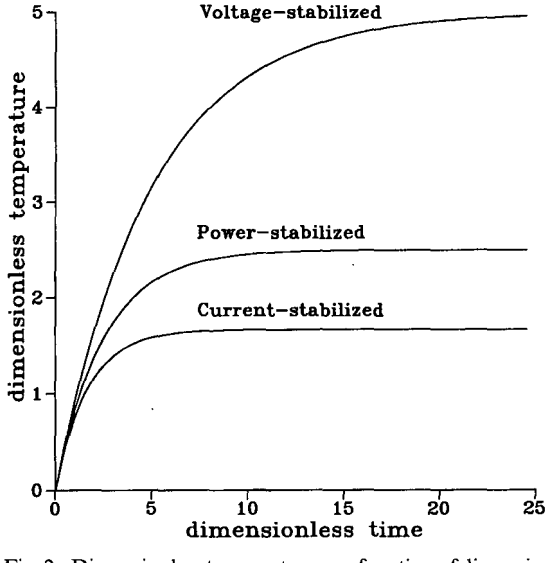

Fig. 2. Dimensionless temperature as a function of dimensionless time (approximate equations) for three possible modes of power supply operation. $Bi_{0A} = 0.2$, $k^2 = 0.2$. Note how the current-stabilized mode corresponds at any given time to the lowest temperature evolution.

modes of operation are calculated for $Bi_{0A} = 0.2$ and $k^2 = 0.2$. It is seen from Fig. 2 that the shortest transient time and the smallest temperature increase correspond to the current-stabilized mode. The longest transient time and the largest temperature increase correspond to the voltage-stabilized mode, while the power-stabilization mode lies in the middle. The difference between these three modes is caused by the temperature dependence of the buffer velocity.

Of course, these effects are pronounced only for the case of relatively small Biot numbers Bi_{0A} (poor cooling conditions) and relatively large values of the autothermal parameter k^2 (high voltage, large diameter of capillary, high buffer conductivity), or, better, for the case when the Biot number and the autothermal parameter are of the same order of magnitude. Thus, if $k = 0$, the values for τ and $\bar{\vartheta}_{a_s}$ (see eqns. 9) will be the same for all three cases. It is also seen from eqns. 9 that the transient time τ and the average buffer temperature for the voltage-stabilized mode increase infinitely if k^2 approaches $2Bi_{0A}$. This result is in agreement with the study of Gobie and Ivory [2], who called this phenomenon the "autothermal runaway". It is interesting that neither τ nor $\bar{\vartheta}_{a_s}$ is affected by the autothermal parameter k^2 in the power stabilization mode. It should be stressed that this approximate theory is limited to the case of a capillary with a relatively thin wall and coating.

UNSTEADY HEAT TRANSFER IN A POWER-STABILIZED MODE

This part aims at presenting results of mathematical modelling of the transient heat transfer in the power-stabilized mode governed by eqns. 1–6. In order to calculate temperature profiles across the capillary and transient times, we used the procedure described in Part I [11].

As the temperature regime depends significantly on the capillary dimensions and on the cooling conditions, we shall distinguish three types of capillaries and three modes of cooling.

The capillary types are thin, with I.D. < 50 μm, intermediate, with 50 μm $<$ I.D. < 150 μm, and thick, with I.D. > 150 μm. The thermal properties of the fused-silica wall and polyimide coating were taken from the Standard Product List of Polymicro Technologies (Phoenix, AZ, USA). The thermal properties of the buffer are assumed to be identical with those of water and the electrical conductivity of the buffer and its thermal coefficient were taken from ref. 2. All data used are presented in Table I.

As representative examples of thin, intermediate and thick capillaries we chose those with I.D. = 50 μm, O.D. = 363 μm for thin, I.D. = 150 μm, O.D. = 363 μm for intermediate and I.D. = 530 μm, O.D. = 700 μm for thick. The thickness of the polyimide coating was assumed to be 15 μm in all instances.

The three modes of cooling we distinguish are lack of forced cooling, forced air cooling and forced liquid cooling.

The heat-transfer coefficient for the case of lack of forced cooling was evaluated by using eqns. 4e and g with parameters corresponding to dry air at 25°C and the characteristic temperature difference (for evaluation of the Rayleigh number) equal to 30°C.

The values of heat-transfer coefficients in air and liquid cooling systems used in the Beckman apparatus for the capillary with $R_P = 165$ μm are $h_{air} = 239.54$ W/m^2 · K for the air cooling system and $h_{liq} = 1136$ W/m^2 · K for the liquid cooling system (data kindly provided by Dr. K. Anderson, Beckman Instruments, Palo Alto, CA, USA). We recalculate the heat transfer coefficients by multiplying these values by the factor $(R_P/165)^{-0.6}$, according to eqns. 4f and e.

The evolution of temperature profiles across the

TABLE I

PHYSICAL PARAMETERS USED FOR COMPUTER SIMULATIONS

Parameter	Value	Parameter	Value
ρ_L[a]	1 g/cm^3	χ_L[c]	0.61 W/mK
ρ_W	2.15 g/cm^3	χ_W	1.5 W/mK
ρ_P	1.42 g/cm^3	χ_P	0.15 W/mK
C_{PL}[b]	4.18 J/g	σ_0[d]	7.5 mS/cm
C_{PW}	1 J/g	α[e]	2.17 · 10^{-2} K^{-1}
C_{pP}	1.1 J/g		

[a] Density.
[b] Specific heat capacity.
[c] Thermal conductivity.
[d] Electric conductivity of the buffer.
[e] Thermal coefficient of electric conductivity.

corrected 26 Oct 92 On page 107, 1st column, last sentence: this sentence should be deleted

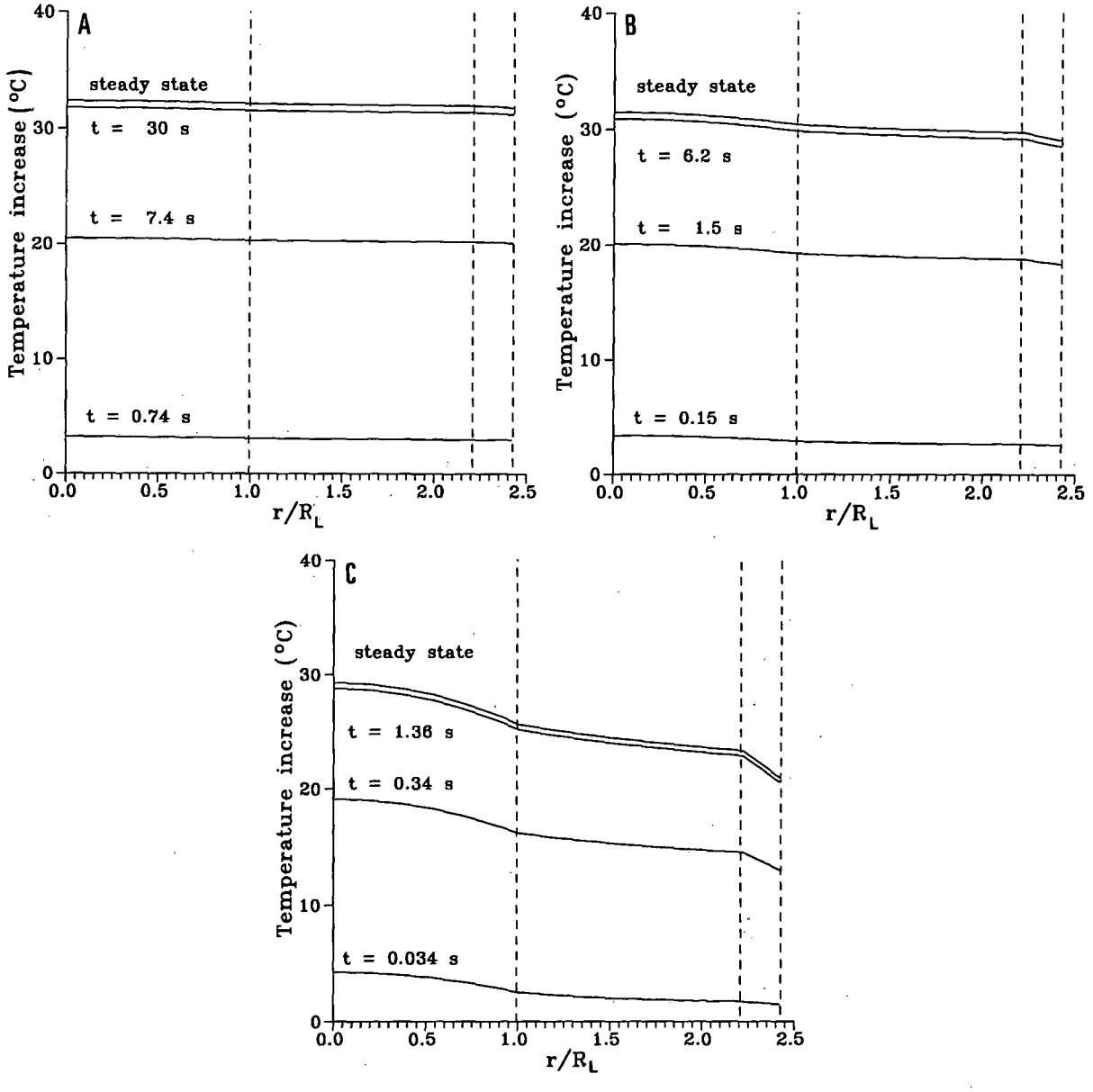

Fig. 3. Temperature profiles across the capillary at different times as a function of the r/R_L ratio (where r = distance between any point in the section of Fig. 1, up to RP, and the centre of the capillary; R_L = radius of the lumen of the capillary). In all three simulations, the lower three curves represent time points equal to 0.1τ, τ and 4τ. The upper curve in all figures corresponds to the steady-state temperature distribution. (A) Lack of forced cooling, voltage gradient 90 V/cm; (B) air-cooling, voltage gradient 190 V/cm; (C) liquid cooling, voltage gradient 360 V/cm. Note that, in all simulations, the value of zero on the abscissa represents the centre of the lumen of the capillary; therefore, a full representation of the temperature profile in the entire capillary should correspond to a specular doubling of the image on the left-hand side of each figure. The vertical dashed lines represent at $x = 1$, end of the lumen; at $x = 2.22$, end of the wall; and at $x = 2.42$, end of the polyimide coat of the capillary.

TABLE II

TRANSIENT TIME AS A FUNCTION OF COOLING MODE AND CAPILLARY SIZE (CALCULATED AT $\Delta T \approx 30°C$)

Type of capillary	Parameter	Type of cooling		
		None	Air cooling	Liquid cooling
Thin (I.D. = 50 μm, O.D. = 363 μm)	E (V/cm)	250	550	1050
	τ_{tr} (s)	25	5.2	1.2
Intermediate (I.D. = 150 μm, O.D. = 363 μm)	E (V/cm)	90	190	360
	τ_{tr} (s)	29.6	6.2	1.4
Thick (I.D. = 530 μm, O.D. = 700 μm)	E (V/cm)	28	65	125
	τ_{tr} (s)	120	21	4.8

capillary of the intermediate type for three modes of cooling is shown in Fig. 3. The curves on the figures correspond to temperature profiles at time points equal to 0.1τ, τ and 4τ. The last one was defined above as the transient time. The highest curve in all figures corresponds to the steady-state temperature distribution. The voltage was chosen so as to provide an approximately equal (about 30°C) temperature increase in all instances. It can be seen from Fig. 3A that the temperature profile evolves by remaining almost uniform in the case of lack of forced cooling. It takes approximately 30 s to attain the steady state. The case of air cooling (Fig. 3B) is characterized by shorter transient times in comparison with the lack of forced cooling and greater temperature gradients of the buffer temperature. The electric field providing a temperature increase of 30°C is 190 V/cm, which is considerably greater than the 90 V/cm reported in Fig. 3A. With liquid cooling (Fig. 3C) the voltage is increased up to 360 V/cm and the transient time decreases to 1.36 s. However, the temperature gradient in the buffer becomes more pronounced and assumes a quasi-parabolic profile in the lumen of the capillary.

Results illustrating the influence of cooling and the type of capillary are presented in Table II. We took the temperature increase of 30°C as a reference point and calculated the transient times and electric fields necessary to produce such an elevation of temperature for all combinations of capillary types and cooling conditions. When comparing the values for thin and intermediate capillaries in Table II one might conclude that a threefold increase in capillary inner diameter does not lead to considerable changes in transient times for all modes of cooling. However, an increase in transient times of about 20% occurs. The transition to a thick capillary shows a considerable increase in transient times (by a factor of *ca.* 4). It can be seen from Table II that the transient process should be taken into account when performing separations in the absence of cooling for all type of capillaries, especially for thick ones. With

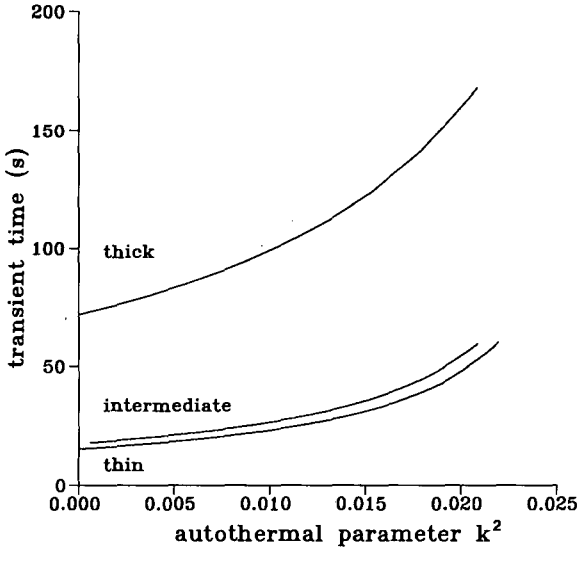

Fig. 4. Dependence of the transient time (in seconds) on the autothermal parameter (k^2) in the case of lack of forced cooling. Thin = capillary of 50 μm I.D. and 363 μm O.D.; intermediate = 150 μm I.D. and 363 μm O.D.; thick = 530 μm I.D. and 700 μm O.D. Note how the thin and intermediate capillaries behave similarly, whereas a large deviation is seen with the thick capillary.

air cooling these effects are pronounced only for thick capillaries and with liquid cooling their influence on separation appears to be negligible.

As the lack of cooling corresponds to longer transient times than other modes of cooling, we present dependences of the transient time on the autothermal parameter, eqn. 7c. This parameter is responsible for the autothermal runaway, as is evident from eqns. 9a and b. Fig. 4 shows these dependences for three types of capillaries and illustrates the progressive increase in transient time with higher values of the autothermal parameter (*i.e.*, increasing power generation).

The dependences of the transient time for the three capillary types on the heat-transfer coefficient are shown in Fig. 5, which generalizes our previous considerations to diverse kinds of coolants, cooling systems, etc. The electric field for each curve was adjusted so as to match the temperature for each capillary type at a given value of heat-transfer coefficient. Fig. 5 shows the importance of the capillary outer diameter on the transient process. It

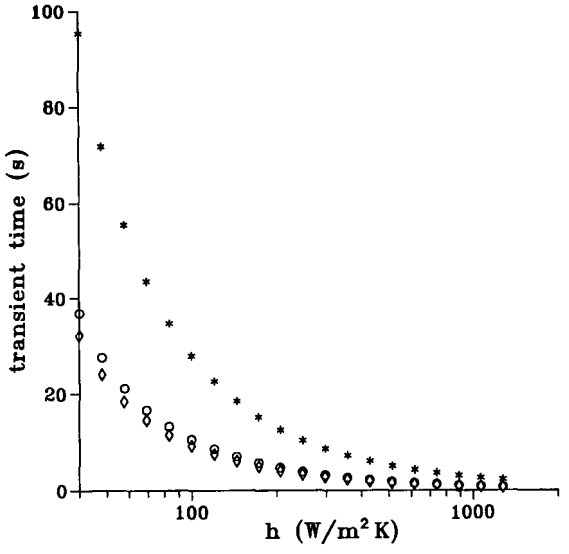

Fig. 5. Dependence of the transient time for three capillary types on the coefficient of heat transfer [h (W/m^2 · K)]. As in Fig. 4, note the very similar behaviour of the thin (◇) and intermediate (○) capillaries and the strong divergence of the thick capillary (✳). Note that, for any given value of the heat-transfer coefficient, the temperature on each of the three curves will coincide (this is obtained by adjusting the electric field strength in each type of capillary). E: ✳ (thick capillary), 32 V/cm; ○ (intermediate capillary), 110 V/cm; ◇ (thin capillary), 260 V/cm.

can be used for choosing a capillary type for a given cooling system or for the determination of the parameters of a cooling system.

CONCLUSIONS

Some practical guidelines can be derived from our simulations of thermal transients as follows.

In systems lacking forced cooling, the best operating mode would be at constant current, as this is the system generating the lowest temperature increase due to Joule heating.

In uncooled capillaries, the highest theoretical plate number will be obtained with the narrowest bore (*e.g.*, 20 μm I.D.), as this will correspond to the minimum radial temperature excursion.

As the thermal transients can last as long as >2 min, they will probably not be relevant in long-duration separations (typical of protein and nucleic acid analyses in gel media) but they might affect short-duration runs, *e.g.*, separations occurring in just a few minutes.

In very large-bore capillaries (*ca.* 500 μm I.D.), if there is a large temperature difference between the axis and the periphery, two phenomena will contribute to zone broadening (decrease in theoretical plate number): (a) radial viscosity gradients, allowing for faster migration of ions at the centre of the lumen (this will automatically generate conductivity differences) and (b) radial pH gradients, due to pK variations of the buffering ions in the background electrolyte (*e.g.*, the dpK/dT value for Tris is 0.03) [12], with a concomitant modulation of the mobility of the analyte ions, especially at background electrolyte pH values close to the pK values of the analytes.

Our results can be generalized to other types of separations, *e.g.*, isoelectric focusing in thin gel slabs (500 μm thickness). As these gels are cooled only on one side (see Fig. 3.13 in ref. 13), it is clear that temperature gradients will be pronounced (with generation of a radial pH gradient, in addition to the longitudinal pH gradient established between the anode and cathode). This definitely calls for gels of much decreased thickness (*e.g.*, 50–100 μm, simulation in progress).

ACKNOWLEDGEMENTS

M.S.B. thanks the European Space Agency (ESA)

for a fellowship enabling him to carry out this work at the University of Milan. P.G.R. thanks ESA, ASI (Agenzia Spaziale Italiana) and Progetto Finalizzato Chimica Fine II (CNR, Rome) for funding these studies.

REFERENCES

1 R. J. Nelson, A. Paulus, A. S. Cohen, A. Guttman and B. L. Karger, *J. Chromatogr.*, 480 (1989) 111–127.
2 W. A. Gobie and C. F. Ivory, *J. Chromatogr.*, 516 (1990) 191–200.
3 H. J. Issaq, I. Z. Atamna, G. M. Muschik and G. M. Janni, *Chromatographia*, 32 (1991) 155–161.
4 E. Grushka, R. M. McCormick and J. J. Kirkland, *Anal. Chem.*, 61 (1989) 241–246.
5 A. E. Jones and E. Grushka, *J. Chromatogr.*, 466 (1989) 219–225.
6 A. Vinther and H. Søberg, *J. Chromatogr.*, 559 (1991) 3–26.
7 G. O. Roberts, P. H. Rhodes and R. S. Snyder, *J. Chromatogr.*, 480 (1989) 37–67.
8 S. Terabe, *Trends Anal. Chem.*, 8 (1989) 129–134.
9 H. S. Carslaw and J. C. Jaeger, *Conduction of Heat in Solids*, Clarendon Press, Oxford, 2nd ed., 1959.
10 S. Kakaç, R. K. Shah and W. Aung (Editors), *Handbook of Single-Phase Conductive Heat Transfer*, Wiley, New York, 1987.
11 M. S. Bello and P. G. Righetti, *J. Chromatogr.*, 606 (1992) 95–102.
12 P. Lundahl and S. Hjertén, *Ann. N. Y. Acad. Sci.*, 209 (1973) 94–111.
13 P. G. Righetti, *Isoelectric Focusing: Theory Methodology and Applications*, Elsevier, Amsterdam, 1983.

Journal of Chromatography, 606 (1992) 113–119
Elsevier Science Publishers B.V., Amsterdam

CHROM. 24 244

Chromatographic behaviour of diastereoisomers

XI.* Steric effects and solvent selectivity effects in retentions on silica of esters of maleic and fumaric acids

M. D. Palamareva and I. D. Kozekov

Department of Chemistry, University of Sofia, Sofia 1126 (Bulgaria)

(First received February 18th, 1992; revised manuscript received March 31st, 1992)

ABSTRACT

The thin-layer chromatographic (TLC) retentions on silica of twenty diastereoisomeric compounds of the type ROOCCH = CHCOOR were studied as the group R varied from methyl to isopentyl and cyclohexyl. Twenty-one mobile phases were used having strengths, ε, in the range 0.215–0.316 and a wide variation of solvent selectivity effects. Owing to a site chelation via the two ester groups, the (*Z*)-maleate was always more strongly retained than the corresponding (*E*)-fumarate. An increase in both steric effects and solvent selectivity effects did not change the relative retention but affected the retention of the diastereoisomers. TLC is suitable for assigning the configurations of other compounds from the group studied.

INTRODUCTION

This series of papers [1] is aimed at a better understanding of the relative retentions of diastereoisomeric pairs of compounds on silica because the problem is connected with the use of normal-phase liquid–solid chromatography (LSC) as a method for configuration determination. Thin-layer chromatography (TLC) on silica of over 130 diastereoisomeric pairs of various groups of compounds with known configurations has shown that the relative retention of the diastereoisomers of a given group usually remains unchanged when steric effects and solvent selectivity effects are varied [2–5]. The exceptions seem reasonable and can be predicted on the basis of Snyder's theory [6–8] and Soczewiński's method [9].

In Part X [1] we reported the TLC on silica of two related groups of diastereoisomeric ethenes having two different complex substituents. The relative retentions found, $E > Z$ and $Z > E$, were attributed to two different models of adsorption of each group of compounds ensuring less steric hindrance of the more strongly retained diastereoisomer. In an attempt to find conformationally rigid diastereoisomeric compounds with two equal strongly adsorbing groups in this work, we studied the TLC separation on silica of esters of maleic and fumaric acid of the type 1 shown. This paper reports the separations of twenty such diastereoisomers showing an increase in the effective volume of R with 21 mobile phases.

Correspondence to: Dr. M. D. Palamareva, Department of Chemistry, University of Sofia, 1 James Bourchier Avenue, Sofia 1126, Bulgaria.

* For Part X, see ref. 1.

0021-9673/92/$05.00

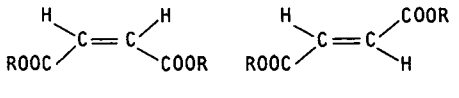

Z (maleates) E (fumarates)

type 1

R = CH_3, C_2H_5, n-C_3H_7, iso-C_3H_7, n-C_4H_9, sec.-C_4H_9, iso-C_4H_9, n-C_5H_{11}, iso-C_5H_{11}, cyclohexyl

EXPERIMENTAL

The synthesis of the diastereoisomeric compounds **1–20** studied was done according to ref. 10, with 37–88% yields.

The ^1H NMR spectra of the compounds were measured in chloroform on a Tesla 80-MHz spectrometer. They were similar to those reported in refs. 11 and 12, showing a chemical shift for the olefinic protons in the region of 6.05–6.28 ppm and 6.68–6.85 ppm for *Z* and *E* isomers, respectively.

TLC was performed as in ref. 3 on silica gel DG (Riedel-de Haën, Hannover, Germany). The solvents used were of analytical-reagent grade. The R_F values were arithmetic means of three to eight measurements. The reproducibility of the R_F values was ± 0.025.

RESULTS AND DISCUSSION

Table I lists the mobile phases used which were characterized by the three parameters strength, ε, localization, m, and polarity, P', introduced by Snyder [6–8]. The values of these parameters and the molar fraction, N_B, in the case of the binary mobile phases were calculated by means of a microcomputer program [13] based on Snyder's theory [6–8].

Table II summarizes the TLC data showing the structure and configuration of the compounds studied, their R_F values and the derived values of sep-

TABLE I

MOBILE PHASES STUDIED AND THE CORRESPONDING COMPUTER-CALCULATED [13] VALUES OF STRENGTH, ε, LOCALIZATION, m, AND POLARITY, P'

N_B is the molar fraction of the second solvent for binary mobile phases 1–11 and 17–21.

No.	Composition (vol.%)	N_B	ε	m	P'
1	Hexane–diethyl ether (80:20)	0.238	0.286	0.63	0.64
2	Hexane–ethyl acetate (88.4:11.6)	0.148	0.286	0.58	0.60
3	Hexane–tetrahydrofuran (87.2:12.8)	0.190	0.286	0.97	0.60
4	Hexane–acetone (95.4:4.6)	0.078	0.286	0.88	0.33
5	Tetrachloromethane–isopropanol (99.76:0.24)	0.003	0.286	–	1.61
6	Hexane–methyl *tert.*-butyl ether (91.6:8.4)	0.091	0.286	0.76	–
7	Tetrachloromethane–diethyl ether (89.0:11.0)	0.102	0.286	0.53	1.73
8	Tetrachloromethane–acetonitrile (96.14:3.86)	0.062	0.286	0.58	1.76
9	Cyclohexane–diethyl ether (82.4:17.6)	0.181	0.286	0.62	0.33
10	Benzene–methylene chloride (37.99:62.01)	0.306	0.286	0.09	2.95
11	Hexane–diisopropyl ether (37.4:62.6)	0.393	0.286	0.10	1.54
12	Cyclohexane–toluene–diethyl ether (81.8:10.0:8.2)		0.270	0.54	0.31
13	Hexane–tetrachloromethane–chloroform–diethyl ether (75.1:10.0:10.0:4.9)		0.270	0.54	0.78
14	Cyclohexane–tetrachloromethane–benzene–methylene chloride–ethyl acetate (87.32:3.33:3.33:3.33:2.68)		0.270	0.51	0.19
15	Cyclohexane–carbon disulphide–toluene–benzene–methylene chloride (14.74:6.67:6.67:6.67:65.26)		0.270	–	2.35
16	Hexane–toluene–benzene–chloroform–diisopropyl ether–diethyl ether (85.5:2.5:2.5:2.5:2.5:4.5)		0.270	0.54	0.50
17	Hexane–ethyl acetate (98:2)	0.026	0.215	0.54	0.19
18	Hexane–ethyl acetate (94:6)	0.078	0.258	0.57	0.36
19	Hexane–ethyl acetate (91.9:8.1)	0.105	0.270	0.58	0.48
20	Hexane–ethyl acetate (87:13)	0.165	0.292	0.58	0.66
21	Hexane–ethyl acetate (80:20)	0.249	0.316	0.59	0.96

TABLE II

EXPERIMENTAL R_F VALUES AND DERIVED VALUES OF LOG α FOR THE DIASTEREOISOMERIC COMPOUNDS **1–20** OF TYPE I

For compositions of mobile phases, see Table I. The values of log α were calculated from R_F values of the corresponding *Z–E* pair using eqns. 1 and 2.

R	Solute		R_F for indicated mobile phase																				
	Configuration	No.	1	2	3	4	5	6	7	8	9	10	11	12	13	14	15	16	17	18	19	20	21
CH_3	*Z*	**1**	0.22	0.22	0.29	0.12	0.03	0.15	0.26	0.16	0.22	0.28	0.42	0.09	0.10	0.06	0.21	0.09	0.03	0.10	0.13	0.22	0.34
	E	**2**	0.43	0.40	0.47	0.25	0.06	0.32	0.45	0.33	0.39	0.40	0.66	0.22	0.20	0.12	0.32	0.21	0.08	0.22	0.27	0.40	0.53
CH_2CH_3	*Z*	**3**	0.32	0.33	0.39	0.17	0.03	0.21	0.34	0.22	0.32	0.31	0.59	0.14	0.13	0.08	0.24	0.13	0.04	0.16	0.20	0.34	0.48
	E	**4**	0.55	0.50	0.57	0.31	0.06	0.40	0.55	0.44	0.52	0.44	0.82	0.31	0.26	0.17	0.38	0.28	0.11	0.32	0.38	0.50	0.64
$CH_2CH_2CH_3$	*Z*	**5**	0.40	0.42	0.47	0.21	0.03	0.28	0.43	0.29	0.41	0.36	0.74	0.21	0.17	0.11	0.30	0.18	0.06	0.23	0.29	0.42	0.58
	E	**6**	0.62	0.56	0.64	0.35	0.07	0.46	0.65	0.54	0.62	0.51	0.93	0.40	0.33	0.20	0.44	0.36	0.13	0.37	0.45	0.57	0.70
$CH(CH_3)_2$	*Z*	**7**	0.41	0.43	0.50	0.22	0.03	0.30	0.42	0.31	0.43	0.34	0.75	0.22	0.17	0.12	0.29	0.18	0.07	0.23	0.30	0.44	0.59
	E	**8**	0.63	0.57	0.65	0.37	0.07	0.48	0.65	0.54	0.63	0.48	0.93	0.40	0.33	0.22	0.42	0.37	0.14	0.38	0.46	0.58	0.72
$CH_2CH_2CH_2CH_3$	*Z*	**9**	0.44	0.46	0.53	0.23	0.03	0.33	0.51	0.35	0.47	0.43	0.82	0.24	0.20	0.14	0.35	0.21	0.08	0.26	0.34	0.50	0.64
	E	**10**	0.68	0.59	0.70	0.38	0.08	0.52	0.71	0.58	0.69	0.57	0.96	0.45	0.36	0.24	0.50	0.42	0.16	0.41	0.49	0.61	0.75
$CH(CH_3)CH_2CH_3$	*Z*	**11**	0.48	0.49	0.54	0.26	0.03	0.35	0.51	0.32	0.49	0.42	0.84	0.27	0.20	0.15	0.33	0.21	0.07	0.27	0.34	0.49	0.64
	E	**12**	0.71	0.60	0.68	0.42	0.09	0.53	0.72	0.57	0.69	0.55	0.95	0.47	0.36	0.24	0.48	0.41	0.16	0.39	0.48	0.60	0.74
$CH_2CH(CH_3)_2$	*Z*	**13**	0.47	0.48	0.53	0.25	0.03	0.35	0.51	0.35	0.49	0.44	0.83	0.27	0.21	0.16	0.37	0.22	0.08	0.27	0.33	0.49	0.64
	E	**14**	0.70	0.59	0.68	0.41	0.09	0.52	0.73	0.59	0.69	0.57	0.96	0.46	0.36	0.24	0.52	0.41	0.16	0.39	0.48	0.60	0.74
$CH_2CH_2CH_2CH_2CH_3$	*Z*	**15**	0.48	0.48	0.54	0.25	0.04	0.35	0.54	0.41	0.51	0.48	0.85	0.29	0.23	0.17	0.40	0.24	0.08	0.28	0.35	0.50	0.65
	E	**16**	0.72	0.60	0.69	0.41	0.10	0.53	0.78	0.65	0.71	0.61	0.98	0.49	0.38	0.25	0.54	0.43	0.16	0.40	0.49	0.60	0.75
$CH_2CH_2CH(CH_3)_2$	*Z*	**17**	0.49	0.48	0.55	0.25	0.05	0.36	0.56	0.44	0.51	0.48	0.86	0.30	0.23	0.17	0.40	0.24	0.08	0.28	0.35	0.50	0.66
	E	**18**	0.73	0.60	0.71	0.42	0.09	0.54	0.79	0.67	0.72	0.61	0.98	0.50	0.38	0.26	0.54	0.43	0.16	0.41	0.49	0.61	0.76
Cyclohexyl	*Z*	**19**	0.46	0.47	0.53	0.24	0.05	0.35	0.57	0.47	0.52	0.46	0.84	0.30	0.21	0.17	0.37	0.21	0.07	0.27	0.35	0.50	0.66
	E	**20**	0.69	0.60	0.70	0.41	0.10	0.53	0.80	0.69	0.73	0.58	0.96	0.51	0.37	0.26	0.50	0.41	0.16	0.40	0.49	0.61	0.77

	Log α for indicated mobile phases																					Range of log α
1–2	0.43	0.37	0.36	0.39	0.32	0.42	0.36	0.41	0.36	0.23	0.43	0.45	0.35	0.32	0.25	0.42	0.45	0.40	0.40	0.37	0.34	0.23–0.45 (0.22)
3–4	0.42	0.31	0.32	0.34	0.32	0.40	0.38	0.45	0.36	0.25	0.50	0.44	0.38	0.37	0.29	0.42	0.47	0.39	0.39	0.29	0.28	0.25–0.50 (0.25)
5–6	0.39	0.24	0.32	0.31	0.39	0.34	0.39	0.46	0.37	0.27	0.67	0.40	0.38	0.31	0.27	0.41	0.36	0.29	0.30	0.26	0.23	0.23–0.67 (0.44)
7–8	0.39	0.24	0.29	0.32	0.39	0.34	0.41	0.42	0.35	0.26	0.64	0.41	0.38	0.32	0.25	0.43	0.33	0.31	0.30	0.24	0.25	0.24–0.64 (0.40)
9–10	0.43	0.23	0.34	0.31	0.45	0.34	0.37	0.41	0.40	0.24	0.72	0.39	0.35	0.29	0.27	0.44	0.34	0.29	0.27	0.19	0.23	0.19–0.72 (0.53)
11–12	0.42	0.20	0.26	0.31	0.51	0.32	0.39	0.45	0.37	0.23	0.66	0.38	0.35	0.25	0.28	0.42	0.40	0.24	0.26	0.20	0.20	0.20–0.66 (0.46)
13–14	0.42	0.19	0.28	0.32	0.51	0.30	0.41	0.43	0.37	0.22	0.69	0.36	0.33	0.22	0.26	0.39	0.34	0.24	0.28	0.20	0.20	0.19–0.69 (0.50)
15–16	0.44	0.21	0.28	0.32	0.43	0.32	0.48	0.43	0.37	0.22	0.94	0.37	0.31	0.21	0.25	0.38	0.34	0.23	0.25	0.18	0.21	0.18–0.94 (0.76)
17–18	0.45	0.21	0.30	0.34	0.28	0.32	0.48	0.41	0.39	0.22	0.90	0.37	0.31	0.24	0.25	0.38	0.34	0.25	0.25	0.19	0.21	0.19–0.90 (0.71)
19–20	0.42	0.23	0.32	0.34	0.33	0.32	0.48	0.40	0.40	0.21	0.66	0.39	0.35	0.24	0.23	0.42	0.40	0.25	0.25	0.19	0.23	0.19–0.66 (0.47)

aration, α, of Z–E pairs calculated by the following equations:

$$\log \alpha = R_{M(Z)} - R_{M(E)} \quad (1)$$

$$R_M = \log k' = \log (1/R_F - 1) \quad (2)$$

where k' is the capacity factor and the subscripts E and Z specify the isomer. Using eqn. 1, the relative retention of the diastereoisomers is expressed in a shorter manner, namely, a positive value of log α corresponds to a stronger retention of the Z compound than that of its E diastereoisomer, as was found (see Table II). This relative retention is valid for all the cases studied independently of the structure of the compounds and mobile phases used.

Table III shows the fit of the data obtained with mobile phases 2 and 17–21 composed of hexane and ethyl acetate in different ratios to Soczewiński's equation [9]:

$$R_M = A - n\log N_B \quad (3)$$

where A is a constant for a given solute and set of mobile phases, N_B is the molar fraction of the more polar solvent ethyl acetate and the slope of the plot, n, is the number of solvent molecules displaced by a solute molecule from the adsorbent surface. Fig. 1 illustrates some of the data in Table III.

A general view on the variation of the separation, α, of the diastereoisomeric pairs with the use of mobile phases of different m is shown in Table IV. Any mobile phase is represented by the average value $\overline{\log \alpha}$ for all compounds studied. Fig. 2 illustrates this variation.

Microcomputer-aided choice of the mobile phases used

The mobile phases used were selected by means of the microcomputer program [13] mentioned above, having the following three main modes: (1) choice of the solvents for the mobile phase, (2) calculation of the values of the parameters ε, m and P' on the basis of the ratio of the solvents input by the user and (3) choice of mobile phases of given strength, ε, desired by the user.

The R_F values of diastereoisomers **1–20** with hexane–diethyl ether (80:20) (mobile phase 1) were in the favourable range 0.22–0.73. Mode 2 of the microcomputer program showed that ε of this mobile phase was 0.286. Using mode 3 of the microcompu-

TABLE III

FIT OF R_M OF INDIVIDUAL COMPOUNDS OBTAINED WITH BINARY MOBILE PHASES 17–19, 2, 20, 21 OF INCREASING ε TO THE EQUATION $R_M = A - n$LOG N_B (EQN. 3), WHERE N_B IS THE MOLAR FRACTION OF THE SECOND SOLVENT

The values of $\Delta A = A_Z - A_E$ were calculated on the basis of A for the indicated isomer.

Solute	n	A	ΔA	S.D.	R
1	−1.24	−0.45	0.28	0.03	−0.998
2	−1.13	−0.73		0.02	−0.999
3	−1.38	−0.81	0.14	0.02	−0.999
4	−1.17	−0.95		0.02	−0.999
5	−1.34	−0.95	0.15	0.03	−0.999
6	−1.21	−1.10		0.02	−0.999
7	−1.30	−0.94	0.18	0.02	−0.999
8	−1.20	−1.12		0.02	−0.999
9	−1.33	−1.04	0.12	0.01	−0.999
10	−1.19	−1.16		0.03	−0.998
11	−1.40	−1.10	0.04	0.03	−0.999
12	−1.18	−1.14		0.02	−0.998
13	−1.33	−1.05	0.08	0.02	−0.999
14	−1.18	−1.13		0.02	−0.999
15	−1.35	−1.08	0.09	0.01	−0.999
16	−1.20	−1.17		0.03	−0.997
17	−1.36	−1.09	0.10	0.02	−0.999
18	−1.21	−1.19		0.03	−0.997
19	−1.42	−1.13	0.07	0.02	−0.999
20	−1.23	−1.20		0.04	−0.996
			Overall	±0.02	−0.999

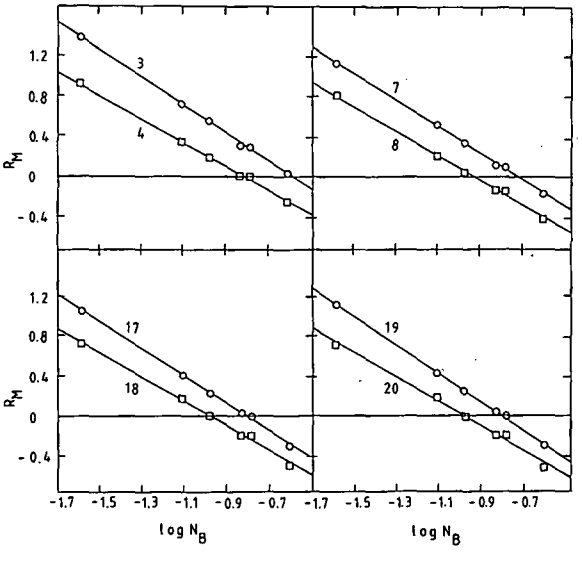

Fig. 1. R_M *vs.* log [molar fraction (N_B)] plots based on the data in Table III for diastereoisomeric pairs **3–4**, **7–8**, **17–18** and **19–20**.

TABLE IV

VARIATION OF AVERAGE VALUES OF SEPARATION, α, WITH LOCALIZATION, *m*, OF THE MOBILE PHASES

$\overline{\text{Log } \alpha}$, $\overline{R_F}$ and $\overline{R_M}$ are average values for compounds **1–20** and a given mobile phase (see Table II). The values of *m* are taken from Table I. Mobile phases 5 and 15 are not included because their *m* values cannot be calculated. The mobile phases are arranged in order of increasing *m*.

ε	Mobile phase	$\overline{\text{Log } \alpha}$	*m*	$\overline{R_F}$	$\overline{R_M}$
0.287	10	0.24	0.09	0.47	0.05
	11	0.68	0.10	0.83	−0.69
	7	0.42	0.53	0.57	−0.12
	2	0.24	0.58	0.49	0.02
	8	0.43	0.58	0.45	0.09
	9	0.37	0.62	0.54	−0.07
	1	0.42	0.63	0.53	−0.05
	6	0.34	0.76	0.39	0.19
	4	0.33	0.88	0.30	0.37
	3	0.31	0.97	0.57	−0.12
0.270	14	0.28	0.51	0.18	0.66
	12	0.40	0.54	0.33	0.31
	13	0.35	0.54	0.26	0.45
	16	0.41	0.54	0.28	0.41
0.215–0.316	17	0.38	0.54	0.10	0.95
	18	0.29	0.57	0.30	0.37
	19	0.30	0.58	0.37	0.23
	2	0.24	0.58	0.49	0.02
	20	0.23	0.58	0.50	0.00
	21	0.24	0.59	0.65	−0.27

ter program, we found other binary mobile phases of the same strength. Thus, the set of mobile phases 1–11 are of equal ε (0.286). Similarly, the set of mobile phases 11–16 containing threee to six solvents

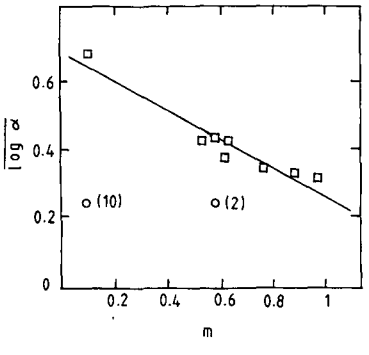

Fig. 2. Log α *vs.* *m* plot from Table IV for mobile phases having ε = 0.286. The numbers in parentheses indicate the mobile phase used.

was selected to have ε equal to 0.270. The set of mobile phases 17–21 composed of hexane and ethyl acetate was chosen by mode 2 of the microcomputer program and has ε in the range 0.215–0.316 as a result of the increase in the amount of ethyl acetate and its N_B.

Table I shows that the properties of mobile phases 1–21 composed of two to six non-localizing and localizing solvents are different because of the following changes in the values of the characterizing parameters: $0.215 \leqslant \varepsilon \leqslant 0.316$, $0.09 \leqslant m \leqslant 0.97$, $0.19 \leqslant P' \leqslant 2.95$. The average values $\overline{R_F}$ and $\overline{R_M}$ in Table IV show that the retention of the compounds studied decreases with increase in ε.

Role of solvent selectivity effects

Solvent selectivity effects change significantly the separation of a given diastereoisomeric pair, as can be seen from the corresponding ranges of log α included in Table II.

The solvent selectivity effects were approximated by the localization, *m*, for mobile phases of constant ε and by the molar fraction of the more polar solvent, N_B, for binary mobile phases with increasing N_B and thus with increasing ε [1, 3–5].

Concerning the set of mobile phases 17–19, 2, 20 and 21, composed of hexane and ethyl acetate and with increasing ε, a very good linear correlation was found between R_M and solvent selectivity effects expressed by N_B, as required by eqn. 3. The mean values of the standard deviation, S.D., and correlation coefficient, *R*, were ± 0.02 and 0.999, respectively, as the molar fraction, N_B, of ethyl acetate varied in the range 0.026–0.249. The plots for the diastereoisomers are almost parallel or show a slight tendency for a better separation at lower N_B (see Fig. 1).

According to Table III, the absolute values of the slope *n* are *ca.* 1, showing that one solute molecule, independently of its configuration, displaces one molecule of the stronger solvent ethyl acetate from the adsorbent surface.

When N_B approaches unity, *A* in eqn. 3 is equal to R_M and the relative parameter $\Delta A = A_Z - A_E$ is equal to log α. Table III shows that ΔA has positive values in all instances and consequently the relative retention of the diastereoisomers will not alter if the mobile phase is mainly composed of ethyl acetate. The same is valid for the remaining range of N_B

because the R_m *vs.* log N_B plots for the diastereoisomers do not cross.

According to Snyder's theory [6–8], there is a linear correlation between log α and m when ε is kept constant, and this has been widely verified (*e.g.*, see refs. 1 and 3). Table IV shows that a significant variation of m is characteristic only for mobile phases 1–11 having $\varepsilon = 0.286$. The corresponding plot in Fig. 2 agrees with the theory except for the data obtained with mobile phases 2 and 10 as the overall S.D. is ± 0.12. The tendency for maximum separation with minimum m is clearly seen. Table IV also shows that mobile phase 11, composed of hexane and diisopropyl ether, has the best selectivity because $\overline{\log \alpha}$ is greatest (0.68). This mobile phase shows a low m value (0.10) and an intermediate P' value (1.54).

The plot in Fig. 2 does not cross the abscissa when m is in the range 0.1–1, *i.e.*, $\log \alpha > 0$. Hence, the retention $Z > E$ established is not expected to alter if other mobile phases with different m are used (*cf.*, refs. 4 and 5).

Role of steric effects

There are examples when a change in steric effects in a series of diastereoisomers of a given type affords a change in the relative retention of the diastereoisomers [2–5]. This phenomenon is attributed to a change in the adsorption model or to the role of solvent selectivity effects in determining the relative retention.

The compounds studied are a good example of diastereoisomers of a given type with varying steric effects because of the significant variation of the group R. Table II shows that the Z isomer is always more strongly retained than the corresponding E isomer independently of the steric effect of R (ref. 14, p. 298). However, the greater the steric effect, the higher is the R_F of the compounds with a given configuration. For instance, the Z isomers show an increase in R_F from 0.22 to 0.49 with mobile phase 1 when R increases from methyl to isopentyl. This decrease in retention should be connected with the corresponding changes in free energy of adsorption with a dominating role of enthalpy over entropy (*cf.*, ref. 6, p. 85). It is interesting that in contrast to this fact, the separation of the diastereoisomers is improved in the same order (see the tendency for increase in the ranges in log α from 0.22 to 0.76 in Table II when passing from solute pair **1–2** to solute pair **17–18**). Thus, a sort of steric acceleration (ref. 14, p. 290) of the separation of the diastereoisomers was established. This could be attributed to relief of steric strain under adsorption (if there is a significant entropy loss when the solutes studied are adsorbed owing to the decrease in their freedom, the steric strain could be reduced).

Deduced model of adsorption

The compounds studied are free from the complication of intramolecular hydrogen bonding because the two ester groups are proton acceptors and a proton-donating group is absent. They are conformationally rigid. The equal values of n for Z and E isomers in Table III indicate that the diastereoisomers adsorb via the same group, which should be the two equal ester groups. Thus, the free energy of adsorption on silica of the ester group is considerably greater than that of the olefinic double bond, being 5.27 and 0.25, respectively (ref. 6, p. 264). In addition, the double bond is conjugated with the two carbonyl groups increasing their adsorption.

Taking into account the two-point adsorption, the stronger adsorption of the Z isomers than that of the corresponding E isomers is a result of the proximity of the two ester groups which adsorb via the so-called site chelation [6] on the same adsorption site. Such a phenomenon is not possible for the

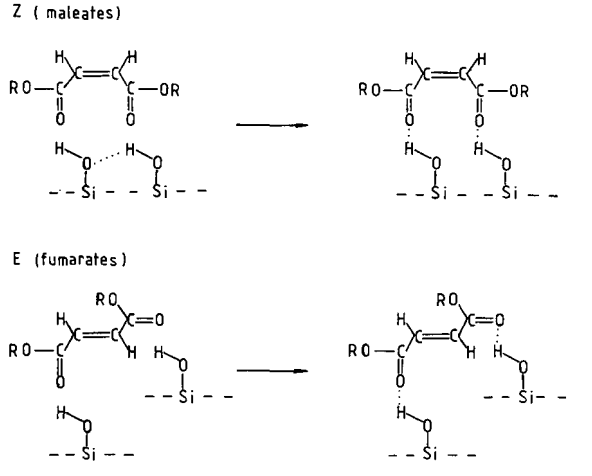

Fig. 3. Schematic representation of the two-point adsorption of the diastereoisomers studied with a site chelation for only Z isomers on a reactive hydroxyl site (ref. 6, p. 315).

E isomers, which also adsorb with the two ester groups but on two separate adsorption sites (see Fig. 3).

The following assumption is possible for the *Z* isomers: site chelation can be compensated for by steric hindrance between the two ester groups at a given effective volume of the group R, leading to the oposite relative retention $Z < E$. However, such a phenomenon was not established. Therefore, TLC seems suitable for configurational assignments of other compounds of similar type [2].

ACKNOWLEDGEMENT

We thank Dr. L. R. Snyder for his support of this study and very helpful comments on the manuscript, especially the drawing of our attention to the fact that an increase in steric effects improves the separation of diastereoisomers.

REFERENCES

1 M. D. Palamareva, B. J. Kurtev and I. Kavrakova, *J. Chromatogr.*, 545 (1991) 161; and references cited therein.
2 M. D. Palamareva, B. J. Kurtev, M. Mladenova and B. Blagoev, *J. Chromatogr.*, 235 (1982) 299; and references cited therein.
3 L. R. Snyder, M. D. Palamareva, B. J. Kurtev, L. Z. Viteva and J. N. Stefanovski, *J. Chromatogr.*, 354 (1986) 107.
4 M. D. Palamareva and L. R. Snyder, *Chromatographia*, 19 (1984) 352.
5 M. Palamareva, B. Kurtev and L. Viteva. *God. Sofii. Univ., Khim. Fak.*, 79 (1985) 258.
6 L. R. Snyder, *Principles of Adsorption Chromatography*, Marcel Dekker, New York, 1968.
7 L. R. Snyder and J. J. Kirkland, *Introduction to Modern Liquid Chromatography*, Wiley-Interscience, New York, 2nd ed., 1979.
8 L. R. Snyder, in Cs. Horváth (Editor), *High-Performance Liquid Chromatography*, Vol. 3, Academic Press, New York, 1983, p. 157.
9 E. Soczewiński, *J. Chromatogr.*, 388 (1987) 91; and references cited therein.
10 G. H. Jeffery and A. I. Vogel, *J. Chem. Soc.*, (1948) 664.
11 L. M. Jackman and R. H. Wiley, *Proc. Chem. Soc.*, (1958) 196.
12 L. M. Jackman and R. H. Wiley, *J. Chem. Soc.*, (1960) 2886.
13 M. D. Palamareva and H. E. Palamarev, *J. Chromatogr.*, 477 (1989) 235.
14 N. S. Isaacs, *Physical Organic Chemistry*, Longman, Harlow, 1987.

Journal of Chromatography, 606 (1992) 121–128
Elsevier Science Publishers B.V., Amsterdam

CHROM. 24 230

Effect of solvent composition and pH on R_F values of metal ions on titanium tungstate-impregnated papers in aqueous nitric acid, acetone–nitric acid and butanol–nitric acid systems

Surendra Dutt Sharma and Smiti Misra

Analytical Research Laboratory, Department of Chemistry, Hindu College, B-3, Jigar Vihar, Moradabad 244001 (India)

(First received January 31st, 1992; revised manuscript received March 18th, 1992)

ABSTRACT

The chromatographic behaviour of 50 cations on titanium (IV) tungstate-impregnated papers in 10^{-5}–5 *M* HNO_3, butanol–8 *M* HNO_3 and HNO_3–acetone–water systems was studied, together with the effect of pH on R_F values. For most cations, $R_F = a + bC^2$, where C is the nitric acid concentration. The effect of mole fractions of HNO_3, acetone and water on R_F values is explained. A large number of analytically important binary and ternary separations are reported. Quantitative separation of Pb^{2+} and Hg^{2+} from binary mixtures containing larger amounts of other metal ions was achieved.

INTRODUCTION

Titanium(IV)-based exchangers have been found to possess promising chemical and thermal stability and have been extensively used in column chromatography [1], thin-layer chromatography [2,3] and paper chromatography [4,5] of metal ions. Of these, titanium(IV) tungstate has proved to be the most stable in acids [1,6] and exhibits good ion-exchange capacity. Qureshi and Husain [7] studied the chromatography of metal ions on titanium(IV) tungstate-impregnated papers. Recently, electrochromatography of a number of metal ions in complex-forming acids and their sodium salts has also been carried out [8]. These papers are very selective and a number of metal ion separations were achieved.

However, in the above studies, no effort was made to study the effect of solvent composition on the retention factor, the effect of pH on the R_F values of metal ions has not been studied and not many ions were studied in a number of aqueous and mixed solvent systems.

In this work, nitric acid was chosen because it is a non-complexing acid and the understanding of the equilibria is simplified. Acetone does not solvate ions significantly and hence it is easy to study the mechanism of migration. Butanol was chosen because of our earlier experience [9,10] that it gives clear and useful separations.

EXPERIMENTAL

Apparatus

Chromatography was performed on 15 × 3.0 cm Whatman No. 1 paper strips in glass jars of 21 × 5 cm I.D. A Bausch and Lomb Spectronic-20 spectrophotometer was used for measurements.

Reagents

Analytical-reagent grade chemicals and reagents

Correspondence to: Dr. S. D. Sharma, Analytical Research Laboratory, Department of Chemistry, Hindu College, B-3, Jigar Vihar, Moradabad 244001, India.

0021-9673/92/$05.00

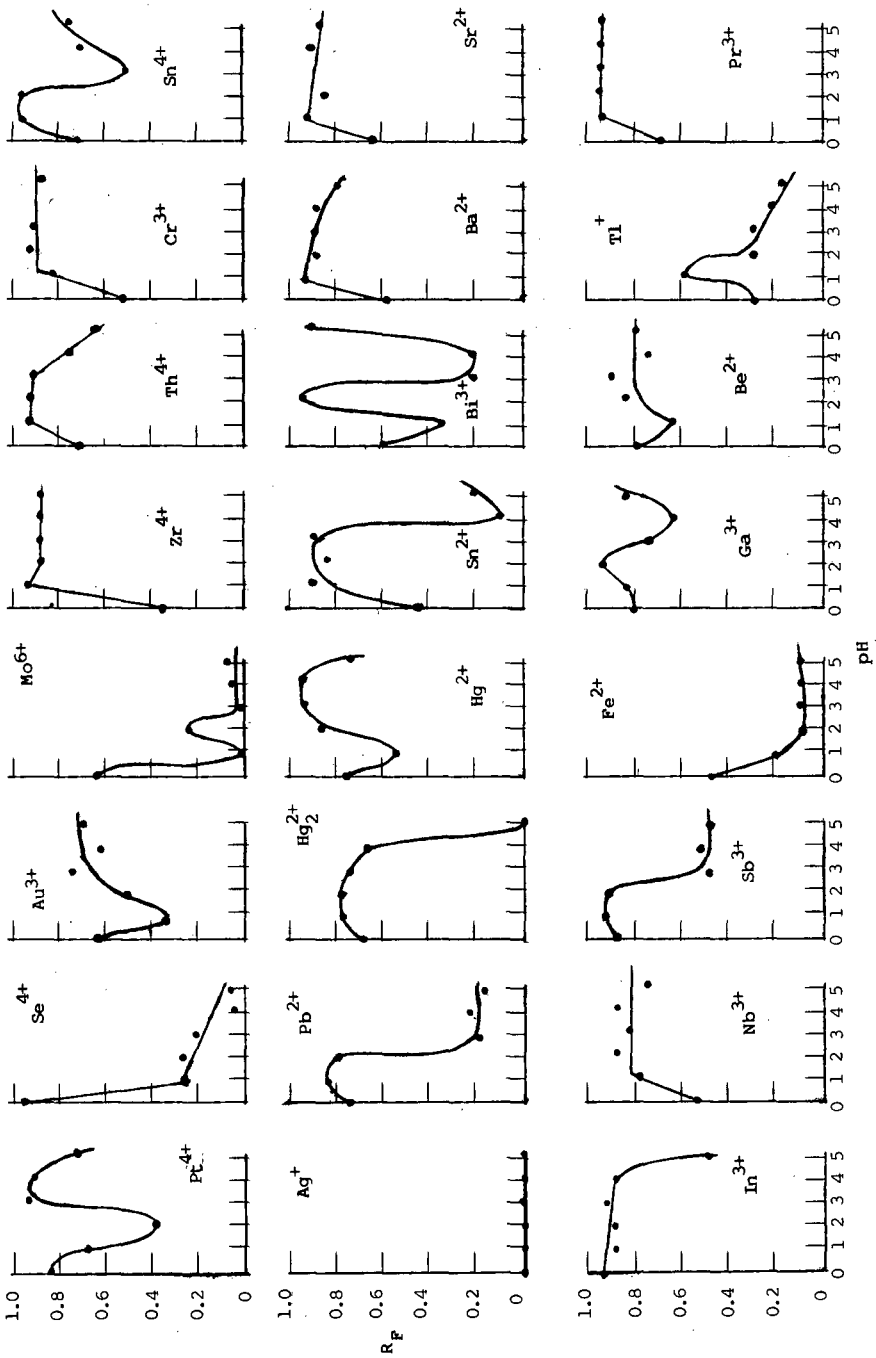

Fig. 1. Plots of R_F *vs.* pH of HNO_3 systems. Pd^{2+}, Fe^{3+}, VO^{2+}, UO_2^{2+}, Cu^{2+}, Ni^{2+}, Co^{2+}, Al^{3+}, Zn^{2+}, Mn^{2+}, Ir^{4+}, Mg^{2+}, K^+, Rb^+, Cs^+, Sr^{2+}, Tl^{3+}, Cd^{2+}, La^{3+}, Ru^{3+}, Ca^{2+}, Y^{3+}, Ce^{3+}, Ce^{4+}, Nb^{5+} and Pr^{3+} have $R_F > 0.75$ at all pH values.

were used. In butanol–HNO_3 systems 8 *M* HNO_3 was used and in pH studies 10^{-5}–1 *M* HNO_3.

Test solutions and detection

Test solutions containing 0.1 *M* chlorides, nitrates or sulphates of cations were prepared in a small amount of the corresponding acids. Conventional spot test reagents were used for detection purposes.

Preparation of ion-exchange papers

A 0.25 *M* solution of titanium(IV) chloride and a 0.25 *M* solution of sodium tungstate were prepared in distilled water. Paper strips were first passed through titanium(IV) chloride solution for 3–5 s and the excess of the chloride was removed by placing the strips on a filter-paper sheet. The strips were then dipped in sodium tungstate solution for 5 s and the excess was drained off. The strips were dried at room temperature overnight, washed three times with distilled water in order to remove excess reagents and finally allowed to dry at room temperature for 12 h and used as such. These papers were found to possess considerable ion-exchange capacity. For K^+ ion (K^+–H^+ exchange), the exchange capacity is 0.35 mequiv. per gram of treated paper as determined by column experiments (saturation method) [11].

Procedure

For qualitative work. The sample solution was applied (one or two spots) on paper strips. The chromatograms were conditioned for 5–10 min, then the solvent was allowed to ascend 11 cm from the starting line on the paper in all instances.

For quantitative work. Stock solutions of lead nitrate and mercury(II) nitrate were prepared in demineralized water. Pb^{2+} and Hg^{2+} were loaded with the help of a lambda pipette in the form of a streak. The cations to be separated were also applied in the amounts shown in Table II. Development was performed in the chosen solvent systems. In all instances, ascent 11 cm from the starting line on titanium(IV) tungstate-impregnated papers was allowed. A pilot paper was run simultaneously in order to locate the exact position of the spot with the help of the chromogenic agent. The area of the working paper corresponding to the detected spot on the pilot paper was cut out and Pb^{2+} and Hg^{2+} were eluted with 1 *M* HNO_3 and 1 *M* H_2SO_4, respectively. The volume of the solution in each instance was then reduced to about 10 ml by heating on a hot-plate. Pb^{2+} and Hg^{2+} were detected spectrophotometrically [12] using dithizone in carbon tetrachloride at 520 and 485 nm, respectively.

Solvent systems

Fifty cations were chromatographed in the following 31 solvent systems: (a) nine HNO_3 systems with concentrations of 1, 2, 3, 5, 0.1, 0.01, 0.001, 0.0001 and 0.00001 *M*; (b) six butanol–8 *M* HNO_3 systems in the proportions (1) 10:0, (2) 9:1, (3) 8:2, (4) 7:3, (5) 6:4 and (6) 5:5; and (c) sixteen solvent systems containing HNO_3–acetone–water in the proportions (1) 1:1:1, (2) 1:1:2, (3) 1:1:3, (4) 1:1:4, (5) 1:1:5, (6) 1:1:6, (7) 1:2:1, (8) 1:3:1, (9) 1:4:1, (10) 1:5:1, (11) 1:6:1, (12) 2:1:1, (13) 3:1:1, (14) 4:1:1, (15) 5:1:1 and (16) 6:1:1.

RESULTS AND DISCUSSION

In order to check the reproducibility of R_F values, five sets of some ions were chromatographed in 1.0, 0.1 and 0.01 *M* HNO_3. It was observed that the variation does not exceed 10% of the average R_F values. The complete R_F data have not been given for the sake of brevity. The effect of pH and solvent composition was studied only for those cations where $R_F < 0.75$. A large number of binary and ternary separations on impregnated papers were achieved as a direct result of the selectivity shown by the ion exchanger and the solvent studied. The few important ones achieved in aqueous HNO_3 systems are Ag^+–Bi^{3+}–Cu^{2+}, Sb^{3+}–Sn^{2+}–Sn^{4+}, Ag^+–Pb^{2+}–Cd^{2+} and Tl^+–Ga^{3+}–Zn^{2+}. Butanol–8 *M* HNO_3 systems were found to be useful in effecting the separations, *viz.*, Al^{3+}–Zn^{2+}–Tl^{3+}, Bi^{3+}–Hg^{2+}–Tl^{3+}, Zr^{4+}–Th^{4+}–Sb^{3+}, Fe^{3+} or Cr^{3+}–Mn^{2+}–Pt^{4+}, Mo^{6+}–VO^{2+}–UO_2^{2+}, Mn^{2+}–Zn^{2+}–Hg^{2+} and Se^{4+}–La^{3+} or Y^{3+}–Au^{3+}. Quaternary separation of Ag^+–Pb^{2+}–Bi^{3+}–Pt^{4+} was also achieved with butanol–8 *M* HNO_3 (1:1). Some useful ternary separations in HNO_3–acetone–water systems are Ba^{2+}–Sr^{2+}–Ca^{2+}, Tl^+–Bi^{3+}–Hg^{2+}, Ag^+–Tl^+–Tl^{3+} and Mo^{6+}–Mn^{2+}–Cr^{3+}.

Aqueous nitric acid systems

In aqueous nitric acid systems (10^{-5}–1 *M*), the plots of R_F *versus* pH (Fig. 1) reveal certain interest-

ing points. For some cations such as Tl^{3+}, Fe^{3+}, Ni^{2+}, Co^{2+}, Ba^{2+}, Sr^{2+}, Mn^{2+}, Pr^{3+}, Cd^{2+}, Zn^{2+}, Al^{3+}, Cr^{3+}, K^+, Rb^+, Cs^+, Y^{3+}, Zr^{4+}, Ce^{3+} and Nd^{3+}, the R_F value first increases from pH 0 to 1 and then becomes almost constant. Above pH 1, there is not much increase in the R_F value for most of the cations, possibly because the pH of the solution does not affect the ion-exchange capacity of titanium(IV) tungstate significantly. Qureshi *et al.* [1] have shown that the ion-exchange capacity of Ti(IV)-based exchangers does not change if the pH of the solution is below 10. However, a sharp increase in ion-exchange capacity is observed as the pH is raised above 10. This is probably due to the hydrolysis of the exchange material at higher pH. According to them, Ti(IV)-based ion exchangers behave like weakly acidic cation exchangers, which differs from the findings of Szirtes *et al.* [13]. Only titanium phosphate shows a moderately strong acid behaviour. For Pb^{2+}, Hg_2^{2+}, Sb^{3+}, Hg^{2+}, Ga^{3+}, Bi^{3+}, Sn^{2+}, Th^{4+} and Mg^{2+} the R_F is maximum at pH 2. With Bi^{3+}, Sb^{3+} and Pb^{2+} there is a sharp decrease in the R_F value beyond pH 2. The same trend is also observed with Sn^{2+}, for which the R_F decreases from 0.9 to 0.1 as the pH increases from 3 to 4. In all these instances, the sharp decrease in R_F value may be due to the excessive hydrolysis of these cations in the acidic solutions.

Ag^+ shows exceptional behaviour, having almost zero R_F value owing to its interaction with the

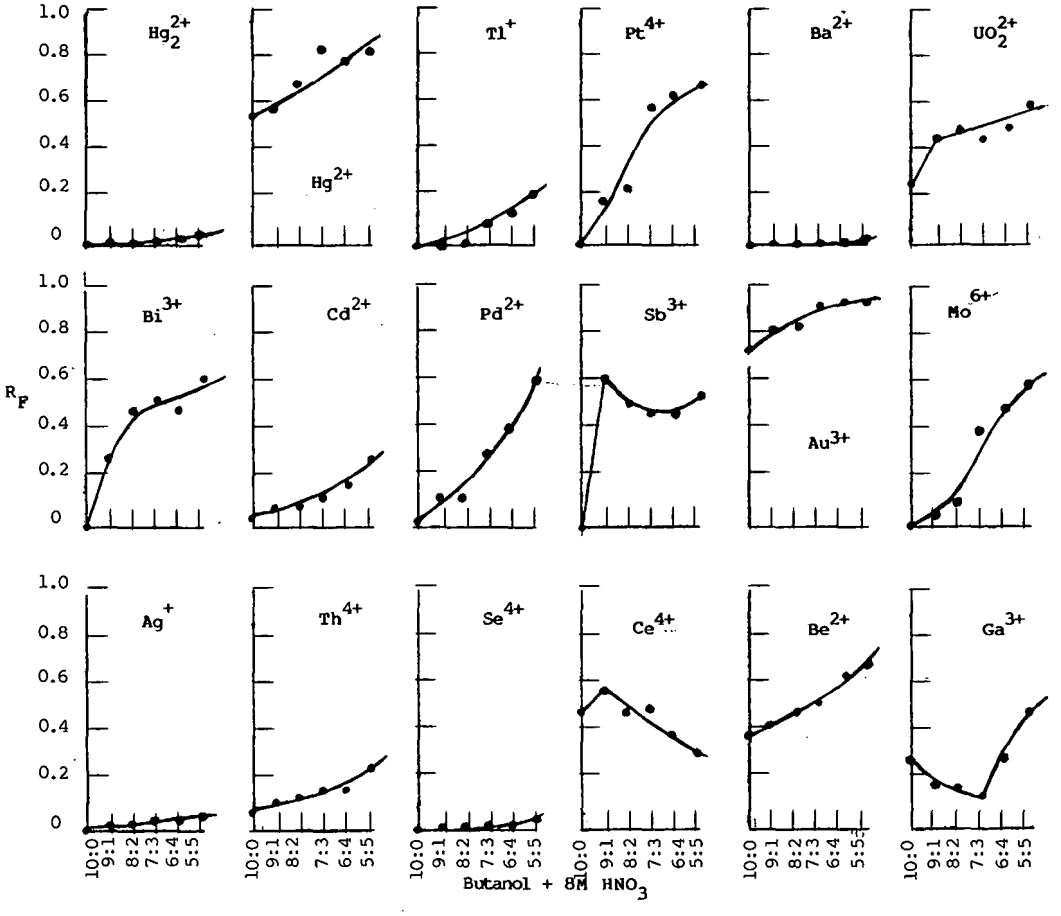

Fig. 2. Plots of R_F *vs.* butanol–8 *M* HNO_3 proportions. Tl^{3+} has $R_F > 0.75$. Pb^{2+}, Fe^{2+}, Sn^{2+}, Sr^{2+}, Cr^{3+}, K^+, Rb^+, Cs^+, Y^{3+}, Zr^{4+}, Ru^{3+}, La^{3+}, In^{3+} and Pr^{3+} have the same trend as Tl^+. Fe^{3+}, Mg^{2+}, Cu^{2+}, Ni^{2+}, Co^{2+}, Al^{3+}, Ca^{2+}, Th^{4+}, Ce^{3+} and Nd^{3+} have the same trend as Cd^{2+}.

exchanger. It has been shown by Murray and Fuerstenau [14], that cations are preferably exchanged when the gel has a negative surface charge. They explained this on the assumption that the adsorption of Ag^+ is due to Ag^+–matrix interaction. At pH 1, Hg^{2+} has a low R_F value whereas the lanthanides have R_F values of almost 1. This can be explained on the basis that on titanium(IV) tungstate columns Hg^{2+} is significantly adsorbed in HNO_3 media having a higher K_d value whereas the lanthanides have the lowest K_d values, thereby showing higher R_F values on titanium(IV) tungstate papers.

Butanol–nitric acid systems

Butanol–8 *M* HNO_3 in various ratios is an excellent solvent system with numerous possibilities for analytically difficult separations. Some of these have actually been achieved. The great advantage of the ion-exchange papers is that the spots are more compact than on the plain papers and therefore there is very little tailing on these papers. It is obvious from Fig. 2 that for most of the monovalent and bivalent ions, as the HNO_3 concentration increases the R_F value also increases. Titanium(IV) tungstate in these systems appears to behave only as a sorbent and not as an exchanger. This may be partly due to the low ion-exchange capacity of titanium(IV) tungstate in butanol–HNO_3 media and partly to the small degree of ionization of metal salts in butanol media.

In order to understand the mechanism of sorption and the effect of nitric acid on this mechanism, it was decided to correlate the R_F values of the metal ions with C, the nitric acid concentration. A plot of R_F *versus* C^2 gave straight lines passing through the origin for K^+, Rb^+ and Cs^+. The same trend was observed for the majority of cations and only in a few instances were significant intercepts obtained, *e.g.*, with Be^{2+}, Hg^{2+} and Au^{3+}. The R_F value can therefore be represented by a simple equation, $R_F = a + bC^2$, where a is the intercept and b is the slope; a is probably dependent on the solubility in butanol of the salt concerned, *e.g.*, KCl if K^+ is chromatographed. Thus, $a = 0$ for K^+, Rb^+ and Cs^+ as their chlorides have very low solubilities (the solubilities of KCl and CsCl are 0.624 and 0.621 wt.%, respectively) in butanol. Hg^{2+} has a large intercept owing to the higher solubility of mercury(II) chloride in butanol (the solubility of $HgCl_2$ is 15.5 wt.%). The data for Be and Au chlorides are not available but they must have significant solubilities in butanol.

It is apparent from Table I that with K^+, Rb^+ and Cs^+ the slope decreases from Cs^+ to K^+ owing to the decrease in the size of the ion. Similarly, the slope decreases as one goes from Rb^+ to Zr^{4+} and from Cs^+ to La^{3+} (right across the Periodic Table). This is due to an increase in charge and a decrease in size. Other cations follow the same trend and the only apparent exception is Fe (0.49) and Co (0.56). In this instance the Pauling radius of Co^{2+} is higher than that of Fe^{3+} and hence the R_F value of Co^{2+} should be greater than that of Fe^{3+}. The charge also favours the smaller R_F for Fe^{3+}.

HNO_3–acetone–water system

A plot of R_F *versus* mole fraction (X) (Fig. 3) gives some interesting results. In order to have a clear idea

TABLE I

VALUES OF b FOR DIFFERENT METAL IONS IN THE EQUATION $R_F = a + bC^2$

Metal ion	b	Metal ion	b	Metal ion	b	Metal ion	b
K^+	0.81	Ca^{2+}	0.56	Fe^{3+}	0.49	In^{3+}	0.75
Rb^+	1.00	Hg^{2+}	0.71	Al^{3+}	0.78	Pr^{3+}	0.75
Cs^+	1.16	Cd^{2+}	0.63	Au^{3+}	0.66	Nd^{3+}	0.25
Tl^+	0.37	Pb^{2+}	0.63	Y^{3+}	0.57	Zr^{4+}	0.48
Co^{2+}	0.56	Mg^{2+}	0.44	Ce^{3+}	0.43	Th^{4+}	0.56
Be^{2+}	0.86	Cu^{2+}	0.54	Ru^{3+}	0.63		
Sr^{2+}	0.82	Ni^{2+}	0.66	La^{3+}	0.72		

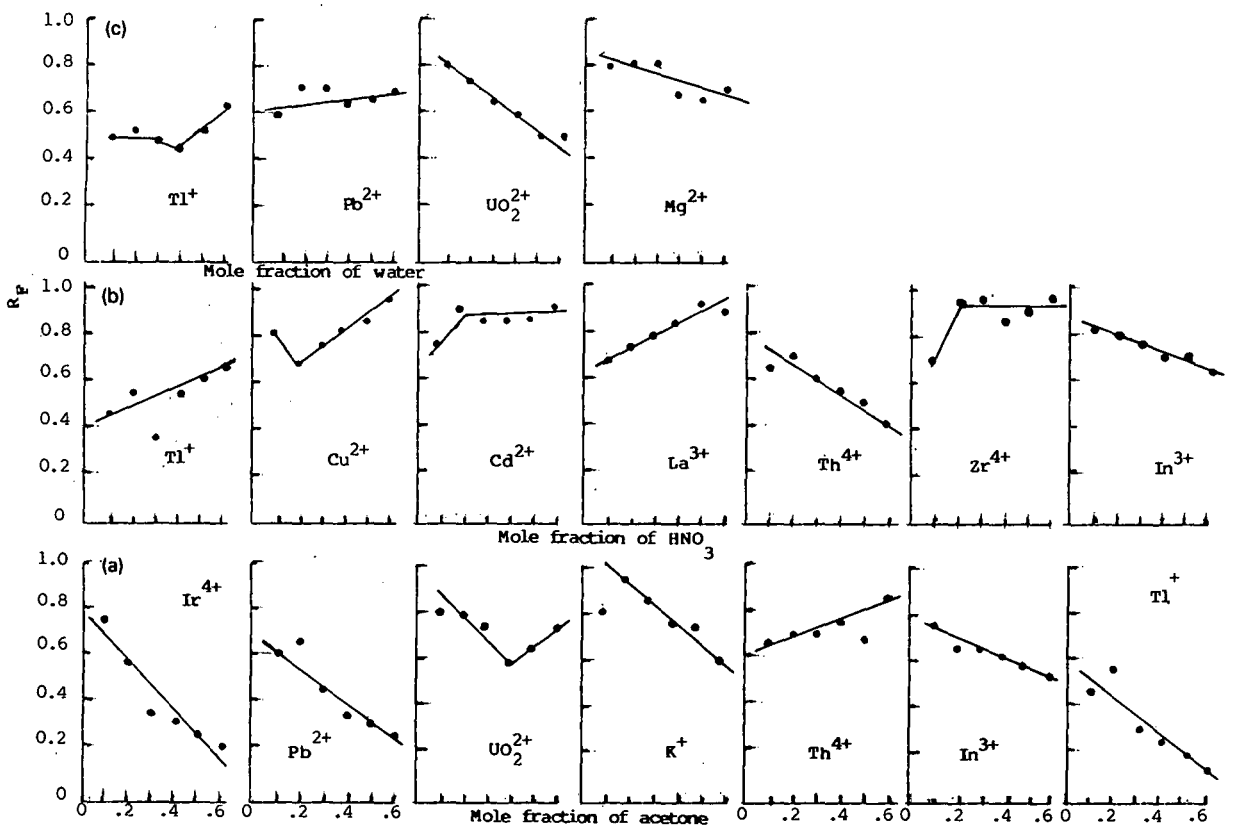

Fig. 3. Plots of R_F *vs.* mole fractions of acetone, HNO_3 and water. (a) Sm^{3+}, Be^{2+}, Mg^{2+}, Pd^{2+}, Al^{3+}, Ba^{2+}, Fe^{3+}, Cu^{2+}, Cd^{2+}, VO^{2+}, Co^{2+}, Ni^{2+}, Zn^{2+}, Mn^{2+} and Zr^{4+} have the same trend as In^{3+}. Tl^{3+} and Ce^{4+} have $R_F > 0.75$ at all pH. (b) Co^{2+}, Zn^{2+}, Ni^{2+}, Mn^{2+}, Y^{3+}, Be^{2+}, VO^{2+}, Sm^{3+}, Mg^{2+}, Pd^{2+}, Al^{3+}, Bi^{3+}, Hg^{2+} and Ce^{4+} have $R_F > 0.75$. Tl^{3+}, Pb^{2+} and Ba^{2+} have the same trend as La^{3+}. (c) Zr^{4+}, Cd^{2+}, Co^{2+}, Ni^{2+}, La^{3+}, Zn^{2+}, VO^{2+}, Sm^{3+}, Pr^{3+}, Cu^{2+}, Y^{3+}, Al^{3+}, Mn^{2+}, Hg^{2+}, Bi^{3+}, Ce^{4+}, In^{3+} and Be^{2+} have $R_F > 0.75$. Th^{4+} has the same trend as Mg^{2+}.

of the effect of solvent composition on R_F values, we shall consider these plots as R_F *versus* the mole fraction of acetone, nitric acid and water.

Effect of mole fraction of acetone on R_F values. Fig. 3a was plotted for the systems in which the mole ratio of water and nitric acid remains constant and only the proportion of acetone is continuously increased, *i.e.*, for HNO_3–acetone–water systems in the volume ratios 1:1:1, 1:2:1, 1:3:1, 1:4:1, 1:5:1 and 1:6:1. With these systems, straight lines are obtained which in most instances are parallel to one another. Surprisingly, there is no effect of charge, size or nature of the cation on the slopes of the lines. Thus, for Co^{2+}, Cd^{2+}, Cu^{2+}, Ni^{2+}, Zn^{2+}, Mn^{2+}, In^{3+}, Sm^{3+}, Mg^{2+}, Pd^{2+}, Al^{3+}, Ba^{2+}, Fe^{3+}, K^+, VO^{2+} and Zr^{4+} the decrease in R_F with increase in mole fraction of acetone is due to the decrease in the number of hydrogen ions competing for the exchange sites. Hence it follows that when the aqueous and non-aqueous solvents are both non-complexing and the HNO_3:H_2O ratio remains constant, the R_F value is almost always dependent on the number of H^+ ions competing for the exchange sites. However, the behaviour of Th^{4+} is different as it gives higher R_F values, perhaps because thorium nitrate is very soluble in acetone [15] and water, in addition to its highly complexing nature in nitrate systems. If the factors of adsorption and ion exchange are neglected, the movement of a substance on a paper chromatogram is a function of its solubility in the

developing solvent. The R_F values of Tl^+ and Pb^{2+} at higher acetone concentrations are low because these ions interact strongly either with the cation or anion of the exchanger.

Effect of mole fraction of HNO_3 on R_F values. Fig. 3b shows the plots for the systems where the water: acetone mole ratio remains constant while the nitric acid mole fraction is constantly increased, *i.e.*, for HNO_3–acetone–water systems in the volume ratios 1:1:1, 2:1:1, 3:1:1, 4:1:1, 5:1:1 and 6:1:1. These curves are also very revealing. The R_F values generally increase linearly with increasing mole fraction of HNO_3 except for Th^{4+}, Ce^{4+} and In^{3+}. The increased R_F is now easily explained in terms of the increase in the number of H^+ ions competing with the cations for the exchange sites. The R_F of Th^{4+} decreases with increase in the mole fraction of HNO_3 because it means a decrease in the acetone concentration and, as explained earlier, Th^{4+} is highly soluble in acetone. In^{3+} is an exception, the R_F value decreasing with increase in the mole fraction of HNO_3. There is no significant change in the R_F value of Ce^{4+}, which remains almost constant with change in HNO_3 concentration.

Effect of mole fraction of water on R_F values. In Fig. 3c we have plotted R_F values for HNO_3–acetone–water systems in the volume ratios 1:1:1, 1:1:2, 1:1:3, 1:1:4, 1:1:5 and 1:1:6, the mole ratio of acetone to nitric acid remaining constant while the mole fraction of water is increased. An increase in the mole fraction of water means an increase in the ionization of HNO_3 and, therefore, the R_F values increase linearly with increasing mole fraction of water. The exceptions are UO_2^{2+}, Pb^{2+}, Th^{4+} and Mg^{2+}. With UO_2^{2+}, with an increase in the mole fraction of water there is a greater formation of the insoluble uranyl tungstate, resulting in a decrease in the R_F value. A similar explanation applies to Pb^{2+} and Th^{4+}.

TABLE II

QUANTITATIVE SEPARATION OF Hg^{2+} AND Pb^{2+} FROM BINARY AND SYNTHETIC MIXTURES IN BUTANOL AND IN 0.001 *M* HNO_3

Amount of Hg^{2+} applied (μg)	Amount of other metal ion applied (μg)	Amount of Hg^{2+} found (μg)	Amount of Pb^{2+} applied (μg)	Amount of other metal ion applied (μg)	Amount of Pb^{2+} found (μg)
100	Hg_2^{2+} 200	95	100	Ag^+ 107	100
100	Tl^+ 204	98	100	Hg^{2+} 200	101
100	Bi^{3+} 208	100	100	Tl^{3+} 204	105
100	Cd^{2+} 112	95	100	Cd^{2+} 112	100
100	Pd^{2+} 106	100	100	Pd^{2+} 106	102
100	Sb^{3+} 121	99	100	Fe^{3+} 55)	100
100	Ag^+ 107	100	100	Cu^{2+} 63	95
100	Pb^{2+} 207	100	100	Ni^{2+} 58	98
100	Fe^{3+} 55	100	100	Co^{2+} 58	100
100	Cu^{2+} 63	95	100	Al^{3+} 26	102
100	Ni^{2+} 58	102	100	Be^{2+} 9	100
100	Co^{2+} 58	105	100	Zn^{2+} 65	100
100	Ba^{2+} 137	100	100	Mn^{2+} 54	101
100	Sr^{2+} 87	104	100	Ba^{2+} 137	104
100	Ca^{2+} 40	100	100	Sr^{2+} 87	100
10	Mixture	10	100	Mg^{2+} 24	102
50	Mixture	49.5	100	Ca^{2+} 40	103
100	Mixture	100	10	Mixture	10
200	Mixture	198	50	Mixture	50
400	Mixture	404	100	Mixture	98
			200	Mixture	197
			400	Mixture	402

Application

The advantage of this work is that Pb^{2+} and Hg^{2+} have been quantitatively separated from binary mixtures containing larger amounts of other metal ions such as Ag^{+}, Tl^{+}, Cd^{2+}, Pd^{2+}, Sb^{3+}, Cu^{2+}, Ni^{2+}, Ba^{2+}, Sr^{2+} and Ca^{2+} (Table II). It has been observed that the method works well within an error range of 5%. The method works satisfactorily even for the separation of Pb^{2+} from alloys containing these metals. Synthetic alloy samples of Pb^{2+} with other metal ions were prepared by mixing various metallic solutions in certain ratios so that they correspond to the actual metallic proportions in standard alloys, and then these samples were tried on titanium(IV) tungstate papers and the metal ion separations were achieved.

CONCLUSION

For most cations, there is a significant adsorption in the pH range 0–1. The sharp decrease in the R_F values of few ions above pH 2 is due to excessive hydrolysis in the acidic media. pH 2 is the most favourable acidity for ion exchange for Pb^{2+}, Hg^{2+}, Hg_2^{2+}, Sb^{3+}, Ga^{3+}, Bi^{3+}, Sn^{2+}, Th^{4+} and Mg^{2+}. Ag^{+} is selectively adsorbed on these papers due to Ag^{+}–matrix interaction. The pH does not affect the ion-exchange capacity of titanium(IV) tungstate significantly in the pH range 0–5, which is in agreement with the observations made by Qureshi *et al.* [1].

In butanol–HNO_3 systems, titanium(IV) tungstate behaves only as a sorbent and not as an exchanger. The R_F values depend on the square of the nitric acid concentration.

In nitric acid–acetone–water systems, at higher acetone concentration the exchange phenomenon is not significant owing to a smaller number of H^{+} ions competing for exchange sites. For most of the ions, the R_F value is linearly dependent on the mole fractions of HNO_3 and H_2O.

ACKNOWLEDGEMENT

The authors are grateful to UGC (New Delhi) for financial assistance.

REFERENCES

1 M. Qureshi, N. Zehra, S. A. Nabi and V. Kumar, *Talanta*, 20 (1973) 609.
2 N. S. Seth and R. P. S. Rajput, *Indian J. Chem., Sect. A*, 22 (1983) 1088.
3 S. D. Sharma and S. Misra, *J. Liq. Chromatogr.*, 8 (1985) 3017.
4 N. S. Seth, R. P. S. Rajput and S. Agarwal, *Ann. Chim.*, 75 (1985) 153.
5 K. V. Surendranath and S. N. Tandon, *J. Liq. Chromatogr.*, 11 (1988) 1433.
6 M. Qureshi and J. P. Gupta, *J. Chem. Soc. A*, (1969) 1755.
7 M. Qureshi and W. Husain, *Sep. Sci.*, 4 (1969) 197.
8 S. D. Sharma and S. Misra, *J. Planar Chromatogr.*, 2 (1989) 399.
9 M. Qureshi and S. D. Sharma, *Anal. Chem.*, 45 (1973) 1283.
10 M. Qureshi, I. Akhtar and K. N. Mathur, *Anal. Chem.*, 39 (1967) 1766.
11 M. Qureshi, R. Kumar and H. S. Rathore, *J. Chem. Soc.*, (1970) 272.
12 F. D. Snell, *Photometric and Fluorometric Methods of Analysis. Metals (Part I)*, Interscience, New York, 1978, pp. 10 and 107.
13 L. Szirtes, L. Zsinka, K. B. Zaboreuko and B. Z. Iofa, *Acta Chim. Acad. Sci. Hung.*, 54 (1967) 215.
14 D. J. Murray and M. C. Fuerstenau, *J. Inorg. Nucl. Chem.*, 30 (1968) 3325.
15 M. Qureshi and S. Z. Qureshi, *J. Chromatogr.*, 22 (1966) 198.

Journal of Chromatography, 606 (1992) 129–132
Elsevier Science Publishers B.V., Amsterdam

CHROM. 24 307

Short Communication

Improvement of peroxyoxalate chemiluminescence detection in liquid chromatography with gradient elution and a long reaction time

Nobuaki Hanaoka and Hiroshi Tanaka

Analytical Instrument Research Laboratory, Shimadzu Corporation, Nakagyo-ku, Kyoto 604 (Japan)

(First received February 19th, 1992; revised manuscript received April 22nd, 1992)

ABSTRACT

In peroxyoxalate chemiluminescence (PO-CL) measurement using bis(2,4,6-trichlorophenyl) oxalate, background emission occurs much faster than that from analytes. By using a long reaction time of more than 15 s in most instances the background level can be reduced while maintaining sufficient analyte intensity. PO-CL detection with a reaction time of 20 s was applied in measurements of dansylated amino acids by liquid chromatography with gradient elution. The background was very low and baseline drift did not influence the detection of femtomole amounts of dansylated amino acids. The detection limits were 2–4 fmol (signal-to-noise ratio = 2).

INTRODUCTION

Since its first application with high-performance liquid chromatography (HPLC) [1], peroxyoxalate chemiluminescence (PO-CL) has become widely acknowledged as a highly sensitive detection method for HPLC, flow-injection analysis (FIA) and various other analytical techniques. One advantage of this method is that the background signal is much lower than that in the conventional fluorescence method owing to the absence of a light source and accounts in large part for the improved sensitivity of PO-CL detection. However, a background signal higher than that of the photomultiplier tube (PMT) dark current is still observed when using a PO-CL detector in an HPLC system [2–4]. There is therefore light emission in the final mixture of column effluent and PO-CL reagent solution without the addition of fluorescent analytes and the detection capacity of the PO-CL detector is limited by fluctuations in the background light intensity.

The existence of background emission also limits the application of the PO-CL method to HPLC with gradient elution. The composition of the final solution changes as the gradient proceeds with a consequent effect on the background intensity, eventually causing baseline drift of the chromatogram. This drift is not negligible particularly in cases of highly sensitive detection and sometimes makes the measurement of analytes impossible.

Little research has been reported on gradient HPLC analysis with PO-CL detection. Weinberger [5] measured dansylated (Dns) steroids by this technique, but the amounts of sample injected were in

Correspondence to: Dr. N. Hanaoka, Analytical Instrument Research Laboratory, Shimadzu Corporation, Nakagyo-ku, Kyoto 604, Japan.

0021-9673/92/$05.00

the range of 5–15 pmol and the measurement was not very sensitive. Miyaguchi *et al.* [6] measured 100 fmol of Dns-amino acids with the flow-rate of the eluent set low (0.3 ml/min) and that of the PO-CL reagent six times higher (1.8 ml/min). Change in the water content in the final solution was therefore small, which resulted in a small baseline drift but a long measurement time (*ca.* 3 h).

The kinetic rates of PO-CL emission were recently found to differ considerably between the analytes and the background when using bis(2,4,6-trichlorophenyl) oxalate (TCPO) [7]. Assessment was made of the influence of various factors on the intensity and kinetic rate of background emission. Based on the data obtaiend, measurement conditions for Dns-amino acids by isocratic HPLC with CL detection were optimized using a long reaction time (t_1) and, as a result, the background level was reduced more than tenfold.

In this study, the application of gradient elution to the optimized HPLC–CL system was investigated. Gradient conditions for the separation of Dns-amino acids were determined by HPLC with UV detection and thirteen Dns-amino acids were measured under these conditions and with PO-CL detection. It was considered that a reduced background level would resulted in a smaller baseline drift and highly sensitive PO-CL detection applicable to HPLC with gradient elution.

EXPERIMENTAL

Reagents

Dns-Amino acids were purchased from Sigma (St. Louis, MO, USA) and TCPO from Tokyo Kasei (Tokyo, Japan). Water was purified with a Yamato WG-25 system. All other chemicals were of analytical-reagent grade.

Apparatus

The gradient HPLC system with a PO-CL detector is shown in Fig. 1. It consisted of Shimadzu Type LC-9A HPLC pumps (P), a DGU-4A degasser (G), an FCV-9AL low-pressure gradient flow

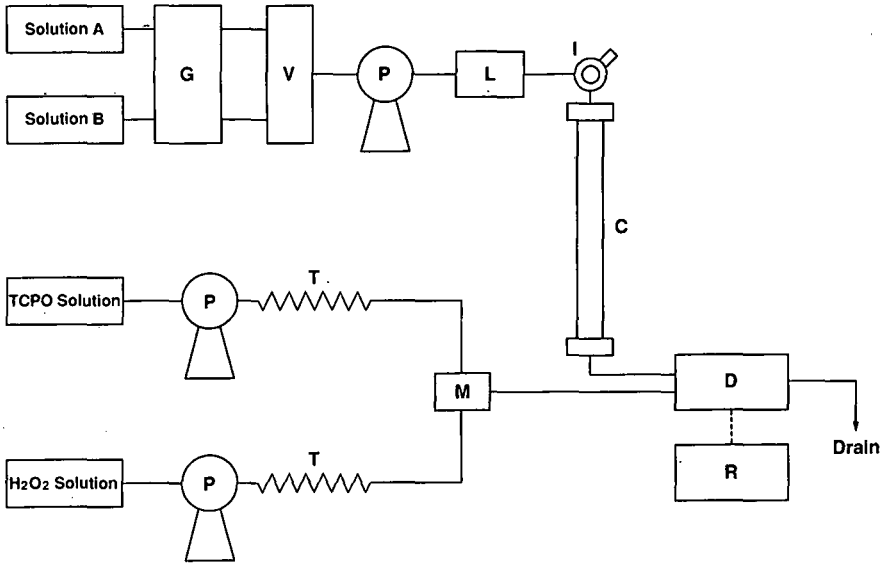

Fig. 1. Schematic diagram of the gradient HPLC system with PO-CL detection. P = pump; G = degasser; V = low-pressure gradient flow control valve; L = mixer for low-pressure gradient; I = injector, C = LC column; M = mixer; D = detector; R = Chromatopac. A stainless-steel tube (T) (2 m × 0.1 mm I.D.) was connected to the output of each pump for the PO-CL reagent. For all other flow lines, stainless-steel tubing (0.5 mm I.D.) was used. Solution A, 1.8 mmol of imidazole dissolved in 1000 ml of water [adjusted to pH 7.0 with nitric acid (pH 7.0, NO_3^-)]; solution B, 1.8 mmol of imidazole in a mixture of 400 ml of water and 600 ml of acetonitrile (pH 7.0, NO_3^-); flow-rate, 0.8 ml/min; TCPO solution, 0.5 mmol of TCPO in 1000 ml of acetonitrile, flow-rate 0.5 ml/min; hydrogen peroxide solution, 40 mmol of hydrogen peroxide in 1000 ml of acetonitrile, flow-rate 1.2 ml/min; voltage applied to photomultiplier tube, −0.8 kV; temperature of detector, 30°C.

control valve (V), a mixer for the low-pressure gradient (L), a Rheodyne Model 7125 injector (I) with a 20-μl sample loop, a Shimadzu Shim-Pak CLC ODS column (C) (150 × 4.6 mm I.D.) and a premixer (M) for a Shimadzu LC-6A pump. The gradient flow control valve was operated by the pump for the eluent according to the manufacturer's instruction. D was the same CL detector as that in the previous study [7], using a PTFE tube (4 m × 0.5 mm I.D.) for the reaction line of the effluent and CL reagents. Output signals were recorded with a Shimadzu Chromatopac C-R6A recorder (R). For the determination of the gradient conditions for Dns-amino acid separation, a Shimadzu SPD-10A UV detector was used instead of the CL detector. A stainless-steel tube (T) (2 m × 0.1 mm I.D.) was connected to the outlet of each reagent pump and stainless-steel tubing (0.5 mm I.D.) was used in all other flow lines.

Determination of gradient conditions

The wavelength for detection was 340 nm [7]. Solution A consisted of 1.8 mmol of imidazole dissolved in 1000 ml of water (pH 7.0, NO_3^-) and solution B was 1.8 mmol of imidazole in a mixture of 400 ml of water and 600 ml of acetonitrile (pH 7.0, NO_3^-). The flow-rate was 0.8 ml/min. A mixture of thirteen amino acids (10 ng each) (see below) dissolved in 20 μl of solution A was injected. All measurements were made at room temperature (*ca.* 23°C).

HPLC–CL measurement of Dns-amino acids

The sample was a mixture of thirteen Dns-amino acids dissolved in 20 μl of solution A. The amounts of the amino acids were as follows: 82 fmol of aspartic acid (Asp), 85 fmol of glutamic acid (Glu), 77 fmol of asparagine (Asn), 62 fmol of glutamine (Gln), 92 fmol of serine (Ser), 80 fmol of threonine (Thr), 75 fmol of alanine (Ala), 67 fmol of proline (Pro), 80 fmol of valine (Val), 22 fmol of lysine (Lys), 42 fmol of isoleucine (Ile), 75 fmol of leucine (Leu) and 63 fmol of phenylalanine (Phe). The column was washed with solution B for 30 min and preconditioned with a mixture of solitions A–solution B (75:25) for 15 min before sample loading. A linear gradient from 75% to 30% A over 35 min was then performed. The column temperature was room temperature (*ca.* 23°C).

The TCPO solution consisted of 0.5 mmol of TCPO in 1000 ml of acetonitrile. The flow-rate was 0.5 ml/min. The hydrogen peroxide solution was 40 mmol of hydrogen peroxide in 1000 ml of acetonitrile and its flow-rate was 1.2 ml/min. The voltage applied to the photomultiplier tube, temperature and response were −0.8 V, 30°C and 3 s, respectively.

RESULTS AND DISCUSSION

Gradient conditions for Dns-amino acid analysis

For gradient measurements of the thirteen Dns-amino acids, the flow-rate of the eluent, concentration of imidazole and solution pH were the same as those optimized in the previous study [7]. Only the water content in the eluent was varied by changing the ratio of solutions A and B. Good separation and minimum time for measurement were achieved under the conditions specified in the Experimental section.

HPLC–CL measurement of Dns-amino acids

For the detection of Dns-amino acids, the following parameters were optimized in the previous study [7]: t_1 of the effluent with PO-CL reagents, the concentration of each reagent, the flow-rate of each reagent solution and the temperature of the detector. As a result, the background level was reduced by as much as twentyfold and the signal-to-noise ratio (S/N) was enhanced more than tenfold. The reaction line of the detector in this study was as long as that used for the optimized t_1 as indicated in ref. 7 and the same detection conditions including t_1 (20 s) were used for HPLC measurements of Dns-amino acids with the optimized gradient elution.

A typical chromatogram obtained is shown in Fig. 2A. When the nonoptimized conditions used in the previous study (t_1 = 5 s, concentration of hydrogen peroxide = 10 mM, temperature of detector = 23°C and imidazole concentration = 2 mM) were applied to this gradient system, the background was high (65 nA at the start of measurement) and the baseline drift was more than ten times that shown in Fig. 2. Quantitative analysis of a sample was virtually impossible. Under the optimum conditions, the background level decreased to 2.7 nA and the ratio of the baseline drift to peak height of Dns-amino acids was almost the same as

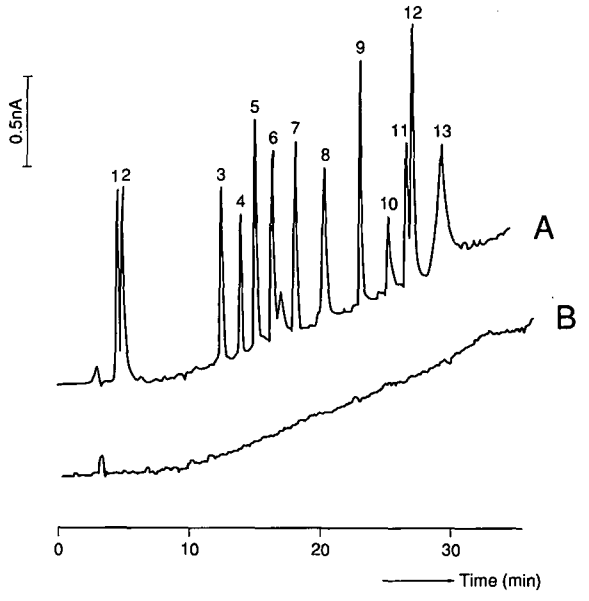

Fig. 2. (A) Chromatogram of Dns-amino acids. Peaks: 1 = 82 fmol of Asp; 2 = 85 fmol of Glu; 3 = 77 fmol of Asn; 4 = 62 fmol of Gln; 5 = 92 fmol of Ser; 6 = 80 fmol of Thr; 7 = 75 fmol of Ala; 8 = 67 fmol of Pro; 9 = 80 fmol of Val; 10 = 22 fmol of Lys; 11 = 42 fmol of Ile; 12 = 75 fmol of Leu; 13 = 63 fmol of Phe. Conditions: linear gradient from 75% to 30% solution A in 35 min. (B) Baseline measured under the same gradient conditions as those in (A) without an LC column.

that for the chromatogram of Miyaguchi *et al.* [6]. It should be noted that the changes in the water content of the eluent (26.2% during measurement) and the final solution (8.4% in the same period) were 1.5 and 3.4 times greater, respectively, and the measurement time was as short as 35 min.

Baseline drift may possibly result from elution of impurities from the LC column. If fluorescent impurities trapped in a column elute gradually with increase in the amount of organic solvent, the background level will increase during the course of measurement. For the evaluation of this effect, the baseline was measured by FIA after replacing the column with a stainless-steel tube (2 m × 0.3 mm I.D.). The baseline obtained is shown in Fig. 2B. In either instance the amount of drift was the same and was concluded not to be generated by changes in the amounts of impurities eluted from the LC column. This agrees well with the previous study in which the PO-CL background may not have been the emission from impurities but reaction intermediates and its intensity and the kinetic rate were influenced by certain factors such as water content [7].

Nevertheless, small, irregular peaks appeared on the chromatograms during measurements and good cleaning and conditioning of the column were found to be essential for their prevention and to obtain reproducible results. The column was washed and preconditioned before each measurement as described in the Experimental section. As a result, the detection limits of Dns-amino acids were 2–4 fmol (S/N = 2) and the R.S.D. of the peak height was less than 3%.

REFERENCES

1 S. Kobayashi and K. Imai, *Anal. Chem.*, 52 (1980) 424.
2 G. Mellbin, *J. Liq. Chromatogr.*, 6 (1983) 1603.
3 K. W. Sigvardson and J. W. Birks, *Anal. Chem.*, 55 (1983) 432.
4 R. Weinberger, C. A. Mannan, M. Cerchio and M. L. Grayeski, *J. Chromatogr.*, 288 (1984) 445.
5 R. Weinberger, *J. Chromatogr.*, 314 (1984) 155.
6 K. Miyaguchi, K. Honda and K. Imai, *J. Chromatogr.*, 303 (1984) 173.
7 N. Hanaoka, H. Tanaka, A. Nakamoto and M. Takada, *Anal. Chem.*, 63 (1991) 2680.

Journal of Chromatography, 606 (1992) 133–135
Elsevier Science Publishers B.V., Amsterdam

CHROM. 24 312

Short Communication

Sensitive and stable Cookson-type reagent for derivatization of conjugated dienes for high-performance liquid chromatography with fluorescence detection

Kazutake Shimada and Tatsuhito Mizuguchi

Faculty of Pharmaceutical Sciences, Kanazawa University, 13–1 Takara-machi, Kanazawa 920 (Japan)

(First received March 24th, 1992; revised manuscript received April 24th, 1992)

ABSTRACT

A sensitive and stable Cookson-type reagent, 4-substituted 1,2,4-triazoline-3,5-dione, having 6-methoxy-2-phenylbenzoxazole as a fluorophore, was prepared for high-performance liquid chromatographic measurements of conjugated dienes. The reagent was purified by sublimation to give stable purple crystals. The reagent quantitatively produced the adduct with provitamin D_3 in 5 min under ice cooling, which was highly responsive to fluorescence detection [detection limit 2 fmol per injection (signal-to-noise ratio = 5)].

INTRODUCTION

In a previous paper we reported the preparation of Cookson-type reagents, 4-substituted 1,2,4-triazoline-3,5-diones, having a chromophore, fluorophore or electrophore at the 4-position, for high-performance liquid chromatographic (HPLC) measurements of vitamin D-related compounds having a conjugated diene [1,2]. The reactivity of these reagents and the properties of their adducts were examined by using provitamin D_3 (7-dehydrocholesterol; 7-DHC) as a model compound. The adduct with 4-[2-(1-pyrenyl)ethyl]-1,2,4-triazoline-3,5-dione was most responsive to detection {fluorescence (FL): detection limit 25 fmol per injection [signal-to-noise ratio (S/N) = 5]}. However, the reagent could not be purified by sublimation or recrystallization, so the reaction mixture of a precursor and an oxidizing agent was used as the derivatization reagent [1,2]. The reagent sometimes gave the problem in the derivatization of sulphated vitamin D metabolites that a deconjugation reaction occurred with the remaining oxidant or its degradation products [3].

This paper deals with the preparation and properties of a new Cookson-type reagent (**IV**) having 6-methoxy-2-phenylbenzoxazole as a fluorophore for the determination of conjugated dienes (Fig. 1).

EXPERIMENTAL

Materials

Ethyl hydrazinecarboxylate and *tert.*-butyl hypochlorite were obtained from Tokyo Kasei Kogyo (Tokyo, Japan). All other chemicals were of analytical-reagent grade. For thin-layer chromatography

Correspondence to: Dr. K. Shimada, Faculty of Pharmaceutical Sciences, Kanazawa University, 13-1 Takara-machi, Kanazawa 920, Japan.

0021-9673/92/$05.00

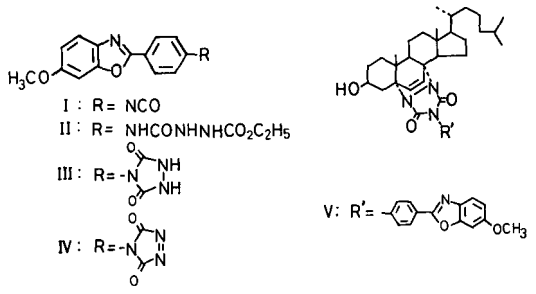

Fig. 1. Preparation of the Cookson-type reagent **IV** and its adduct with 7-DHC (**V**).

(TLC) silica gel HF_{254} precoated TLC plates (0.25 mm) (E. Merck, Darmstadt, Germany) were used and for silica gel column chromatography silica gel 60 (70–230 mesh) (E. Merck) was used.

Apparatus

Proton nuclear magnetic resonance (^{1}H NMR) spectra were obtained with a Jeol (Tokyo, Japan) JNM-EX 270 spectrometer at 270 MHz using tetramethylsilane as an internal standard. The abbreviations used are s = singlet, d = doublet, t = triplet, q = quartet, dd = doublet of doublets, m = multiplet and br = broad. Electron impact ionization mass spectrometry (EI-MS) was carried out on a Hitachi (Tokyo, Japan) M-80 spectrometer.

HPLC was carried out on a Shimadzu (Kyoto, Japan) LC-6A chromatograph equipped with a Hitachi F-1050 FL detector ($\lambda_{ex.}$ 320 nm, $\lambda_{em.}$ 380 nm). A YMC-Gel C_8-120-S5 (5 μm) column (15 x 0.46 cm I.D.) (YMC, Kyoto, Japan) was used at ambient temperature at a flow-rate of 1.0 ml/min.

Preparation of the Cookson-type reagent

Compound II. 4-(6-Methoxy-2-benzoxazolyl) phenyl isocyanate (**I**), prepared according to the procedure described by Kondo *et al.* [4], was treated with ethyl hydrazinecarboxylate as described previously [2] to give the desired ethoxycarbonylsemicarbazide derivative (**II**) as a colourless amorphous substance (xylene): m.p., 218–220°C; ^{1}H NMR [C^2HCl_3–$C^2H_3O^2H$ (1:1)], δ 1.31 (3H, t, J = 7.3 Hz, $-CH_2CH_3$), 3.90 (3H, s, $-OCH_3$), 4.22 (2H, q, J = 7.3 Hz, $-CH_2CH_3$), 6.97 (1H, dd, J = 2.3, 8.7 Hz, benzoxazole-5H), 7.16 (1H, d, J = 2.3 Hz, benzoxazole-7H), 7.57 (1H, d, J = 8.7 Hz, benzoxazole-4H), 7.63 and 8.09 (each 2H, each d, J = 8.9 Hz, phenyl-H); EI-MS, m/z 370 (M^+).

corrected 26 Oct. 92 AP $-CH_2CH_3$

Compound III. Compound **II** (10 mg) was dissolved in ethanol–water (1:1, v/v) (2 ml) containing 2 *M* KOH and stirred at room temperature for 20 min. The reaction mixture was acidified with 5% HCl, the resulting pale yellow precipitate was filtered and the precipitate was washed with water and dried *in vacuo*. Its homogeneity was confirmed by TLC [solvent system chloroform–methanol–water (80:20:2.5, v/v/v); R_F 0.56]; m.p. >300°C; EI-MS, m/z 324 (M^+). The compound was subjected to the following oxidation reaction without further purification.

Compound IV. Compound **III** (4 mg) was suspended in ethyl acetate (1 ml) and treated with *tert.*-butyl hypochlorite (1.7 μl; 1.1 molar ratio) under ice cooling for 15 min. The reaction mixture was filtered to remove the unreacted precursor and the filtrate was evaporated *in vacuo*. The residue obtained was subjected to sublimation at 140°C (bath temperature) (0.2 mmHg) to give purple crystalls (1 mg): m.p., 148–150°C; EI-MS, m/z 322 (M^+); visible spectrum, λ_{max} ethyl acetate 528 nm [2]. The compound was stable for at least 1 month in a refrigerator.

Preparation of the authentic adduct (V) with 7-DHC

A solution of **IV** (5 mg) in ethyl acetate (0.5 ml) was added to a solution of 7-DHC (6 mg) in ethyl acetate (0.5 ml) and the reaction mixture was kept for 15 min under ice cooling. The mixture was applied to a silica gel column (10 x 0.6 cm I.D.) to decompose the excess of the reagent and the eluate was evaporated *in vacuo*. The residue obtained was subjected to preparative TLC using chloroform–ethyl acetate (1:1, v/v) as a developing solvent. The corresponding spot (R_F 0.36) was eluted with ethyl acetate to give the desired adduct (**V**, 4.5 mg) as a colourless amorphous substance (ethanol). ^{1}H NMR (C^2HCl_3), δ 3.20 (1H, dd, J = 4.3, 13.9 Hz, 9α-H), 3.89 (3H, s, $-OCH_3$), 4.46 (1H, br s, 3α-H), 6.26 and 6.43 (each 1H, each d, J = 8.3 Hz, 6,7-H), 6.96 (1H, dd, J = 1.9, 8.8 Hz, benzoxazole-5H), 7.12 (1H, d, J = 1.9 Hz, benzoxazole-7H), 7.64 (1H, d, J = 8.8 Hz, benzoxazole-4H), 7.69 and 8.25 (each 2H, each d, J = 8.3 Hz, phenyl-H).

Reactivity of IV with 7-DHC

A solution of an excess of the reagent (**IV**, about 20 equivalents) in ethyl acetate (0.1 ml) was added to a solution of 7-DHC (1 μg) in ethyl acetate (0.1 ml) under ice cooling. A portion of the reaction mixture was subjected to HPLC at various times. The rate of reaction was measured by comparing the peak area obtained with that of an authentic sample [2].

RESULTS AND DISCUSSION

The design of a useful derivatization reagent for conjugated dienes in HPLC–FL detection requires two structural features, *viz.*, a functional group reactive toward the conjugated dienes and a fluorophore responsive to FL detection with high sensitivity. In previous work we used 1,2,4-triazoline-3,5-dione as the functional group and anthracene or pyrene as a fluorophore, but the reagents obtained were not sensitive and stable as described above [1,2]. Subsequently, Shimizu *et al.* [5] and Jordan *et al.* [6] also reported the same type of reagent, but their reagents were not purified by recrystallization or sublimation.

Recently, Kondo *et al.* [4] and Naganuma *et al.* [7] reported 6-methoxy-2-phenylbenzoxazole as a sensitive fluorophore. These results prompted us to prepare a new Cookson-type reagent having this fluorophore at the 4-position of a 1,2,4-triazoline-3,5-dione, 4-[4-(6-methoxy-2-benzoxazolyl) phenyl]-1,2,4-triazoline-3,5-dione (**IV**), according to the procedure described previously [2]. The reagent was easily obtained from the known compound **I** and purified by sublimation to give stable crystals. The reactivity of the reagent was examined by using 7-DHC as a model compound and the reagent quantitatively produced the stable adduct **V** in 5 min under ice cooling as did other reagents of the same type [2]. The adduct **V** gave a single peak with the theoretical shape on HPLC and was highly responsive to FL detection [detection limit 2 fmol per injection (S/N = 5)] (Fig. 2).

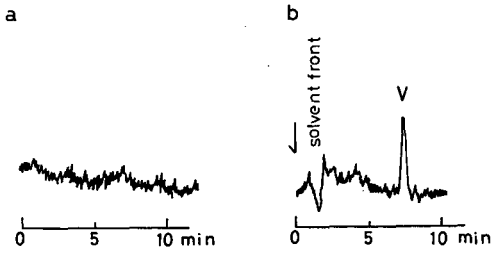

Fig. 2. HPLC of compound **V**. Solvent system: acetonitrile–water (9:1, v/v). For other conditions, see Experimental. (a) Blank chromatogram. (b) Compound **V** (1.3 fmol/in 10 μl of ethanol).

Although the Cookson reagent 4-phenyl-1,2,4-triazoline-3,5-dione was purified by sublimation [8], this is the first reported instance of a Cookson-type derivatization reagent having a sensitive fluorophore and being purified by sublimation. Studies of the application of this reagent to the determination of vitamin D_3 metabolites including conjugates are in progress.

ACKNOWLEDGEMENTS

This work was supported in part by a grant from the Ministry of Education, Science and Culture, Japan. We are indebted to Dr. Y. Kawahara (Sankyo, Tokyo) for valuable suggestions.

REFERENCES

1 K. Shimada and T. Oe, *Anal. Sci.*, 6 (1990) 461.
2 K. Shimada, T. Oe and T. Mizuguchi, *Analyst (London)*, 116 (1991) 1393.
3 K. Shimada and H. Kaji, in preparation.
4 J. Kondo, K. Watanabe and Y. Kawahara, *The 9th Symposium on Analytical Chemistry of Biological Substances, Tokyo, 1990*, Abstracts of Papers, pp. 109–112.
5 M. Shimizu, S. Kamachi, Y. Nishii and S. Yamada, *Anal. Biochem.*, 194 (1991) 77, and references cited therein.
6 P. H. Jordan, G. Read and T. Hargreaves, *Analyst (London)*, 116 (1991) 1347.
7 H. Naganuma, J. Kondo and Y. Kawahara, *J. Chromatogr.*, 532 (1990) 65.
8 R. C. Cookson, S. S. Gupte, I. D. R. Stevens and C. T. Watts, *Org. Synth.*, 51 (1971) 121.

Journal of Chromatography, 606 (1992) 136–140
Elsevier Science Publishers B.V., Amsterdam

CHROM. 24 301

Short Communication

Determination of the polymeric light stabilizer Chimassorb 944 in polyolefins by isocratic high-performance liquid chromatography

R. Matuška, L. Preisler and J. Sedlář

Chemopetrol, Litvínov, Research Institute of Macromolecular Chemistry, 656 49 Brno (Czechoslovakia)

(First received April 22nd, 1991; revised manuscript received April 14th, 1992)

ABSTRACT

A procedure is described for the determination of Chimassorb 944 in polyolefins. The method is based on high-performance liquid chromatographic (HPLC) analysis of an extract obtained through disintegration of the polymer sample in boiling toluene. The dissolved polymer is then precipitated with methanol, containing triethylamine which prevents sorption of Chimassorb 944 on laboratory glassware and filter-paper. The HPLC determination employs the calibration line method. If the calibration is carried out with Chimassorb 944–Irganox 1010 mixture then an accurate determination of both additives is possible. The detection limit is 0.02% (w/w), the relative standard deviation being lower than 10%.

INTRODUCTION

Hindered amine light stabilizers (HALSs) have been widely applied in the plastics industry to protect polymers against photooxidation. New types of stabilizers are being developed with the aim of suppressing their volatility and extractability from polymers. Chimassorb 944 (Fig. 1) stabilizer may serve as an example of this type of additive. It is an oligomer with a molecular mass of 2500–3000.

Compared with monomeric stabilizers, the determination of such oligomeric structures in polymer matrices usually represents a serious analytical problem. Methods for determining Chimassorb 944 are mainly based on the determination of the nitrogen content in the polymer (polyolefin) by Kjeldahl digestion [1] or on the hydrogenolysis [2] of the sample. This is applicable only when the stabilizer is the only nitrogen-containing component in the system. Another approach makes use of the measurement

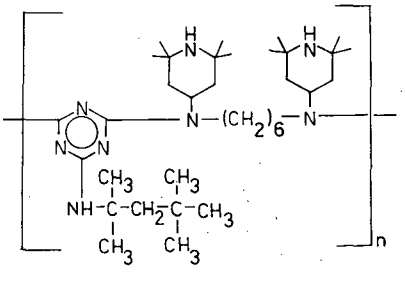

Fig. 1. Structure of Chimassorb 944.

Correspondence to: Dr. R. Matuška, Chemopetrol, Litvínov, Research Institute of Macromolecular Chemistry, 656 49 Brno, Czechoslovakia.

0021-9673/92/$05.00

of the UV absorbance of the polymer dissolved in decalin and extracted with sulphuric acid [3] or the measurement of the IR absorption of the stabilizer triazine group [4,5]. Chromatographic methods include pyrolysis–gas chromatography [6] or high-performance liquid chromatography (HPLC) using Styragel and Ultragel columns with the flame ionization detection [7] and reversed-phase gradient elution HPLC [8].

This paper describes a simple isocratic elution HPLC method using a size-exclusion column and UV detection. Particular attention has been paid to the elimination of the adsorption of Chimassorb 944 on the polymer and the filter during the sample preparation. In this way, an almost complete recovery has been attained.

EXPERIMENTAL

Apparatus

A Hewlett-Packard Model 1050 liquid chromatograph equipped with a Rheodyne Model 7125 sampling valve (20-μl sample loop), a UV detector operated at 244 nm, sensitivity 0.5 AUFS, and a Hewlett-Packard Model 3396 A integrator was used. The analytical columns (250 × 7 mm I.D.), made of stainless steel and packed with LiChrogel PS4 and PS1, were connected in series and operated at room temperature (gel permeation chromatographic exclusion limits $2 \cdot 10^3$ D for LiChrogel PS1 and $5 \cdot 10^3$ D for LiChrogel PS4). A 1.5 g/l solution of diethanolamine (DEA) in tetrahydrofuran (THF) (inlet pressure 40 bar, flow 1 ml/min) was employed as a mobile phase.

Solvents and chemicals

Toluene, methanol (analytical-reagent grade), triethylamine (TEA), DEA (both of technical grade) were obtained from Lachema (Brno, Czechoslovakia). The TEA was dried with molecular sieve 5A and distilled before use. THF stabilized with 0.025% of 2,6-diterebutyl-4-methylphenol (BHT) was obtained from Merck (Darmstadt, Germany) and Chimassorb 944 from Ciba-Geigy (Basle, Switzerland). The calibration solution was prepared by dissolving 100 mg of Chimassorb 944 in 250 ml of THF. Three model samples of polypropylene with known stabilizer content (0.05% BHT and 0.05%, 0.1% and 0.3% of Chimassorb 944) were also prepared.

Procedure

A 1-g polyolefin sample was placed in a 250-ml round-bottomed flask and disintegrated by refluxing with 30 ml of toluene for 40 min on an oil-bath at 130°C. After cooling to about 60°C, 75 ml of 1% TEA solution in methanol were added through the reflux condenser. The mixture was agitated, allowed to cool to laboratory temperature and filtered through a filter-paper impregnated with 1% TEA solution in methanol. The filter cake was washed twice with 10 ml of the same TEA solution. The combined filtrate was evaporated to dryness and the residue dissolved in 5 ml of THF or in 5 ml of THF–toluene (1:1) when the stabilizers were incompletely dissolved in THF alone. A volume of 20 μl of this solution was injected into the chromatograph. A typical chromatogram is shown in Fig. 2.

The Chimassorb 944 content in the polymer sample was calculated by comparing the peak heights of the calibration solution with those of the sample solution.

RESULTS AND DISCUSSION

It is not possible to separate polymeric HALSs (Chimassorb 944, Tinuvin 622) quantitatively from

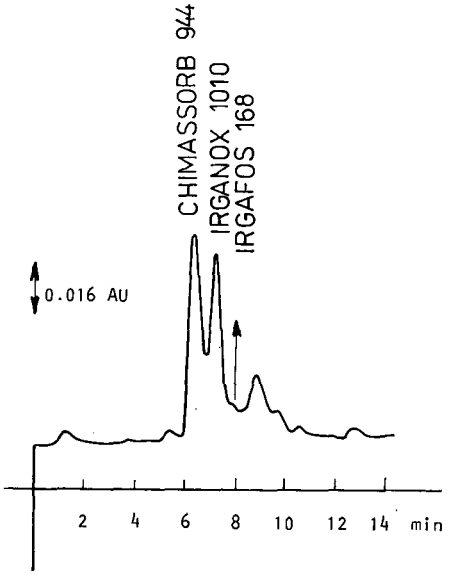

Fig. 2. Typical chromatogram of sample containing 0.3% Chimassorb 944, 0.3% Irganox 1010 and 0.3% Irganox 168. Sample after exposure for 1000 h at 80°C.

TABLE I

INFLUENCE OF TEA ADDITION ON THE RECOVERY OF CHIMASSORB 944 FROM A POLYMER MATRIX

Model Sample	Treatment			
	Without TEA		With TEA	
	Chimassorb 944 found (%)	s_R[a]	Chimassorb 944 found (%)	s_R[a]
Ch 05: 0.05% Chimassorb 944, 0.05% BHT in PP[b]	0.041	0.004	0.049	0.005
Ch 1: 0.10% Chimassorb 944, 0.05% BHT in PP	0.087	0.005	0.103	0.004
Ch 3: 0. 30% Chimassorb 944, 0.05% BHT in PP	0.265	0.005	0.308	0.007

[a] s_R = Standard deviation = $K_n \cdot R$ (n = 6).
[b] PP = polypropylene.

the polymer matrix by a simple extraction. To achieve this, it is necessary to boil the sample containing Chimassorb 944 in toluene or decalin and after its disintegration to precipitate the polymer (*e.g.*, with methanol). The precipitated polymer, however, can sorb the stabilizer on its large surface. The stabilizer can also be sorbed on the glass walls of vessels and on a filter during the sample treatment.

The phenomena caused a lowering of the results when model samples were analysed. Our observations correspond well with those published by Freitag [8], who achieved only an 83% recovery in analyses where 0.05% Chimassorb was present in polypropylene. We have found that the recovery of Chimassorb 944 after its separation from polyolefin can be considerably increased by using TEA and inducing competitive sorption. For this reason, we impregnated with TEA all the glassware and the filter used in handling the stabilizer extract. TEA was also added to the methanol used for the polymer precipitation. The results of analyses obtained both in the presence and in the absence of TEA are shown in Table I. The results indicate that the TEA treatment permits the quantitative recovery of HALSs.

To separate Chimassorb 944 from polyolefin oligomers and from other components of the stabilizing system we used LiChrogel packings. For these gels (styrene–divinylbenzene copolymers) mobile phases such as THF, acetone, dimethylformamide and chloroform are generally recommended. However, the use of THF alone as a mobile phase did not lead to the elution of Chimassorb 944. This was rendered possible only after the addition of DEA to the mobile phase.

An increase in the DEA concentration in THF progressively reduced the retention time and improved the Chimassorb 944 peak symmetry. The former phenomenon was observable up to a concentration of 0.5 g/l of DEA in THF in the mobile phase. Further increase in DEA concentration led only to the improvement of the Chimassorb 944 peak shape. A concentration of DEA of 1.5 g/l in THF was chosen as the optimum in the mobile phase.

THF used for the mobile phase was stabilized with 0.025% of 2,6-di-*tert.*-butyl-4-methylphenol and the UV spectra show that the absorbance minimum of the mobile phase can be matched satisfactorily with the absorbance maximum of Chimassorb 944 (244 nm). The recommended values of the wavelength and the mobile phase composition are optimum also from the viewpoint of demands on the sensitivity of the method and the separation of Chimassorb 944 from the other stabilizers, especially Irganox 1010.

When determining Chimassorb 944 in the presence of a phenolic component, such as Irganox 1010, it is recommended that the sample size taken for analysis is as small as possible. Another possibility is to carry out the calibration with Chimassorb 944–Irganox 1010 mixture in a ratio corresponding to that used in the stabilizer package. In this way the interference of the phenolic component is min-

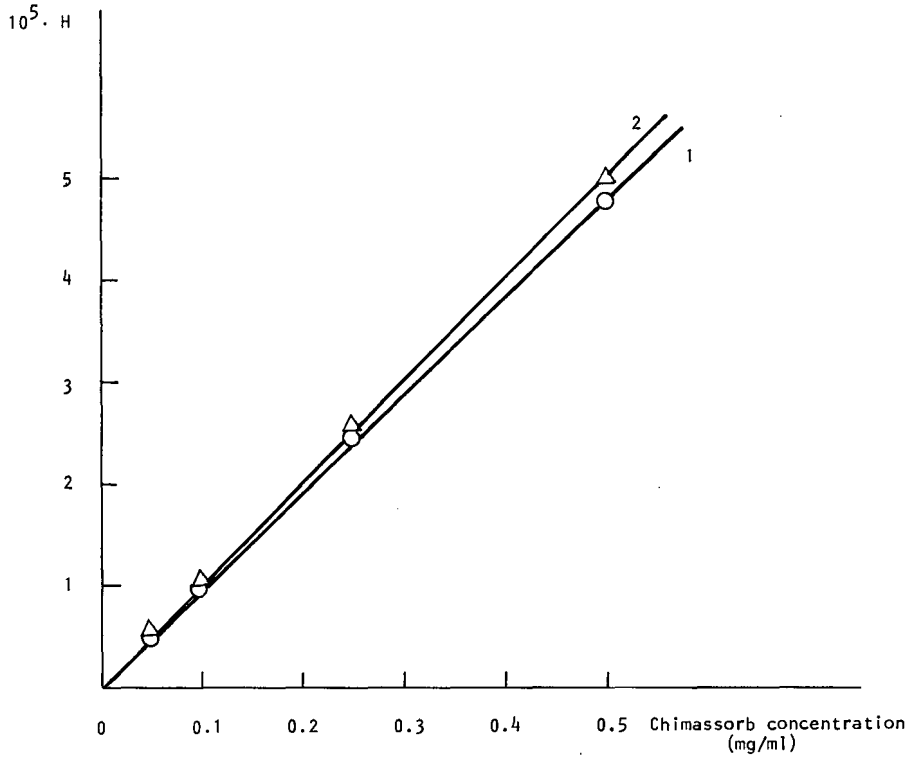

Fig. 3. Effect of addition of Irganox 1010 on the slope of the Chimassorb 944 calibration curve. 1 = Without addition Irganox 1010; 2 = Chimassorb 944 + Irganox 1010 (1:3, w/w). H = height of peaks.

imised (see Fig. 3). When the calibration is carried out in the absence of Irganox 1010 then the systematic error of Chimassorb 944 determination may be as high as 10%, the overall stabilizer concentration being within the range 0.1–0.5% (w/w). The following example illustrates the analysis of commercial fibre-grade polypropylene Tatren (Slovnaft, Bratislava, Czechoslovakia). The concentration of Chimassorb 944 was determined both in pellets and in the corresponding fibre (see Table II). The presence of other components of the stabilizer package (*i.e.*, phenolics and phosphites) did not interfere with the analysis.

TABLE II

DETERMINATION OF CHIMASSORB 944 IN THE COMMERCIAL POLYPROPYLENE TATREN AND FIBRE MADE THEREFROM

	Chimassorb 944 (%, w/w)	
	Pellets	Fibre
	0.123	0.093
	0.116	0.112
	0.121	0.097
Mean	0.120	0.100
s_R	0.004	0.011

Although the scatter of experimental values was higher in the case of fibre, the accuracy of the determination was still sufficient to show the effect of processing on the concentration of HALSs in the final product. The demanding operations connected with the conversion of pellets into fibre and subsequent thermal treatment of the latter reduce the stabilizer concentration. This decrease is, however, far less pronounced than with low-molecular-mass (monomeric) HALSs.

CONCLUSION

The proposed method represents a very simple

way of determinating Chimassorb 944 by HPLC in a basic instrumental configuration. No special detector, gradient elution system or device for baseline subtraction is necessary. The method can be used to determine 0.02–1.0% (w/w) of Chimassorb 944 in polyolefins. No interferences from other additives currently used for the stabilization of polyolefins were noted.

In practice, phenolic and phosphite stabilizers are most likely to be present in the stabilizer package containing Chimassorb 944. Their concentration is usually of the same order of magnitude as that of Chimassorb 944. Frequently, their level is even lower than that of HALSs. Chimassorb 944, being a typical stabilizer of choice for fibre-grades PPs, is unlikely to be combined with UV screeners such as Tinuvin 327 or benzophenones. For this reason only the above-mentioned phenol–phosphite combinations with Chimassorb 944 were analysed in the test runs. The results showed a good separation of this HALS from other components even when the latter were present in a threefold excess.

REFERENCES

1 *Chimassorb 944 Determination in Polypropylene, High Density Polyethylene and Low Density Polyethylene by the Total Nitrogen Content; Analytical Method KC-65/1*, Ciba-Geigy, Basle 1980.
2 V. Mika, L. Preisler and J. Sodomka, *Polym. Degrad. Stabil.*, 28 (1990) 215.
3 W. Freitag, *Fresenius' Z. Anal. Chem.*, 316 (1983) 495.
4 Li, Peiji *et al.*, *Fenxi Huaxue*, 13 (1985) 664; *C.A.*, 104 (1986) 51459e.
5 *Chimassorb 944 and Chimassorb 81 Determination in Polyolefins*, Analytical Method KC-71/2, Ciba-Geigy, Basle, 1982.
6 P. Perstein and P. Orme, *J. Chromatogr.*, 325 (1983) 87.
7 S. G. Gharfeh, *J. Chromatogr.*, 389 (1987) 211.
8 W. Freitag, *J. Chromatogr.*, 450 (1988) 430.

Journal of Chromatography, 606 (1992) 141–146
Elsevier Science Publishers B.V., Amsterdam

CHROM. 24 304

Short Communication

Determination of diclazuril in animal feed by liquid chromatography

Jan De Kock, Maurits De Smet and Rudy Sneyers

Analytical Research Department, Janssen Research Foundation, Beerse (Belgium)

(First received January 17th, 1992; revised manuscript received April 21st, 1992)

ABSTRACT

A method is described for the determination of diclazuril (Janssen Research Compound R64433; trademark Clinacox) in chicken feed at the 1 mg kg^{-1} level. Compound R062646, a structure analogous to diclazuril, was used as the internal standard. The drug was extracted from food with acidified methanol. Diclazuril was then isolated by means of solid-phase extraction with a cartridge containing a C_{18} phase. The eluate was evaporated and the residue redissolved in dimethylformamide. An aliquot was injected onto a reversed-phase high-performance liquid chromatographic column and the drug substance quantified at 280 nm by an ultraviolet detector. Extraction (absolute) recoveries of 85% for both internal standard and diclazuril were obtained. The method is suitable for diclazuril concentrations ranging from 0.1 to 1.5 mg kg^{-1}. Method validation data are presented.

INTRODUCTION

Diclazuril (I, Fig. 1) was developed as a potent and broad-spectrum anticoccidial in broiler chickens [1–3]. For the control of coccidiosis, diclazuril is admixed in the feed at a concentration of 1 mg kg^{-1}. This can be achieved by the inclusion of 200 g of the 0.5% Clinacox premix per ton of feed.

Until now no liquid chromatographic (LC) method has been published for the determination of diclazuril. We report a robust high-performance liquid chromatographic (HPLC) assay for the quantitation of the anticoccidial in feed. Analyses of the samples have shown that the medicated feed is stable for at least 6 months. A possible degradation compound (III, Fig. 1), resulting from stress-decomposition studies of the drug substance, is not found in these aged samples.

An extended clean-up procedure allows the analysis of feed samples of different origin. It is well known that, because it is dependent upon the availability of the ingredients, the composition of a feed can vary to a high degree. Hence the level of the feed excipients that are co-extracted can change.

To enhance the ruggedness of the method, an internal standard (II, Fig. 1) was taken through the whole clean-up procedure.

EXPERIMENTAL

Instrumentation

The type of equipment used for the development of the method and batch control is described below. Any instrument equivalent to that described can be used. A liquid chromatograph equipped with an autosampler and a variable UV wavelength detector

Correspondence to: Dr. M. De Smet, Analytical Research Department, Janssen Research Foundation, Beerse, Belgium.

0021-9673/92/$05.00

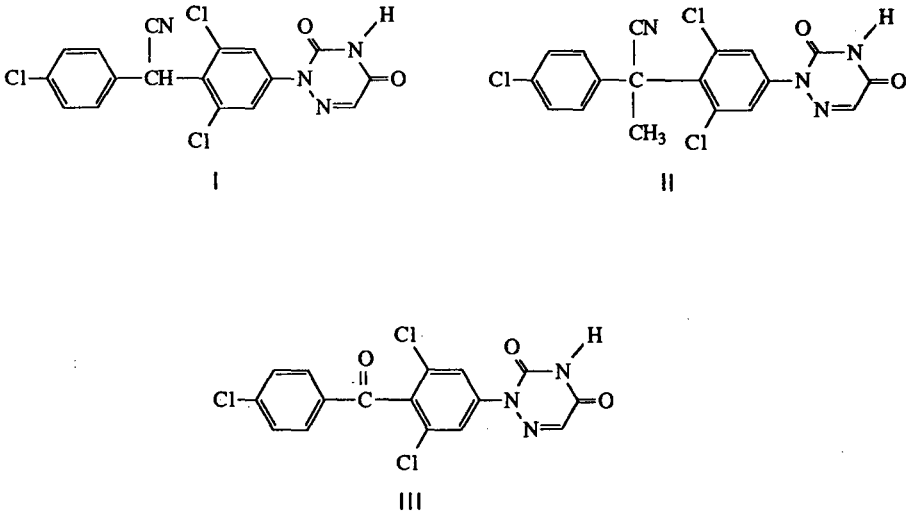

Fig. 1. Structures of dicluzaril (I), the internal standard (II) and a possible degradation product of dicluzaril (III).

(Hewlett-Packard Series 1050, Wallbron, Germany) was used. Quantitation was done at 280 nm. A flow-rate of 2 ml/min and an injection volume of 20 μl were used. The elution mode was a ternary gradient. Solvents A, B and C were, respectively, 0.5% ammonium acetate and 0.01 *M* tetrabutylammonium hydrogen sulphate in water, acetonitrile and methanol. The initial conditions were 60% A, 20% B and 20% C. These were held for 10 min and then followed by a gradient elution lasting 30 min to 45% A, 20% B and 35% C. The column was then flushed with acetonitrile for 10 min.

Reagents, materials and eluent

The model compounds (I, II and III) used in this study were reference standard grade from Janssen Pharmaceutica (Beerse, Belgium). Deionized water was purified through a Milli-Q4 System (Millipore, Brussels, Belgium). Acetonitrile and methanol were of HPLC quality (Janssen Chimica, Geel, Belgium). Inorganic compounds were all of p.a. quality.

The solid-phase extraction cartridges (Mega Bond C_{18}) were obtained from Analytichem (Harbor City, CA, USA). The analytical column was a stainless-steel tube (100 mm × 4.6 mm I.D.) packed with Hypersil ODS or BDS (3-μm particles, Shandon Scientific, Astmoor, UK).

Standard and sample preparations

An internal standard solution of 0.05 mg of II per ml of dimethylformamide was used. A reference solution was prepared containing 2 μg of diclazuril and II each per ml of a water–dimethylformamide mixture (60:40, v/v). Both solutions were prepared preferably in amber-coloured flasks and stored in the refrigerator at −4°C.

The extraction solvent (acidified methanol) was prepared by addition of 5 ml of hydrochloric acid to 1000 ml of methanol.

Meal (mash) and pellets were ground in order to be homogenized. From the ground food about 50 g were accurately weighed into a suitable glass container. Pellets were ground before sampling. Exactly 1 ml of the internal standard solution and 200 ml extraction solvent were added. The mixture was stirred overnight. The supernatant (20 ml) was transferred into a suitable vessel and diluted with 20 ml of water. This solution was put onto a Mega-Bond (C_{18}) column. Vacuum was applied with a waterjet and the cartridge was washed with 25 ml of acidified methanol–water (65:35, v/v). The fraction collected was discarded and the model compounds were eluted from the Mega-Bond column with 25 ml of acidified methanol–water (80:20 v/v). The eluate was evaporated to dryness at 60°C. The residue was

redissolved in 1 ml of dimethylformamide and 1.5 ml of water.

It is recommended the final sample solution be filtered over a 0.45-μm chemically resistant filter (Gelman) before injection.

Sample analysis

Before injection of a sample sequence the analytical column was flushed with 100% acetonitrile for at least 15 min followed by equilibration with the initial elution solvents for 10 min. During the sequence the gradient composition described in the *Instrumentation* section was followed.

The amount of diclazuril present in the feed sample, expressed as weight percentage, was calculated from:

$$\text{Diclazuril}(\%) = \frac{H_{c,s}}{H_{i,s}} \times \frac{H_{i,r}}{H_{c,r}} \times \frac{C_{c,r}}{C_{a,s}} \times 100$$

where $C_{c,r}$ is the concentration of diclazuril in the reference solution, $C_{a,s}$ is the concentration of the theoretical amount of diclazuril analyte in the final sample solution and $H_{c,r}$, $H_{i,r}$, $H_{c,s}$ and $H_{i,s}$ are the peak heights measured for diclazuril (c) and internal standard (i) in the reference (r) and sample (s) solutions.

Absolute recovery

A set of two blank feed samples (50 g) were taken; one was spiked with internal standard and diclazuril, the other with internal standard only. Spiking amounts were at the 1 mg kg^{-1} level. Both sets were then subjected to the whole work-up procedure. At the end diclazuril was added (1 mg kg^{-1} level) to the samples containing only internal standard. The recovery was calculated from the peak height ratios measured on the chromatograms. The same procedure was repeated for the recovery of the internal standard (one set of samples contained internal standard only).

Linearity

The linearity for diclazuril was determined in the 50–150% range with the nominal batch level of 1.0 mg kg^{-1}.

Blank feed (50 g) was spiked three times with 50 μg of internal standard and 25, 50 and 75 μg of diclazuril (corresponding to 50, 100 and 150%) and analysed according to the method described.

Accuracy and precision

Blank feed was spiked with diclazuril in various amounts (concentrations between 0 and 1.5 mg kg^{-1}) and analysed according to the method described.

Precision (repeatability and reproducibility) studies were performed on a broiler feed sample produced by a commercial feed mill in Brazil at the 1 mg kg^{-1} level.

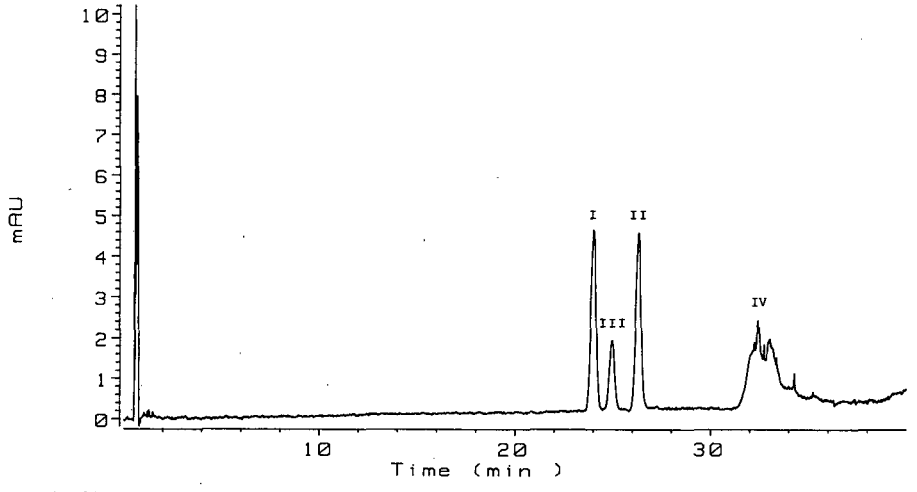

Fig. 2. Chromatogram demonstrating the selectivity of the method. Peaks: I = diclazuril; II = internal standard; III = possible degradation compound (each 2 μg ml^{-1}); IV = mobile phase impurities.

RESULTS AND DISCUSSION

Selectivity

Stress-decomposition studies on the drug substance revealed the formation of compound III. Because of the similar structure of this compound, a gradient elution is necessary to obtain a separation between the three model compounds. In Fig. 2 a specimen chromatogram demonstrating the selectivity is shown. Furthermore, the gradient enhances the selectivity against possible feed excipients. It was noted during development of the assay that proper adjustment of the gradient for some samples is necessary to eliminate interference from the excipients.

Determination at wavelength 280 nm gave a good signal-to-noise ratio.

Extraction procedure and absolute recovery

In the laboratory for gas chromatography (GC) [4] in our analytical department, similar studies were performed. The results indicated that the extraction procedure described gives the highest recovery. Stirring overnight is not necessary, but because the

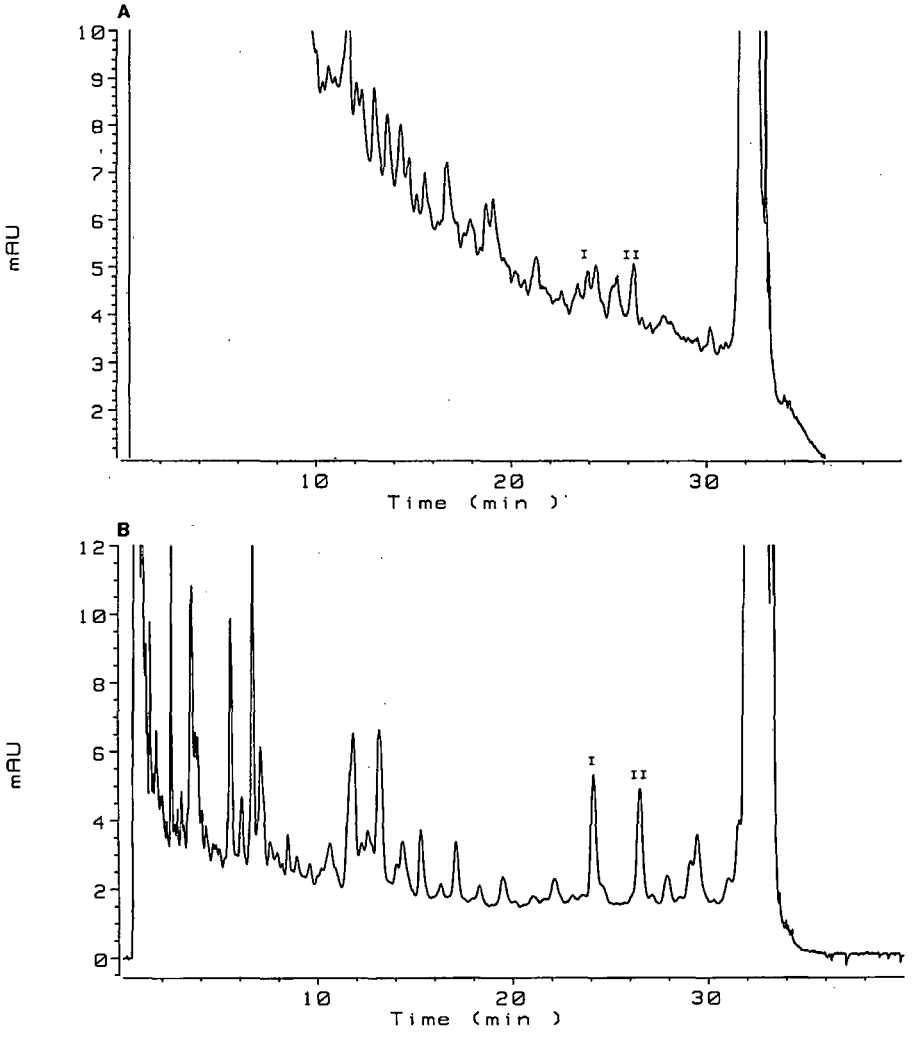

Fig. 3. (A) Chromatogram before the solid phase extraction. (B) Chromatogram after clean-up with a C_{18} cartridge. Peaks: I = diclazuril; II = internal standard.

TABLE I

REPEATABILITY, REPRODUCIBILITY ACCURACY AND LINEARITY AT THE 1 mg kg^{-1} LEVEL

	n	Concentration found (mean ± S.D.)	R.S.D.[a] (%)
Repeatability	6	1.00 ± 0.02 mg kg^{-1}	2.3
Reproducibility	6	0.95 ± 0.05 mg kg^{-1}	5.0
Accuracy[b]	14	92.7 ± 9.7%	10.4

Linearity (0.5–1.0–1.5 mg kg^{-1})
Regression: $y = -0.33 + 1.26x$ $r^2 = 0.997$

[a] R.S.D. = relative standard deviation.
[b] Diclazuril concentrations between 0 and 1.5 mg kg^{-1}.

liquid extraction period is at least 6 h it can be a time-saving step. The solid phase extraction step is necessary to remove most of the excipients (see Fig. 3). No loss of model compound was noted during the first wash step of the clean-up procedure. The liquid extraction and the solid-phase clean-up procedure gave for both model compounds I and II an absolute recovery of 85%.

Validation of the method

The linearity was checked at the anticipated level of 1 mg kg^{-1}. In the 50–150% range a good relationship between the peak-area ratio of diclazuril and internal standard and the injected amount of diclazuril was obtained. The equation of the linear regression line together with the correlation is given in Table I.

The accuracy can be evaluated through the analysis of samples spiked with known amounts of diclazuril. The tolerance for anticoccidials at this low level is 20%. The results in Table I show that the method is accurate at an extended level of the nominal concentration of 1 mg kg^{-1}.

From the point of view of system suitability and quality assurance it is advisable to analyse a control sample before each sample sequence. This sample may be a laboratory-made sample or a production batch containing a known concentration of diclazuril, preferably at the 1 mg kg^{-1} level.

The precision (repeatability) of the entire analytical method was measured by six replicate determinations of diclazuril by one analyst using the same liquid chromatograph. The reproducibility study was performed over a 4-week period by different analysts in different laboratories with different chromatographs. The results and statistical evaluation of this study are given in Table I.

In order to demonstrate the reliability of the method a comparative study was set up. Samples from different origins were analysed with a GC method [4] and with the LC method described. The results expressed in mg kg^{-1} are shown in Table II. The results of both methods were obtained by one single analysis of the sample.

The data of the precision and accuracy studies together with the results of the comparative test prove the ruggedness of the method.

TABLE II

ASSAY OF DICLAZURIL IN FEED SAMPLES; A COMPARATIVE STUDY OF LC AND GC

Sample origin	LC result (mg kg^{-1})	GC result (mg kg^{-1})
Columbia	0.88	0.89
Yugoslavia	0.20	0.20
Australia	0.69	0.71
Austria	1.04	1.01
Brazil	1.11	0.93
Venezuela	0.20	0.18
South Africa	1.54	1.53

CONCLUSION

A reliable method has been developed for the determination of diclazuril in animal feed at a concentration of 1 mg kg^{-1}. An extended extraction procedure is necessary to cover a wide range of feed samples.

ACKNOWLEDGEMENT

The authors are grateful to the quality assurance laboratory of the analytical research department for the follow-up of the method validation.

REFERENCES

1 O. Vanparijs, R. Marsboom and L. Despenter, *Poult. Sci.*, 68 (1989) 489–495.
2 O. Vanparijs, R. Marsboom, L. Hermans and L. Van Der Flaes, *Poult. Sci.*, 68 (1989) 496–500.
3 O. Vanparijs, R. Marsboom, L. Hermans and L. Van Der Flaes, *Poult. Sci.*, 69 (1990) 60–64.
4 M. De Smet, G. Nijsmans and H. Quintelier, *Internal Report ST-GC 90-38*, Janssen Research Foundation, Beerse, 1990.

Journal of Chromatography, 606 (1992) 147–151
Elsevier Science Publishers B.V., Amsterdam

CHROM. 24 103

Short Communication

Ionophoretic technique in the study of mixed-ligand complexes of biochemical importance in the Co(II)/Cu(II)–adenosine diphosphate nitrilotriacetate system

Amita Yadav and R. K. P. Singh

Electrochemical Laboratories, Department of Chemistry , University of Allahabad, Allahabad 211002 (India)

(First received November 7th, 1991; revised manuscript received February 13th, 1992)

ABSTRACT

A method involving the use of an ionophoretic technique (paper electrophoresis) is described for the study of equilibria in mixed-ligand complex systems in solution. The method is based on the migration of a spot of a metal ion (m), with the complexants added to the background electrolyte (0.1 *M* perchloric acid). For the study of ternary complexes, the concentration of one of the complexants, adenosine diphosphate (ADP), is kept constant, while that of the second ligand, nitrilotriacetate (NTA), is varied. A graph of mobility against − log[MTA] is used to obtain information on the formation of the mixed-ligand complex and to calculate the stability constants. The overall stability constants of –ADP and M–ADP–NTA complexes were found to be $10^{5.9}$ and $10^{11.9}$ for Cu(II) and $10^{4.3}$ and $10^{9.7}$ for Co(II) complexes at $\mu = 0.1$ and 30°C.

INTRODUCTION

Paper electrophoresis has previously been applied to the study of metal complexes in solution and attempts have been made to determine the stability constants of the complex species [1,2]. In previous work a method was developed for the study of stepwise complex formation [3–5]. Although the use of paper electrophoresis for the study of metal complex systems with a single ligand seems to be well established, there has been no systematic study on mixed-ligand complexes. However, Czakis Sylikowska [6] made some observations on the formation of mixed halide complexes of Hg(II), but the studies were only qualitative and did not throw light either on the nature of the species or on their stabilities. Previous papers [7–10] described a method for the study of mixed-ligand complexes. The present work represents an extension of that technique and this paper reports our observation on the mixed-ligand system Cu(II)/Co(II)–adenosine diphosphate (ADP)–nitrilotriacetate (NTA).

EXPERIMENTAL

Horizontal–vertical-type electrophoresis equipment (Systronics Model 604) was used together with various accessories. In each instance electrophoresis was carried out for 60 min at 200 V at 30°C. Whatman No. 1 paper strips (25 × 1 cm) were used.

Correspondence to: Dr. A. Yadav, Electrochemical Laboratories, Department of Chemistry, University of Allahabad, Allahabad 211002, India.

0021-9673/92/$05.00

pH measurements were made with an Elico Model L_{1-10} pH meter using a glass electrode.

Metal perchlorates were prepared by an appropriate method and the final concentrations were kept at $5.0 \cdot 10^{-3}$ *M*. 1-(2-Pyridylazo)-2-naphthol (PAN) [0.1% (w/v) in ethanol] was used for detecting Cu(II) and Co(II) ions. A saturated solution of silver nitrate in acetone was sprayed on the paper and subsequently fumed with ammonia to detect glucose spots.

The background electrolyte for the study of binary complexes was 0.1 *M* perchloric acid–0.002 *M* ADP–$3.3 \cdot 10^{-3}$ *M* NTA with sodium hydroxide added to produce the desired pH, and for the study of ternary complexes it was 0.1 *M* perchloric acid–0.002 *M* ADP with various amounts of NTA, maintained at pH 8.5 by addition of sodium hydroxide solution.

Procedure for binary complexes

Whatman No. 1 paper strips (25 × 1 cm) in duplicate are spotted in the middle with metal ion solutions. An extra strip is marked with glucose. The strips are sandwiched between two insulated hollow metal plates and the temperature of the system is maintained by water supply within the plates at a fixed temperature. The plates are then mounted on the electrophoresis equipment with the end of the paper strips dipping in the two tanks of the instrument. Electrophoresis is carried out for 60 min. The strips are then removed from tank and dried and the migrated spots are detected with specific reagents. The movement of a metal spot towards the negative electrode is taken as positive mobility and in the reverse direction as negative mobility. Duplicate strips always recorded less than a 5% variation in the distance travelled and the mean of the two was taken for calculation of mobility. The movement of glucose is used as a correction factor for electroosmosis. The electrophoretic migration of metal spots on the paper was observed at different pH values of the background electrolyte. Movements divided by potential gradient yield mobilities, which are plotted in Figs. 1 and 2.

Procedure for ternary complexes

Strips are marked with metal ion solutions in duplicate along with an additional strip marked with glucose. After drenching the strips with the background electrolyte, electrophoresis is carried for 1 h at the same potential difference as for binary complexes. For subsequent observations, the NTA solution (pH 8.5) is added progressively and the ionophoretic mobility is recorded. Mobility is plotted against $-\log$ [NTA] (Fig. 3).

RESULTS AND DISCUSSION

M–ADP system

The plot of the overall electrophoretic mobility of a metal spot against pH gives a curve with two plateaux as shown in Fig. 1. A plateau is obviously an indication of the pH range where the speed is virtually constant. This is possible only when a particular complex is overwhelmingly formed. Thus, every plateau indicates the formation of a certain complex species. The first plateau corresponds to the region in which metal ions are uncomplexed. It lies in a low pH range, where the concentration of protonated species of ADP is obviously maximum. Hence it is concluded that this protonated species of ADP is non-complexing. Subsequently the metal ion spot has a progressively decreasing velocity and hence complexation of the metal ion should be taking place with other ionic species of ADP whose concentration increases progressively with increase in pH. The second plateau in each instance with a negative mobility indicates the formation of a 1:1 negatively charged metal complex. Further increases in the pH of the background electrolyte has no effect on the mobility of metal ions. Hence it is concluded that the complexing species of the ligand is ADP^{3-}. This is in conformity with the findings of other workers [11–13].

The metal spot on the paper is thus a combination of uncomplexed metal ions and a 1:1 complex. This spot is moving under the influence of the electric field, its overall mobility being given by the equation

$$U = \sum_n U_n f_n \tag{1}$$

where U_n and f_n are the mobility and mole fraction of a particular complex species, respectively. This equation is transformed into the following form on taking into consideration different equilibria:

$$U = \frac{U_0 + U_1 K_1 [\mathrm{L}]}{1 + K_1 [\mathrm{L}]} \tag{2}$$

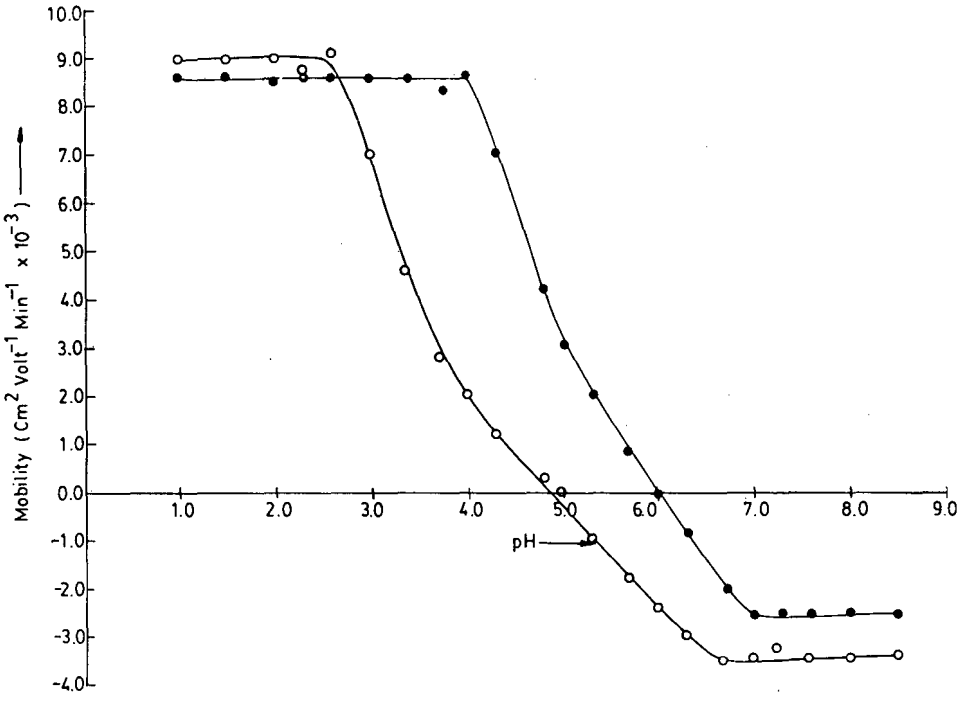

Fig. 1. Plots of mobility *versus* pH for the metal–ADP system. ○ = Cu(II); ● = Co(II).

where U_0 and U_1 are the mobilities of the uncomplexed metal ion and 1:1 metal complex, respectively, and L is the total ligand concentration. This equation was used for calculating the stability constants of the complexes of metal ions with ADP.

For calculating the stability constant K^{M}_{M-ADP}, the region between the first and second plateaux is pertinent. The overall mobility U will be equal to the arithmatic mean mobility of the uncomplexed metal ion U_0 and that of the 1:1 metal complex U_1 at a pH where $K^{M}_{M-ADP} = 1/[L]$. With the help of the dissociation constants of ADP ($k^{ADP^-}_{ADP^{2-}} = 10^{4.1}$ and $k^{ADP^{2-}}_{ADP^{3-}} = 10^{6.4}$) [14], the concentration of the ADP anion $[L^{3-}]$ is determined at a particular pH, from which K^{M}_{M-ADP} can be calculated. These calculated values are given in Table I.

TABLE I

STABILITY CONSTANTS OF SOME BINARY AND TERNARY COMPLEXES OF Cu(II) AND Co(II) WITH ADP AND NTA

Ionic strength = 0.1 *M*; temperature = 30°C.

Stability constant	Cu(II)		Co(II)		Ref.
	Calculated value	Literature value	Calculated value	Literature value	
Log K^{M}_{M-ADP}	5.9	5.90	4.3	4.20	19
Log K^{M}_{M-NTA}	12.2	12.94	10.1	10.38	20
Log $K^{M-ADP}_{M-ADP-NTA}$	6.0	–	5.4	–	–
Log $K^{M}_{M-ADP-NTA}$	11.9	–	9.7	–	–

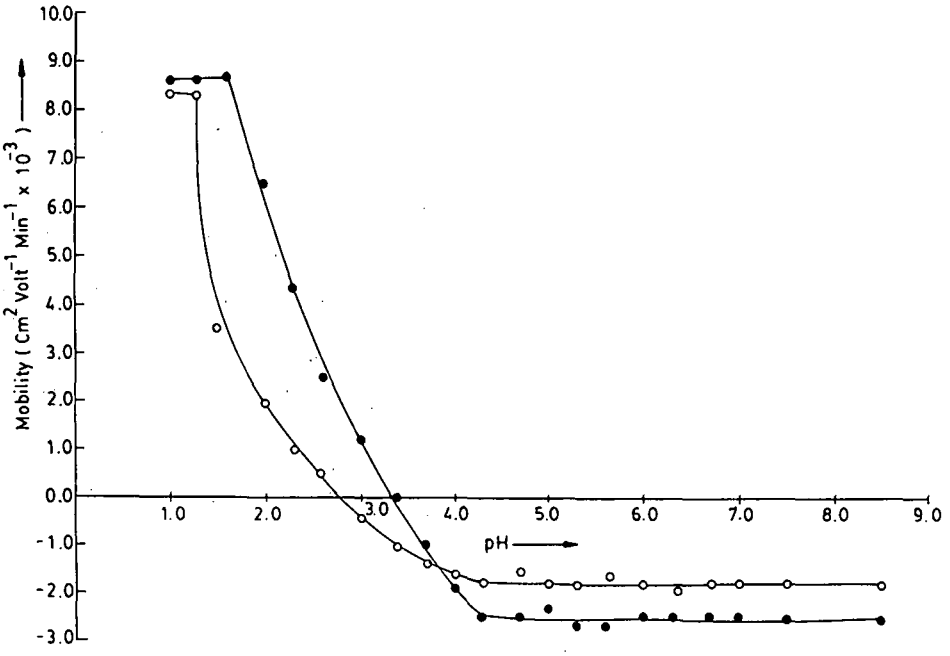

Fig. 2. Plots of mobility *versus* pH for the metal–NTA system. O = Cu(II); ● = Co(II).

M–NTA system

The overall mobilities of the metal spots in the presence of NTA at different pH values are represented in Fig. 2. It is evident that with all the metal ions two plateaux are obtained, the mobility of the second plateau lying in the negative region, showing the negatively charged nature of the complex. Hence only one NTA anion is assumed to combine with one bivalent metal ion to give a 1:1 M–NTA complex, which is in conformity with the findings of other workers [15–18]. The stability constants of complexes with NTA (K^{M}_{M-NTA}) were calculated as described for the M–ADP system and are given in Table I.

M–ADP–NTA system

This system was studied at pH 8.5 with a specific purpose. It was observed from the mobility curves for M–ADP and M–NTA binary systems that binary complexes $(M–ADP)^-$ and $(M–NTA)^-$ are formed up to pH 8.5. Hence it would be desirable to study the transformation of the $(M–ADP)^-$ complex into the $(M–ADP–NTA)^{4-}$ complex at pH 8.5 in order to avoid any side interactions.

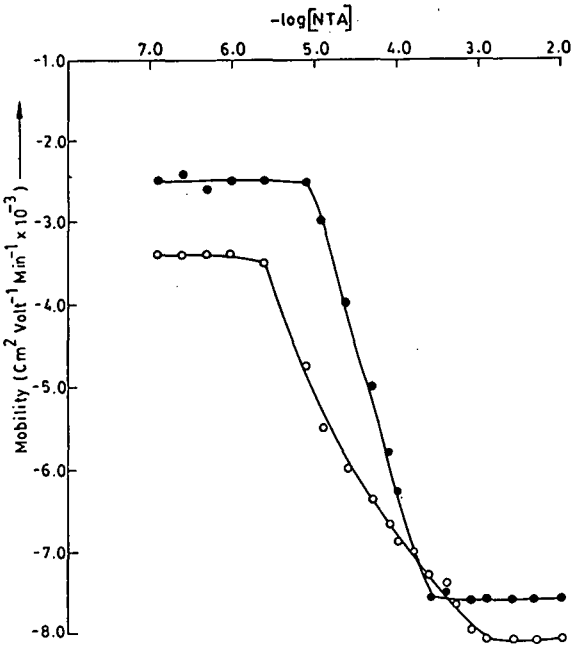

Fig. 3. Plots of mobility *versus* −log[NTA] for the metal–ADP–NTA system. O = Cu(II); ● = Co(II).

The plots of mobility against logarithum of concentration of added NTA are shown in Fig. 3 and exhibit two plateaux. The negative mobility in the region of the first plateau is obviously due to 1:1 M–ADP$^-$ complexes (see Fig. 1 at pH 8.5). The mobility corresponding to the second plateau is more negative than that of the first plateau, indicating the formation of a more negatively charged complex. However, as the mobility for the last plateau does not agree with the mobility of a 1:1 M–NTA complex (Fig. 2), it is inferred that the species corresponding to the second plateau is due to the coordination of the NTA^{3-} anion to a 1:1 M–ADP$^-$ moiety, resulting in the formation of a 1:1:1 $(M–ADP–NTA)^{4-}$ mixed complex according to

$$(M–ADP)^- + NTA^{3-} \overset{K_1}{\rightleftharpoons} (M–ADP–NTA)^{4-} \quad (3)$$

In the present electrophoretic study, the transformation of a simple complex into a mixed complex takes place, the overall mobility being given by

$$U = U_0 f_{M–ADP} + U_1 f_{M–ADP–NTA} \quad (4)$$

where U_0 and U_1 are the mobilities and $f_{M–ADP}$ and $f_{M–ADP–NTA}$ the mole fractions of M–ADP and M–ADP–NTA complexes respectively.

From Fig. 3, the total concentration of NTA at which the overall mobility is mean of the mobilities of the two plateaux was determined. For this the concentration of the NTA^{3-} anion at pH 8.5 was calculated. $K^{M–ADP}_{M–ADP–NTA}$ is obviously equal to 1/[L]. For the calculation of the overall stability constants ($K^{M}_{M–ADP–NTA}$), the stability constant of the M–ADP complex was multiplied by $\log K^{M–ADP}_{M–ADP–NTA}$. All these values of stability constants are given in Table I.

REFERENCES

1 V. Jokl, *J. Chromatogr.*, 14 (1964) 71.
2 J. Biernat, *Rocz. Chem.*, 38 (1964) 343; *C.A.*, 61 (1964) 6456b.
3 R. K. P. Singh, J. K. Sircar, J. R. Yadava, P. C. Yadava and K. L. Yadava, *Electrochim. Acta*, 26 (1980) 395.
4 R. K. P. Singh, J. K. Sircar, R. Khelawan and K. L. Yadava, *Chromatographia*, 13 (1980) 709.
5 R. K. P. Singh, J. R. Yadava, P. C. Yadava and K. L. Yadava, *Z. Phys. Chem. (Leipzig)*, 3 (1983) 264.
6 M. Czakis Sylikowska, *Zesz. Nauk. Politech. Lodz. Chem.*, 6 (1967) 2038; *C.A.*, 65 (1966) 1746e.
7 P. C. Yadava, A. K. Ghose, K. L. Yadava and A. K. Dey, *Chromatographia*, 9 (1976) 416.
8 J. R. Yadava, J. K. Sircar and K. L. Yadava, *Electrochim. Acta*, 26 (1981) 391.
9 R. K. P. Singh, J. R. Yadav and K. L. Yadava, *J. Electrochem. Soc. India*, 30 (1981) 250.
10 R. K. P. Singh and K. L. Yadava, *Trans. SAEST*, 16 (1981) 3.
11 M. M. Taquikhan and A. E. Martell, *J. Am. Chem. Soc.*, 89 (1967) 5585.
12 M. M. Taquikhan and A. E. Martell, *J. Am. Chem. Soc.*, 84 (1967) 3037.
13 C. M. Fray and J. E. Stuehr, *J. Am. Chem. Soc.*, 94 (1972) 8898.
14 A. Yadav, R. K. P. Singh and K. L. Yadava, *J. Electrochem. Soc. India*, (1991) in press.
15 T. R. Bhat, R. R. Das and J. Shanker, *Indian J. Chem.*, 5 (1967) 324.
16 D. Hopgood and R. J. Angelici, *J. Am. Chem. Soc.*, 90 (1968) 2508.
17 O. K. Borggaard, O. Farver and V. S. Anderson, *Acta Chem. Scand.*, 25 (1971) 3541.
18 J. Israeli, J. R. Coyouette and R. Volpe, *Talanta*, 18 (1971) 737.
19 A. E. Martell and R. M. Smith, *Critical Stability Constant —Amines*, Vol. II, Plenum Press, New York, 1974, p. 281.
20 R. M. Smith and A. E. Martell, *Critical Stability Constants —Amino Acids*, Vol. I, Plenum Press, New York, 1974, p. 141.

Journal of Chromatography, 660 (1992) 152
Elsevier Science Publishers B.V., Amsterdam

CHROM. 24 330

Book Review

Cell separation science and technology, edited by D.S. Kompala and P. Todd, American Chemical Society, Washington, DC, 1991, 301 pp. US$ 69.95 ISBN 0-8412-2090-5.

Cell Separation Science and Technology, edited by Dhinakar S. Kompala of the University of Colorado and Paul Todd of the National Institute of Standards and Technology, is a volume of the *American Chemical Society (ACS) Symposium Series* developed from the Symposium sponsored by the Division of Industrial and Engineering Chemistry, Inc., and Biochemical Technology at the *199th National Meeting of the ACS* held in Boston, MA, on April 22–27, 1990.

There are, no doubt, several ways in which to call for contributors, motivate them and edit the volume to obtain a compact, exhaustive and up-to-date result. It is the reviewer's opinion that an optimal result was achieved with this ACS Symposium Series volume. The book is composed of 17 contributions (chapters) divided into four main groups distinguishing different principal methodologies applied for cell separations.

The first chapter is an introductory review summarizing the reasons, objectives and methods for separating the living cells. The following four groups of chapters concern: Flow sorting and optical methods, Sedimentation and flow methods, Affinity, adsorption and extraction methods and Electrophoretic and magnetic methods.

The individual contributions are written by leading experts in their respective fields in a very convenient, uniform way. Each contribution presents a short introduction to the described method, an explanation of its fundamentals and a description of the typical applications in cell separation. Without exception, each also contains a representative list of recent fundamental papers, reviews and books, thus opening up to the reader wide possibilities for easy access to more detailed information concerning the corresponding specialized literature.

A simple look at the contents of the book gives a full impression of the extent of the covered topics. The titles of the individual contributions are as follows: Separation of living cells; High-resolution separation of rare cell types; Rare-earth chelates as fluorescent markers in cell separation and analysis; Automated cell separation techniques based on optical trapping; Separation techniques used to prepare highly purified chromosome populations: sedimentation, centrifugation, and flow sorting; Separation of cells by sedimentation; High-capacity separation of homogeneous cell subpopulations by centrifugal elutriation; Cell separations using differential sedimentation in inclined settlers; Separation of cells by field-flow fractionation; Separation of cells and measurement of surface adhesion forces using a hybrid of field-flow fractionation and adhesion chromatography; High-capacity cell separation by affinity selection on synthetic solid-phase systems; Population heterogeneity in blood neutrophils fractionated by continuous flow electrophoresis and partitioning in aqueous polymer two-phase systems; Separation of lymphoid cells using combined countercurrent elutriation and continuous flow electrophoresis; Comparison of methods of preparative cell electrophoresis; Separation of small-cell lung cancer cells from bone marrow using immunomagnetic beads; Analytical- and process-scale cell separation with bioreceptor ferrofluids and high-gradient magnetic separation.

This covers most of the methods used recently for the analytical and preparative separation of living cells. There are no comments to be added. The book could serve in many research laboratories as a reference handbook to interested individuals, and it seems that it could be successfully introduced as a textbook for various university course levels.

Paris (France) Josef Janča

Chromatography, 5th edition

Fundamentals and Applications of Chromatography and Related Differential Migration Methods

edited by **E. Heftmann**, *Orinda, CA, USA*

These are completely new books, organized according to the successful plan of the previous four editions. While avoiding repetition of material covered in the previous editions, the authors have succeeded in presenting a coherent and comprehensive picture of the state of each topic. The books provide beginners as well as experienced researchers with a key to understanding current activities in various separation methods. They will also serve as textbooks for graduate courses in technical, medical and engineering schools as well as all universities offering science courses.

Part A: Fundamentals and Techniques

Journal of Chromatography Library Volume 51A

Part A covers the theory and fundamentals of such methods as column and planar chromatography, countercurrent chromatography, field-flow fractionation, and electrophoresis. Affinity chromatography and supercritical-fluid chromatography are covered for the first time. Each topic is treated by one of the most eminent authorities in the field.

Contents Part A: 1. Theory of chromatography *(L.R. Snyder)*. 2. Countercurrent chromatography *(Y. Ito)*. 3. Planar chromatography *(S. Nyiredy)*. 4. Column liquid chromatography *(H. Poppe)*. 5. Ion-exchange chromatography *(H.F. Walton)*. 6. Size-exclusion chromatography *(L. Hagel and J.-C. Janson)*. 7. Affinity chromatography *(T.M. Phillips)*. 8. Supercritical-fluid chromatography *(P.J. Schoenmakers and L.G.M. Uunk)*. 9. Gas chromatography *(C.F. Poole and S.K. Poole)*. 10. Field-flow fractionation *(J. Janca)*. 11. Electrophoresis *(P.G. Righetti)*. Manufacturers and dealers of chromatography and electrophoresis supplies. Subject Index.

1992 xxxvi + 552 pages
Price: US $ 179.50 / Dfl. 350.00
ISBN 0-444-88236-7

Parts A & B Set
Set price: US $ 333.50 / Dfl. 650.00
ISBN 0-444-88404-1

Part B: Applications

Journal of Chromatography Library Volume 51B

Part B presents various applications of these methods. New developments are reviewed and summarized. Important topics such as environmental analysis and the determination of synthetic polymers and fossil fuels, are covered for the first time.

Contents Part B: 12. Inorganic species *(P.R. Haddad and E. Patsalides)*. 13. Amino acids and peptides *(C.T. Mant, N.E. Zhou and R.S. Hodges)*. 14. Proteins *(F.E. Regnier and K.M. Gooding)*. 15. Lipids *(A. Kuksis)*. 16. Carbohydrates *(S.C. Churms)*. 17. Nucleic acids, their constituents and analogs *(N-I Jang and P.R. Brown)*. 18. Porphyrins *(K. Jacob)*. 19. Phenolic compounds *(J.B. Harborne)*. 20. Drugs *(K. Macek and J. Macek)*. 21. Fossil fuels *(R.P. Philp and F.X. de las Heras)*. 22. Synthetic polymers *(T.H. Moury and T.C. Schunk)*. 23. Pesticides *(J. Sherma)*. 24. Environmental analysis *(K.P. Naikwadi and F.W. Karasek)*. 25. Amines from environmental sources *(H.A.H. Billiet)*. Manufacturers and dealers of chromatography and electrophoresis supplies. Subject Index.

1992 xxxii + 630 pages
Price: US $ 189.50 / Dfl. 370.00
ISBN 0-444-88237-5

Elsevier Science Publishers

P.O. Box 211, 1000 AE Amsterdam, The Netherlands
P.O. Box 882, Madison Square Station, New York, NY 10159, USA

Announcement from the Publisher

ELSEVIER SCIENCE PUBLISHERS

prefers the submission of electronic manuscripts

Electronic manuscripts have the advantage that there is no need for the rekeying of text, thereby avoiding the possibility of introducing errors and resulting in reliable and fast delivery of proofs.

The preferred storage medium is a $5\frac{1}{4}$ or $3\frac{1}{2}$ inch disk in MS-DOS format, although other systems are welcome, e.g. Macintosh.

Your disk and (**exactly matching**) printed version (printout, hardcopy) should be submitted together to the accepting editor. In case of revision, the same procedure should be followed such that, on acceptance of the article, the file on disk and the printout are **identical**. Both will then be forwarded by the editor to Elsevier.

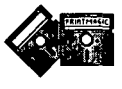

Please follow the general instructions on style/arrangement and, in particular, the reference style of this journal as given in 'Instructions to Authors'.

Please label the disk with your name, the software & hardware used and the name of the file to be processed.

Further information can be found under 'Instructions to Authors - Electronic manuscripts'.

Contact the Publisher for further information.

ELSEVIER SCIENCE PUBLISHERS B.V.
P.O. Box 330, 1000 AH Amsterdam
Netherlands
Fax: (+31-20) 5862-304

PUBLICATION SCHEDULE FOR 1992

Journal of Chromatography and *Journal of Chromatography, Biomedical Applications*

MONTH	O 1991–F 1992	M	A	M	J	J	
Journal of Chromatography	Vols. 585–593	594/1 + 2 595/1 + 2	596/1 596/2 597/1 + 2	598/1 598/2 599/1 + 2 600/1 600/2	602/1 + 2 603/1 + 2 604/1	604/2 605/1 605/2 606/1	The publication schedule for further issues will be published later.
Cumulative Indexes, Vols. 551–600					[a]		
Bibliography Section		610/1			610/2		
Biomedical Applications	Vols. 573 and 574	575/1 575/2	576/1	576/2 577/1	577/2	578/1 578/2	

[a] Cumulative Indexes will be Vol. 601, to appear early 1993.

INFORMATION FOR AUTHORS

(Detailed *Instructions to Authors* were published in Vol. 558, pp. 469–472. A free reprint can be obtained by application to the publisher, Elsevier Science Publishers B.V., P.O. Box 330, 1000 AH Amsterdam, The Netherlands.)

Types of Contributions. The following types of papers are published in the *Journal of Chromatography* and the section on *Biomedical Applications:* Regular research papers (Full-length papers), Review articles and Short Communications. Short Communications are usually descriptions of short investigations, or they can report minor technical improvements of previously published procedures; they reflect the same quality of research as Full-length papers, but should preferably not exceed five printed pages. For Review articles, see inside front cover under Submission of Papers.

Submission. Every paper must be accompanied by a letter from the senior author, stating that he/she is submitting the paper for publication in the *Journal of Chromatography*.

Manuscripts. Manuscripts should be typed in double spacing on consecutively numbered pages of uniform size. The manuscript should be preceded by a sheet of manuscript paper carrying the title of the paper and the name and full postal address of the person to whom the proofs are to be sent. As a rule, papers should be divided into sections, headed by a caption (*e.g.*, Abstract, Introduction, Experimental, Results, Discussion, etc.). All illustrations, photographs, tables, etc., should be on separate sheets.

Introduction. Every paper must have a concise introduction mentioning what has been done before on the topic described, and stating clearly what is new in the paper now submitted.

Abstract. All articles should have an abstract of 50–100 words which clearly and briefly indicates what is new, different and significant.

Illustrations. The figures should be submitted in a form suitable for reproduction, drawn in Indian ink on drawing or tracing paper. Each illustration should have a legend, all the *legends* being typed (with double spacing) together on a *separate sheet*. If structures are given in the text, the original drawings should be supplied. Coloured illustrations are reproduced at the author's expense, the cost being determined by the number of pages and by the number of colours needed. The written permission of the author and publisher must be obtained for the use of any figure already published. Its source must be indicated in the legend.

References. References should be numbered in the order in which they are cited in the text, and listed in numerical sequence on a separate sheet at the end of the article. Please check a recent issue for the layout of the reference list. Abbreviations for the titles of journals should follow the system used by *Chemical Abstracts*. Articles not yet published should be given as "in press" (journal should be specified), "submitted for publication" (journal should be specified), "in preparation" or "personal communication".

Dispatch. Before sending the manuscript to the Editor please check that the envelope contains four copies of the paper complete with references, legends and figures. One of the sets of figures must be the originals suitable for direct reproduction. Please also ensure that permission to publish has been obtained from your institute.

Proofs. One set of proofs will be sent to the author to be carefully checked for printer's errors. Corrections must be restricted to instances in which the proof is at variance with the manuscript. "Extra corrections" will be inserted at the author's expense.

Reprints. Fifty reprints of Full-length papers and Short Communications will be supplied free of charge. Additional reprints can be ordered by the authors. An order form containing price quotations will be sent to the authors together with the proofs of their article.

Capillary Electrophoresis

Principles, Practice and Applications

by **S.F.Y. Li**, *National University of Singapore, Singapore*

Journal of Chromatography Library Volume 52

Capillary Electrophoresis (CE) has had a very significant impact on the field of analytical chemistry in recent years as the technique is capable of very high resolution separations, requiring only small amounts of samples and reagents. Furthermore, it can be readily adapted to automatic sample handling and real time data processing. Many new methodologies based on CE have been reported. Rapid, reproducible separations of extremely small amounts of chemicals and biochemicals, including peptides, proteins, nucleotides, DNA, enantiomers, carbohydrates, vitamins, inorganic ions, pharmaceuticals and environmental pollutants have been demonstrated. A wide range of applications have been developed in greatly diverse fields, such as chemical, biotechnological, environmental and pharmaceutical analysis.

This book covers all aspects of CE, from the principles and technical aspects to the most important applications. It is intended to meet the growing need for a thorough and balanced treatment of CE. The book will serve as a comprehensive reference work and can also be used as a textbook for advanced undergraduate and graduate courses. Both the experienced analyst and the newcomer will find the text useful.

Contents:

1992 xxvi + 586 pages
Price: US$ 225.50 / Dfl. 395.00
ISBN 0-444-89433-0